2015

Development of Novel Chemical Biology Tools for Probing Structure-Function Relationships in G Protein-Coupled Receptors

Tian He

DEVELOPMENT OF NOVEL CHEMICAL BIOLOGY TOOLS FOR PROBING STRUCTURE-FUNCTION RELATIONSHIPS IN G PROTEIN-COUPLED RECEPTORS

A Thesis Presented to the Faculty of

The Rockefeller University

in Partial Fulfillment of the Requirement for

the degree of Doctor of Philosophy

by

He Tian

June 2015

DEVELOPMENT OF NOVEL CHEMICAL BIOLOGY TOOLS FOR PROBING STRUCTURE-FUNCTION RELATIONSHIPS IN G PROTEIN-COUPLED RECEPTORS

He Tian, Ph.D.

The Rockefeller University 2015

G protein-coupled receptors (GPCRs) constitute a large family of transmembrane receptors that transduce extracellular signals into intracellular biochemical responses. Understanding with chemical precision how GPCRs function in cellular membranes is an active area of biological research, but despite recent reports of X-ray crystal structures of several GPCRs, some important questions remain unresolved. For example, the kinetics and thermodynamics of ligand-receptor interactions that lead to receptor activation and how allosteric modulators affect receptor signaling need to be addressed. In addition to basic understanding of transmembrane signaling, studies of GPCRs can provide insights that might advance drug discovery since a large proportion of existing therapeutic agents target GPCRs. The first aim of my thesis project was to develop a strategy for the bioorthogonal labeling of GPCRs with useful chemical probes or chemically reactive handles at specific defined sites. Several strategies were explored to label unnatural amino acid residues genetically encoded into GPCRs expressed in mammalian culture. Using the visual pigment rhodopsin (Rho) as a model GPCR, the strain-promoted [3+2] azide-alkyne cycloaddition reaction (SpAAC) between dibenzocyclooctyne (DIBO) and

p-azido-L-phenylalanine (azF) was shown to be a suitable strategy for attaching labels to GPCRs. While characterizing the specificity, kinetics, topology-dependent reactivity of the labeling chemistry, the reaction rate of SpAAC with azF situated in the transmembrane region of the receptor was enhanced by up to 1000-fold, which was attributed to DIBO partitioning into the hydrophobic core of micelles. Then a fluorescence resonance energy transfer (FRET) assay was developed for the labeled Rho to demonstrate its functionality with respect to ligand binding. Rho consists of a chromophore ligand, 11-*cis*-retinal, bound to the opsin via a Schiff base bond. The photoisomerization of 11-*cis*-retinal to all-*trans*-retinal activates the receptor to trigger the downstream signaling cascade in photoreceptor cells. The Schiff base bond in the active conformation is prone to hydrolysis, allowing all-*trans*-retinal to dissociate from the ligand-binding pocket. The ligand-free opsin then recombines with 11-*cis*-retinal to complete the visual cycle. The FRET assay used to measure the reaction rates of bioorthogonal labeling chemistries also enabled measurement of retinal entry kinetics and was utilized first to address the energetics of the recombination reaction between opsin and 11-*cis*-retinal. The activation energy for retinal binding was obtained from the temperature-dependent retinal entry kinetics. The reaction enthalpy was measured by isothermal titration calorimetry (ITC). The activation energy for the reverse reaction was measured by chromophore exchange of the bound 11-*cis*-retinal with exogenous 9-*cis*-retinal. Based on these results, the complete energy diagram was derived for the binding between 11-*cis*-retinal and opsin. Additional studies were carried out to determine how retinal entry and release kinetics were affected by site-directed mutagenesis of set of highly conserved amino acid residues postulated to be in the pathway for retinal entry

and/or release. A set of mutations located at the fifth and sixth transmembrane (TM) helices was found to exert a much greater influence on the retinal entry kinetics than on the retinal release kinetics. Three criteria were used to evaluate the influence of these mutations: 1) the correlation between side-chain size and entry kinetics; 2) the change in the activation energy for retinal entry; 3) the effect of increasing polarity at these sites. Based on these findings, a model was proposed to describe the retinal entry pathway leading from the membrane-embedded receptor surface to the ligand-binding site in the transmembrane core. In summary, the methods described in this thesis add to the chemical biology tool kit for probing the structure-function relationship in GPCRs. As a specific application of the methodology a detailed analysis is presented that describes the kinetics and thermodynamics of ligand binding and release in the prototypical GPCR rhodopsin. Additional applications of the current methodology include, for example, single-molecule studies of the GPCR signaling complex.

Acknowledgements

I would like to thank my advisor, Dr. Thomas Sakmar, for accepting me into his laboratory to carry out my Ph.D. research project. I appreciate his thoughtful guidance and generous support, as well as insightful advice on career development. My doctoral study has been built on the open and collaborative research environment he has cultivated within the lab and in the broader scientific community.

It has been a great experience to work with the members of the Sakmar lab. My special gratitude goes to Dr. Thomas Huber, who showed me how to think critically about a scientific question and rigorously execute the experiments. He has proven to be an invaluable source of scientific knowledge and he has stimulated endless discussions. I thank Manija Kazmi, for being a tremendously efficient and helpful lab manager. I would like to acknowledge Dr. Minyoung Park, Dr. Shixin Ye, Dr. Saranga Naganathan, and Dr.Thomas Haines, for sharing scientific thoughts and providing feedback on my research. I also thank Dr. Adam Knepp, Dr. Amy Grunbeck, and Dr. Ruchi Gupta for teaching me laboratory techniques in the beginning phase of my graduate study. I express my appreciation to all members of the Sakmar Lab, present or former, for making a supportive and conductive lab environment.

I acknowledge the Proteomic Resource Center and the High-Throughput Screening Center at the Rockefeller University for training and help with the core instruments and facilities. I thank the Dean's Office of the Rockefeller University and the Tri-institutional Program in Chemical Biology for funding.

Finally, I thank my parents and my friends, especially Stefanie Gerstberger, Han Guo, Cindy Meyer, and Aitor Garzia, for their support throughout my graduate studies,

and for making my time in the New York City a great adventure and an enlightening life experience.

TABLE OF CONTENTS

LIST OF FIGURES

LIST OF TABLES

LIST OF ABBREVIATIONS

AcF	*p*-acetyl-L-phenylalanine
AIDS	acquired immunodeficiency syndrome
azF	*p*-azido-L-phenylalanine;
BzF	*p*-benzoyl-L-phenylalanine
β_2AR	β_2-adrenergic receptor
cAMP	cyclic adenosine monophosphate
cGMP	cyclic guanosine monophosphate
CHAPS	3-[(3-cholamidopropyl)-dimethylammonio]-1-propanesulfonate
CHS	cholesteryl hemisuccinate
CMC	critical micelle concentration
CNBr	cyanogen bromide
CuAAC	copper (I)-catalyzed [3+2] azide–alkyne cycloaddition;
DIBO	dibenzocyclooctyne
DBCO	dibenzocyclooctyne
DM	*n*-dodecyl-β-D-maltoside
EC	extracellular
FlAsH	fluorescein arsenical hairpin binder
FRET	fluorescence resonance energy transfer
GAP	GTPase activating protein
GEF	guanine nucleotide exchange factor
GFP	green fluorescent protein

GPCR	G protein-coupled receptor
GRK	G protein-coupled receptor kinase
HIV	human immunodeficiency virus
IC	intracellular
IgG	immunoglobulin G
ISA	immunosorbent assay
isoRho	isorhodopsin
mAb	monoclonal antibody
PDE	phosphodiesterase
ROS	rod outer segment
Rho	rhodopsin
SpAAC	strain-promoted [3+2] azide–alkyne cycloaddition
Tyr-RS	Tyr-tRNA synthetase
uaa	unnatural amino acid
wt	wild type
OG	*n*-octyl-*β*-D-lucoside
PSB	protonated Schiff base
SB	Schiff base
SDS-PAGE	sodium dodecyl sulfate-polyacrylamide gel electrophoresis
TIRF	total internal reflection fluorescence
TM	transmembrane
Trp	tryptophan

Chapter One: Introduction

1.1. G protein-coupled receptors as important drug targets

The G protein-coupled receptor (GPCR) superfamily constitutes the largest group of transmembrane receptors. All GPCRs share seven transmembrane helices as a common structural framework and several highly conserved amino acid residues reside within the transmembrane domain and define receptor sub-classes. As discussed below, the ligand-binding pocket for class A GPCRs is generally situated within the transmembrane core region. The extracellular N-terminus, intracellular C-terminus and the loops between transmembrane helices are much less well conserved but nevertheless play critical roles in defining receptor trafficking and receptor-G protein interaction, among other functions.

Despite the common structural features, GPCRs respond to a wide array of stimuli that are chemically (photon, ions, small molecules, lipids, peptides, proteins) and functionally (hormones, neurotransmitters, cytokines, ordorants, *etc*.) divergent. Not surprisingly, GPCRs mediate a myriad of physiological processes and are widely implicated in diseases, making them the most important category of all the known drug targets (Overington et al., 2006). Notable examples include *β* blockers targeting β adrenergic receptor for treating hypertension, and HIV entry blockers targeting the chemokine CCR5 receptor for treating AIDS.

The GPCR superfamily is further divided into five classes named after their representative member: *rhodopsin* (class A), *Secretin* (class B), *Adhesion* (originally class B), *Glutamate* (class C), and *Frizzled/Taste2* (Bockaert and Pin, 1999). The *rhodopsin*

receptor family is the largest category, covering a number of nearly 700 receptors (Lagerstrom and Schioth, 2008).

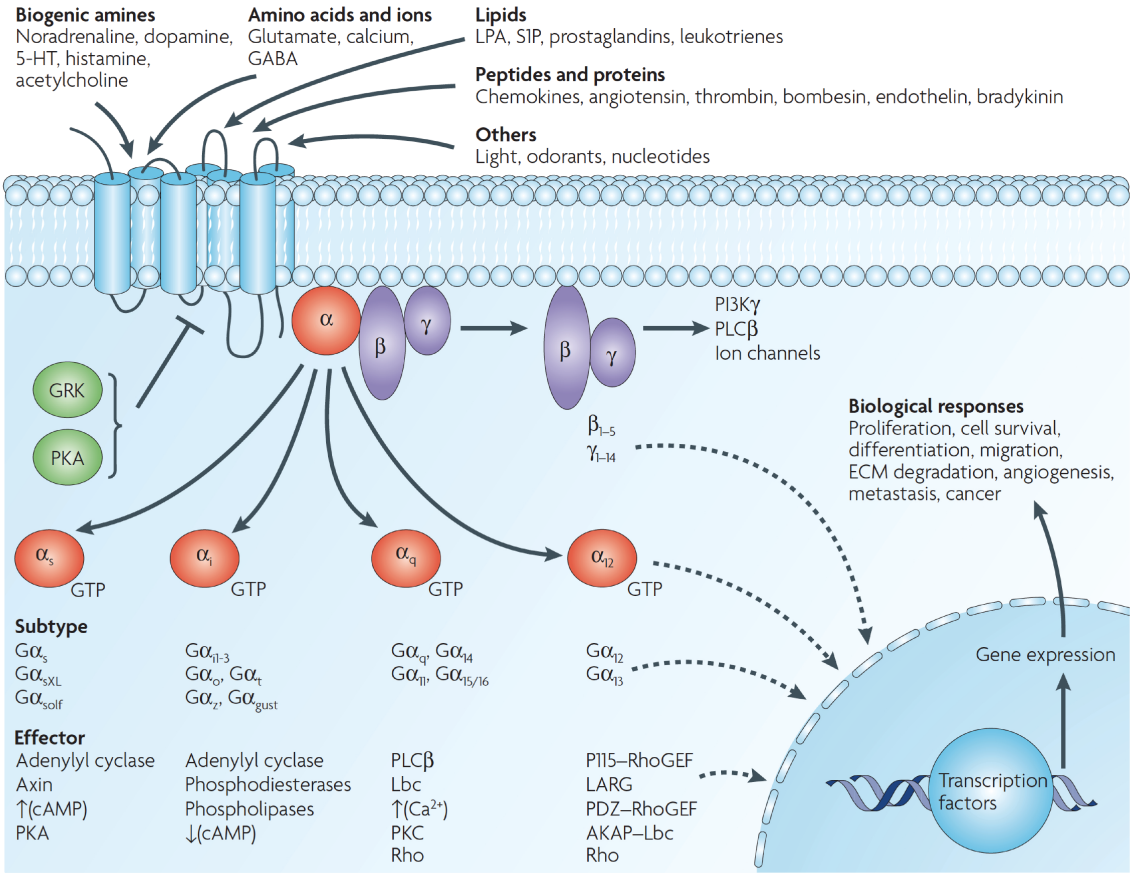

Figure 1-1. The GPCR signaling pathway. A wide range of ligands can activate GPCRs. The activated receptor activates the heterotrimeric G protein. The downstream signaling pathway is determined by the type of Gα being activated by the receptor. The four classes of Gα are specialized to activate adenylyl cyclase (G_s), inhibit adenylyl cyclase (G_i), activate phospholipase C (G_q), and regulate guanine nucleotide exchange ($G_{12/13}$). The biological response may range from transient events (*e.g.*, opening of ion channel) to long-term change (*e.g.*, gene expression). Figure taken from (Dorsam and Gutkind, 2007).

1.2 Intracellular signaling through GPCRs

GPCRs are exquisitely regulated signaling machines. As the name suggests, the canonical signaling pathway involves the coupling between the receptor and G protein. Unlike many other important transmembrane receptors, such as ligand-gated ion channel receptors and enzyme-coupled receptors, GPCRs lack catalytic activity and requires the heterotrimeric G protein (G$\alpha\beta\gamma$) to serve as an intermediate between receptor and effector. Specifically, GPCR activation by agonist binding leads to GDP-GTP exchange in the Gα subunit and subsequent decoupling of Gα with G$\beta\gamma$ and receptor. In this regard, GPCRs functions as a guanine nucleotide exchange factor (GEF). Gα is a weak GTPase whose activity is regulated by GTPase activating proteins (GAPs). The hydrolysis of GTP to GDP deactivates Gα and eventually results in the re-association of Gα with Gβγ (Oldham and Hamm, 2008).

Besides the G protein cycle, the duration of signaling is also regulated through a process termed desensitization. The receptor can be phosphorylated by GPCR kinases (GRKs) to induce arrestin binding, which prevents further interaction between receptor and G protein, and induces endocytosis of the receptor to reduce the density of receptors on the cell surface.

The picture described here, however, is quite primitive, with many key questions to be tackled. One important question open to debate concerns the allosteric regulation of GPCRs. In the classic scenario, ligand-receptor binding precedes receptor-G protein binding (the "free collision" model). Meanwhile, there is increasing evidence suggesting that G protein may engage receptor prior to agonist binding (the "pre-coupling" model), which in turn increases receptor's affinity to the ligand (Oldham and Hamm, 2008;

Nobles et al., 2005). Whether the pre-assembled receptor-G protein complex exists in the cellular context, and if so, what is their physiological significance, is being actively investigated. Another pharmacologically significant question is the biased signaling of GPCRs. A particular ligand may not elicit the full repertoire of downstream signaling, but selectively activate some of the pathways (Violin and Lefkowitz, 2007). Because many GPCRs mediate more than one downstream signaling pathway with important physiological consequence, these biased ligands may be exploited to precisely target the most relevant pathway while leave the rest undisrupted. Addressing these questions often require a detailed understanding on the conformational dynamics and heterogeneity of GPCRs.

1.3 Rhodopsin as a Model System for Studying GPCR: a Historical Perspective

This thesis presents novel chemical approaches for studying GPCR signaling complex, using the visual photoreceptor rhodopsin as the model system, an excellent prototypical receptor for class A GPCRs. Here I would like to briefly review the history of research on rhodopsin to illustrate how knowledge accumulated for a particular receptor contributed to the grand picture of GPCRs.

1.3.1 The early years of research on rhodopsin

The scientific quest on the biochemistry of visual process has a long-standing history dating back to the 1830s, when microscopic anatomists began to investigate the fine structure of the eye and its associated parts. These efforts led to the identification of the layer structure of retina, including the outer layer consisting of cones and rods, and the connectivity between retina and nerve fiber. Although the overall importance of retina in visual function was evident, it remained controversial on which element of retina mediates the light-sensing function. Heinrich Müller, an anatomist working in Würzburg, showed that the nerve fibers terminates at the rods and cones, supporting the view that rods and cones are responsible for light-sensing (Schickore, 2000). Moreover, Müller was the first to describe the reddish color of vertebrate rod cells.

The significance of Müller's seminal finding was made clearer by the work of Franz Boll, who described in 1876 that the red-purple color of rod changed to yellow upon photobleaching in a wavelength-dependent manner, and that the red color could be regenerated in the live animal in the dark (Boll, 1876). The reversible change of color strongly suggested a direct connection between rod cells and the visual action, and immediately inspired Willy Kühne, a physiologist well acquainted with chemical

approaches, to pursue this question. Kühne decided that purple was more suitable than red for describing the color of rod, and coined the neologism “visual purple (sehpurpur)”, and later “ rhodopsin” to refer to this colored substance. Kühne, together with his assistants, produced a strikingly large body of knowledge into the chemistry of visual system that remained unsurpassed for the next fifty years. They found that in contrary to Boll’s claim, visual purple was not degraded upon death of animal. The photobleaching of this purple substance involved an intermediate yellow species and the rate of photobleaching was dependent on the wavelength and intensity of incident light. The regeneration of visual purple required direct contact between retina and fresh pigment epithelium. They extracted visual purple with bile salt, and performed the recombination reaction *in vitro* by combining the retina and pigment epithelium extraction. Because visual purple could be salted out, but did not penetrate semi-permeable membrane, Kühne inferred it to be a protein (Gamgee, 1877; Kühne, 1878; Wolf, 2001).

The pioneering works by the physiologists in the 19th century established the idea that visual function involved a chemical process in the rod cells of retina. The subsequent development of spectrophotometry enabled quantitative verification of Kühne’s qualitative description. Selig Hecht, a biophysicist at Columbia University, proposed a conceptual scheme for this reversible chemical process. Visual excitation is initiated by the dissociation of the photosensitive pigment (S) into two molecules ($S \rightarrow P+A$), and one of the resulting products mediates the photo excitation. In turn, the pigment was regenerated by the recombination of P and A, or a variant P +B (Wald, 1968). A major contribution by Hecht was the recognition of the quantal nature of visual photochemistry. He showed that visual excitation only required 5 to 8 photons, an incredibly small

number, thus the visual system must possess an exceptional efficient signal amplification mechanism (Hecht et al., 1942).

In 1930s, various lines of evidence suggested visual purple was a protein with a colored prosthetic group (Hecht, 1942). George Wald, Hecht's pupil, made a crucial step towards uncovering the chemical nature of rhodopsin. Inspired by the observation that dietary night blindness resulted from vitamin A deficiency, Wald showed by UV-Vis spectroscopy that the chloroform extraction from retina contained a considerable concentration of vitamin A (Wald, 1933), and proposed that rhodopsin was a carotenoid-bound protein (Wald, 1934). In the ensuing years, Wald studied every species he could possibly obtain, and concluded all the visual pigments, including the cone receptors for photopic color vision and rod receptor for scotopic vision, shared a similar architecture: a molecule of retinal bound to a colorless protein opsin, and it was the difference in opsins that produced the characteristic absorption spectrum for each pigment (Wald, 1953, 1964). The abundance of rhodopsin in bovine retina made it possible for enough material to be obtained in large quantity, which was non-trivial in an era prior to the advent of recombinant protein technology. Using bovine rhodopsin as the model system, Wald and his co-workers delineated the serial conversion of retinoids in the visual cycle (Wald et al., 1950; Wald and Brown, 1950; Hubbard and Wald, 1952), and elucidated how retinal was attached to the apoprotein opsin (Bownds and Wald, 1965; Bownds, 1967). These findings were summarized in Figure 1-2.

1.3.2 Rhodopsin found to be a GPCR

By the year of 1967 when Wald was awarded the Nobel Prize in Physiology or Medicine, his relentless investigation had pushed the research on rhodopsin to the

boundary of the contemporaneous chemical and spectroscopic methodologies. Nonetheless, how rhodopsin could convert photo-signal into neuroelectric signal could not be answered without explicit knowledge on the action of opsin. In the late 1970s sequencing of soluble globular protein was routine. However, sequencing a highly hydrophobic molecule like rhodopsin remained a formidable challenge. Paul Hargrave, a leading peptide biochemist, overcame a series of technical difficulties to determine the N- and C-terminal sequence of rhodopsin (Hargrave and Fong, 1977; Hargrave et al., 1982a), locate the lysine that formed a Schiff base bond with retinal (Wang et al., 1980; Hargrave et al., 1982b), and characterize the oligosaccharides attached to the N-terminus (Fukuda et al., 1979, 1982).

From 1982 to 1983, the Ovchinnikov group based in Moscow (Ovchinnikov, 1982) and the Hargrave group (Hargrave et al., 1983) independently published their magnum opus: the complete amino acid sequence of rhodopsin. The primary structure yielded the critical insight that the polypeptide of rhodopsin folded into seven transmembrane helices (Figure 1-3) (Ovchinnikov, 1982; Hargrave et al., 1983). It also suggested a structural and functional homology between rhodopsin and another known retinal-bound protein bacteriorhodopsin (Ovchinnikov, 1982).

Figure 1-2. Summary of the knowledge on the visual cycle by 1968. **A)** The structures of 11-*cis*-retinal (**1**), 11-*cis*-retinol (**2**), all-*trans*-retinal (**3**), all-*trans*-retinol (**4**) and all-*trans*-retinyl ester (**5**). **B**) The proposed diagram of rod visual cycle. The enzymes in the visual cycle identified after 1968 are colored in *red*. The question mark represents the enzymes Ward hypothesized to exist. The photobleaching of rhodopsin by light causes 11-*cis*-retinal to isomerize to all-*trans* retinal that subsequently dissociates from opsin. All-*trans*-retinal is then reduced to its alcohol form by all-trans retinol dehydrogenase (all-*trans* RDE) (Rattner et al., 2000), the only enzymatic activity identified in the visual cycle by 1968(Koen and Shaw, 1966). All-*trans*-retinol then forms all-*trans* retinyl ester with fatty acid by the activity of lecithin retinol acyltransferases (LRAT) (Saari and Bredberg, 1989; Ruiz et al., 1999). All-*trans*-retinyl ester is isomerized and de-esterified to yield 11-*cis*-retinol by the activity of RPE65 isomerohydrolase, without producing 11-*cis*-retinyl ester. The long-awaited retinoid isomerase was first identified through mouse genetics (Redmond et al., 1998), then characterized by biochemical approach (Jin et al., 2005; Moiseyev et al., 2005; Moiseyev et al., 2006). 11-*cis*-retinol was oxidized to 11-*cis*-retinal by 11-*cis*-retinol dehydrogenase (Simon et al., 1995; Simon et al., 1996). Rhodopsin is synthesized by the recombination of opsin and 11-*cis*-retinal, thus completing the visual cycle. **C)** The photoactivation of rhodopsin. Light causes the bound 11-*cis*-retinal to isomerize to all-*trans* retinal. The all-*trans*-retinal bound opsin undergoes through a series of short-lived photo-intermediates (λ_{max} indicated in the bracket): the 543-nm species (pre-lumi, now commonly referred to as “batho”), the 497-nm species (lumi), 478-nm species (Meta-I), 380-nm species (Meta-II), ending in the dissociation of retinal. These were characterized at low temperatures. The photobleaching of opsin results in the exposure of new chemical groups, including two thiols groups (Wald and Brown, 1953) and one proton-binding group. However, Wald incorrectly positioned retinal on the surface of opsin. The first clue indicating retinal is located in the hydrophobic core of the disc membrane came the FRET study by the Stryer group (Thomas and Stryer, 1982). Figure adapted from (Wald, 1968; Nobel Prize lecture)

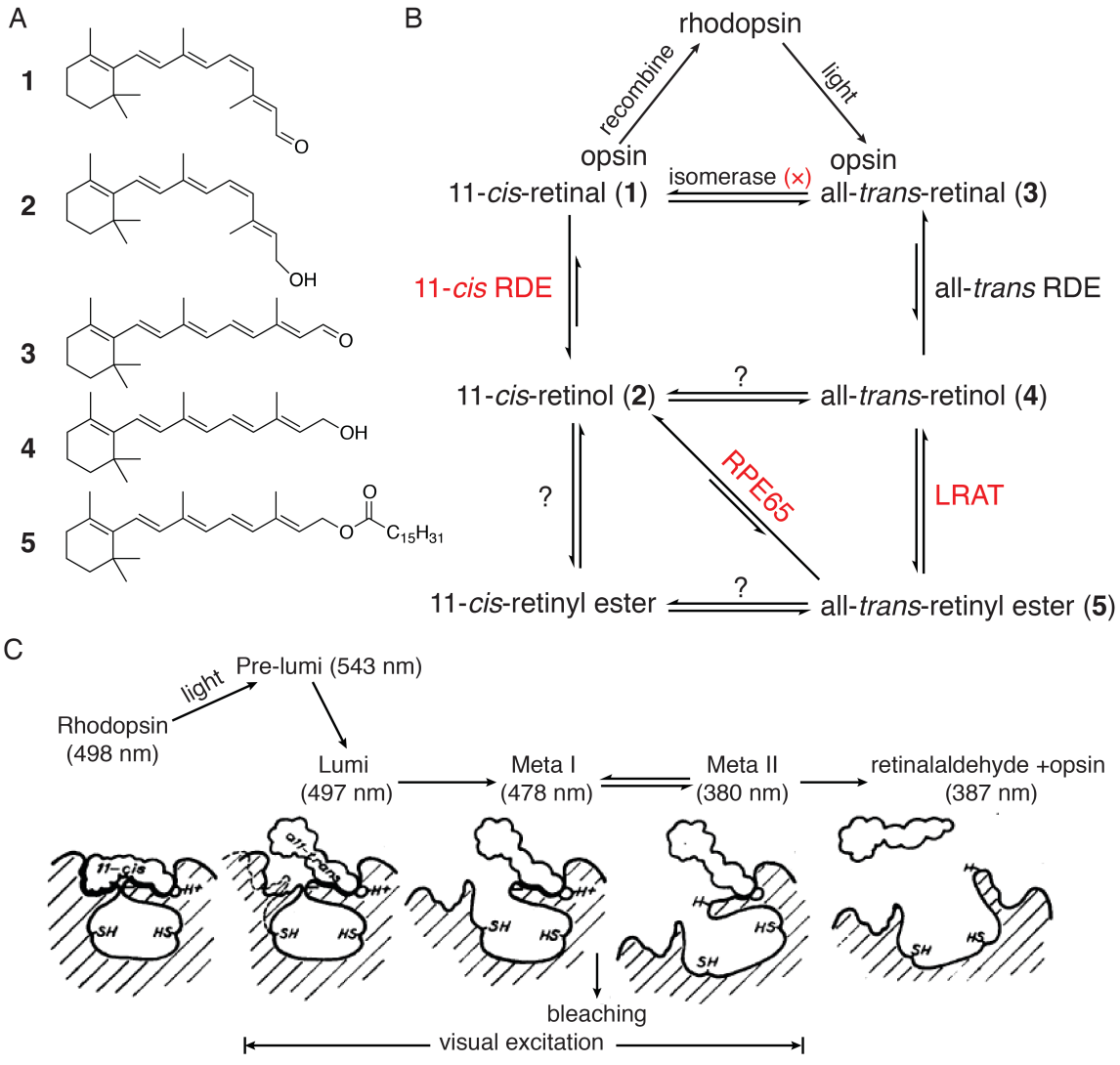
A
1
2
OH
3
4
OH
5
O
$C_{15}H_{31}$
B
rhodopsin
recombine
light
opsin
opsin
11-*cis*-retinal (**1**)
isomerase (×)
all-*trans*-retinal (**3**)
11-*cis* RDE
all-*trans* RDE
11-*cis*-retinol (**2**)
?
all-*trans*-retinol (**4**)
?
RPE65
LRAT
11-*cis*-retinyl ester
?
all-*trans*-retinyl ester (**5**)
C
light
Pre-lumi (543 nm)
Rhodopsin
(498 nm)
Lumi
(497 nm)
Meta I
(478 nm)
Meta II
(380 nm)
retinalaldehyde +opsin
(387 nm)
11-cis
all-trans
H+
SH
HS
bleaching
visual excitation

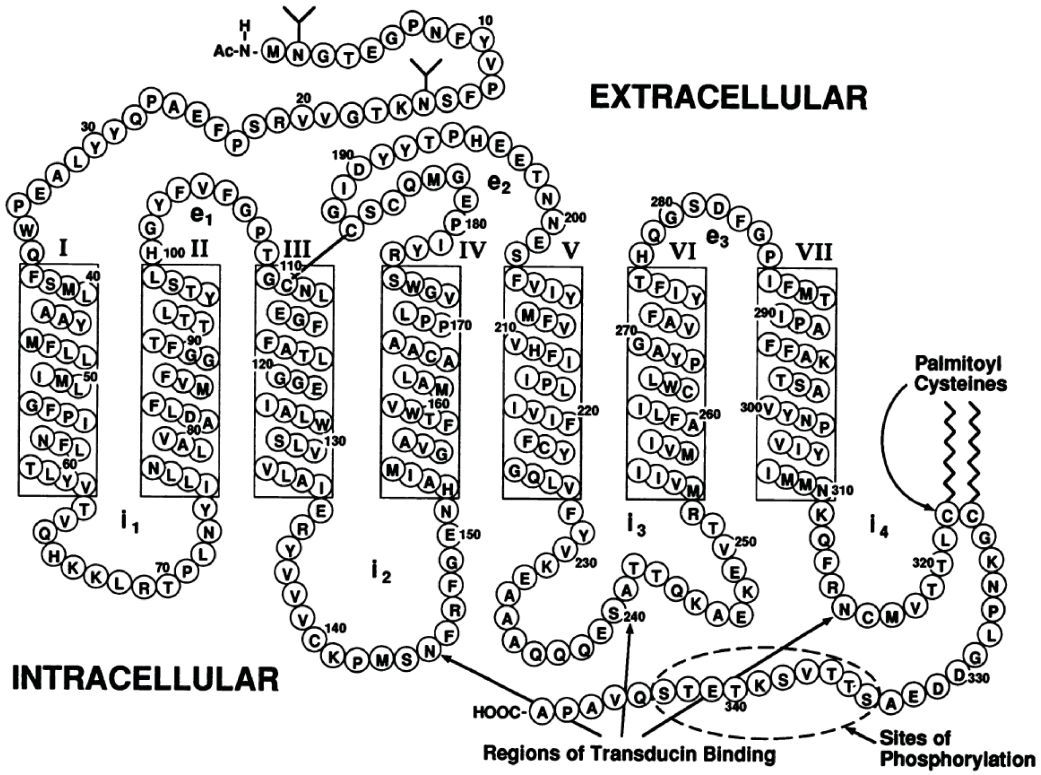

Figure 1-3. The topological model of rhodopsin, with functionally important sites highlighted. Compared with the model proposed in 1983, this model differs slightly in the assignment of the boundary between the helices and loops. It also incorporated the information on the site of glycosylation (Fukuda et al., 1979), palmitoylation(Moiseyev et al., 2006), a critical disulfide bond (Karnik et al., 1988), and molecular determinants for transducin binding and activation (Franke et al., 1988; Franke et al., 1990). Figure taken from (Hargrave and Mcdowell, 1992).

The disclosure of the peptide sequence of rhodopsin quickly led to the advent of molecular biology of vision: the cloning of the gene encoding bovine rhodopsin (Nathans and Hogness, 1983), human rhodopsin (Nathans and Hogness, 1984), fruit fly rhodopsin (Zuker et al., 1985), and human cone receptors for color vision (Nathans et al., 1986).

In the mid-1980s, a groundbreaking advance closely related to rhodopsin was made at a different frontier. The cloning of β-adrenergic receptor (Dixon et al., 1986; Frielle et al., 1987)and α-adrenergic receptor (Kobilka et al., 1987) shed light on the similarity between rhodopsin and adrenergic receptors, which was naturally predicted to possess seven transmembrane helices. It was quickly appreciated that the similarities between the visual photoreceptors and endocrine receptors was beyond simple sequence and structural homology; they resembled each other in the pattern of signaling.

Since late 1950s, the idea of intracellular signal transduction through secondary messenger has seized intense attention. In fact, the canonical stimulatory G protein (G_s)-adenylyl cyclase pathway was first elucidated for the epinephrine system. It embarked with the discovery of the first secondary messenger, cyclic adenosine monophosphate (cAMP) (Rall et al., 1957; Rall and Sutherland, 1958). Four years later, the synthetic enzyme adenylyl cyclase (Sutherland et al., 1962) and degrading enzyme phosphodiesterase (Butcher and Sutherland, 1962) of cAMP were purified. It was not long before another cyclic nucleotide, cyclic guanosine monophosphate (cGMP), joined the class of secondary messenger molecules (Ashman et al., 1963). In the 1970s, it was found that the production of cAMP requires guanosine triphosphate (GTP) (Rodbell et al., 1971a; Rodbell et al., 1971b) and a protein component with GTPase activity, later known as the G protein (Ross and Gilman, 1977a, b).

In the beginning of 1980s, the cyclic GMP cascade in rod cells had come into prominence. The observed dramatic hydrolysis of cGMP in rod cells upon illumination (Woodruff and Bownds, 1979; Yee and Liebman, 1978) and depolarization of ROS plasma membrane caused by exogenously injected cGMP (Miller and Nicol, 1979) were consistent with the key features of the visual system: 1) exceptional capability of signal amplification and 2) coupling between chemical reaction and neuroelectric signal. The major enzymatic components, cyclic GMP phosphodiesterase (Bitensky et al., 1975; Miki et al., 1975; Keirns et al., 1975) and GTPase transducin (Wheeler and Bitensky, 1977; Fung et al., 1981), as well as their interdependence (Kühn, 1980) had been characterized by the collective efforts of several groups, notably the Bitensky group at Yale University, the Stryer group at Stanford University and the Kühn group in the Federal Republic of Germany. In fact, years before the cloning of β_2-adrenergic receptor, the analogy between the light-activated signaling pathway in rod outer segment and epinephrine-stimulated signaling pathway in hormone-sensitive cells had been articulated first by Bitensky (Shinozawa et al., 1979; Bitensky et al., 1981; Stein et al., 1982; Bitensky et al., 1982), then by Stryer (Stryer, 1983, 1986). The flow of information involved the common steps: 1) the extracellular signal activates the receptor; 2) the receptor then stimulates the GDP-GTP exchange in a G protein; 3) the GTP-bound G protein acts on a enzyme that catalyzes the degradation (phosphodiesterase for light-activated pathway) or synthesis (adenylyl cyclase for the epinephrine-stimulated pathway) of a cyclic nucleotide (Figure 1-4). The sequence and structural homology between photoreceptors and adrenergic receptors cemented the parallelism, which is now known as the classic G protein-coupled receptor signaling pathway (Dohlman et al., 1987). The new realization rectified the old

thought that seven transmembrane helices was the structural hallmark of light-sensing protein.

The conservation of GPCR pathway implied that the findings about rhodopsin might also hold true for other receptors. One excellent example was the cloning of arrestin, the protein regulating the desensitization of GPCRs. In 1983, it was recognized that agonist-induced desensitization of β_2-adrenergic receptor was dependent on phosphorylation (Stadel et al., 1983; Lefkowitz et al., 1983). However, purified β_2-adrenergic receptor (GRK2) lost its ability to desensitize the β_2-adrenergic receptor, suggesting an essential component was missing (Benovic et al., 1987a). Around the same time, the Kühn group identified and purified a 48-kDa protein in rod outer segment that binds with photoactivated rhodopsin and quenches the cGMP cascade (Pfister et al., 1985; Wilden et al., 1986). It was quickly shown this 48-kDa protein, later renamed arrestin, restored the ability of β_2-adrenergic receptor kinase to desensitize β_2-adrenergic receptor (Benovic et al., 1987b). The cloning of rhodopsin arrestin (Shinohara et al., 1987) enabled design of a appropriate hybridization probe leading to the cloning of β-arrestin (Lohse et al., 1990). The role of GRK and arrestin in GPCR desensitization turned out to be a general mechanism for regulating GPCR signaling (Premont and Gainetdinov, 2007).

If we consider Boll's work in 1876 marked the beginning of visual chemistry (Boll, 1876), and the research on adrenergic receptor commenced with the isolation of epinephrine by Takamine in 1900 (Bennett, 1999; Rubin, 2007), the two fields have evolved independently for multiple decades before they intersected in the mid 1980s. It is worth noting that this discovery also inspired the cloning of a large family of olfactory

receptors (Buck and Axel, 1991), which earned Linda Buck and Richard Axel the 2004 Nobel Prize in Physiology or Medicine.

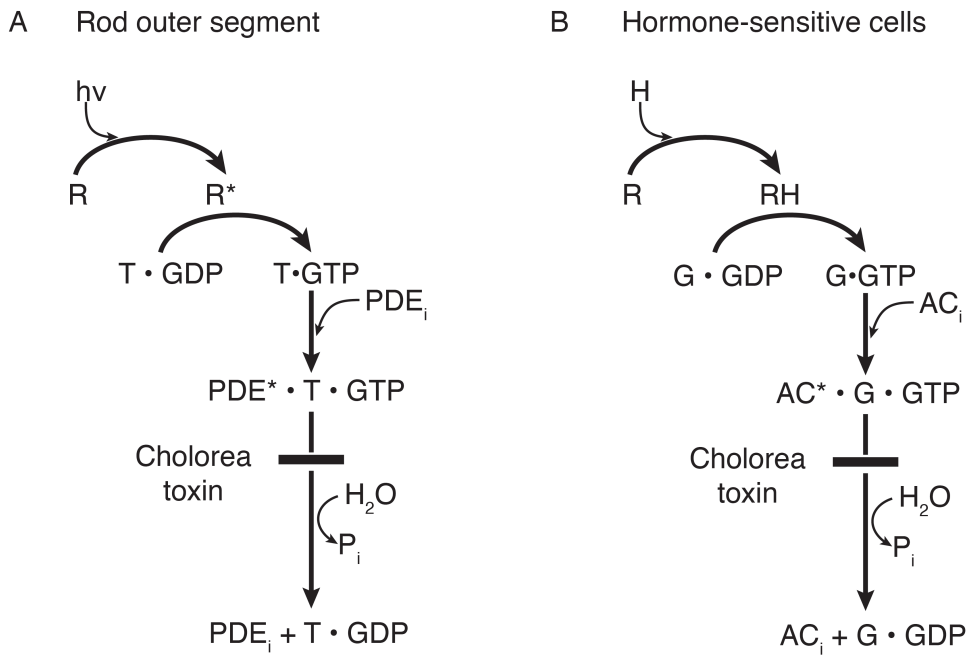

Figure 1-4. Comparison of the signaling pathway in rod outer segment (A) and hormone-sensitive cells (B). R: rhodopsin or the adrenergic receptor at the basal state; hν: photon; H: hormone (e.g. epinephrine); R*: photoactivated rhodopsin; RH: hormone-receptor complex; T: transducin; G: stimulatory G protein (G_s); AC_i and AC*: inhibited and activated form of adenylyl cyclase; PDE_i and PDE*: inhibited and activated forms cGMP phosphodiesterase. Both pathways terminate with the hydrolysis of bound GTP through the GTPase activity of T or G. Another parallel is that cholera toxin catalyzes the ADP-ribosylation of both T and G, and blocks their GTPase activity. Figure adapted from (Stryer, 1983)

1.3.3 Rhodopsin as a model system for understanding the structure-function relationship of GPCRs

The discovery of the seven transmembrane helices of GPCRs was both illuminating and tantalizing. One way to decode the seven helices was to see how small perturbation to the integral structure would alter the function. The Khorana group designed the first synthetic gene for bovine rhodopsin (Ferretti et al., 1986), and demonstrated the heterologous expression of rhodopsin in mammalian cell culture (Oprian et al., 1987), which paved the way for site-directed mutagenesis study of rhodopsin. From the late 1980s to 1990s, this approach proved extremely prolific in understanding the precise structure–function relationship of rhodopsin, yielding information on the molecular determinants for maintaining the correct folding of the receptor (Karnik et al., 1988), modulating the stability prorogated Schiff base (Sakmar et al., 1989, 1991; Nakayama and Khorana, 1991); defining rhodopsin-transducin interaction (Franke et al., 1990); leading to retinal diseases (Liu et al., 1996; Garriga et al., 1996; Mollaaghababa et al., 1997), and conferring constitutive activity in the absence of photoactivation (Kim et al., 1997; Han et al., 1998).

A crucial insight from the mutagenesis study was that rhodopsin activation involved the rigid-body movement of TM3 and TM6. Spin labels attached to the cytoplasmic end of TM3 and TM6 indicated a change in their distance in response to photoactivation (Farrens et al., 1996). When its cytoplasmic end of TM3 and TM6 were held together by metal ion binding (Sheikh et al., 1996) or by disulfide crosslinking (Farrens et al., 1996) illuminated rhodopsin failed to activate transducin. These findings

demonstrated that the relative movement between TM3 and TM6 was essential for rhodopsin activation.

Another strategy for understanding the seven transmembrane helices was to examine the structure at higher resolution. In 1993, Schertler and his co-workers obtained projection structure of rhodopsin at 7-9 Å resolution, providing the first clue for the arrangement of the seven helices (Schertler et al., 1993). The first high-resolution X-ray crystal structure of rhodopsin was published in 2000 by Palczewski and his co-workers (Palczewski et al., 2000). More refined structures that revealed the conformation of 11-*cis*-retinal bound in the binding pocket and internal water network ensued within a few years (Teller et al., 2001; Li et al., 2004; Okada et al., 2004). These structures of rhodopsin served as a framework for interpreting the previous biochemical data accumulated through the mutagenesis studies (Sakmar et al., 2002). It also enabled the identification of "switches" motifs responsible for maintaining rhodopsin at its basal state. In 2007, the Kabila group and the Stevens group reported the high-resolution structures of engineered β_2-adrenergic receptor at its inactive state (Rosenbaum et al., 2007; Rasmussen et al., 2007; Cherezov et al., 2007). A comparison on the structures of rhodopsin and β_2-adrenergic receptor again revealed a high degree of similarity (Figure 5-A), proving the utility of rhodopsin as a mode system for studying GPCRs.

The follow-up efforts were devoted to capture functionally relevant conformations of rhodopsin. The structures of bathorhodopsin(Murakami and Kouyama, 2011; Nakamichi and Okada, 2006a), lumirhodopsin(Nakamichi and Okada, 2006b), a photoactivated deprotonated intermediate (Salom et al., 2006), and electron crystallography map of Meta I (Ruprecht et al., 2004)were obtained between 2004 and

2006. Two year later, the crystal structures of ligand-free opsin(Park et al., 2008) and opsin in its G protein-interacting form (Scheerer et al., 2008) were acquired, followed by the structure of Meta-II rhodopsin (Choe et al., 2011), constitutively active mutant (Standfuss et al., 2011; Deupi et al., 2012a), and disease mutant (Singhal et al., 2013). Thus rhodopsin became the first GPCR whose inactive, active and discrete intermediate states have been crystallized. Comparison of the inactive and the active conformation confirmed the helix movement model for receptor activation proposed based on the biochemical studies of rhodopsin in 1990s (Figure 5-C) (Farrens et al., 1996; Sheikh et al., 1996), and shed light on how photoisomerization transforms retinal from an inverse agonist to an agonist (Choe et al., 2011; Standfuss et al., 2011). These structures together provided a framework for understanding the molecular basis of GPCR activation (Deupi and Kobilka, 2010; Deupi et al., 2012b; Deupi, 2014). Dark-state rhodopsin is thought to represent the most energetically stable conformation of GPCRs, and activation involves the accumulative local structural changes that culminate in pronounced helix movement, particularly the outward tilt of TM6 (Deupi et al., 2012b). It also renovated the simplistic two-state model for GPCR activation: between the two extremes of the fully inactive and the fully active conformation there are a series of intermediates; the role of ligand is to shift the equilibrium of population by altering the energy landscape (Deupi and Kobilka, 2010).

The crystal structures of rhodopsin facilitated rational design of biophysical experiment to track the sequence and dynamics of conformational changes in receptor activation (Altenbach et al., 2008a; Ye et al., 2010). Moreover, they served as templates for homology modeling of GPCRs for virtual drug screening (Archer et al., 2003; Evers

and Klabunde, 2005), and enabled molecular dynamic simulations to receptor self-assembly in the context of lipid bilayer (Periole et al., 2007; Periole et al., 2012).

In 2011, two structures of β_2-adrenergic receptor at its active state, one stabilized by a nanobody (Rasmussen et al., 2011a), the other stabilized by irreversible agonist binding (Rosenbaum et al., 2011), were resolved by the Kobilka group. The active-state structures of β_2-adrenergic receptor are remarkably similar to that of rhodopsin (Figure 5-C), thus completely validating the helix movement model of GPCR activation. At the same time, the GPCR field witnessed another important breakthrough: for the first time an active GPCR in complex with its G-protein partner was crystallized (Rasmussen et al., 2011b). This structure revealed important contacts on the receptor-G protein interface and conformational changes that lead to the opening of nucleotide binding pocket.

Currently the number of GPCR crystal structures are still rapidly increasing (Stevens et al., 2013). In addition to class A GPCRs, class B (Siu et al., 2013) and the transmembrane domain of class C receptors (Wu et al., 2014; Dore et al., 2014) have also been successfully obtained. Despite the wealth of knowledge produced from the structural studies, crystallography has its inherent limitations. First of all, obtaining a structure for any GPCR remains an expensive and time-consuming task. The reasons underlying this difficulty include low expression level of receptors in most expression systems, hydrophobicity of membrane proteins, and the intrinsic structural instability associated with the basal activity exhibited by most GPCRs. Consequently, except for rhodopsin, extensive engineering is often required for increasing the thermal stability of receptors, such as point mutagenesis, T4 lysozyme fusion in the intracellular loop, and antibody stabilization. However, these altered regions are implicated in receptor-G

protein or receptor-arrestin interaction. This has complicated the interpretation of the structures. Second, GPCR activation involves more than two “on” and “off” states, while a structure only gives the “snapshot” of one conformation. It is particularly challenging to capture the active state that naturally tends to relax to the energetically favored inactive state. Not surprisingly, so far active-state structures have been obtained only for a few extensively characterized GPCRs. For most other GPCRs it will be a formidable task to obtain enough structures to cover all the relevant conformations. Third, the static nature of crystal structures provides little insights into the dynamics of receptor activation. All these considerations raise a need for developing new methodologies.

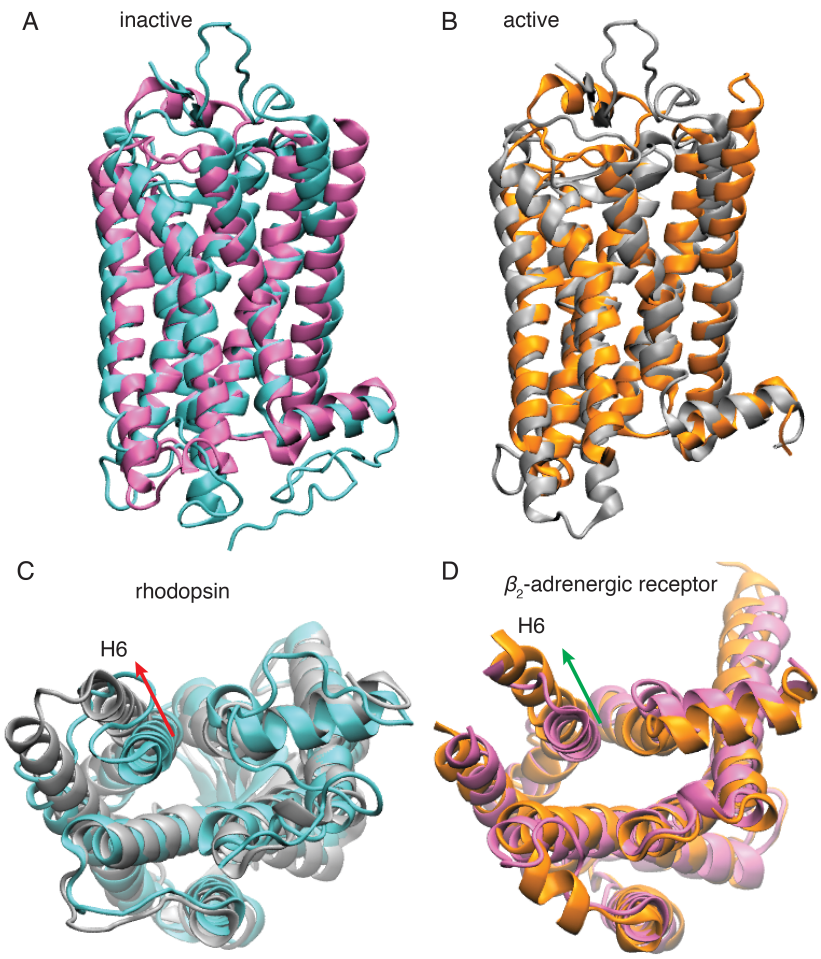

Figure 1-5. Comparison of the structures of rhodopsin and β_2-adrenergic receptor. **A)** The structures of inactive rhodopsin (*cyan*, PDB 1U19) (Okada et al., 2004) and inactive β_2-adrenergic receptor (*mauve*, 2RH1) (Rasmussen et al., 2007). **B)** The structures of active metarhodopsin (*grey*, 3PQR) (Choe et al., 2011) and active-state β_2-adrenergic receptor (*orange*, 3CAP) (Rasmussen et al., 2011a). Comparison of the intracellular side of **C)** inactive rhodopsin and inactive β_2-adrenergic receptor and **D**) active metarhodopsin and active β_2-adrenergic receptor. In the active conformation, the outward tilt of the cytoplasmic end of TM6 is 6-7 Å and 11 Å in rhodopsin and β_2-adrenergic receptor, respectively.

1.4 Chemical approaches for studying GPCRs

A unique craft of chemists is to tailor the property of molecules for tackling biological problems, which has contributed tremendously to the GPCR field on various topics, for example, mapping the ligand-receptor binding mode. Before it became possible to crystallize GPCRs, crosslinking ligand to the receptor was one of the few ways to interrogating ligand-receptor binding. Even with the great advance in structural biology of GPCR, the resources needed to acquire the crystal structure for a ligand-receptor complex make it beyond a routine process. More importantly, many ligand-receptor complex are simply too unstable to be crystallized. Therefore, crosslinking often represents a more practical option (Grunbeck and Sakmar, 2013). This approach, despite the trials and errors involved to validate the function of the derivatized ligand, has produced valuable insights. The Khorana designed a photocrosslinking 11-*cis*-retinal analog by modifying the *β*-ionone ring with a diazirine group (Nakayama and Khorana, 1990a). Subsequent photocrosslinking experiment with opsin unambiguously assigned the *β*-ionone between TM3 and TM6 (Nakayama and Khorana, 1990b), and mapped the residues in proximity with retinal (Nakayama and Khorana, 1991). Based on this photocrosslinking analog, the Nakanishi group further locked the *cis*-double bond by adding a six-membered ring. This analog could not undergo the *cis*-*trans* photoisomerization, so it was possible to selectively crosslink retinal with the inactive receptor. They found that the relative position of *β*-ionone ring was closer to TM6 in the dark-state, but shifted to TM3 in the Meta-II state (Zhang et al., 1994). These findings from photocrosslinking experiments were one decade ahead of the crystal structures (Palczewski et al., 2000; Choe et al., 2011).

Nonetheless, understanding the ligand binding mode should not be narrowly interpreted as knowing the contacts between the ligand and the binding pocket, but how these contacts are correlated to the function of the receptor. For example, adrenergic receptor has never been crystallized in complex with important native ligands like epinephrine or norepinephrine. Yet as early as 1910 the functional groups important for stimulating the sympathetic response were defined through systematic variation of the chemical structure of epinephrine (Barger and Dale, 1910). The knowledge on the structure-activity relationship of adrenergic ligands played an indispensible role in drug development and fundamental scientific inquiry, including developing the high-affinity ligands for treating asthma, hypertension, depression, etc. These ligands also proved powerful tools for investigating fundamental biological questions. For example, the existence of adrenergic receptors on cell membrane as distinct molecular entities was open to debate even at the beginning of 1970s. To prove the receptor theory, one needs to show that ligands specifically bind to surfaces of the cells expected to express the receptors. This was a challenging experiment, because the adrenergic receptor only constitutes a small population among the cell-surface proteins. The well-characterized native ligands were generally not ideal reagents for such purpose, primarily due to their low affinities and lack of selectivity between α- and β-subtypes. Therefore, when Lefkowitz and his co-workers set out to search for adrenergic receptors, they chose [^{3}H] alprenolol for β-adrenergic receptor (Lefkowitz et al., 1974) and [^{3}H]dihydroergocryptine for α-adrenergic receptor (Williams and Lefkowitz, 1976), both were synthetic high-affinity antagonists with an unsaturated double bond. The tritium labeling was done through the textbook palladium-catalyzed hydrogenation reaction of alkenes. They were

able to show that these ligands could bind with the cell membrane in a manner fulfilling all the properties predicted by the physiological studies: competitive, subtype-selective, and stereospecific, thereby fully establishing the receptor theory.

For a long period of time, the focus of the chemical toolkit for studying GPCRs has been on the ligands. In the recent years, our laboratory has expanded the horizon by developing a general platform for modifying the chemical properties of receptors, which shall be discussed in greater details in Chapter Two.

Chapter Two: Bioorthogonal Labeling of Functional GPCRs

2.1 Summary

We have developed a general approach for site-specific bioorthogonal labeling of G protein-coupled receptors (GPCR). We utilized rhodopsin (Rho), a prototypical class A GPCR as the model system to study the labeling chemistry. We incorporated ketone and azide functionality into the receptor by uaa mutagenesis. We performed a comparative study for two labeling strategies, one targeting the keto group and the other targeting the azido group. We carried out kinetic analysis of the model reactions, and quantified the extent of non-specific labeling. We demonstrated the superior bioorthogonality of the azido group, and concluded that strain-promoted [3+2] azide–alkyne cycloaddition (SpAAC) reaction of dibenzocyclooctyne (DIBO) with azF is a suitable choice for labeling discrete sites located in the EC, IC and TM region of Rho with fluorophores. We found that azF residues situated on the transmembrane surface of detergent-solubilized receptors exhibit up to 1000-fold rate enhancement compared with azF residues on water-exposed surfaces. We showed that the amphipathic moment of the labeling reagent, consisting of hydrophobic DIBO coupled to hydrophilic Alexa dye, results in strong partitioning of the DIBO group into the hydrocarbon core of the detergent micelle and consequently high local reactant concentrations. The observed rate constant for the micelle-enhanced SpAAC was comparable with the fastest bioorthogonal labeling reactions known. Finally, we utilized the azF-Rho labeled with Alexa488 to measure the kinetics of ligand uptake in a membrane-mimetic bicelle system. We found that the modification barely perturb the behavior of the receptor with respect to ligand binding.

2.2 Introduction

2.2.1 Approaches for labeling GPCRs with chemical probes

Biophysical and biochemical studies of GPCRs often rely on the attachment of appropriate probes to receptors. When designing such experiments, three interrelated issues need to be taken into consideration: what kind of probes should be introduced, which region of receptor should be modified with the probe, and how to anchor the probe to the site of interest. The ideal methodology should be general, *i.e.*, not dependent on the specific property of the receptor, minimally perturbs its intrinsic functionality, and allow for flexibility in choosing where to attach the label.

The choice of probe is dictated by the particular question being asked. The possible probes vary greatly in term of chemical property and span a wide range of molecular size, from fusion proteins, to small molecules, and to isotopic labels. Among various types of probes that have been successfully applied to GPCRs, fluorescence is a particularly powerful and versatile tool. Its high sensitivity allows experiments to be performed with limited amount of material. The temporal resolution of fluorescence measurement, combined with the spatial resolution of FRET, is ideally suited for probing the conformational changes and sequence of events in GPCR signaling.

Fluorescent proteins (Shaner et al., 2005) and organic dyes (Goncalves, 2009) have been the most popular choice for fluorescent probes. In the recent years, novel fluorescent reporters like quantum dots (Alivisatos et al., 2005) and rare earth ions (Selvin, 2002) have received increasing attention. Attaching different types of fluorescent probes to GPCRs require specialized methodologies. One possibility to visualize GPCR by fluorescence is to harness the specific interaction between receptor and ligand, or

between receptor and antibody. In these cases, the fluorescent labels are conjugated to the ligand or the antibody, and brought into proximity of the receptor by molecular recognition. However, this thesis is primarily concerned with the strategies for directly attaching a fluorescent probe to the receptor.

The structural hallmark of GPCRs is the seven transmembrane (TM) helices that are connected together with extracellular (EC) or intracellular (IC) loops. Prior to the disclosure of high-resolution structures, it has been learned that the N-terminus, C-terminus, and the loops of the heptahelical receptors may have the structural flexibility to accommodate major modifications, such as fusion with fluorescent proteins or luciferase (Kobilka et al., 1988; Barak et al., 1997; Tarasova et al., 1997; Angers et al., 2000; Gales et al., 2005; Bohme and Beck-Sickinger, 2009; Lohse et al., 2012). With the development of molecular cloning and recombinant protein technology, fluorescent protein fusion has evolved to a powerful tool for studying the behavior of GPCRs *in vivo*. Receptors tagged with a fusion protein were characterized for ligand binding, downstream signaling, and trafficking, and often found to maintain the wild-type behaviors (Gales et al., 2005). These constructs were widely used to assess the dimerization between receptors and the interaction between receptor and downstream signaling protein. However, alteration of the native behavior of receptors remains a concern, which requires careful case-by-case evaluation. Moreover, fluorescent proteins often suffer from a high probability of photobleaching and low quantum yield. By comparison, small-molecule fluorophores offers greater brightness and photostability, and cover a wider range of spectrum.

Further improvement has been pursued in two directions. The first strategy is aimed at reducing the length of polypeptide that needs to be inserted into the receptor.

For example, fluorescein arsenical hairpin binder (FlAsH/ReAsH) technology utilizes the coordination between sulfur and arsenic to chelate a biarsenical derivative of fluorescein to a tetracysteine peptide motif. FlAsH was paired with cyan fluorescent protein to monitor the conformational change in receptor activation. The reduced size of FlAsH greatly enhanced the FRET signal and sensitivity (Hoffmann et al., 2005; Hoffmann et al., 2010). Unlike FlAsH/ReAsH, chemoenzymatic labeling methods create covalent linkage, instead of coordination interaction, between short peptide/probe pair (Rashidian et al., 2013). Typically, enzymes catalyzing post-translational modification are re-purposed to add a probe or a reactive handle to a peptide sequence genetically encoded into the target protein. In the case of formylglycine generating enzyme (FGE) (Rush and Bertozzi, 2008) and sortase (Popp et al., 2007) the acceptor sequence can be as short as five residues. An important direction of chemoenzymatic labeling research is to alter the substrate specificity of these post-translational modification enzymes to incorporate unique functional groups that are bioorthogonal, *i.e.*, not naturally present in biomolecules, into the target protein. The Ting group has created biotin ligases that are capable of ketone, alkyne or azide analogues of biotin to a 15-mer acceptor peptide (Chen et al., 2005; Slavoff et al., 2008). The earliest report on chemoenzymatic labeling of a GPCR dates back to 1978, when the Stryer group used transglutaminase to inserted small-molecule fluorophores into the third intracellular loop of Rho (Pober et al., 1978). So far the applications of chemoenzymatic labeling to GPCRs have remained relatively rare. Nonetheless, the rapid expansion of chemoenzymatic labeling toolkit makes it a promising tool to the GPCR community.

The second strategy substituted the fluorescent or luminescent protein for self-labeling proteins, which, unlike the post-translational modification enzymes described above, catalyze the covalent modification of themselves rather than a different target protein. For instance, mammalian O-6-methylguanine-DNA methyltransferase has been engineered to accept benzylguanine derivatives as substrate (Keppler et al., 2003; Keppler et al., 2004). This approach, known as SNAP/CLIP-tag, has expanded the repertoire of fluorescent reporters to include organic dyes (Maurel et al., 2008) and rare earth metal ions (Emami-Nemini et al., 2013). The second member in the category of self-labeling proteins is Halo-tag, a modified haloalkane dehalogenase (Los et al., 2008). In a recent report, cAMP receptor carrying Halo-tag was labeled with tetramethylrhodamine and imaged for single-particle tracking in live cells (Snaar-Jagalska et al., 2013). Compared with fluorescent proteins, self-labeling proteins combine the advantage of fusion protein tag and covalent labeling and promise a greater freedom in choosing fluorescent reporters with desired photophysical properties (Gronemeyer et al., 2005).

The approach of fusion protein, despite numerous successful demonstrations, is inherently limited by the shear size of protein tag. Bulky fusion proteins often prove inadequate when subtle conformational changes, particularly those in the transmembrane region of GPCRs, are being studied. In addition, the EC surfaces of GPCRs can be critical for receptor-ligand binding, and the IC surface for receptor-G protein interaction. Hence for certain applications it is desirable to leave the EC and IC surface intact. Therefore, approaches that enable attachment of a probe to a single residue has a decisive

advantage over the methodologies described above for investigating the structure-function relationship of GPCRs.

Covalent labeling of protein residues has been extensively studied (Glazer, 1970; Sletten and Bertozzi, 2009). Classic methods rely on bioconjugation chemistries targeting the reactive groups of the amino acid residues, such as the primarily amine of lysine, the thiol group of cysteine, the side chain of tyrosine and tryptophan, and the N-terminal amino group (Glazer, 1970). Apparently, except for the N-terminal amino group, none of these reactive residues is likely to occur for once in the protein. While the reactivities of the same residue in one protein can be differently modulated by sterical factors or pH, and some selectivity can be achieved by judicious choice of reaction conditions, the optimization process can be laborious. Unlike globular proteins, GPCRs are hydrophobic membrane proteins, expressed at low level, and often unstable without bound ligands. Therefore, the reactions for labeling GPCRs are expected to proceed under mild conditions, exhibit good kinetics, yield stochiometrically-labeled product without chromatographic purification, and minimally depend on solvent accessibility. Meanwhile, removal of the naturally occurring reactive residues by site-directed mutagenesis may result in functional alteration.

Among these classic protein labeling chemistries, maleimide and methane thiosulfonate chemistries targeting cysteine thiol groups have been a popular choice, because cysteines is one of the rarest amino acids in the composition of proteins, and the number of reactive cysteines can be further reduced by the formation of disulfide bond. Not surprisingly, tremendous efforts have been made to understand the cysteine chemistry for prototypical GPCRs like Rho (Rousselet and Devaux, 1978; Chen and

Hubbell, 1978; Resek et al., 1993; Yang et al., 1996) and β_2-adrenergic receptor (Gether et al., 1997) to achieve site-specific labeling of the receptors. These studies yielded important insights into the structure-function relationship of GPCRs. The FRET experiment in the Stryer group in 1972 with Rho (Wu and Stryer, 1972) provided early insights into the physical dimension of this molecule. It is worth noting that this study was among the first demonstrations how FRET could be applied as a molecular ruler for macromolecules (Stryer, 1978). Site-directed spin labeling of the cytoplasmic end of Rho in 1990s revealed the rigid-body helix movement in receptor activation, a feature subsequently confirmed by crystal structures (Farrens et al., 1996; Altenbach et al., 1996). Later, spin labeling of the TM helices of Rho enabled high-resolution distance mapping of the helix movement of Rho (Hubbell et al., 2003; Altenbach et al., 2008b). Fluorescence spectroscopy involving conformational-sensitive probes have been exploited to probe the activation of Rho (Farrens and Khorana, 1995; Dunham and Farrens, 1999), as well as the ligand-specific conformation (Ghanouni et al., 2001; Yao et al., 2006) and oligomerization (Mathiasen et al., 2014) of β_2-adrenergic receptor.

However, as all GPCRs possess multiple cysteines, generating the cysteine-free background and validating the functional integrity of the mutant receptor remain a cumbersome process (Resek et al., 1993; Yang et al., 1996; Gether et al., 1997). The long histories of the research on Rho and β_2-adrenergic receptor have produced sufficient experience for manipulating these two prototypical GPCRs and characterizing the functionality of their cysteine-free mutants, a legacy not necessarily available to researchers working on an expanding list of therapeutically interesting receptors.

Moreover, reactive cysteines exist in abundance in cells, thereby limiting the applicability of sulfhydryl chemistries practically to purified receptors.

2.2.2 Unnatural amino acid (uaa) mutagenesis of GPCR

To develop a general approach for site-specific labeling of GPCRs, we have opted for an alternate strategy to introduce bioorthogonal functionalities into receptors using unnatural amino acid (uaa) mutagenesis (Davis and Chin, 2012; Huber and Sakmar, 2014).

Incorporating uaas into protein was realized in 1989, by combining non-sense suppression and chemically acylated suppressor tRNA in an *in vitro* translation system (Noren et al., 1989). This method was used to generate uaa-containing soluble globular proteins, such as *β*-lactamase (Noren et al., 1989), T4 lysozyme (Mendel et al., 1991), staphylococcal nuclease (Judice et al., 1993), and Cytochrome P450 (Kimata et al., 1995). Owing to the difficulty in delivering chemically acylated suppressor tRNA into cells, *in vivo* suppression was possible only for giant cells (*e.g.* Xenopus oocytes) (Nowak et al., 1995). However, synthesis of functional membrane proteins requires the coordinated actions of multiple organelles to fold the polypeptide, add post-translational modifications, and transport them to the correct membranes. Such conditions can be very difficult to reconstitute *in vitro*.

An ingenious solution to this problem was reported in 2001, when Wang *et al* presented a general methodology for *in vivo* non-sense suppression by engineering an archaebacterial tyrosyl tRNA/synthetase pair that is orthogonal to the endogenous tRNA/synthetase pairs of *E. coli* and yet effectively utilized by the ribosome (Wang et al., 2001). In 2002, a new pair of mutant *E. coli* Tyr-tRNA synthetase and *B.*

stearothermophilus suppressor $tRNA^{Tyr}$ was generated to enable non-sense suppression in mammalian cells (Sakamoto et al., 2002). Further genetic screening for *E. coli* Tyr-RS variants in the yeast system expanded the range of uaas that can be incorporated into protein with high specificity (Deiters et al., 2003; Chin et al., 2003a; Chin et al., 2003b).

Based on these discoveries, our laboratory pioneered in incorporating uaas into mammalian GPCRs. The first successful example of incorporating a uaa into GPCR was done in the yeast system (Huang et al., 2008), which is of limited use to the majority of GPCRs. We has greatly improved the suppression efficiency of amber codon suppression in mammalian cell culture by creating a novel chimera of *H. sapiens* and *B. stearothermophilus* $tRNA^{Tyr}$ that forms an orthogonal pair with the existing *E. coli* Tyr-RS in the human HEK293T cell line. As most GPCRs cannot be expressed in bacterial culture, and even in mammalian cell cultures their expression levels are generally low, uaa mutagenesis would not have become a practical approach for studying GPCRs without achieving reasonable suppression efficiency.

We have adapted this orthogonal pair of suppressor tRNA and tRNA synthetase to incorporate analogues of phenylalanine, namely *p*-acetyl-L-Phe (AcF), *p*-azido-L-Phe (azF), and *p*-benzoyl-L-Phe (BzF), into GPCRs heterologously expressed in transiently transfected cells (Ye et al., 2008; Ye et al., 2009). In this way we are able to incorporate several bioorthogonal functionalities, namely the keto group in AcF, the azido group in azF, and the benzophenone group in BzF, into various GPCRs (Figure 2-1). We found that these uaas can be specifically inserted into the intracellular, extracellular, and transmembrane region of GPCRs, as long as the original residues are not structurally or functionally critical.

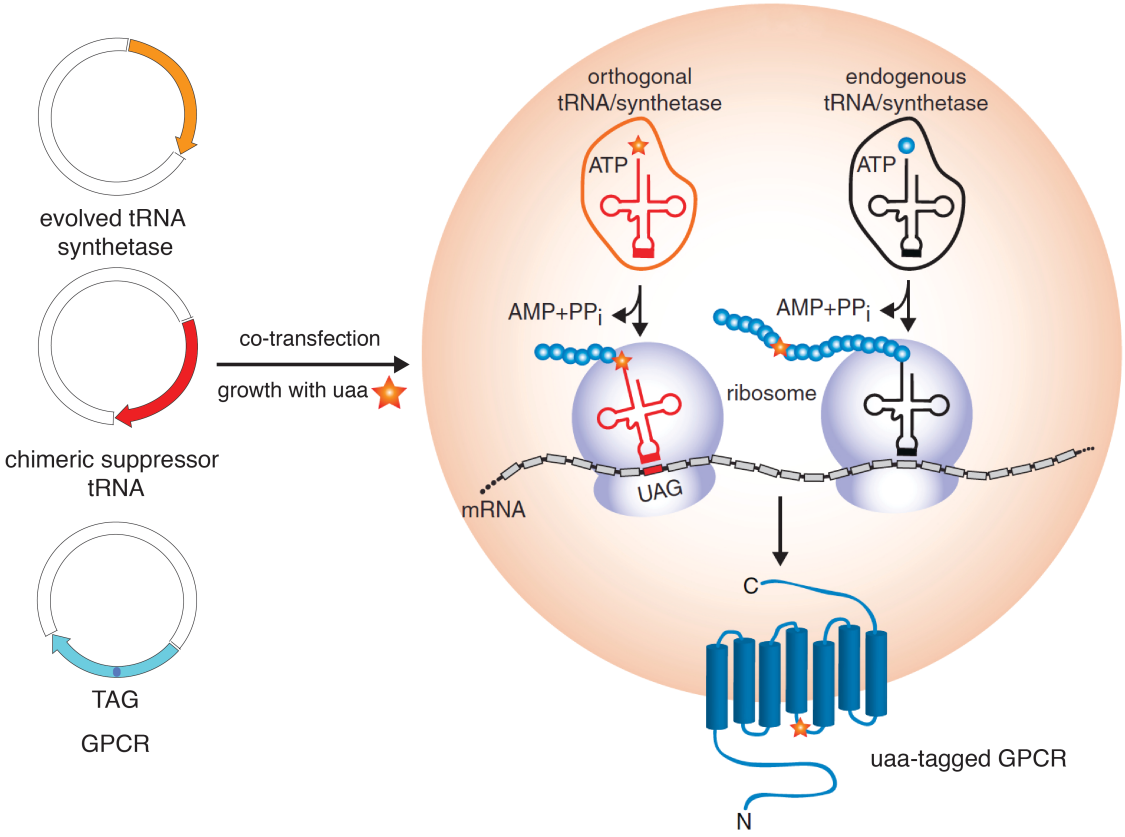

Figure 2-1. Incorporation of unnatural amino acids (uaas) into GPCRs by amber codon suppression. HEK293T or HEK293F cells are co-transfected with three different plasmids encoding the evolved aminoacyl synthetase gene, the chimeric suppressor tRNA gene, and the GPCR gene with an in-frame amber (TAG) mutation at a specific position. The transfected cells are cultured in the presence of the uaa corresponding to the tRNA synthetase. The bacterial orthogonal tRNA/synthetase pair is orthogonal to the endogenous mammalian tRNAs and synthetases, thereby preventing incorrect translation of the codons for natural amino acids. The ribosome is capable of utilizing the suppressor tRNA charged with the uaas to suppress the normal function of amber stop codon, resulting in a full-length receptor tagged with a uaa at the desired position (figure adapted from Daggett and Sakmar, 2011).

We further developed several applications based on the individual spectroscopical or chemical reactivity of these uaas. The azido group in azF exhibits a vibrational signature distinct from that of the native residues in the infrared spectrum and thus serves as a probe for the local electrostatic environment. The engineered azF-Rho enabled us to track the conformational changes involved in Rho activation (Ye et al., 2010; Ye et al., 2009). BzF and azF are also photoactivatable crosslinkers, and were used to map the ligand binding modes for the chemokine receptors CCR5 and CXCR4 (Grunbeck et al., 2011; Grunbeck et al., 2012), the substance P receptor NK1 in native cell membrane (Valentin-Hansen et al., 2014), as well as the binding sites of the chemokine receptors with conformation-sensitive monoclonal antibody (Ray-Saha et al., 2014). This targeted photocrosslinking approach using genetically encoded uaas bypassed the need of adding photoactivatable groups to ligands, which may alter the binding mode, particularly in the case of small-molecule ligands (Grunbeck and Sakmar, 2013). Unnatural amino acid mutagenesis has also been successfully applied to ligand-gated channels (Zhong et al., 1998), voltage-gated ion channels (Dougherty, 2000; Pless et al., 2011), and ionotropic glutamate receptors (Klippenstein et al., 2014) to probe ligand-receptor interaction and protein conformational changes (Pless and Ahern, 2013).

2.2.3 Site-specific fluorescent labeling of GPCRs

Here we present a detailed study on site-specific fluorescent labeling of functional GPCRs by combining uaa mutagenesis and bioorthogonal labeling chemistry (Figure 2-2). Previous applications of similar approaches for protein labeling mostly involved highly expressing, soluble proteins, such as superoxide dismutase (Deiters et al., 2004), T4 lysozyme (Brustad et al., 2008), myoglobin (Nguyen et al., 2011), maltose-binding

protein (Seo et al., 2011; Seo et al., 2014), GFP (Plass et al., 2011; Reddington et al., 2012; Borrmann et al., 2012), calmodulin (Wang et al., 2014), etc. By comparison, GPCRs are low-expressing, hydrophobic membrane proteins that are easily denatured under the conventional protein labeling conditions. Hence, bioorthogonal labeling of GPCRs requires careful optimization based on their specific properties.

We chose Rho, a prototypical class A GPCR, as the model system to study the labeling chemistry. We have previously demonstrated incorporation of AcF and azF into various sites of Rho (Ye et al., 2010; Ye et al., 2008; Ye et al., 2009). Ketones and azides are both bioorthogonal reactive handles, for which a wealth of bioconjugation chemistries has been accumulated. However, we have observed non-specific labeling of wt rhodopsin by chemistries targeting ketone. Therefore, the first issue addressed in this chapter is the bioorthogonality of the two labeling strategies, one targeting the keto group in AcF and the other targeting the azido group in azF. We showed that azF is a superior bioorthogonal reactive handle compared with AcF. We also found that chemistries with azF generally exhibit greater kinetics. Based on these findings, we concluded that strain-promoted [3+2] azide–alkyne cycloaddition (SpAAC) reaction of dibenzocyclooctyne (DIBO) with azF is a suitable choice for labeling GPCRs.

The second question is whether this labeling strategy is general. We tested multiple sites located in the EC, IC and TM region of Rho with different DIBO derivatives, and found the reaction to be robust and modular. While characterizing the kinetics of SpAAC between DIBO and azF-rhodopsin, we found the reaction to be much faster than the SpAAC involving two small molecules. Hence the third task we have accomplished here is to explain the observed rate enhancement by a model based on the partitioning of

DIBO derivatives into micelles. This finding added new insights into the practical application of bioorthogonal labeling to GPCRs. Finally, we evaluated the functional integrity of labeled Rho with a steady-state fluorescence-quenching assay. We showed that attaching to a fluorophore to the fourth helix of Rho does not significantly perturb the behavior of receptor with respect to ligand binding.

2.3 Results

2.3.1 The bioorthogonality of keto group and azido group as labeling handles

We conducted a comparative study for the labeling chemistries utilizing the two reactive handles incorporated into GPCRs through amber codon suppression. We chose oxime ligation to biotinylate AcF-tagged Rho (Figure 2-3A), and the strain-promoted [3+2] azide–alkyne cycloaddition (SpAAC) for azF-tagged Rho (Figure 2-3B), respectively.

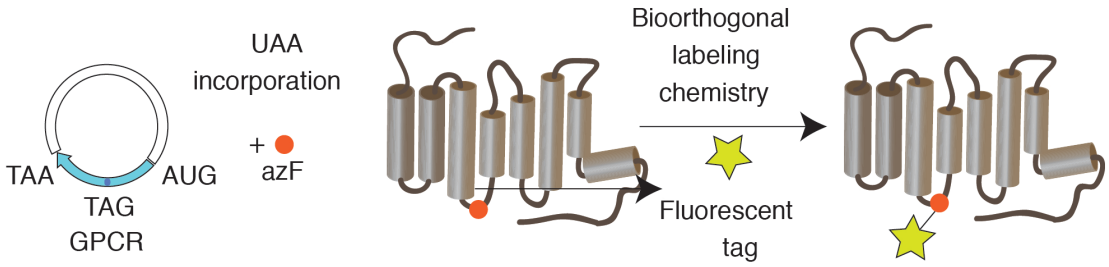

Figure 2-2. Bioorthogonal labeling of uaa-tagged GPCRs. The uaa-tagged mutant GPCR was heterologously expressed in mammalian cell culture. A fluorescent tag is conjugated to the uaa through a bioorthogonal labeling chemistry.

We chose S144 located at the second IC loop of Rho as the target site for studying the reaction kinetics. This site has good uaa incorporation efficiency and reactivity towards labeling reagents. S144azF Rho was solubilized in *n*-dodecyl-*β*-D-maltoside (DM) micelles, captured to an immunoaffinity matrix (1D4 mAb-sepharose 2B) via its C-terminal epitope, and reacted with labeling reagents reagent. The 1D4 mAb is specific to the C-terminal epitope of Rho (Molday and Mackenzie, 1983). The excess unbound reagents were washed away before the labeled receptor was specifically eluted. (Figure 2-3C) The reaction of azF with DIBO-biotin was performed at pH 7.2. The reaction of AcF

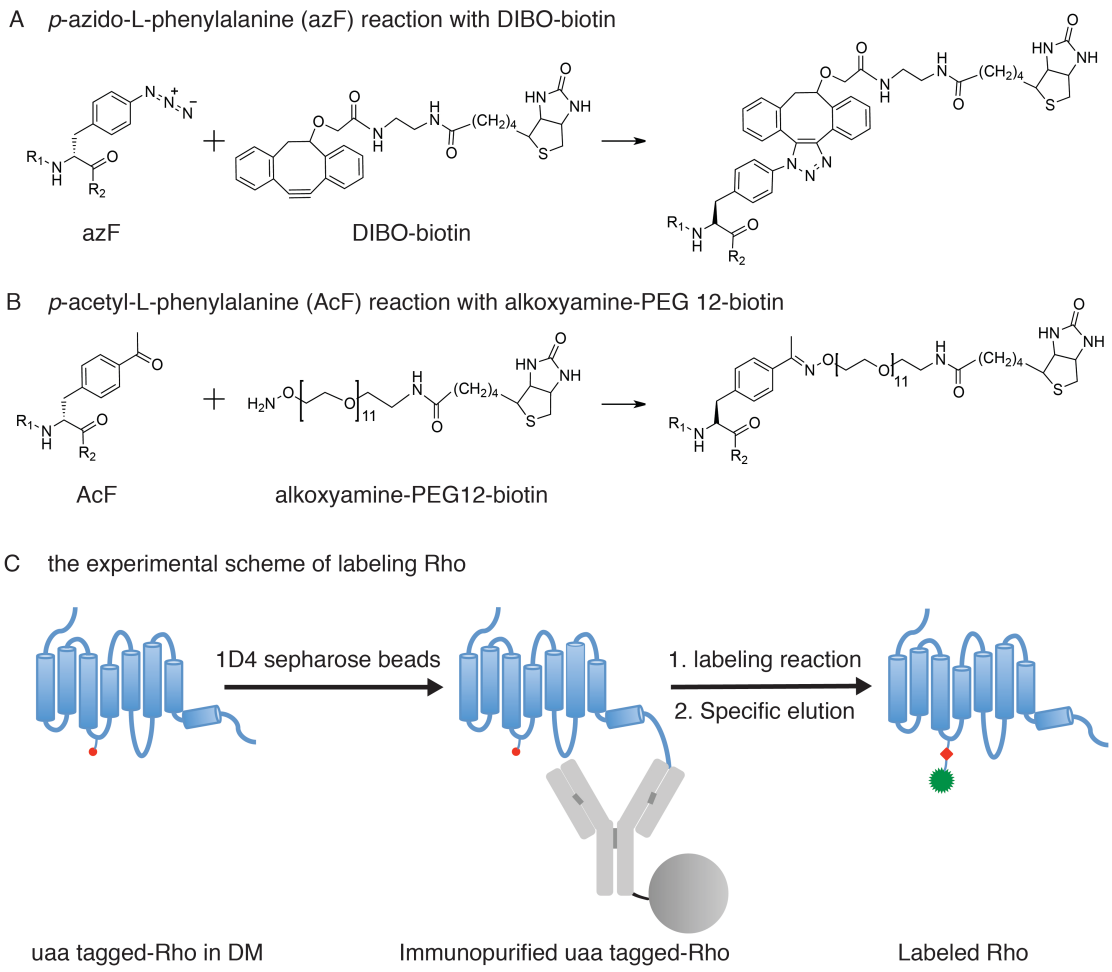

Figure 2-3. Bioorthogonal reaction for labeling the azido group and the keto group in GPCRs. A) The strain-promoted [3+2] azide-alkyne cycloaddition (SpAAC) between *p*-azido-L-phenylalanine (azF) and dibenzocyclooctyne-biotin (DIBO-biotin). **B)** The oxime ligation between *p*-acetyl-L-phenylalanine (AcF) and alkoxyamine-PEG12-biotin. **C)** The experimental scheme for labeling uaa-tagged rhodopsin (Rho). The heterologously expressed Rho was solubilized in *n*-dodecyl-*β*-D-maltoside (DM) and immunopurified with the C-terminal specific 1D4 antibody. The receptor bound to the resin was subjected to the labeling reaction. After the excess labeling reagent was washed away, the labeled Rho was specifically eluted from the resin.

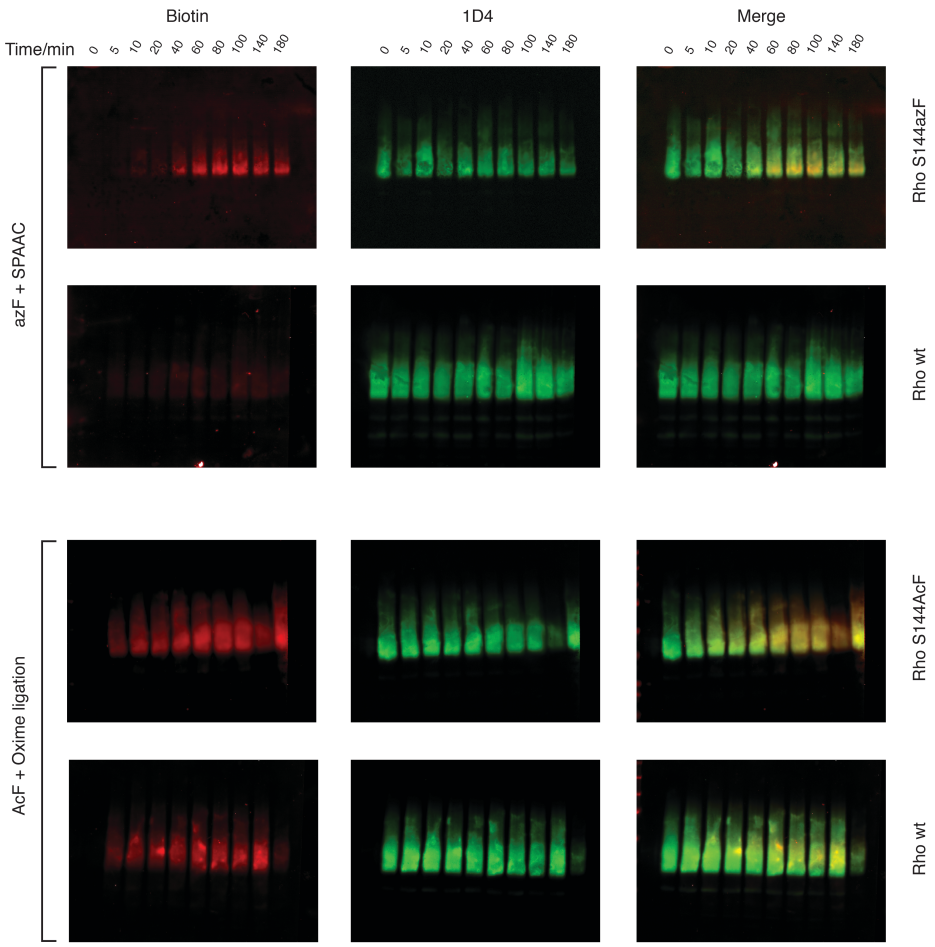

Figure 2-4. Kinetic study of labeling chemistries for azF-tagged Rho and AcF-tagged Rho. Upper panel: Rho S144azF and Rho wt reacted with 50 μM DIBO-biotin. Lower panel: Rho S144AcF and wt Rho reacted with 10 mM alkoxyamine-PEG12-biotin. Red: 700-nm channel for streptavidin IRDye 680RD (biotinylation signal). Green: 800-nm channel for IRDye800CW goat anti-mouse secondary antibody (1D4 signal). Yellow: 700-nm and 800-nm channel merged together. In order to clearly visualize any possible background labeling for Rho wt, higher detector sensitivity for the 700-nm channel was chosen during image acquisition.

with alkoxyamine-PEG12-biotin was performed under a more acidic condition of pH 6.0, as a balance between reaction rate and maintenance of the protein integrity. We performed kinetic studies for the two model reactions. The time-series samples were analyzed by dual-color IR-based quantitative Western blot. The possibility of two-channel detection eliminates the need of performing extra loading controls (Figure 2-4)

We found that the combination of SpAAC and azF exhibited reaction kinetics that was faster by two orders of magnitude (Table 2-1), and also displayed higher specificity (Figure 2-5). The combination of oxime ligation and AcF resulted in substantial background labeling for wt Rho (~0.1, Figure 2-5B). Interestingly, the rate of the non-specific reaction was faster than that of the specific reaction and complete within half an hour. The receptor was photobleached prior to SDS-PAGE separation and did not contain a covalently-bound retinal. Thus the aldehyde group of retinal can be ruled out as the cause of background labeling.

Table 2-1. The reaction kinetics of the bioorthogonal chemistries

	Second-order rate constant ($M^{-1} s^{-1}$)		
Labeling reagent	Biotin-DIBO	Biotin-alkoxyamine	
Rho substrate	S144azF	S144AcF (specific)	WT (non-specific)
Measurement 1	9.6 ± 1.5	0.026 ± 0. 005	0.044 ± 0. 009
Measurement 2	7.6 ± 1.1	0.028 ± 0.007	0.22 ± 0.05
Average	8.6 ± 1.3	0.027 ± 0.006	0.13 ± 0.04

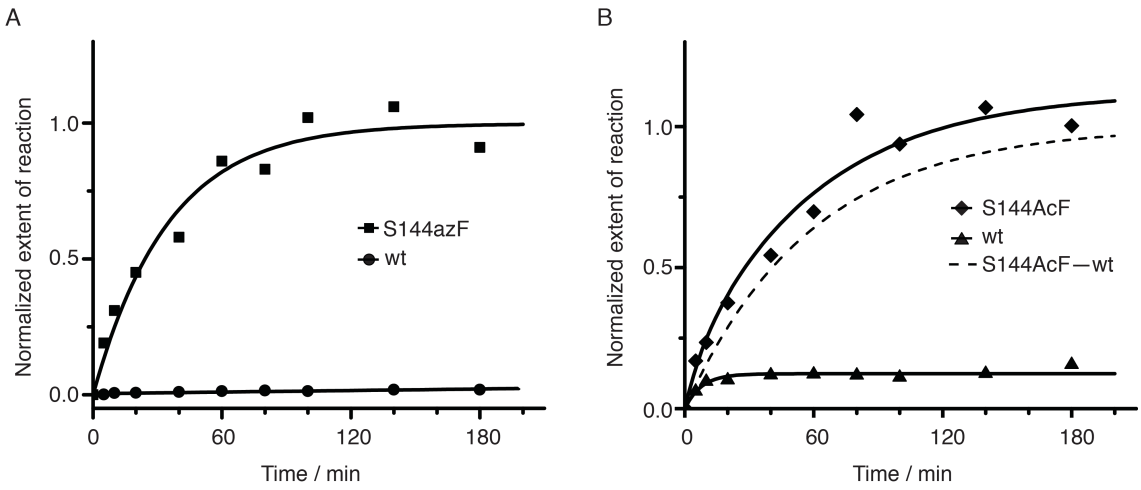

Figure 2-5. **Comparison of labeling chemistries for azF- and AcF-Rho.** The time-series samples were analyzed using dual-color quantitative Western blot. As the labeling reagents have different linker lengths and detectabilities, the Western blot signals from two chemistries cannot be directly compared. Therefore, to simplify the interpretation of data, the extent of labeling (ξ) was normalized under the assumption that ξ for the specific component for each labeling chemistry, upon the completion of reaction, is assigned to 1.0. **A)** The kinetic study for the azF-Rho and wt Rho reacted with 50 μM DIBO-biotin. The background labeling for wt Rho was negligible. The second-order reaction rate (k_2) for Rho S144azF with DIBO-biotin is 8.6 ± 1.3 M^{-1} s^{-1}. **B)** Kinetic study for the AcF-Rho and wt Rho reacted with 10 mM alkoxyamine-PEG12-biotin. The specific k_2 for Rho S144AcF with alkoxyamine-PEG12-biotin is 0.027 ± 0.006 M^{-1} s^{-1}, two orders of magnitude lower than that of azF with DIBO-biotin. There was a substantial non-specific component for this reaction, based on the background labeling of wt Rho. The non-specific k_2 for wt Rho with alkoxyamine-PEG12-biotin is 0.13 ± 0.04 M^{-1} s^{-1}.

After testing different choices of uaas and bioorthogonal chemistries, we concluded that the combination of azF and DIBO is a suitable strategy to label GPCRs, as it exhibits higher specificity and faster kinetics.

2.3.2 Choice of site for fluorescent labeling

The structural hallmark of GPCRs is their seven TM helix bundle connected with three EC loops and three intracellular IC loops. We chose an EC site Y102 that has been shown to be amenable for covalent modification (Ye et al., 2008). On the cytoplasmic surface, we chose C140 located at the end of TM3, S144 in the second IC loop, and A234 in the third IC loop, and A246 at the end of TM6. For the transmembrane region, we selected TM4, which is positioned distal to the main helix bundle and it is generally not involved in the helix rotation required for GPCR activation (Farrens et al., 1996; Park et al., 2008; Scheerer et al., 2008; Rasmussen et al., 2011b). Compared with all other TMs, the residues of TM4 are least likely to contribute to the ligand binding pocket (Venkatakrishnan et al., 2013). Thus, we reasoned that modification of residues in TM4 would have minimal effects on the intrinsic functionality of the receptor (Figure 2-6). We generated amber stop codon at every turn of TM4 (N151, M155, A158, V162, L165, A169, V173). These residues were chosen because their side chains point outward from the helix bundle (Figure 2-7). We avoided mutating the residues involved in the conserved non-covalent contact between TM3 and TM4 (in the case of Rho they correspond to W161, A164, A168) (Venkatakrishnan et al., 2013). Except for L165amb (not shown), all the constructs yielded expression of full-length receptor containing azF (Figure 2-8). While the TM region of Rho in DM micelles is expected to be shielded by the alkyl chain of DM. The variation of the local environment on protein surface allows us to systematically assess the behavior of SpAAC for labeling a transmembrane protein.

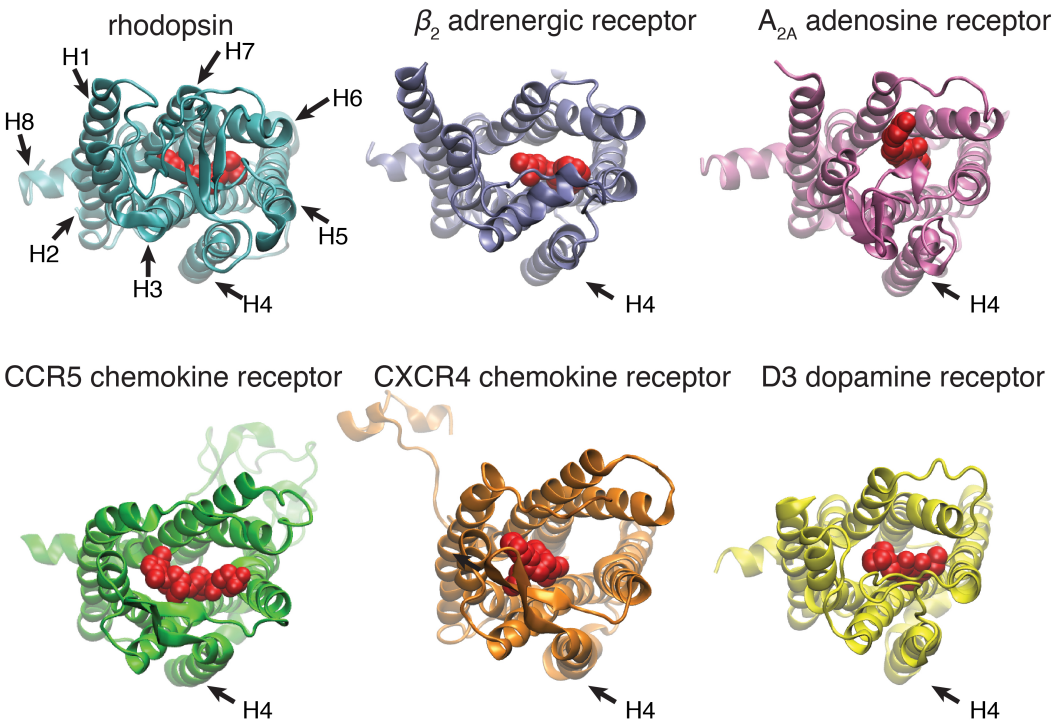

Figure 2-6. **Comparison of the crystal structures of different Class A GPCRs with bound ligands:** 1) Rho and 11-*cis*-retinal (protein data base access code 1GZM) (Li et al., 2004); 2) β_2 adrenergic receptor and carazolol (2RH1) (Cherezov et al., 2007); 3)A_{2A} adenosine receptor and ZM241385 (3EML) (Jaakola et al., 2008); 4) CCR5 chemokine receptor and maraviroc (4MBS) (Tan et al., 2013); 5) CXCR4 chemokine receptor and IT1t (3ODU) (Wu et al., 2010); 6) D3 dopamine receptor and eticlopride (3PBL) (Chien et al., 2010). Viewed from the EC side, with the ligands shown in *red*. The TM4 of these receptors (indicated by an arrow) are positioned outside the helix bundle and not in contact with the ligands.

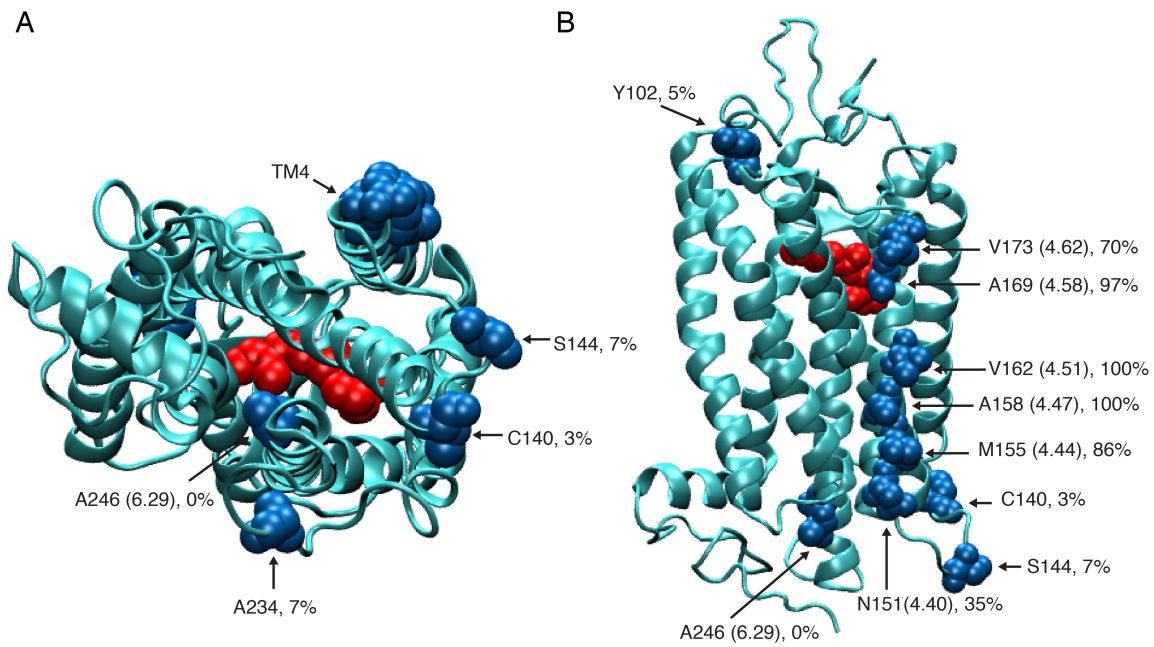

Figure 2-7. Structure of bovine Rho with 11-*cis*-retinal and the tested amino acid residues (PDB: 1U19. *red:* 11-*cis*-retinal; *blue*: TM4 sites). **A)** Cytoplasmic view. **B)** Side view. For the TM sites, the Ballesteros-Weinstein notation is shown in parentheses (Ballesteros and Weinstein, 1995). The hydrophobicity of the local environment at these sites is estimated by the percent of lipid contacts versus water contacts. The values give the fraction of the surface exposure of these residues to lipids as observed in molecular dynamics simulations of Rho in a phospholipid bilayer membrane (Huber et al., 2004).

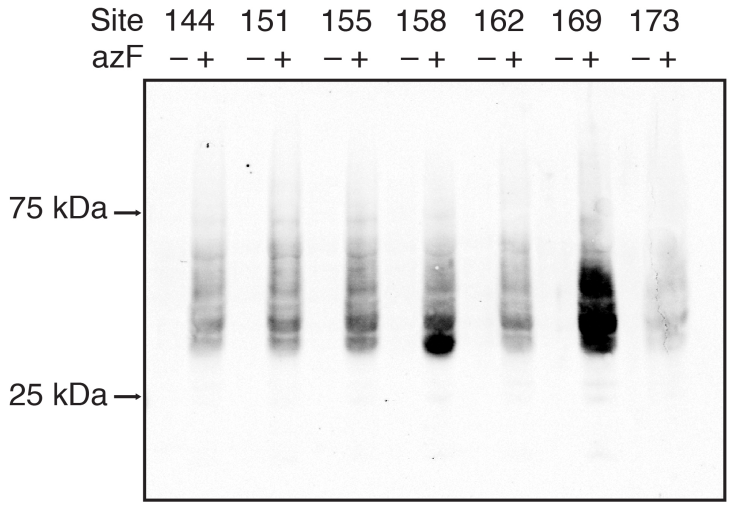

Figure 2-8. The heterologous expression of Rho with single azF substitution at the indicated positions. HEK293F cells were transfected with three plasmids encoding the suppressor tRNA, the aminoacyl tRNA synthetase, and Rho with an amber mutation. The cell lysates were analyzed by Western blot (100 μg total protein per lane). The receptor was probed with 1D4 mAb specific to the C-terminus of Rho, followed by goat-anti-mouse 800 CW (LI-COR). The full-length receptor was detected only when the expression medium was supplemented with azF, indicating specific incorporation of azF into Rho.

2.3.3 Fluorescent labeling of Rho with Alexa488-DIBO at different sites

We utilize DIBO derivatives of Alexa fluors to generate fluorescently labeled Rho by SpAAC (Figure 2-9).

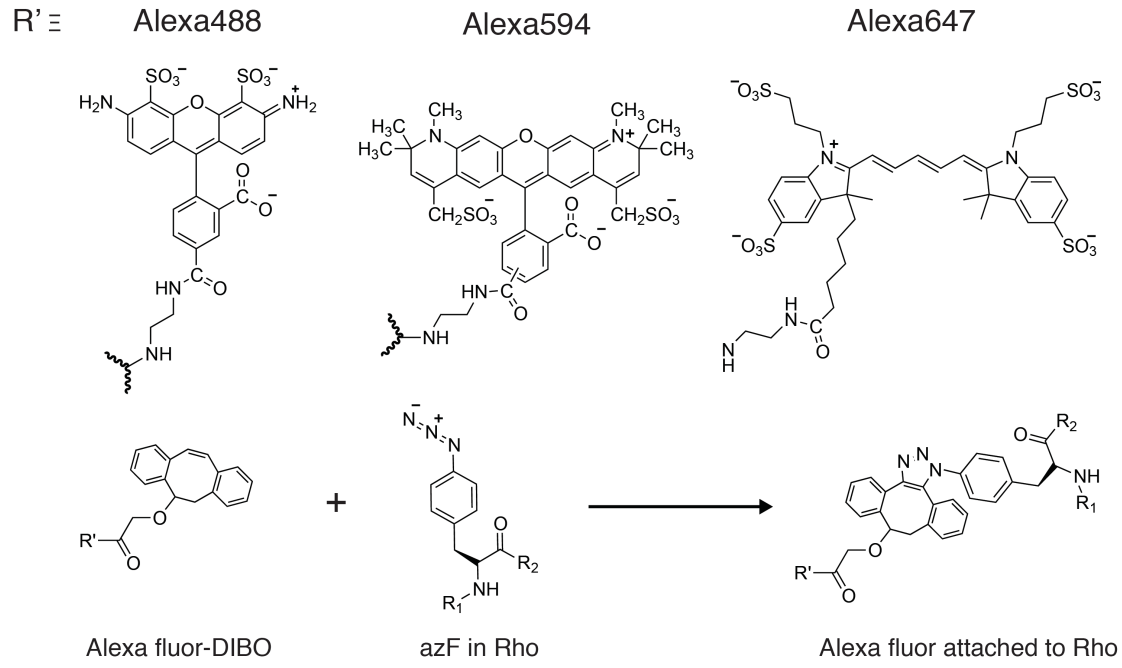

Figure 2-9. The SpAAC reaction Alexa488-DIBOs and azF. Alexa555-DIBO was also used in the present study. However, its chemical structure has not been disclosed by the manufacturer.

Figure 2-10 shows the results obtained for a typical reaction of azF-Rho samples treated for 18 h with 50 μM Alexa488-DIBO at 25ºC. The in-gel fluorescence shows a prominent fluorescent band for all the azF-Rho variants, whereas the wt sample does not show a fluorescent band above background level. Among all the azF-Rho variants, the signal from Y102-Alexa488 Rho was weaker compared with all other variants. Due to glycosylation and oligomerization, Rho appeared as a smear in the SDS-PAGE gel. To confirm the purity of the sample, we treated the purified S144-Alexa488 Rho with PNGaseF to remove the glycans. We found no other fluorescently labeled protein was

present in the sample, except for Rho visualized as monomer, dimer and trimer in the gel. The robust labeling of the TM region is particularly interesting, because the hydrophobic alkyl chain of DM might be expected to shield the TM region of Rho in DM micelles.

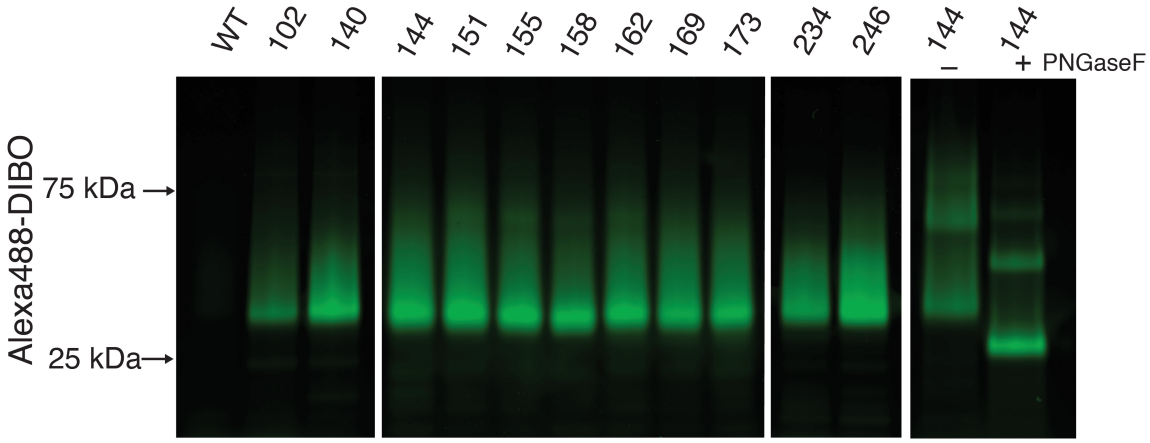

Figure 2-10. Fluorescent labeling of azF-Rho with Alexa488-DIBO. After labeling reactions, samples were separated by 4–12% SDS-PAGE and the gel image was taken with a confocal 488-nm laser fluorescence scanner using an emission filter set optimized for Alexa488 detection. Strong fluorescent bands were observed for the all the mutants, whereas that for Y102azF was significantly weaker. No band was observed for wt Rho treated under the same condition.

Rho utilizes a chromophore 11-*cis*-retinal as its native ligand (Figure 2-11). Dark-state Rho exhibits a characteristic absorption band centered at 500 nm. After photobleaching in the presence of NH_2OH, 11-*cis*-retinal isomerizes to all-*trans*-retinal and dissociates from the binding pocket. In the resulting spectrum, the 500-nm band of Rho shifts to 370 nm, revealing the absorption peak of the fluorophore. Thus the concentrations of 11-*cis*-retinal-bound Rho and fluorophore can be quantified from their respective absorption peaks. In the representative spectra, the labeling ratio for S144azF-

Rho was 1.13, while that of wt Rho is only 0.04 (Figure 2-11), demonstrating that this reaction was specific with azF-Rho.

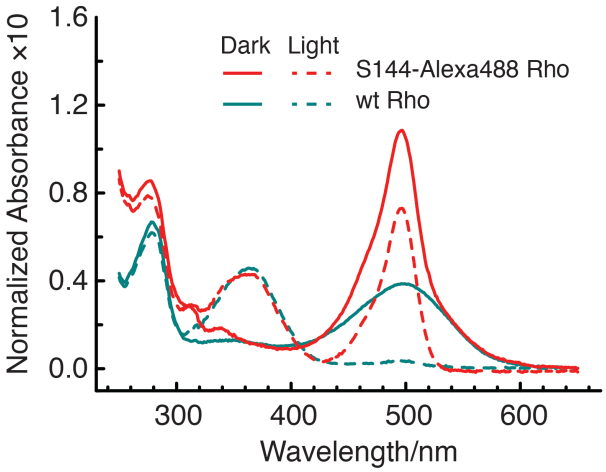

Figure 2-11. UV-Vis spectra of wt and S144azF Rho treated with Alexa488-DIBO. The dark state (dark) and illuminated (light) spectra are normalized to the amount of Rho using the 380-nm absorbance of the illuminated sample (light). Comparison of the absorbance at 495 nm illustrates the small amount of Alexa488 present in the purified wt sample mainly due to co-purification and to a lesser extent due to background labeling.

We quantified the labeling stoichiometries for Alexa488-labeled azF-Rho variants by UV-Vis spectroscopy (Figure 2-12). Except for Y102azF Rho, which was clearly under labeled with a labeling stoichiometry of 0.56, all the azF-Rho variants exhibited a dye/protein ratio above 1.0, ranging from 1.05 for A234azF Rho to 1.68 for V173azF-Rho (Figure 2-12). The super-stoichiometry possibly resulted from a fraction of receptors that did not regenerate with 11-*cis*-retinal.

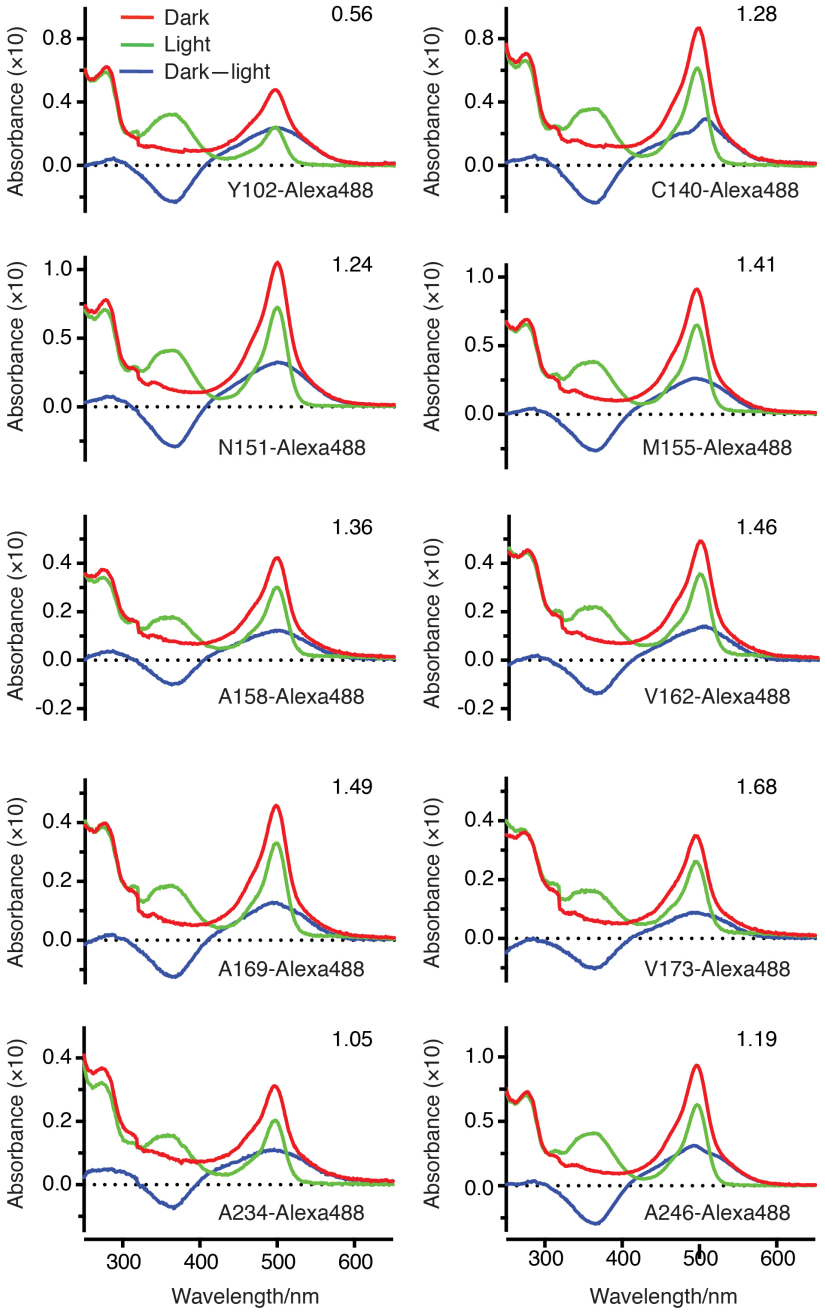

Figure 2-12. **The UV-Vis spectra of azF-Rho variants with Alexa488 attached to different sites.** *Red*: dark-state Rho; *green*: photobleached Rho; *blue*: the difference spectrum (dark–light). The dark−light difference spectrum at 500 nm was used to calculate the concentration of Rho (c_{Rho}) using an extinction coefficient of 40,600 M^{-1} cm^{-1}. The Alexa488 concentration (c_{Alexa488}) was calculated from 495-nm absorbance in the light spectrum using the extinction coefficient 73,000 M^{-1} cm^{-1}. The label-to-protein ratio was calculated as $c_{\mathrm{Alexa488}}/c_{\mathrm{Rho}}$ and indicated in the upper right corner.

To enhance the yield of functional receptors, we followed a purification procedure shown to reduce impurities from partially folded receptors (Ridge et al., 1995; Reeves et al., 1999). Alternatively, it is possible that the extinction coefficient of Alexa488 varies with the chemical environment of a particular labeling position. A detailed analysis of this issue is beyond the scope of this paper, but we are confident that this observation is not the result of background reactivity of DIBO with sites other than azF, since the labeling ratio for wt Rho is only 0.04 (*cf.* Figure 2-10).

2.3.4 Optimizing the concentration of Alexa488-DIBO for labeling Rho

We performed the labeling reaction with S144azF-Rho under different concentrations of Alexa488-DIBO and analyzed the labeled products by in-gel fluorescence and UV-Vis spectroscopy. Figure 2-13A shows the in-gel fluorescence of Rho reacted with 50, 20, 10 and 5 μM of Alexa488-DIBO (approximately 100 to10-fold molar excess of the receptor. Panel B shows the dark state (Dark), photobleached (Light), and the difference (Dark–Light) spectra of these samples. The corresponding apparent labeling stoichiometries are 1.84, 1.15, 1.14, and 1.13, respectively. We speculated two possible reasons for the unexpectedly high stoichiometry of S144azF Rho labeled with 50 μM Alexa488-DIBO in this particular reaction. First, a higher concentration of Alexa488-DIBO might be more difficult to wash away, resulting in an increase of co-purified free dyes in the elution. Second, the estimate for the amount of Rho used in this particular reaction might be low. Consequently, the relative percentage of unbound dyes would be higher compared to other samples. The control experiment with wt Rho also disfavors the possibility of a high degree of non-specificity. In the reactions where the concentrations of Alexa488-DIBO were reduced to 20, 10 and 5 μM and there was more

Rho to start with, the resulting stoichiometries are consistent and close to the expected value 1.0. The in-gel fluorescence data also support our hypothesis: the receptor bands exhibit similar intensities, while the 50-μM reaction gives a much more pronounced band for the unbound dye (in order to normalize the amount of receptor, a larger volume of 50-μM sample was loaded to the SDS-PAGE gel.) Taken together, the data suggest that the super-stoichiometry observed from the spectra is likely to represent the presence of unbound Alexa488, rather than promiscuous labeling. We recommend keeping the DIBO reagent at 10-fold molar excess.

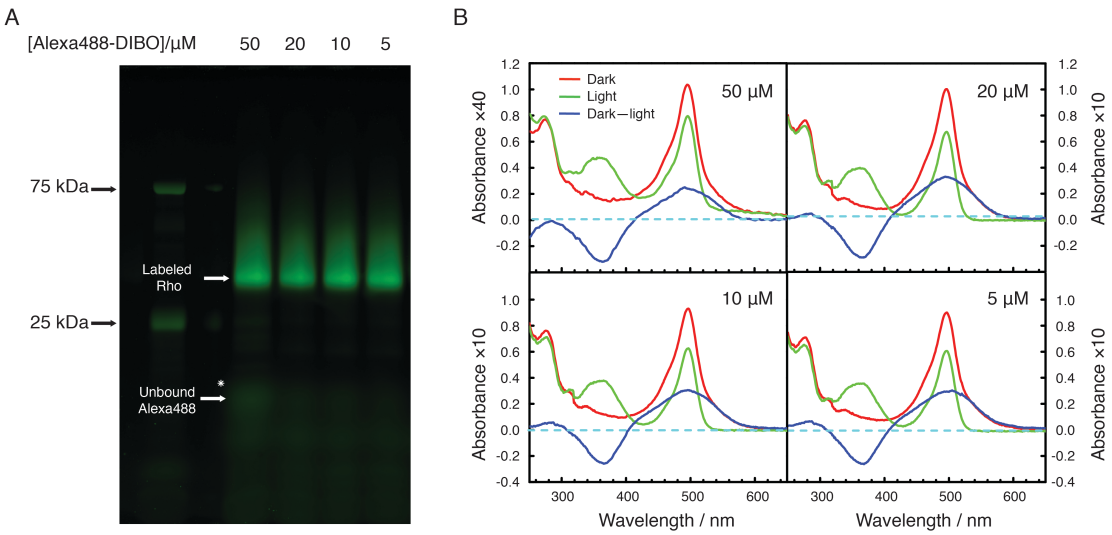

Figure 2-13. Labeling of Rho at position S144 with various concentration of Alexa488-DIBO. A) The in-gel fluorescence and **B)** UV–Vis spectra of Rho reacted with 50, 20, 10 and 5 μM of Alexa488-DIBO. For the in-gel fluorescence assay, 50 ng of sample was loaded into each lane. The apparent labeling stoichiometries determined from the spectra are 1.84, 1.15, 1.14, and 1.13 correspondingly. In addition to the receptor, the in-gel fluorescence also reveals unbound Alexa488-DIBO, which decreases with the concentration of the labeling reagent. For the 50-μM reaction, the band of free dye is particularly pronounced (marked by the white star).

2.3.5 Labeling azF-Rho using DIBO derivatized with different Alexa fluorophores

To evaluate whether the labeling reaction for azF-Rho is dependent the fluorophores conjugated to DIBO, we also tested Alexa555-DIBO, Alexa594-DIBO, and Alexa647-DIBO. Figure 2-14 shows the fluorescent labeling of azF-Rho at site 144 with different Alexa fluor-DIBO. The apparent dye-to-protein ratio for S144-Alexa555-, S144-Alexa594-, and S144-Alexa647-Rho are 1.11, 1.20, and 1.03, respectively. By comparison, for wt Rho treated under the same condition, the resulting labeling stoichiometries were below 0.04. These results demonstrated that the labeling strategy is specific and modular.

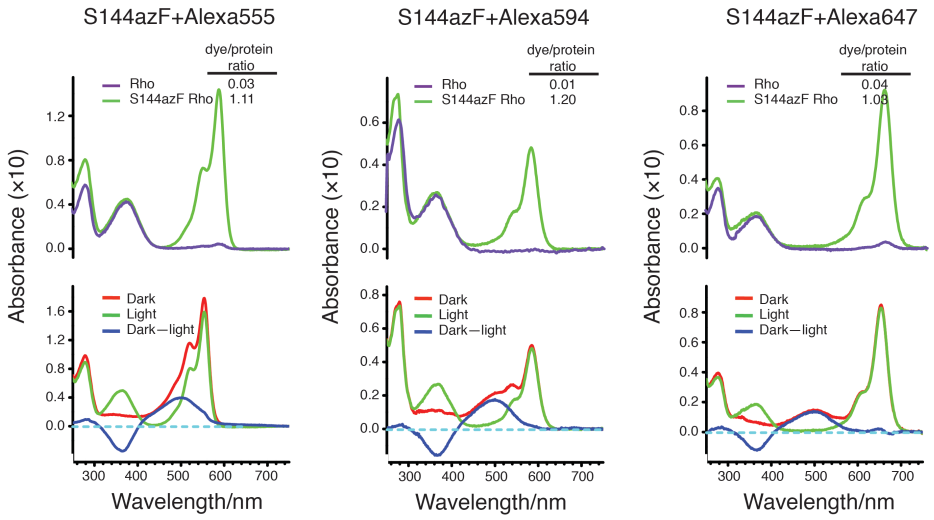

Figure 2-14. Fluorescent labeling of azF-containing Rho at site S144 with different Alexa-DIBOs. Upper panel: the normalized spectra for Rho S144-Alexa fluor and Rho wt treated under the same conditions. Lower panel: the dark-state, light-state, and difference UV-Vis spectra of Rho labeled at S144. The initial concentration of Alexa488-DIBO is 5 μM; for Alexa555-DIBO 50 μM; for Alexa594-DIBO 5 μM; for Alexa647-DIBO 20 μM. The extinction coefficients for Alexa488-DIBO, Alexa555-DIBO, Alexa594-DIBO, and Alexa647-DIBO are assumed to be 71, 000 M^{-1} cm^{-1}, 155, 000 M^{-1} cm^{-1}, 92, 000 M^{-1} cm^{-1}, and 239, 000 M^{-1} cm^{-1}. The apparent dye-to-protein ratio for azF-Rho and wt Rho are indicated in the figure.

2.3.6 Kinetic study of SpAAC between azF-Rho and Alexa-DIBO

The knowledge on the kinetics of the SpAAC reaction for azF-Rho would guide the rational optimization of the reaction conditions. In principle, the reaction kinetics can be determined more accurately using UV-Vis spectroscopy. However, it requires large amount of samples (each measurement requires approximately 1 μg of purified azF-Rho). Therefore, we chose in-gel fluorescence and silver staining for quantifying the relative extent of reaction (Figure 2-15A). As predicted, the conjugation reaction between S144azF Rho and Alexa488-DIBO was pseudo-first order (Figure 2-15B), giving a second-order rate constant for the coupling reactions (k_2) of 62 M^{-1} s^{-1}.

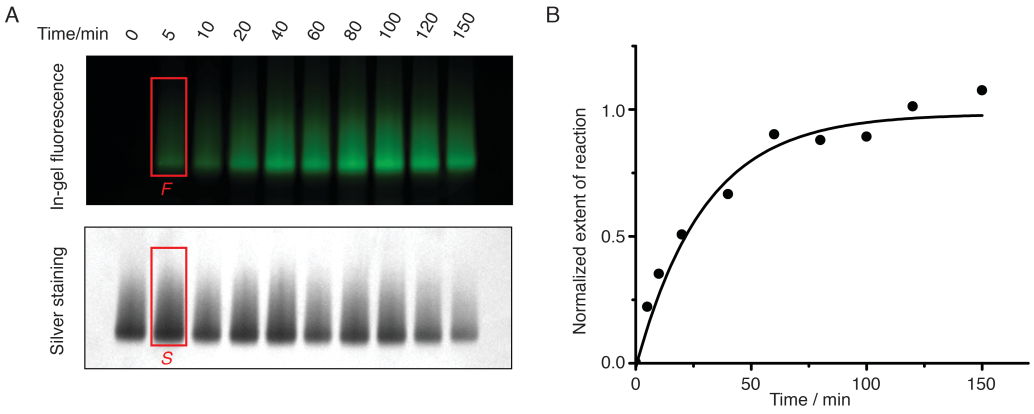

Figure 2-15. The kinetic study of SpAAC between S144azF-Rho and different Alexa 488-DIBO. A) The time course of the reaction shown by in-gel fluorescence. For each time point, 10 μL of sample was loaded to the SDS-PAGE gel. The fluorescence signal was quantified using ImageJ. The amount of protein loading was obtained from silver staining of the same gel, and quantified using ImageJ. The fluorescence intensity corrected for protein loading was calculated as $I = F/S$. **B)** The normalized extent of reaction versus the reaction time. The extent of reaction upon completion is assigned to 1.0. The data was fitted using pseudo first-order kinetic model. The k_2 for Rho S144azF with Alexa488-DIBO is 62 ± 12 M^{-1} s^{-1} based on two independent sets of experiments.

We also determined the reaction rates between S144azF-Rho and other Alexa fluor-DIBO reagents (Figure 2-16). The k_2 of Alexa555-DIBO and Alexa594-DIBO were close to that of Alexa488-DIBO. Alexa647-DIBO reacted slower with S144azF-Rho. Overall, all the Alexa fluor-DIBO reagents exhibited significantly enhanced kinetics that was 2~3 orders of magnitude higher than the reaction rate (0.17 M^{-1} s^{-1}) reported for the SpAAC between benzyl azide and DIBO in methanol (Ning et al., 2008; Debets et al., 2011).

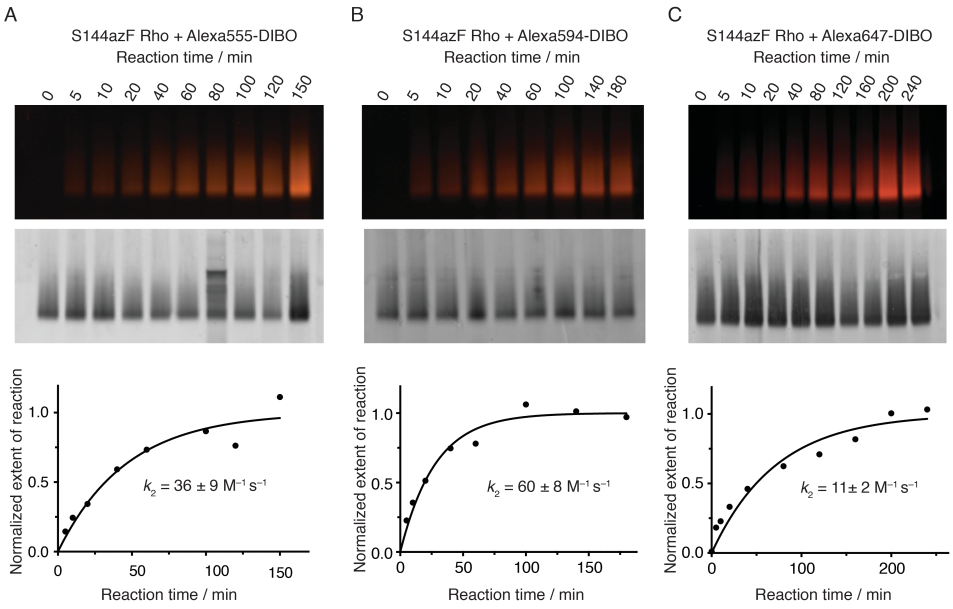

Figure 2-16. The kinetic study of strain-promoted azide-alkyne cycloaddition between S144azF-Rho and different Alexa-DIBOs. A) Alexa555-DIBO, **B)** Alexa594-DIBO, and **C)** Alexa647-DIBO. The resulting k_2 are 36 ± 9 M^{-1} s^{-1} , 60 ± 8 M^{-1} s^{-1}, and 11 ± 2 M^{-1} s^{-1}, respectively.

To quantitatively assess how the local environment on the TM surface contributes to the reactivity of SpAAC. We measured the reaction rates of SpAAC at two sites, M155azF and V162azF, both of which are located in the middle of TM4 (Figure 2-17).

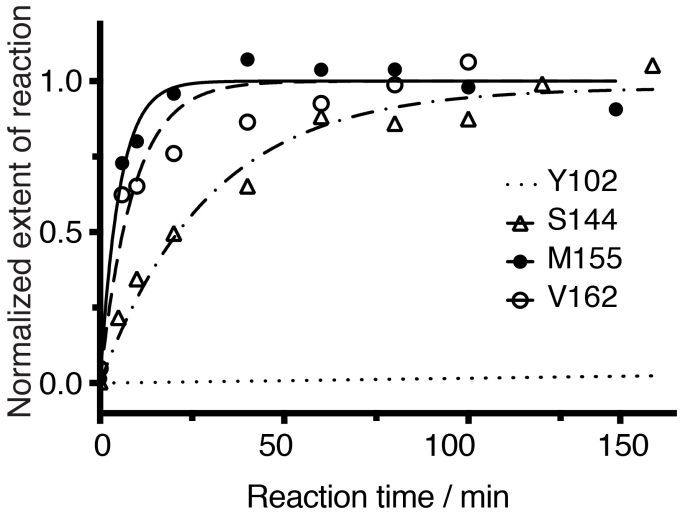

Figure 2-17. The location of azF modulates the kinetics of the SpAAC reaction between azF-Rho and Alexa488-DIBO. Reaction time course of three azF-Rho variants, S144 (IC2), M155 (TM4), and V162 (TM4) were measured based on the method described earlier (*cf*. Figure 2-15). The data points were fitted using pseudo first-order kinetic model. The calculated k_2 is 62 ± 12 M^{-1} s^{-1} for S144azF-Rho, (3.2 ± 0.4)×10^2 M^{-1} s^{-1} for M155azF-Rho, and (1.9 ± 0.5) ×10^2 M^{-1} s^{-1} for V162azF-Rho. The curve for Y102azF-Rho was simulated based on the k_2 (0.27 M^{-1} $s^{-1)}$ estimated from single time point labeling stoichiometry data (dye/protein ratio = 0.56 after 18 h).

The k_2 for M155azF-Rho and V162azF-Rho were (3.2 ± 0.4)×10^2 M^{-1} s^{-1} and (1.9 ± 0.5) ×10^2 M^{-1} s^{-1}, respectively (Figure 2-17). The labeling reaction of Y102azF-Rho with 50 μM Alexa488-DIBO for 18 h yielded a stoichiometry of 0.56, which corresponded to a second order rate constant of 0.27 M^{-1} s^{-1}. This value is similar to the rate observed for the SpAAC reactions between two small molecules (Ning et al., 2008;

Debets et al., 2011). The crystal structure of Rho shows that Y102 is a solvent-accessible site with the side chain pointing towards the EC space. Molecular dynamics simulations of Rho in a phospholipid bilayer membrane show that Y102 is water exposed with only minimal (5%) contacts to lipids (*cf.* Figure 2-7) (Huber et al., 2004). Thus, a 10^3-fold enhancement of SpAAC kinetics was observed for azF residues located in the TM region as compared with the polar region, demonstrating that the local environment near the TM surface greatly accelerates the cycloaddition reaction.

2.3.7 The accelerated SpAAC in the TM region can be explained by the partitioning of Alexa488-DIBO between DM micelles and water

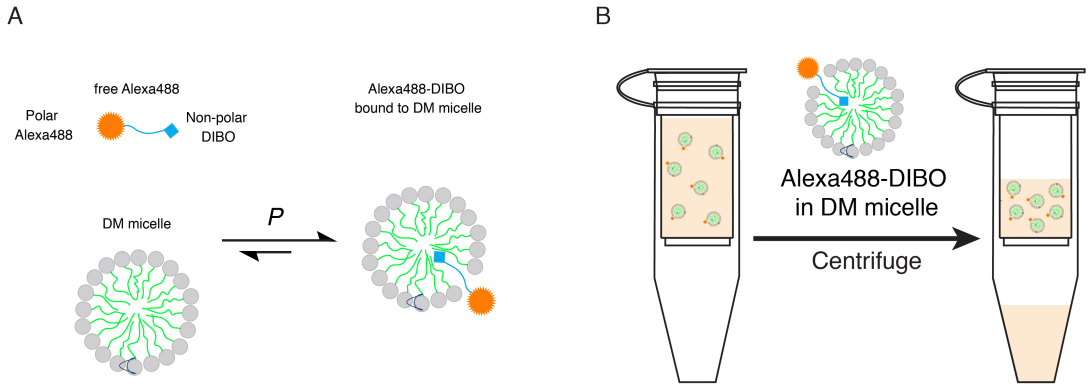

Figure 2-18. **The scheme of filtration experiment to determine the partition coefficient of Alexa488-DIBO between micelles and wate**r. **A)** The partition equilibrium of Alexa488-DIBO between DM micelle and water. **B)** The filtration experiment with spin filter. Alexa488-DIBO solution with DM was added into the spin filter. The experiment is based on the different molecular weight of Alexa488-DIBO (MW = 1039.23) and DM micelles (~50 kDa). The molecular weight cut-off of the microporous membrane is 10 kDa. Therefore, the heavier DM micelles, together with the Alexa488-DIBO partitioning into them, are expected to remain in the retentate fraction, while the free Alexa488-DIBO will flow through the membrane.

The micelles formed by amphiphilic detergents consist of a non-polar core covering the hydrophobic protein surface and a polar envelope surrounding the hydrophobic core. A straightforward explanation for the observed rate enhancement would be that Alexa488-DIBO molecules partition into the DM micelles, resulting in an increased local concentration of the reactive moiety around azF. To test this hypothesis, we designed a filtration experiment, where Alexa488-DIBO was mixed with various concentrations of DM micelles and centrifuged in spin filter units with regenerated cellulose membrane with a molecular weight cut-off of 10 kDa. The larger DM micelles, together with the Alexa488-DIBO partitioning into them, are expected to remain in the retentate fraction, while the free Alexa488-DIBO will flow through the membrane (Figure 2-18) (Strop and Brunger, 2005).

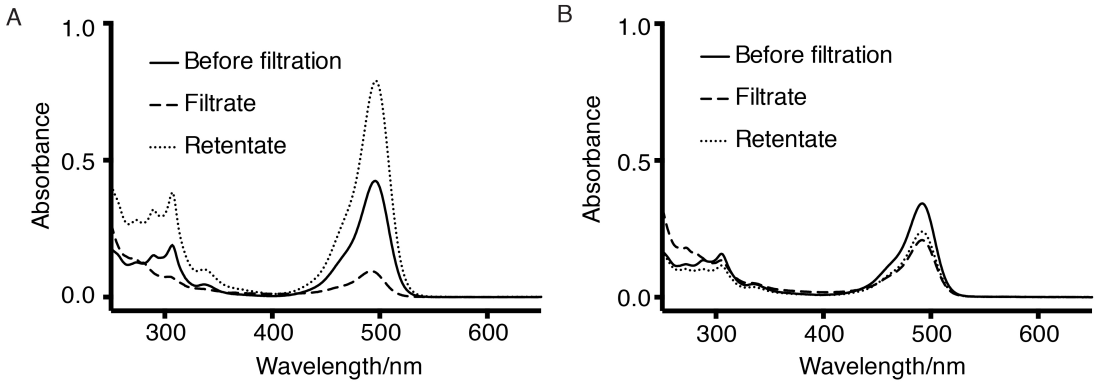

Figure 2-19. Representative spectra for the filtration experiment. A) Alexa488-DIBO solution (~5 μM) prepared in DPBS with 0.1% DM. *Solid*: the Alexa488-DIBO solution before filtration; *dash*: the filtrate; *dot*: the retentate. In the presence of DM, the recovery of Alexa488-DIBO was approximately 100%. **B)** Alexa488-DIBO solutions in DPBS. *solid*: before filtration; *dash*: the filtrate; *dot*: the retentate. In the absence of DM, the recovery of Alexa488-DIBO was lowered to approximately 67%. The concentration of Alexa488-DIBO was calculated from the 492-nm absorbance (ε_{495nm} = 73, 000 M^{-1} cm^{-1}).

The concentration of Alexa488-DIBO the filtrate and retentate were quantified by UV–Vis spectroscopy (Figure 2-19 and Table 2-2). We showed that the total concentration of Alexa488-DIBO in the retentate increased with the weight/volume percent of DM (Table 2-2).

Table 2-2. The concentrations of Alexa488-DIBO and the volumes of filtrate and retentate

f_0 of DM (%)	c_1 (μM)	V_1 (μL)	c_2 (μM)	V_2 (μL)	c_0 (μM)	Recovery* (%)
0	2.86	190	3.28	210	4.69	66
0	3.05	170	4.13	220	5.40	68
0.05	2.12	185	9.05	210	5.76	101
0.10	1.33	200	10.5	210	5.74	105
0.10	1.37	180	9.29	210	5.74	98
0.25	0.562	180	10.2	205	5.64	101
0.25	0.557	180	9.58	220	5.64	98
0.50	0.519	185	10.6	210	5.70	103
0.50	0.423	195	11.8	200	5.81	106
1.00	0.325	175	10.8	220	5.92	104

*Note: The recovery of Alexa488-DIBO was calculated as $\frac{c_1V_1 + c_2V_2}{c_0\left(V_1 + V_2\right)}$.

We calculated the partition coefficient of Alexa488-DIBO between DM micelles and buffer at different DM concentrations. (Table 2-3; and Figure 2-20; the detailed procedures are explained in Appendix I). We found that when the concentration of DM is 0.1% (*w*/*v*), the effective local concentration of Alexa488-DIBO in DM micelles was increased by a factor of 7.8×10^2, a value in good agreement with the observed rate

enhancement (1.2×10^3-fold for M155azF and 7.0×10^2-fold for V162azF as compared to Y102azF). Therefore, the effect of partition suffices to explain the rate enhancement (Table 2-3 and Figure 2-20).

Table 2-3. Calculation of the partition coefficient at different DM concentrations

f_0 of DM (%)	$\frac{(c_2 - c_1)V_2}{c_1(V_1 + V_2)}$	P ($\times10^3$)	Rate enhancement
0	0.08	N.A.	N.A.
0	0.20	N.A.	N.A.
0.05	1.74	4.21	1.35×10^3
0.10	3.53	3.81	795
0.10	3.11	3.41	773
0.25	9.13	3.78	362
0.25	8.91	3.69	361
0.50	10.3	2.10	183
0.50	13.6	2.77	187
1.00	18.0	1.82	95

2.3.8 Evaluation of the functionality of the labeled Rho

We then addressed whether the engineered Rho variants carrying the fluorescent label remained functional. We utilized a fluorescence-quenching assay to assess their photoactivation and ligand binding (Figure 2-21). This assay is based on the energy transfer between Alexa488 (the donor), and the bound 11-*cis*-retinal (the acceptor). The emission spectrum of Alexa488 overlaps with the absorption band of dark-state Rho centered at 500 nm, causing significant quenching of Alexa488 fluorescence by 11-*cis*-retinal. Upon photoactivation, 11-*cis*-retinal isomerizes to all-*trans*-retinal to generate the active-state metaRho II (Meta-II), and the retinal absorption peak shifts to 380 nm. This

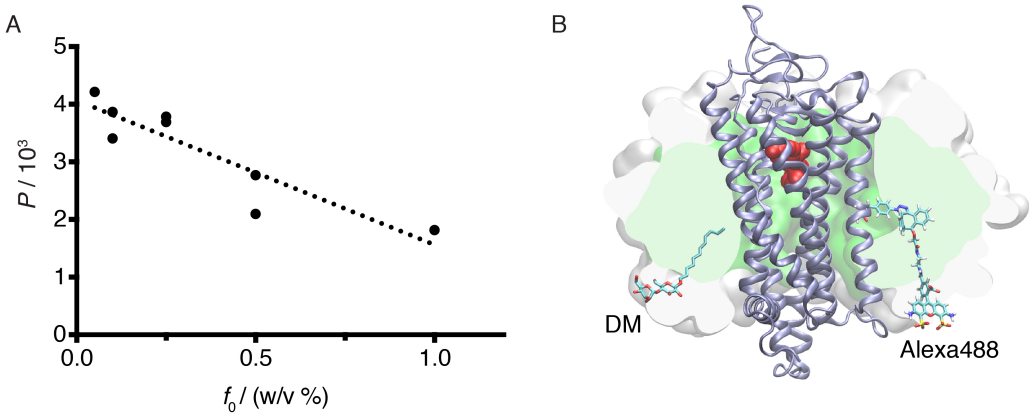

Figure 2-20. **Alexa488 DIBO partitions into the micelle. A)** Partition coefficient (water to micelle) from ultrafiltration experiment with various concentrations of DM. The observed partition coefficients (*P*) were plotted as against the weight/volume percent of DM (f_0). We found empirically a linear correlation between *P* and f_0 ($R^2 = 0.81$). **B)** Atomic model of Rho (PDB:1GZM) embedded in a micelle (150 DM molecules). The SpAAC conjugated V162azF-DIBO-Alexa488 is shown as sticks including hydrogens. For size comparison, one of the 150 DM molecules is shown in sticks but without hydrogens. The protein backbone is shown as a cartoon (*ice blue*). 11-*cis*-retinal is shown in spheres (*red*). The hydrophobic core of the micelle is rendered as a green surface sliced by the image plane just behind the dye. The white surface shows the extension of the head groups of the micelle sliced in the same plane. The model of Alexa488-DIBO was generated with Schrödinger's small-molecule drug discovery suite, and the model of DM micelle was constructed by charmm-gui micelle builder (Cheng et al., 2013). A short molecular dynamics simulation (1.3 ns) was performed with namd2.10 (Phillips et al., 2005) to relax the DM micelle around the receptor.

spectral shift results in loss of quenching and an increase in the Alexa488 signal. Then 11-*cis*-retinal dissociates from the binding pocket, giving opsin with the empty binding pocket (Menon et al., 2001). Therefore the Alexa488 signal can serve as a reporter for the recombination reaction between 11-*cis*-retinal and the apoprotein opsin. Upon addition of exogenous 11-*cis*-retinal, the Alexa488 signal decrease as retinal enters the binding pocket of opsin and forms the protonated Schiff base linkage. It is worth noting that the excitation light for Alexa488 may also cause photoisomerization of 11-*cis*-retinal, which can be further enhanced by the energy transfer between Alexa488 and 11-*cis*-retinal. This energy transfer may result in a lower apparent recombination rate. Therefore it is important to minimize the excitation intensity by using very narrow band-pass filter to reduce such a systematic error.

A typical fluorescent quenching experiment with S144-Alexa488 Rho is shown in Figure 2-21, Panel A. After 5 min (arrow a') we added 30 mL of Rho sample (typically 0.3–1.0 mg) into lipid/detergent micelles to a final concentration of 15–50 nM. Upon illumination (arrow b′), we observed a fast increase of fluorescence signal. This is because photoisomerization of 11-*cis* to all-*trans*-retinal, accompanied by a change from a protonated Schiff base (Rho state) to a deprotonated Schiff base (Meta-II state), causes disappearance of spectral overlap between Rho and Alexa488, and consequent loss of quenching. While the system was allowed to equilibrate for 45 min, all-*trans*-retinal was released as the Meta-II state decayed, and the apoprotein opsin became the dominant species. Upon addition of 1.5 mM (1.48–1.59 mM) 11-*cis*-retinal (30–100-fold excess) (arrow c′), we observed a gradual decrease of the fluorescence signal for the Rho S144-Alexa488 sample, corresponding to the kinetics of 11-*cis*-retinal binding and formation of

the dark state Rho. The regenerated species was further illuminated twice (arrow d′ and e′) to demonstrate the formation of photoactivable pigment. After the addition of NH_2OH (arrow f′), the photobleached Rho (arrow g′) could not be regenerated by 11-*cis*-retinal. The first regeneration process was fit to a monoexponential model yielding a time constant (Figure 2-21B). This time constant corresponds to the pseudo-first-order process of Rho formation from opsin under excess 11-*cis*-retinal. The second order rate constant was calculated for each experiment using the exact retinal concentration (Henselman and Cusanovich, 1976). The quenching efficiency between Alexa488 and retinal and the degree of regeneration were calculated as explained in Figure 2-22, Panel A. Based on more than three measurements, the regeneration of S144-Alexa488 Rho was 96 ± 4%. Therefore, S144-Alexa488 Rho retained its wt behavior with respect to ligand binding.

The wt Rho sample treated under the identical reaction conditions with Alexa488-DIBO was tested using the same fluorescent quenching assay (Figure 2-22, *turquoise*). In contrast to the results from S144-Alexa488 Rho, almost no visible change in the fluorescence signal was observed throughout the assay for wt Rho, confirming that little or no Alexa488-DIBO was covalently attached to the wt receptor without an azido handle. This is consistent with the absence of a fluorescent band in the SDS-PAGE gel (*cf.* Figure 2-10 and 2-11). To assure there is no significant change in fluorescence for the wt sample, we modified the experiment by increasing the excitation intensity by approximately 4-fold, and found that after correction for the larger excitation intensity, the increase in signal due to photoactivation is approximately 1% relative to the S144azF mutant.

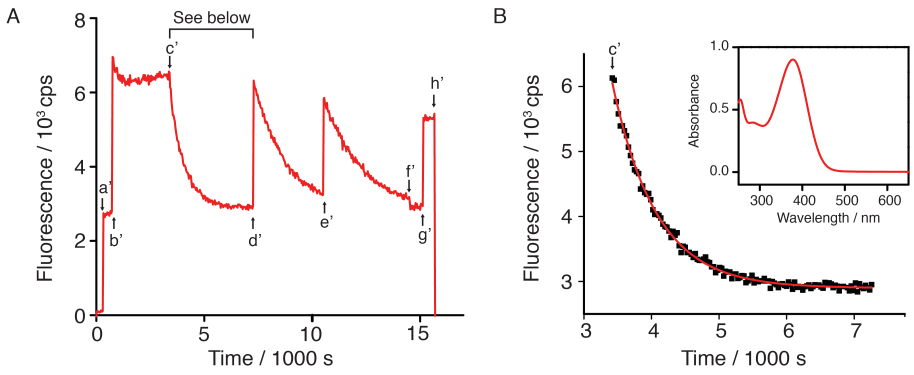

Figur 2-21. The fluorescence-quenching experiment to assess the functionality of Alexa488 labeled Rho. A) The full fluorescence time course of the Alexa488-Rho variants in steady-state fluorescence quenching assay. Fluorescence spectroscopy was performed at 28°C on a SPEX Fluorolog spectrofluorometer in photon counting mode. During time scan experiments the excitation wavelength was 488 nm with 0.2-nm band-pass to minimize photobleaching, and the emission was measured at a wavelength of 525 nm with 15-nm band-pass. The Alexa488-labeled Rho elutions (30 μL) were added into the cuvette (indicated by a′) at a final concentration of 15–50 nM to the assay buffer under constant stirring. Rho was photoactivated with green light (b′). The decay of the photoproducts to the apoprotein opsin was monitored for 45 min before 11-*cis*-retinal (final concentration ~1.5 μM) was added (c′). The exponential decay of the fluorescence back to the pre-illuminated levels indicated a pseudo first-order reaction regenerating Rho from opsin. Repeated illumination (d′) resulted in a fluorescence change of similar magnitude but opposite sign as the regeneration reaction. Repeated bleaching (e′) resulted in a similar change of signal. The two additional illuminations at d′ and e′ illustrated the reversibility of the process. However, in this case opsin that forms by decay of the Meta-II state immediately regenerated to the dark state due to the presence of excess 11-*cis*-retinal. We added 50 mM hydroxylamine (NH_2OH) at pH 6 (f′) to inactivate retinal by oxime formation. Bleaching in presence of hydroxylamine (indicated by g′) resulted in fast decay of the photoproducts to yield opsin. The shutter was closed at the end of the experiment (h′). **B)** The kinetics of the regeneration of S144-Alexa488-Rho. Inset: the absorption spectrum of 11-*cis*-retinal working solution.

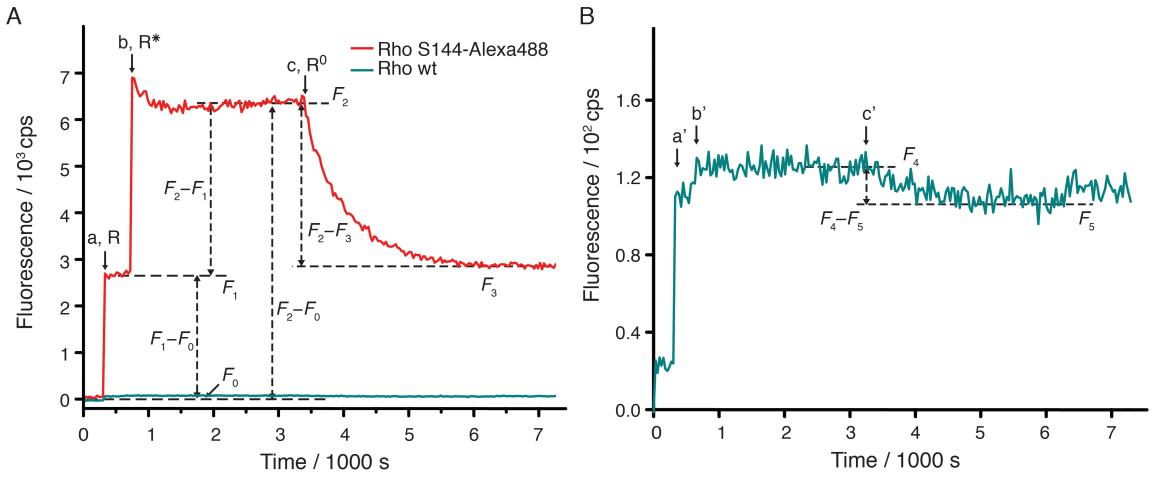

Figure 2-22. Comparison of Alexa488-Rho and wt Rho in the steady-state fluorescence-quenching assay. A) The S144Alexa488-Rho shows increase in fluorescence upon photoactivation and subsequent quenching with 11-*cis*-retinal. The small increase in fluorescence signal at a′ for the wt Rho is due to free label (~3% as compared to S144-Alexa488 Rho), since subsequent illumination or 11-*cis*-retinal addition did not show significant fluorescence changes (less than 1% of the amplitude compared to S144-Alexa488 Rho). Together these results confirm that little or no Alexa488 was covalently attached unless the azF was present and that the site-specifically labeled Rho was fully functional in terms of photoactivation and regeneration. The quenching efficiency is calculated from $E = 1 - F_{DA} / F_D = 1 - (F_1 - F_0)/(F_2 - F_0)$). The degree of regeneration is calculated as $(F_2 - F_3)/(F_2 - F_1)$. **B)** Background labeling is estimated from the retinal uptake amplitude for the wt and S144azF samples ($\left[(F_4 - F_5) I_{\text{Alexa488}} c_{\text{Alexa488}}\right] / \left[(F_2 - F_3) I_{\text{wt}} c_{\text{wt}}\right]$) , accounting for the relative intensity of the excitation light (I) and the concentration of the sample (c). The background labeling in the wt sample appears to be less than 1% of all Rho molecules.

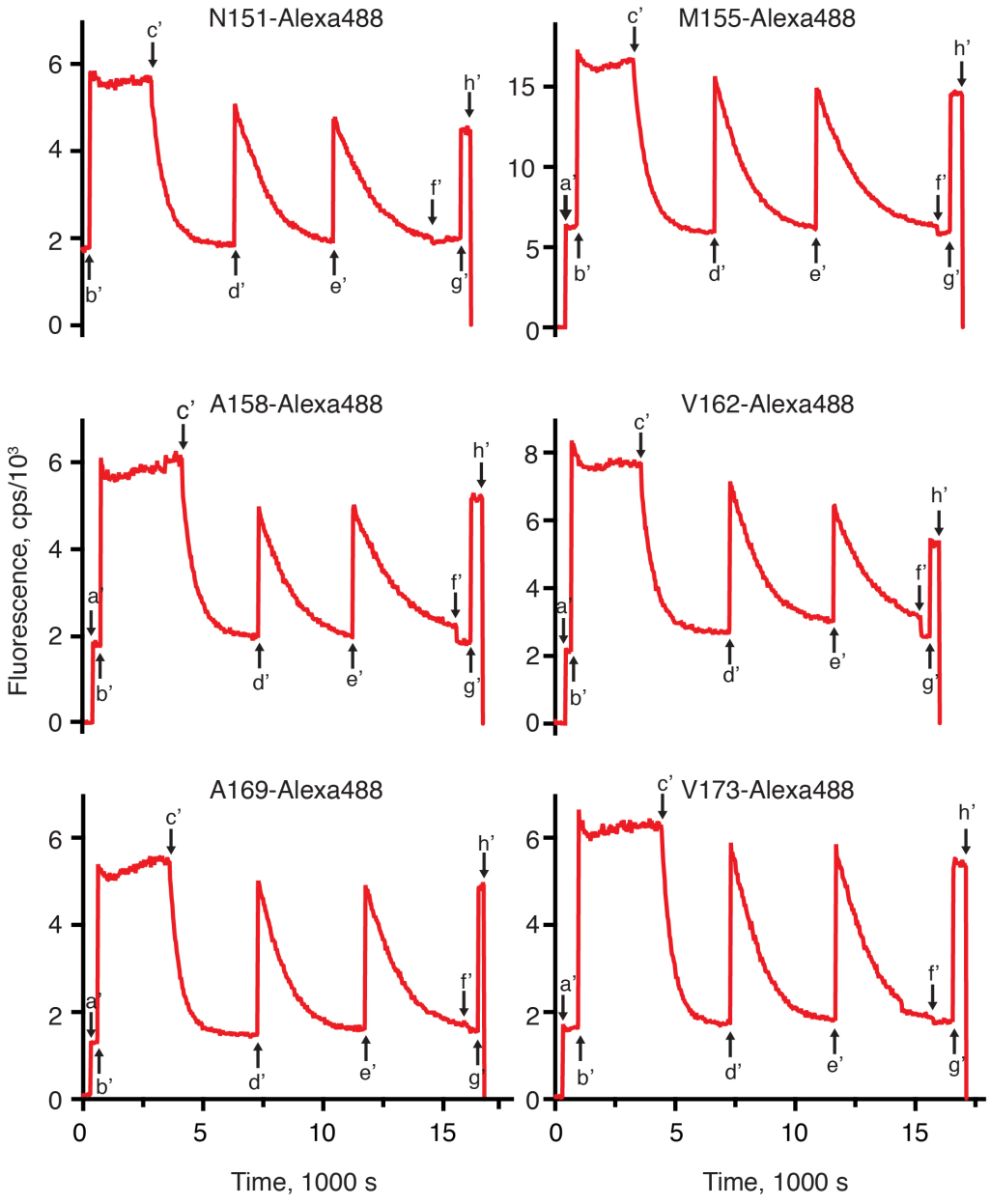

Figure 2-23. The full fluorescence time course of the azF-Rho variants labeled at TM4 in the steady-state fluorescence-quenching assay.

Rho (90%). All the regenerated Rho variants can be repeatedly photoactivated, demonstrating the formation of a functional pigment (Figure 2-23). The rates of recombination reactions between 11-*cis*-retinal and N151-, M155-, A158-, and V162-Alexa488 Rho are consistent with the value obtained for S144-Alexa488 Rho (Figure 2-24). The regeneration kinetics of A169- and V173-Alexa488 Rho are slightly faster (30-40%) compared with S144-Alexa488 Rho (Figure 2-24A). While the difference was not significant, we would like to discuss some possible effects. Differences in energy transfer efficiency between Alexa488 and retinal in Rho could change the sensitivity of the experiment bleaching artifacts due to the probe light. Sites 169 and 173 are closer to the binding pocket and Alexa488 attached to these two sites exhibits higher energy transfer efficiency than when the fluorophore was conjugated to site 144. Higher transfer efficiency between Alexa488 and retinal in Rho would lead to higher bleaching rates and consequently reduced observed regeneration kinetics. Thus, we ruled out the possibility that the faster recombination kinetics for A169-Alexa488 and V173-Alexa488 Rho was an artifact embedded in the energy transfer scheme, as greater energy transfer between Alexa488 and retinal should cause the measured kinetics to be even slower. An alternate explanation would be that modification of the sites in proximity to, although not a part of, the binding pocket caused slightly altered ligand binding kinetics.

The energy transfer efficiencies of these Alexa488-labeled variants are dependent on the distance between the site of labeling and the binding pocket (Figure 2-24B). Among all the Alexa488-labeled azF-Rho variants, S144-Alexa488 Rho showed the lowest quenching efficiency (0.55 ± 0.04), while A169-Alexa488 Rho showed the highest quenching efficiency (0.76 ± 0.04). This result is consistent with distance measurements

based on with the crystal structure of Rho and the site-dependent quenching efficiency thus provides an additional line of evidence for the site-specificity of the labeling strategy. It should be pointed out that here we used the *z*-axis coordinates of the alpha carbon of the labeled sites and the center of 11-*cis*-retinal to estimate the distance between Alexa488 and retinal. A rigorous treatment should take into account the dipole orientations of Alexa488 and 11-*cis*-retinal, the length and conformation of the linker between the alpha carbon and the fluorophore, and the angular distribution of the linker relative to TM4, which is beyond the scope of this study.

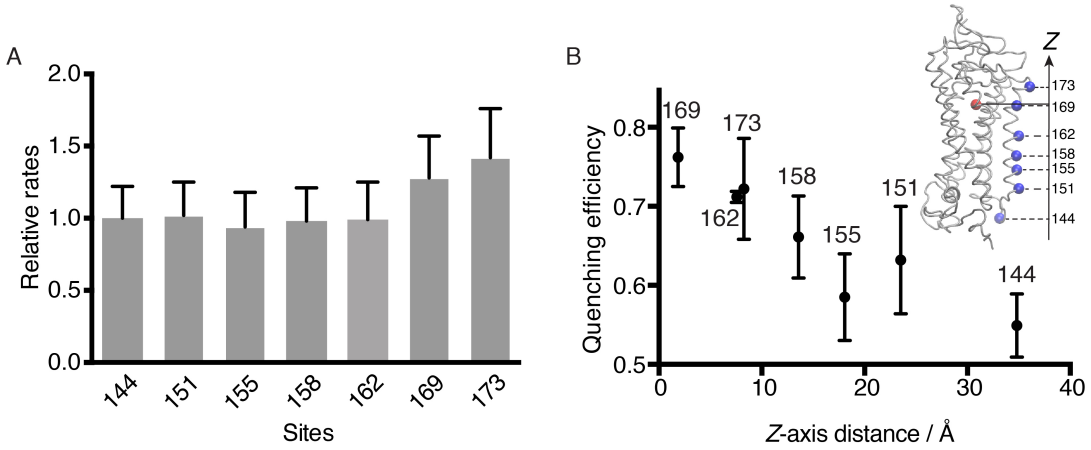

Figure 2-24. The binding kinetics and energy transfer efficiency between Alexa488-Rho variants and 11-*cis*-retinal. A) The second-order rate constants (k_2) of 11-*cis*-retinal uptake by different Alexa488-Rho variants. S144-Alexa488 Rho was used as a reference to normalize the reaction rates of other variants. **B)** The energy transfer efficiencies between 11-*cis*-retinal (acceptor) and Alexa488 (donor) attached to different sites of Rho plotted versus the *Z*-axis distance between the alpha carbon of the labeled site (*blue* dot), and the center of mass of the retinal molecule (*red* dot), as determined from the crystal structure (inset, PDB 1U19) (Okada et al., 2004).

2.4 Discussion

2.4.1 The non-specific reactivity of chemistries selective for the keto group

Our aim in this present study was to identify highly selective and robust labeling chemistries that could exploit site-directed uaa mutagenesis of GPCRs. Initially we focused on the keto group in AcF (Ye et al., 2008). Because keto groups have been studied for site-specific fluorescent labeling in several model systems (Cornish et al., 1996; Hang and Bertozzi, 2001). Under roughly physiological conditions, ketones and aldehydes react specifically with hydrazide (or aminooxy) reagents through hydrazone (or oxime) ligation (Bayer et al., 1988; Wang et al., 2003). These reactions have been used to label proteins at genetically encoded N-terminal aldehyde tags (Shi et al., 2012), and with more flexibility at site-specifically incorporated uaas (Cornish et al., 1996; Fleissner et al., 2009). However, in our initial attempts to label AcF tagged Rho with a fluorescein-hydrazide, we observed substantial covalent modification of wt Rho in the absence of AcF (Ye et al., 2008). In order to determine if such background reactivity was specific to a membrane glycoprotein, like Rho, we studied a soluble, non-glycosylated protein, recombinant firefly luciferase. While we were able to label AcF-tagged luciferase, we also found similar background reactivity in wt luciferase with different reagents selective for ketone and aldehyde (Huber et al., 2013).

Previous studies have reported that cellular oxidation processes often convert some amino acid residues to carbonyl derivatives (i.e., ketone and aldehyde) that can react with hydrazide reagents (Ahn et al., 1987; Stadtman and Levine, 2003). These reactive carbonyl groups normally present in proteins are known to originate from unusual post-translational oxidation processes to the side-chains of lysine, histidine and cysteine

residues under oxidative stress (Stadtman, 1993). More recently, a role of reactive lipid hydroperoxides has been described in a phenomenon known as "protein carbonylation" (Grimsrud et al., 2008). In our study, we obtained the rate constants of the reaction specific for the AcF handle, and the non-specific reaction for the wild-type receptor, and found the latter to be significantly faster than the former. This finding is consistent with the hypothesis that protein oxidation may involve the generation of aldehyde group, which has a more reactive carbonyl group than the ketone group in AcF. We suggested earlier (Huber et al., 2013) that these reactive carbonyl groups have been previously overlooked as the origin of background labeling in protein tagging experiments, possibly because low molecular weight proteins (Wang et al., 2003; Zhang et al., 2003) or highly modified components were employed as the model systems (Zeng et al., 2009). Therefore, the chemistries for aldehyde and ketone should be chosen with caution to achieve the desired protein modification.

2.4.2 A comparative study of labeling chemistries for the azido group

After carefully evaluating the non-specific reaction with labeling ketone, we explored the alternative of using azido groups as reactive handles to label proteins. Azides react specifically with phosphines through the Staudinger-Bertozzi ligation (Kiick et al., 2002; Saxon and Bertozzi, 2000), with alkyne reagents through copper (I)-catalyzed [3+2] azide–alkyne cycloaddition (CuAAC), with oxanorbornadienes through tandem [3+2] cycloaddition–retro-Diels–Alder (tandem crDA) (van Berkel et al., 2007), or with cyclooctynes through SpAAC (Debets et al., 2011; Agard et al., 2004; Sletten and Bertozzi, 2011).

Encouraged by the previous reports of Staudinger ligation to label azido-containing proteins (van Berkel et al., 2007; Tsao et al., 2005; Debets et al., 2010; Schilling et al., 2011), we investigated the possibility of using fluorescein-phosphine to label azF-tagged luciferase and Rho. We found the Staudinger ligation reaction of azF-luciferase with the phosphine reagents gave essentially no background as compared with the hydrazone and oxime ligations, indicating the true bioorthogonality of azido group over the keto group (Huber et al., 2013). However, when we applied the Staudinger ligation to label the membrane protein Rho, we experienced difficulties with the hydrophobicity of the fluorescein-phosphine label. Moreover, we found that the overall utility of the Staudinger ligation was limited by its relatively slow reaction kinetics and sub-stoichiometric ratio of labeling. The Staudinger ligation only achieved 30% labeling of Rho after reacting for 12 h at room temperature (Huber et al., 2013), in spite of the nearly stoichiometric conjugation of azF in other recombinant proteins with fluorescein-phosphine as reported previously (Tsao et al., 2005). In agreement with our findings, a recent report of Staudinger ligations targeting two different azido amino acids showed that azF was only incompletely modified by phosphines, which was attributed to the shorter linker length between the backbone and the azide (Yanagisawa et al., 2008).

We also considered the CuAAC reaction, commonly referred to as the copper-catalyzed click chemistry. However, we were concerned about the potential damage from Cu to the purified protein and live cells, as Cu can switch its oxidative states easily, thereby inducing undesirable chemical modifications to proteins and cells. This drawback of CuAAC prompted a hunt for reagents that react with azide in the absence of metal catalysts.

A report in 1953 mentions an explosive reaction of cyclooctyne with phenyl azide forming a viscous liquid product (Blomquist and Liu, 1953), later identified as 1-phenyl-4.5-cycloocteno-1.2.3-triazol (Wittig and Krebs, 1961). In 2004, the Bertozzi group capitalized on these pioneering studies on the chemistry of many-membered rings in 1950s and 1960s and introduced SpAAC of cyclooctynes and azides as efficient bioconjugation reagents (Agard et al., 2004). In order to overcome problems such as low reactivity, poor reagent stability, and difficult synthetic pathways of the earlier cyclooctynes for bioconjugation, Boons and colleagues introduced dibenzocyclooctyne derivatives for bioconjugation by SpAAC (Brustad et al., 2008) based on a 1969 report on the spontaneous reaction of dibenzocyclooctyne with phenyl azide (Seitz et al., 1969). Despite the reports of degradation of the cyclooctyne BARAC in presence of glutathione (Jewett et al., 2010), it was generally believed that SpAAC involving the cyclooctynes results in low background labeling (Sletten and Bertozzi, 2011). In a recent study, three cyclooctynes, DIBO, BCN, and DIBAC were used to evaluate azide-independent labeling of proteins, demonstrating that all of these reagents exhibited undesirable reactivities to varying extents, by a radical-based thiol-yne addition mechanism that modifies cysteine residues in proteins (van Geel et al., 2012). Interestingly, DIBO appeared to have drastically reduced background labeling as compared with BCN and DIBAC (van Geel et al., 2012).

2.4.3 The non-specific reactivity of DIBO for protein labeling

We present three independent lines of evidence that can be used to estimate the background labeling by DIBO in wt Rho: 1) the absence of Alexa488 absorbance (<5%) in UV-Vis spectrum; 2) the absence of Alexa488 fluorescence emission in the in-gel

fluorescence image (~5%); and 3) negligible change in fluorescence signal upon photoactivation in the fluorescence-quenching assay (<1%). We contend the steady-state fluorescence-quenching assay provided the most accurate information for non-specific covalent labeling, because the energy transfer is critically dependent on the distance between the donor and the receptor.

Another concern is the potential reduction of azide to amine in the cellular context, which would decrease the number of reactive handles present in Rho. The *in vitro* reduction of aryl azide by thiols to aryl amines has been reported (Staros et al., 1978), and the reduction product of azF might be utilized by the aminoacyl synthetase (Nehring et al., 2012). Reduction of genetically encoded azido group to amino group has also been observed by mass spectroscopy (Kiick et al., 2002; Liu et al., 2007). However, in the case of unnatural amino mutagenesis, it is not clear whether the degradation of azF occurred before or after incorporation into protein. Reduction of azF would lead to a decrease of the labeling stoichiometry and might contribute to the apparent sub-stoichiometry for Y102azF Rho. Y102azF is exposed to the oxidizing extracellular environment rather than the reducing environment of the cytosol. Theoretically, compared with Y102azF, S144azF is more likely to be degraded in the cellular environment. Due to the difficulty of mass spectroscopy experiment with GPCRs, we do not have direct experimental evidence to test this possibility. Overall, we believe that the slow reaction kinetics, rather than the reduction of azF, is the major cause for the sub-stoichiometrical labeling for residues like Y102azF.

As mentioned earlier, it has been reported that such azide-independent background labeling of proteins with cyclooctyne reagents was primarily due to reactive cysteine

thiols (van Geel et al., 2012) in analogy to radical, photoinitiated thiol-yne additions (Fairbanks et al., 2010; Hoogenboom, 2010). In Rho there are four membrane-embedded cysteines, three cytoplasmic cysteines, and three extracellular or intradiscal cysteines (Karnik et al., 1988). Among them, two cytoplasmic cysteines (C140 and C316) have been shown to be highly reactive towards traditional thiol-specific reagents (Mielke et al., 2002). The normally S-palmitoylated cysteines (C322 and C323) may be incompletely palmitoylated and available for derivatization (Resek et al., 1993; Blaskovic et al., 2013), since S-palmitoylation is a reversible post-translational modification (Blaskovic et al., 2013). Consequently, except for the two cysteines that form a disulfide bond (C110 and C187), from two to eight remaining cysteines are potentially reactive towards DIBO. We estimate based on 1% background labeling of wild-type Rho that the selectivity factor of DIBO for azF over cysteine is between 200:1 and 800:1, which is sufficient to achieve good bioorthogonality in a chemically defined system.

The present study was primarily focused on labeling purified protein for *in vitro* experiments, but it also gave some insight into application of cyclooctyne reagents in live cell labeling. Considering the selectivity of DIBO reagents, the applicability of this approach depends on the relative abundance of the targeted azido groups over thiol groups from cysteine-containing proteins. The GPCRs are difficult targets that are generally expressed at low levels on the cell surface. Rho is among the best-expressing GPCRs in mammalian cells (6×10^6 molecules/cell) and the expression levels of other GPCRs are likely to be lower than Rho (Oprian et al., 1987; Sarramegna et al., 2003). Moreover, based on our experience, uaa-tagged Rho has significantly lower expression levels (10–20% compared to the wild-type receptor). We do not have direct information

regarding the abundance of cysteines reactive to cyclooctyne, but we can estimate the number of cysteines in membrane proteins per cell. Membrane proteins constitute approximately 30% of the human proteome (Almen et al., 2009) and membrane proteins in the post-nuclear fraction comprise ~9% of total protein mass in human HeLa cells (Bosmann et al., 1968), which corresponds to ~21 pg per cell or ~3.3×10^8 membrane proteins considering each protein molecule has on average 350 amino acids (Milo, 2013). Cysteine has been shown to vary from 0.2% to 0.5% in the total amino acid composition of cultured cells (Okayasu et al., 1997). Assuming membrane proteins have a similar length and composition of amino acids, the total number of cysteines in the membrane proteins is no less than 2×10^8 copies/cell. Therefore, on cell surface the abundance of cysteine is likely to be 2×10^2-fold greater than that of azF in the well-expressing GPCR Rho. With about 200:1 selectivity of DIBO for azF over cysteine, we would expect an equal contribution from specific labeling and background reactivity with cysteines. The situation would be much worse for receptor densities typically employed for single-molecule fluorescence tracking experiments (~1 μm^{-2}) (Hern et al., 2010; Calebiro et al., 2013), which corresponds to only 2500 receptors per cell (Sommerhage et al., 2008). The oxidative state of cysteine thiols should also be taken into account; the exposed cysteines in the extracellular side are likely to be oxidized to disulfide bonds, while the transmembrane and intracellular cysteines more likely in the reduced form. However, considering the hydrophobicity of cyclooctynes, we cannot exclude that possibility that these reagents would partition into lipid bilayer and react with the transmembrane cysteines. Also, certain cyclooctyne derivatives are designed to permeate the membrane (Beatty et al., 2011). Taken together, owing to the cross reactivity with cysteines, it can

be challenging to achieve an ideal signal-to-noise ratio for labeling and imaging low-abundance molecules on live cells using cyclooctyne reagents, as the chemistry is selective over the major non-specific reaction by only two orders of magnitude. Not surprisingly, successful applications of cyclooctyne reagents to live cell labeling normally necessitate the choice of high-abundance target molecules (*e.g.*, peracetylated N-azidoacetyl mannosamine) in the cell surface (Jewett et al., 2010), or promiscuous incorporation of azido uaas into multiple protein molecules (Beatty et al., 2010). Thus, we contend that the cross-reactivity with thiols should be evaluated in parallel with hydrophobicity for the development of new cyclooctyne derivatives for live-cell labeling.

2.4.4 Accelerated SpAAC in micellar environment

While the reaction kinetics of SpAAC with azF-Rho varies with the specific chemical and structural properties of the labeling reagent and the location of the azF residue, it has proven generally satisfactory for our purpose. Interestingly, we noted in our system a substantial rate enhancement effect (from 4-fold to 1000-fold) for the SpAAC reaction (8.6 ± 1.3 M^{-1} s^{-1} for DIBO-biotin or 62 ± 12 M^{-1} s^{-1} for Alexa488-DIBO and Rho-S144azF) as compared with model reactions of DIBO and benzylazide in methanol (0.17 M^{-1} s^{-1}) or water/acetonitrile (1:4 v/v) (2.3 M^{-1} s^{-1}) (Ning et al., 2008; Debets et al., 2011).

The unexpectedly high reaction rates of SpAAC between the ~40-kDa biomolecule S144azF-Rho and DIBO prompted us to postulate that the reactivity of the DIBO reagent is modulated by the local environment on the protein surface, and that the hydrophobicity of the local environment contributes to the observed reactivity enhancement. Therefore, we determined the kinetics for two TM4 azF-Rho variants, M155azF- and V162azF-Rho,

and found even greater rate enhancement effect. To explain this observation, we designed a filtration experiment to determine the partition coefficient of Alexa488-DIBO between micelle and water. We hypothesized that the partitioning of Alexa488-DIBO resulted in a higher local concentration of DIBO around azF, and hence the accelerated reaction. We found such a simple model suffices to explain the order of magnitude of the rate enhancement effect for SpAAC with azF-Rho in micelles.

A popular method to predict the stickiness of cyclooctynes and fluorescent dyes, and their applicability for fluorescent labeling, is based on *in silico* calculation of the *n*-octanol/water partition coefficient (cLogP) (Debets et al., 2011; Hughes et al., 2014). We used ChemBioDraw 14 to calculate cLogP = –11.8 for Alexa488-DIBO. Thus the high value of the measured partition coefficient (Log 780 = +2.9) of Alexa488-DIBO between DM micelles and water seems counterintuitive. However, the cLogP of DIBO was calculated as +4.4 (Debets et al., 2011), suggesting a strong tendency for DIBO to partition into the hydrophobic core of DM micelles. The linker length between the hydrophobic DIBO and the hydrophilic Alexa488 enabled the polar moiety to reside outside the water/detergent interface (Figure 4D). Overall, the amphiphilicity of Alexa488-DIBO makes it thermodynamically favorable to partition into the micelle and adopt the orientation that brings the reactive DIBO moiety into proximity of azF. This finding also supports an earlier report that the calculated cLogP does not robustly predict lipid membrane interactions of fluorescent dyes (Hughes et al., 2014).

The partition effect also helps to explain several earlier observations. The k_2 for S144azF-Rho (62 ± 12 M^{-1} s^{-1}) is two orders of magnitude higher than the reaction rate for the EC site Y102azF, but one order of magnitude lower than that of TM4 sites

M155azF and V162azF. Site S144 is located in the IC2 loop that exhibits higher flexibility than the rigid site Y102 (Huber et al., 2004). Although the residue S144 is largely exposed to water with only 7% lipid contacts (*cf.* Figure 2-7), substitution of serine for azF increases the hydrophobicity of this site, and consequently its probability to partition into the lipidic environment. Recently, we found that a site located in a hydrophobic cavity on the EC side of the CCR5 chemokine receptor was much more efficiently labeled by SpAAC than other EC sites (Naganathan et al., 2015). Interestingly, recent labeling experiments with azF-tagged GFP showed large variation of SpAAC reaction rates for different labeling positions. The most highly reactive site (k_2 = 17.8 M^{-1} s^{-1}) had the least surface exposure of all tested sites and was in a non-charged but polar local environment with an adjacent aromatic phenylalanine residue (Reddington et al., 2012). Taken together, a strong determinant for the SpAAC reactivity of DIBO is the hydrophobicity of the local environment in which azF resides.

2.4.5 Alternate uaas for site-specific labeling of proteins

In the recent years, the pyrrolysyl-tRNA synthetase/tRNA pair (Srinivasan et al., 2002; Polycarpo et al., 2004; Blight et al., 2004) has been developed as an alternative to evolved tyrosyl-tRNA synthetase/tRNA pairs for amber suppression, first in *E.coli* (Neumann et al., 2008), later in yeast (Hancock et al., 2010) and mammalian cells (Hancock et al., 2010). A major advantage of the pyrrolysyl synthetase is its high substrate side-chain promiscuity (Wan et al., 2014). In addition to azido and alkynyl groups for CuAAC or SpAAC (Nguyen et al., 2009), the engineered pyrrolysyl synthetases have enabled a wider range of bioorthogonal reactive group to be genetically encoded into protein, including 2-aminothiols for cyanobenzothiazole condensation

(Nguyen et al., 2011), strained alkynes for SpAAC (Plass et al., 2011) or tetrazine ligation (Borrmann et al., 2012; Lang et al., 2012), strained alkenes for Diels-Alder reaction (Plass et al., 2012), norbornene that reacts with nitrile-imines (Kaya et al., 2012) or tetrazine (Lang et al., 2012), tetrazines with trans-cyclooctyenes (Seitchik et al., 2012), acrylamide with nitrile imine (Lee et al., 2013), etc. The list will continue to grow in the foreseeable future.

An appealing feature about some of these newly developed labeling methods is their ultrafast reaction kinetics, with k_2 up to 10^4 M^{-1} s^{-1} (Lang and Chin, 2014a, b). However, most of the proof-of concept studies were based on globular proteins that are routine to express and purify, and their applicability to proteins of greater biological significance is yet to be demonstrated.

To prepare fluorescently labeled proteins for research applications, reaction kinetics is certainly one of the important concerns, but not the predominant one. Non-specificity can be an issue as well. The strained alkenes (Hoyle and Bowman, 2010), strained alkynes (van Geel et al., 2012) and tetrazines (Jewett and Bertozzi, 2010) all have been suggested or demonstrated to react with thiols, which raises the possibility that these genetically encoded reactive handle may also suffer from cross-reactivity with neighboring cysteines, or with intracellular cysteines in the course of protein folding and trafficking.

Non-specificity can be an issue as well. The strained alkenes (Hoyle and Bowman, 2010), strained alkynes (van Geel et al., 2012), and tetrazines (Jewett and Bertozzi, 2010) all have been suggested or demonstrated to react with thiols, which raises the possibility that these genetically encoded reactive handle may also suffer from cross-

reactivity with neighboring cysteines, or with intracellular cysteines in the course of protein folding and trafficking. In our hands, we found the non-specific reaction between DIBO and free cysteine in Rho to be less than 1%, which would meet our need for subsequent fluorescence experiment.

Based on our own experience gleaned from labeling GPCRs, we contend that characterization of reaction specificity, kinetics, and topology-dependent reactivity, and protein functionality are much needed for successful application of the bioorthogonal chemistries to protein labeling.

2.4.6 The fluorescent quenching assay based on Alexa488 fluorescence

Earlier kinetics studies of chromophore binding and regeneration in Rho utilized tryptophan (Trp) fluorescence (Farrens and Khorana, 1995; Schadel et al., 2003; Sanchez-Martin et al., 2013). However, this approach relies intrinsic Trp residues that are sensitive to ligand-binding or ligand-induced conformational changes and thus has significant limitations. First, due to the low quantum yield of Trp, studying intrinsic fluorescence requires up to 10 times more protein (>10 μg or 0.5 μM) (Schadel et al., 2003; Sanchez-Martin et al., 2013) than needed when the receptor is labeled with extrinsic fluorophores with higher quantum yields (<1 μg/50 nM in our study). In addition, native Trp residues are not necessarily well positioned to serve as active-site probes. Moreover, so-called inner filter effects limit the useful concentration of UV-absorbing 11-*cis*-retinal in Trp-fluorescence experiments. Furthermore, in terms of more general applications, not all GPCR ligands will be able to quench or otherwise alter Trp fluorescence, which limits its general applicability to other GPCR systems. We thus developed a fluorescent quenching assay to circumvent these limitations of Trp

quenching studies and subsequently show that the site-specifically labeled azF-Rho remain functional photoreceptors with respect to ligand binding and release. Our results highlight the advantage of utilizing an extrinsic fluorescent reporter, which allows the flexibility of choosing the optimal photophysical properties to address a specific question, instead of relying on the intrinsic Trp fluorescence.

We envision this assay to be implemented to study the Rho mutations implicated found in various retinal diseases, such as congenital stationary night blindness (Rattner et al., 1999). The applications of this steady-state fluorescence-quenching assay are described in Chapter Three and Chapter Four. Furthermore, it could potentially provide a general scheme for studying the ligand-receptor interaction *in vitro*, especially for the peptide ligands available as fluorophore conjugates. While many previously-reported ligand binding assays similarly exploit the energy transfer between ligand and receptor (Middleton and Kellam, 2005), our methodology is advantageous in two significant ways: 1) it does not involve a fluorescent fusion protein or fluorescent antibody, and is less likely to give an artifact due to extensive modification on native state of receptors; 2) it might provide insights into the mode of binding by comparing receptors specifically labeled at different positions.

2.4.7 The advantage of targeting the TM region of GPCRs

Attaching probes to the TM region of membrane proteins have been a major technical challenge in the field (Pless and Ahern, 2013). To our knowledge, the fluorescent reporters have anchored to the TM region only by incorporation of fluorescent uaas (Cohen et al., 2002; Pantoja et al., 2009). While the fluorescent uaas benefit from short linker length between the protein backbone and the fluorophore, the

photophysical properties of the fluorophores are often limited by the small size of the fluorophore. Unlike maleimide/cysteine chemistry, which involves a thiolate anion intermediate and preferably labels sites exposed to aqueous environment (Li et al., 2002), the DIBO/azF combination readily modifies sites in the hydrophobic TM region. This property of SpAAC offers several opportunities for future work. First, the EC surfaces of GPCRs are often critical for receptor-ligand binding, and the IC surface for receptor-G protein interaction. Thus for numerous applications it is desirable to leave the EC and IC surface intact. Second, the sequence of molecular events in GPCR activation has received increasing interest (Ye et al., 2010; Altenbach et al., 2008b). The capability to anchor a probe to a particular site in the TM region of GPCRs will be a valuable tool for such studies. Third, it is expected to facilitate FRET study on the structure-function relationship of GPCRs. The energy transfer efficiency of FRET is sensitive to the distance between donor and acceptor, making it a popular tool for probing the small changes in protein conformation at the ensemble and single molecule level (Wu and Stryer, 1972; Stryer, 1978; Roy et al., 2008). However, the transfer efficiency also depends on the dipole orientation of fluorophores as well as refractive index of medium, making it difficult to obtain the absolute distance between the donor and the acceptor from FRET alone, and additional structural information is often crucial for correct interpretation of the results. However, for most GPCRs high-resolution structures are still not readily available. The conservation of the TM4 in Class A GPCRs makes it an ideal internal “molecular ruler”, enabling the FRET data to be understood in the context of a homology model (Costanzi, 2011). The TM4 sites shown to be suitable for SpAAC reaction can be extrapolated to other GPCRs (Ballesteros and Weinstein, 1995).

The preference of SpAAC with sites embedded in hydrophobic environment provides a unique possibility for studying membrane proteins. We anticipate that the micelle-enhanced bioorthogonal labeling strategy reported here will be useful to investigate receptor oligomerization, lipid-receptor interactions, and single-molecule FRET of GPCR-ligand interactions (Huber and Sakmar, 2014; Bockenhauer et al., 2011; Huber and Sakmar, 2011).

2.5 Material and Methods

2.5.1 Materials

E. coli TOP10 (Invitrogen) was used for plasmid propagation and isolation. Oligonucleotides were obtained from eOligo or Fisher Scientific. Plasmid DNA was purified using standard Maxi Prep Kits from Qiagen. AcF (RSP Amino Acids LLC) and azF (Chem-Impex International) were used without further purification. The plasmid pSVB.Yam is a tRNA expression vector carrying a humanized chimeric gene encoding an amber suppressor tRNA derived from the *B. stearothermophilus* $tRNA^{Tyr}$ (Ye et al., 2008). pcDNA.RS-Tyr is a protein expression vector based pcDNA3.1 (+)/neo (Invitrogen) with a gene encoding *E. coli* Tyr-RS with a C-terminal FLAG tag (Ye et al., 2008), pcDNA.RS-AcF (*E. coli* Tyr-RS-Y37I/D182G/F183M/L186A) and pcDNA.RS-azF (*E. coli* Tyr-RS-Y37L/D182S/F183M/L186A) are the tRNA synthetase for AcF and azF, respectively (Ye et al., 2008; Ye et al., 2009), and pMT4 carries the synthetic gene encoding wt bovine Rho (Franke et al., 1988). We introduced amber mutations into the Rho gene by QuikChange mutagenesis (Stratagene). The primers are listed in Table 2-4. All plasmid constructs were confirmed by automated DNA sequencing. The HEK293F cell lines, the transfection reagents (FreeStyle MAX), and expression media (OptiPRO SFM reduced serum medium, serum-free FreeStyle 293 expression medium) were obtained from Invitrogen/Thermo Fisher Scientific. Sepharose 2B was purchased from Sigma. 1D4-Sepharose 2B was prepared from 1D4 mAb and CNBr-activated Sepharose 2B (2 mg IgG per mL packed beads) as described below. Alexa488-DIBO was obtained from Molecular Probes/Thermo Fisher Scientific as dry powder, and dissolved in DMSO at 5 mM and stored at -20°C.

Table 2-4 The primers for site-directed mutagenesis

Mutation	Forward (5'→3')	Reverse (5'→3')
Y102amb	cctctctccatgggtagttcgtcttcggtcc	ggaccgaagacgaactacccatggagagagg
C140amb	cggtacgtggtggtgtagaagcccatgagcaac	gttgctcatgggcttctacaccaccacgtaccg
S144amb	gtgcaagcccatgtagaacttccgcttcggtga	tcaccgaagcggaagttctacatgggcttgcac
N151amb	cttccgcttcggtgagtagcacgccatcatg	catgatggcgtgctactcaccgaagcggaag
M155amb	gaaccacgccatctagggcgtcgccttcacc	ggtgaaggcgacgccctagatggcgtggttc
A158amb	cgccatcatgggcgtctagttcacctgggtc	gacccaggtgaactagacgcccatgatggcg
V162amb	gtcgccttcacctggtagatggctctggcc	ggccagagccatctaccaggtgaaggcgac
L165amb	cacctgggtcatggcttaggcctgtgcggcc	ggccgcacaggcctaagccatgacccaggtg
A169amb	gctctggcctgtgcgtagccgccgctcgtc	gacgagcggcggctacgcacaggccagagc
V173amb	ggccccgccgctctagggctggtctagatac	gtatctagaccagccctagagcggcggggcc
A234amb	gtcaaggaggcttaggcccagcagcaggag	ctcctgctgctgggcctaagcctccttgac
A246amb	gccaccactcagaagtaggagaaggaggtc	gacctccttctcctacttctgagtggtggc

2.5.2 Heterologous expression of wt and mutant Rho in suspension cells

HEK293F suspension cells were cultured in serum-free FreeStyle 293 expression medium in a 125-mL disposable, sterile, polycarbonate Erlenmeyer flask (Corning) at 37°C in 5% CO_2 atmosphere. The cell culture was shaken on an orbital shaker at 125 rpm. For amber codon suppression, the cell culture was diluted to a density of 10^6 cells/mL in a 30-mL culture supplemented with 1 mM uaas (AcF or azF) before transfection. Plasmid DNA (38.6 μg in total, 18.4 μg of pMT4.Rho containing the amber codon, 18.4 μg of pSVB.Yam, and 1.84 μg pcDNA.RS) was added into OptiPRO SFM (a total volume of 0.6 mL) reduced serum medium. In another sterile tube, transfection reagent FreeStyle MAX (38.6 μL) was diluted in into OptiPRO SFM (a total volume of 0.6 mL). The diluted transfection reagent was gently combined with the DNA. The mixture was let

stand at room temperature for 10 minutes and then added into the cell culture (total cell number 3×10^7). The cells were harvested 96 hours post-transfection. The total cell number upon harvesting normally ranged from 6×10^7 to 8×10^7.

2.5.3 Regeneration of heterologously expressed Rho

The harvested cells were resuspended in DPBS (Gibco, supplemented with leupeptin and aprotinin, Sigma) at a density of 10^7 cells/mL in a 15-mL conical, polypropylene tube (Falcon). In the dark room, 11-*cis*-retinal (1.4 mM ethanol solution) was added into the cell suspension to a final concentration of 5 μM (Oprian et al., 1987; Starace and Knox, 1998). The suspension was nutated at 4°C overnight. Excess 11-*cis*-retinal was removed by spinning down the cells and discarding the supernatant fraction. The regenerated cells can be immediately used, or may be stored at −20°C for several months.

2.5.4 Coupling 1D4 mAb with CNBr-activated sepharose 2B resin.

The method was based on earlier literature(Oprian et al., 1987; Knepp et al., 2011). In a typical preparation, 50 mL of 1D4 antibody stock solution (0.92 mg/mL in PBS) is coupled to 25 mL of CNBr-activated sepharose 2B. Before the coupling reaction, 1D4 mAb stock solution (50 mL) was concentrated by centrifugation (2,800 × g) at 4 °C using Amicon centrifugal filter unit (Ultra 15, 10 kDa MWCO) until the volume was reduced to 2 mL. The concentrated 1D4 mAb was diluted in Coupling buffer (10 mM borate, 150 mM NaCl, pH 8.2) with 60 mL coupling buffer and centrifuged again until the remaining volume was 2~3 mL. The concentrated mAb solution was transferred into a polypropylene falcon tube and measured for its concentration and volume to determine the recovery yield. Meanwhile, the sepharose 2B resin was washed with ultrapure water

(3 times the volume of resin) for 5 times to remove the ethanol in the storage buffer, followed by two washes with bicarbonate buffer (1M sodium bicarbonate, pH 11.0). After the washes, the resin was resuspended in equal volume of bicarbonate buffer to make a 50% slurry and kept on ice before use. The CNBr activation of sepharose was done in ice bath to maintain the temperature below 5 °C. During the reaction, the pH and temperature of the reaction mixture was monitored with a pH meter and a thermometer. The CNBr solution (approx. 2.55 g CNBr in 2-3 mL acetonitrile) was gently added to the sepharose under mixing by a tissue-culture magnetic stirrer. The reaction was allowed to proceed from 10 to 30 min. During this time 10 M NaOH was added dropwise to neutralize HBr and keep the pH approximately constant. When the reaction was close to completion, the decrease of pH should slow down. The activated sepharose was instantly transfer into a Büchner funnel connected to a suction flask to remove the unreacted CNBr. The flask was filled with ~100 mM Fe (II)SO_4 (3 g in 100 mL water) to destroy the unreacted CNBr. The resin was washed 4 times with ice-cold ultrapure water (50 mL each time) and twice with ice-cold coupling buffer (50 mL each time). Then the activated sepharose resin was transferred into 50-mL Falcon tube and resuspended in coupling buffer to make 50% slurry. Transfer slurry to tubes for coupling. The concentrated 1D4 resin was immediately added into the slurry and thoroughly mixed it by ten inversions. The mixture was kept on nutator at 4 °C overnight to allow the primary amines of the mAb to react with the CNBr-activated resin. After the reaction was complete, the mixture was centrifuged to remove the supernatant (check whether supernatant is free of protein; A280 should be ≤ 0.05). Then resin was washed with 4-5 volumes of 10 mM glycine in DPBS for 20 min on a nutator at 4 °C to deactivate the excess CNBr. In the end the resin

was washed twice with 4~5 volumes of DPBS and resuspended in DPBS as 50% slurry. The 1D4 mAb sepharose 2B resin was stored as 50% slurry in PBS with NaN_3 (10 mM) at 4 °C.

2.5.5 Purification of heterologously expressed Rho

The regenerated cells were lysed with the solubilization buffer (1 mL per 10^7 cells, 1% (w/v) DM, 50 mM HEPES or Tris-HCl, pH 6.8, 100 mM NaCl, 1 mM $CaCl_2$ with complete EDTA-free protease inhibitor cocktail) for at least 1 h at 4°C. All the regenerated samples were maintained in the dark and handled in a darkroom using red safe lights. The cell lysates were centrifuged at 100,000 × g for 30 min at 4°C. The supernatant fraction was mixed with 1D4-Sepharose-2B resin (50 μL or 100 μL) and incubated overnight at 4°C. The resin was then transferred into a microporous centrifugal filtering unit (Microcon-MC pore size 0.48 μm, Millipore), which allows for efficient removal of washing buffer. The resin was first washed with DPBS containing 0.1% (w/v) DM for three times (30 min incubation each time), and then with a low-salt buffer (0.1% (w/v) DM in 2 mM phosphate buffer, pH 6.0). Eventually, the receptor was eluted with the elution buffer (100 μL, no less than the volume of the resin; 0.1% (w/v) DM and 0.33 mg/mL C9 peptide in 2 mM phosphate buffer, pH 6.0). The resin was incubated with the elution buffer on ice for at least 1 h. The purified receptor was collected in a clean 1.5 mL Eppendorf tube. Two elutions should recover 70–80% of the receptor. The Rho yield from 10^7 HEK293F cells is typically 5−8 μg for wt and 0.5−1 μg for azF variants.

2.5.6 UV–Vis spectroscopy of the purified Rho

The dark-state absorption spectrum of Rho was recorded on a Lambda-800 spectrophotometer (PerkinElmer Life Sciences) in a 50-μL micro-cuvette with a 10-mm path length. The receptor was then photobleached by irradiating the sample for 30 s with a 335-mW 505-nm LED light source (Thorlabs) placed on top of the cuvette before acquiring the light spectrum. The dark−light difference spectrum at 500 nm was used to calculate the concentration of Rho using an extinction coefficient of 40,600 $M^{-1}cm^{-1}$. The Alexa-488 concentration was calculated from 495-nm absorbance in the light spectrum using the extinction coefficient 73,000 M^{-1} cm^{-1}. The labeling stoichiometry is the ratio of the Alexa-488 and Rho concentrations determined this way.

2.5.7 Bioorthogonal labeling of Rho

The 11-*cis*-retinal regenerated cells were lysed with the solubilization buffer (1 mL per 10^7 cells, 1% (w/v) DM, 50 mM HEPES or Tris-HCl, pH 6.8, 100 mM NaCl, 1 mM $CaCl_2$ with complete EDTA-free Protease Inhibitor Cocktail, Roche) for at least 1 h at 4°C. The lysate was cleared by centrifugation at 100,000 × g for 30 min and incubated overnight at 4°C with 1D4-mAb-sepharose 2B (100 μL). The resin was transferred into a 1.5-mL Eppendorf tube and washed three times for 30 min each with 0.5 mL reaction buffer. Then the reaction buffer (200 μL) was mixed with the resin (100 μL) to give 300-μL slurry.

The reaction was stopped by centrifugation and removal of the supernatant fraction. The resin was then transferred into a microporous centrifugal filtering unit (Microcon-MC pore size 0.48 μm, Millipore). The resin was first washed with the reaction/wash buffer for three times (30 min incubation each time) to deplete the unreacted dyes, and

then with a low-salt buffer (0.1% (w/v) DM, 2 mM sodium phosphate buffer, pH 6.0). The receptor was eluted with elution buffer (100 μL, no less than the volume of the resin; 0.33 mg/mL C9 peptide in 0.1% (w/v) DM, 2 mM sodium phosphate buffer, pH 6.0). The resin was incubated with the elution buffer on ice for at least 1 h. The purified receptor was collected in a clean 1.5-mL Eppendorf tube. The elution was repeated a second time. The combined elutions were supplemented with 150 mM NaCl and characterized by UV-Vis spectroscopy and in-gel fluorescence. Purified samples were stored at −80°C and thawed on ice before use.

2.5.8 Kinetic study of SpAAC and oxime ligation

The reaction was performed under the same condition as described above. The starting mixture consists of uaa-tagged Rho or wild-type Rho bound to 1D4-sepharose 2B resin (100 μL), and reaction buffer (200 μL). At different time points, an aliquot of the resin/buffer mixture (30 μL) was taken out and added into 0.4 mL of pre-cooled reaction/wash buffer in a clean 1.5-mL Eppendorf tube to quench the reaction. The resin was centrifuged and the supernatant containing unreacted labeling reagents was removed. The resin was washed once with 0.4 mL of wash buffer (30 minutes) to remove the remaining labeling reagent. The labeled Rho was eluted with the elution buffer containing the C9 peptide (15 μL elution buffer × 2). The time-series samples were separated by SDS-PAGE gel (10 μL eluate for each time point) and analyzed with dual-color quantitative western blot using 1D4 mAb as primary antibody, IRDye800CW goat anti-mouse secondary antibody (LI-COR), and IRDye680RD Streptavidin (LI-COR) for biotin detection. The degree of labeling was measured as the ratio of the biotinylation signal to 1D4 signal (protein loading). The extent of labeling reaction (ξ) was calculated

as the ratio of biotinylation signal (700-nm channel) to 1D4 signal (800-nm channel) (i.e., $\xi = I_{700}/I_{800}$). Because the blots from two membranes are subject to random variations for each chemistry, the uaa-tagged Rho and wt Rho time-series samples were further analyzed on the same SDS-PAGE gel for comparison. The ξ was plotted as a function of the reaction time, and fitted using the first-order exponential model to obtain the pseudo first-order rate constant k_1. The reaction rate constant k_2 was calculated as k_1/c (labeling reagent).

2.5.9 Dual-color quantitative Western blot analysis

Appropriate amount of labeled Rho was separated by SDS-PAGE under reducing conditions. The sample was transferred to Immobilon-FL Transfer Membrane (Millipore), blocked with 1% BSA in PBS (20 mM phosphate saline buffer, pH 7.2) at room temperature for 1 h, and stained with 1D4 monoclonal antibody (5000-fold dilution from 1 mg/mL 1D4 stock solution in PBST: 20 mM phosphate saline buffer, pH 7.2, with 0.1% Tween20) against the C-terminal epitope of Rho. After washing with 1× PBST (5 min × 4), the membrane was blotted simultaneously with IRDye800CW goat anti-mouse secondary antibody (20,000-fold dilution, LI-COR) and IRDye680RD Streptavidin (5,000 × dilution, LI-COR). The unbound secondary antibody and streptavidin were washed away with 1× PBST (5 min × 4). The membrane was scanned with Odyssey SA Infrared Imaging System to quantify the biotinylation signal (700-nm channel) and the amount of loaded protein (800-nm channel). The image was analyzed with Image Studio (LI-COR software). Rho as a glycosylated membrane protein runs as a smear on the SDS-PAGE gel. Thus the entire region of the smear was selected to measure the biotin and 1D4 signal intensity.

2.5.10 Kinetic study of SpAAC using Alexa488-DIBO

The reaction was performed under the same condition as described above. The initial concentration of the labeling reagents (10 μM) was approximately 20-fold excess molarity. At different time points, an aliquot of the resin/buffer mixture (30 μL) was taken out and added into a clean 1.5-mL Eppendorf tube. The reaction was quenched by adding the wash buffer (0.4 mL; 0.1% DM (w/v) DPBS, pH 7.2) and centrifugation. Washing and elution were done as described in the previous section. The labeled Rho was first separated by SDS-PAGE electrophoresis, and then visualized by in-gel fluorescence. Silver staining was performed for the same gel in order to normalize the sample concentration.

2.5.11 In-gel fluorescence to detect covalent Rho labeling

The labeled and purified Rho sample (50−100 ng) was separated by SDS-PAGE under reducing conditions. In order to minimize protein aggregation, the sample was not heated prior to loading. Gels were briefly washed in ultrapure water and then visualized on a confocal Typhoon 9400 fluorescence scanner (GE) with 488-nm laser excitation and 510–520 nm band-pass for the fluorescence emission.

2.5.12 Silver staining to quantify protein concentration.

After electrophoresis, the SDS-PAGE gel was rinsed in the fixative buffer (40% water, 50% methanol, 10% acetic acid) for at least one hour with two or three changes of buffer. Then the gel was transferred into ultrapure water to remove the residual acid and methanol. The staining buffer was prepared fresh by adding solution A (0.4 g silver nitrate dissolved in 2 mL water) drop wise into solution B (0.7 mL 30% ammonium

hydroxide added into 10.5 mL 0.36% sodium hydroxide solution) under constant stirring. Following the clearing of the brown precipitate, the total volume of the staining buffer was brought to 50 mL with ultrapure water. The gel was stained under gentle agitation for 10 to 15 minutes, and briefly washed with ultrapure water to remove the staining buffer. Meanwhile, the developing buffer was prepared as follows: mix 30% formaldehyde (50 μL) with 1% citric acid (0.5 mL), and add water to 100 mL. The time needed for achieving best contrast may vary from one experiment to another. Typically, when the background began to turn yellow, we stopped development by transferring the gel into 1% acetic acid. After through washing in water, the silver-stained gel was scanned and analyzed with ImageJ.

2.5.13 Determination of the partition coefficient of Alexa488-DIBO between micelle and water

Approximately 5 μM Alexa488-DIBO solution was prepared in 1× DPBS buffer containing various concentrations of DM micelles (up to ~ 1% (w/v)). 400 μL of the solution was placed in an ultrafiltration spin filter (Amicon Ultra 0.5 mL centrifugal filters, MWCO 10 kDa) and centrifuged at 14,000 × g for 5~7 min until the volume of the filtrate was approximately 200 μL. The accurate volumes of the filtrate and the retentate were determined by pipetting. The concentrations of Alexa488-DIBO in the filtrate and retentate were quantified by UV-Vis spectroscopy (ε_{495nm} = 73, 000 M^{-1} cm^{-1}).

2.5.14 Functional characterization of labeled Rho by steady-state fluorescence

Fluorescence spectroscopy was performed at 28 °C on a SPEX Fluorolog spectrofluorometer in photon counting mode. The time course experiments were done by adding Alexa488-labeled receptor elutions (30 μL) at a final concentration of 15–50 nM

to the assay buffer (450 μL; 10 mg/mL POPC, 10 mg/mL CHAPS, 125 mM KCl, 25 mM MES, 25 mM HEPES, 12.5 mM KOH, pH 6.0) under constant stirring. During time scan experiments the excitation wavelength was 480 nm with 0.2-nm band-pass to minimize photobleaching, and the emission was measured at a wavelength of 525 nm with 15-nm band-pass. The 11-*cis*-retinal stock solution in ethanol was diluted in the assay buffer, and 20 mL of this working dilution was added to the cuvette to a final concentration of 1.5 μM (1.48–1.59 μM) retinal. For each measurement, the concentration of freshly diluted retinal (c_{retinal}) was determined from its 378-nm absorbance (extinction coefficient 24,400 $\text{M}^{-1}\ \text{s}^{-1}$). The pseudo-first order rate constant (k_1) was obtained by fitting the fluorescence signal with monoexponential decay model. The second-order recombination reaction rate constant (k_2) was calculated as k_1/c_{retinal}.

Chapter Three: Kinetics and Thermodynamics of the Chromophore Binding Reaction in Rhodopsin

3.1 Summary

The fundamental molecular event underlying dark adaptation is the recombination reaction between opsin and 11-*cis*-retinal after photobleaching of rhodopsin. We report here a detailed analysis of the kinetics and thermodynamics of this "regeneration" reaction. To enable FRET-based measurement of the recombination between opsin and 11-*cis*-retinal, we prepared a recombinant rhodopsin with a genetically encoded azido-Phe (azF) that was subsequently modified with Alexa488 fluorophore in a quantitative bioorthogonal labeling reaction. We also utilized a phospholipid/detergent bicelle system that provided a thermostabilizing lipid bilayer environment over the long timescales required for the experiments. The recombination reaction followed a second-order rate law. The temperate-dependent kinetics of the recombination reaction and the dissociation reaction were measured to derive the enthalpic and entropic changes required to achieve the transition state. We were also able to quantify for the first time *in vitro*, the very slow dissociation rate of 11-*cis*-retinal from rhodopsin. Isothermal titration calorimetric was used to obtain the total change in enthalpy for the 11-*cis*-retinal binding reaction. We considered all of the experimental results obtained to derive an energy landscape plot for the rhodopsin regeneration reaction. These results provide insights relevant to dark noise and dark adaptation in the visual system as well as to ligand-binding reactions in related G protein-coupled receptor systems.

3.2 Introduction

3.2.1 Rhodopsin regeneration and dark adaptation

The rod cell visual photoreceptor rhodopsin (Rho), responsible for scotopic, or dim-light vision, consists of a heptahelical transmembrane apoprotein opsin and a chromophore, 11-*cis*-retinal (Wald, 1968; Schertler et al., 1993; Palczewski et al., 2000). In the dark state, opsin and 11-*cis*-retinal are covalently linked together through a protonated Schiff base (PSB) (Bownds and Wald, 1965; Bownds, 1967). The interactions between the amino acid side chains in the ligand-binding pocket and 11-*cis*-retinal give Rho its characteristic absorption band centered at 500 nm (Shichi, 1970). Upon photoactivation, the chromophore 11-*cis*-retinal absorbs a photon to isomerize to all-*trans*-retinal (Hubbard and Wald, 1952), triggering a series of conformational changes that eventually results in the Meta-II state to activate heterotrimeric G protein (transducin) for downstream signaling (Stryer, 1986; Sakmar et al., 2002). The decay of Meta-II is accompanied by the hydrolysis of the Schiff base bond and subsequent dissociation of retinal from its binding pocket. To recycle the photoreceptor, the apoprotein opsin recombines with 11-*cis*-retinal to from rhodopsin, a process referred to as regeneration.

Regeneration of Rho in the dark after photobleaching is the fundamental molecular event underlying visual dark adaptation. The correlation between the fraction of Rho and visual sensitivity under various lighting conditions is described by the Dowling-Rushton relation (*i.e.*, the fraction of unregenerated Rho is proportional to the log threshold elevation) (Rushton, 1961; Lamb and Pugh, 2006). Furthermore, efficient regeneration of Rho is required for preventing the deterioration of rod outer segment

(ROS) morphology (Dowling and Wald, 1960). Therefore, it is of great importance to understand the chemical mechanism of the recombination reaction between opsin and 11-*cis*-retinal. However, compared to the photoisomerization of retinal and the receptor activation process (Cooper, 1981; Schick et al., 1987), the energetics of the regeneration reaction remains much less well understood.

3.2. 2 The reconstitution method for studying rhodopsin regeneration

Kühne and his assistant Ewald described the first *in vitro* regeneration experiment of Rho in 1878 (Wolf, 2001; Kühne, 1978). After many failed attempts to reproduce this initial observation, it was confirmed nearly fifty years later by Hecht and his co-workers (Hecht et al., 1936; Chase and Smith, 1940). It was found that regeneration occurred only for Rho freshly extracted with bile salt or digitalin crystals at nearly neutral pH. Wald later demonstrated that the regeneration process was the recombination reaction between opsin and 11-*cis*-retinal (Wald and Brown, 1950).

The kinetic characterizations for this recombination reaction were carried out under a variety of conditions with respect to the method of receptor reconstitution, concentration of retinal, temperature, pH, ionic strength, etc., and the resulting reaction rates reported in the literature span three orders of magnitude (10^2~10^5 M^{-1} s^{-1}) (Henselman and Cusanovich, 1976; Zorn and Futterman, 1973; Matsumoto and Yoshizawa, 1975; Matsumoto et al., 1978; Mccaslin and Tanford, 1981; Sakamoto and Khorana, 1995; Gross et al., 2003a; Gross et al., 2003b; Piechnick et al., 2012). It was often observed that Rho solubilized in detergent micelles could not be fully regenerated (Sanchez-Martin et al., 2013; Mccaslin and Tanford, 1981; Sakamoto and Khorana,

1995), with the notable exception of digitonin, a nonionic steroidal glycoside (Wald and Brown, 1950; Matsumoto and Yoshizawa, 1975; Matsumoto et al., 1978).

We initially hypothesized that the observed poor regeneration efficiency were due to the low thermostability of opsin in these detergent micelle systems. The regeneration reaction begins with the apoprotein opsin, which is unstable in most detergent systems, and irreversibly loses its ability to bind with retinal with a half-life ranging from minutes to hours, depending on the specific detergent. Among the studied detergents, digitonin confers highest thermostability for opsin (Degrip, 1982a). However, digitonin has several practical disadvantages, such as inhomogeneity, variable solubility, a low CMC, a high micelle molecular weight, difficulty to remove by dialysis (Degrip, 1982a; Hjelmeland and Chrambach, 1984). These properties make digitonin cumbersome to use. Thus the mild and highly soluble detergents like *n*-octyl-*β*-glucoside (OG) or *n*-dodecyl-*β*-D-maltoside (DM) have gained a greater popularity for studying Rho and other GPCRs.

Some studies utilized Rho with a pair of mutations N2C/D282C (Xie et al., 2003) that introduced a thermostabilizing disulfide bond to achieve enhanced regeneration in DM micelles (Gross et al., 2003a; Gross et al., 2003b; Piechnick et al., 2012). Nonetheless, the possibility of generating an artifact from the additional disulfide bond close to the retinal binding pocket remains a concern. Phospholipid additives (Sakamoto and Khorana, 1995) or reconstitution of Rho into liposomes (Sanchez-Martin et al., 2013) facilitated the regeneration process. However, addition of phospholipids only increases the yield to approximately 80% regeneration (Sakamoto and Khorana, 1995) and the preparation of liposome and subsequent insertion of Rho into the liposome is a laborious process (Sanchez-Martin et al., 2013).

Our aim was to study the recombination reaction between opsin and retinal using a suitable platform that provides a lipid bilayer environment and is easy to manipulate. Therefore we turned to the bicelles, a model lipid bilayer system comprises of long-chain phospholipids and either detergents or short-chain phospholipids (Sanders and Prosser, 1998). The long-chain phospholipids form planar lipid bilayer fragments, which are edge-stabilized by detergents or short-chain phospholipids that provide enhanced solubility in the aqueous phase (Whiles et al., 2002). An increasing number of studies involving membrane proteins reconstituted into bicelles suggest that in the presence of the lipid environment the membrane proteins are more likely to retain their native activities than when reconstituted in detergent systems (Durr et al., 2012).

3.2.3 Deriving energy diagram for the chromophore binding reaction in rhodopsin

In order to draw the energy diagram for a ligand-receptor binding reaction with a single transition state (TS), minimally two out of three of the following measurements need to be made: 1) the activation energy of the forward reaction $\Delta^{\neq}G_{\text{on}}$, 2) the activation energy of the reverse reaction $\Delta^{\neq}G_{\text{off}}$, and 3) the energy difference between the reactants and the products under a particular state $\Delta G°$' (Figure 3-1). Based on the transition state theory:

$$k = \frac{k_B T}{h} e^{-\frac{\Delta^{\neq} G}{RT}} = \frac{k_B T}{h} e^{-\frac{\Delta^{\neq} H - T\Delta^{\neq} S}{RT}}$$

Where $\Delta G^{\neq}$ is the Gibbs energy of activation, $\Delta H^{\neq}$ is the enthalpy of activation, $\Delta S^{\neq}$ is the entropy of activation, k_{B} is Boltzmann's constant, and h is Planck's constant.

$\Delta G_{on}^{\neq}$ and $\Delta G_{off}^{\neq}$ need to be obtained by kinetic measurements, while $G°'$ requires a method to measure the energy difference between the reactants and the products.

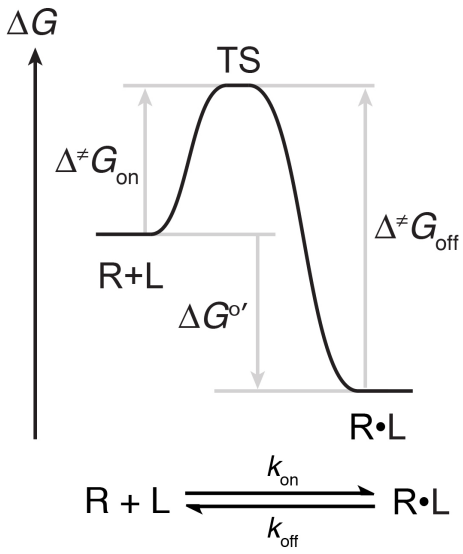

Figure 3-1. Energy diagram for the recombination reaction between receptor and ligand based on transition state (TS) theory. The forward reaction refers to the association between the receptor and the ligand. The reverse reaction refers to the dissociation of the ligand from the receptor. The free energy of activation for the forward reaction is defined as $\Delta^{\neq}G_{on} = G_{TS} - (G_R+G_L)$, for the reverse reaction as $\Delta^{\neq}G_{off} = G_{TS} - G_{R\bullet L}$. The overall change of free energy under a particular state is defined as $\Delta G°' = G_{R\bullet L} - (G_R+G_L)$. The reaction rates of the forward reaction and the reverse reaction are defined as k_{on} and k_{off}, respectively.

Based on the linear form of the Eyring-Polanyi equation:

$$\frac{k}{T} = -\frac{\Delta^{\neq}H}{R}\cdot\frac{1}{T} + \ln\frac{k_B}{h} + \frac{\Delta^{\neq}S}{R}$$

By measuring the temperature-dependent reaction kinetics, it is possible to separate the enthalpic and entropic contribution to free energy required for activation.

We measured the kinetics of the forward reaction (k_{on}) of the recombination between 11-*cis*-retinal and opsin using novel FRET-based assays. We utilized expressed recombinant Rho with a genetically encoded *p*-azido-Phe (azF) at position 144 that was labeled with Alexa488 using a robust bioorthogonal labeling reaction. The S144Alexa488-Rho and unlabeled Rho purified from bovine ROS enabled precise kinetic measurement of the regeneration reaction. We employed a 1-palmitoyl-2-oleoylphosphatidylcholine/3-[(3-Cholamidopropyl) dimethylammonio]-1-propanesulfonate (POPC/CHAPS) bicelle system to reconstitute Rho. We then measured the kinetics of the very slow reverse dissociation reaction of 11-*cis*-retinal from Rho (k_{off}) by monitoring the exchange of the 11-*cis*-retinylidene chromophore with 9-*cis*-retinal *in vitro*. Finally, we measured the enthalpy of the reaction using isothermal titration calorimetry (ITC). In summary, using FRET, UV-Vis spectroscopy, and ITC assays, we were able to derive the kinetic and thermodynamic properties of the reversible regeneration reaction between 11-*cis*-retinal and rhodopsin and derive an energy landscape diagram.

3.3 Results

3.3.1 The thermostability of photobleached Rho

To analyze the recombination reaction between opsin and retinal, we need a reconstitution method that stabilizes opsin at its functional state. We developed a POPC/CHAPS bicelle system to mimic the native membrane environment for the receptor. Previous studies on Rho reconstituted into DMPC/CHAPS bicelles has demonstrated that bicelles of various composition confers an increased thermostability to opsin(Reeves et al., 1999; McKibbin et al., 2007, and facilitates the formation of rhodopsin-Gt high-affinity complex {Kaya, 2011 #1044). Moreover, compared to liposome vesicles, bicelles are easier to prepare, and produce less background signal in spectroscopic studies (Durr et al., 2012). We used the ability of binding with 11-*cis*-retinal as a criterion for correctly-folded, functional opsin, which can be quantified based on the recovery of 500-nm absorbance. Rho purified from ROS was solubilized in *n*-dodecyl-*β*-D-maltoside (DM) micelles or POPC/CHAPS bicelles, photobleached by 505-nm irradiation, and subsequently incubated at 28 °C for various lengths of time. Then the photobleached samples were supplemented with fresh 11-*cis*-retinal, and kept in the dark until the regeneration was complete. The samples were then analyzed using UV-Vis spectroscopy (Figure 3-2). The extent of regeneration was assessed based on the recovery of 500-nm absorbance. We found that the DM-solubilized samples lost the potential to recombine with 11-*cis*-retinal with a half-life of 2.1 h (Figure 3-2F). By comparison, more than 98% of the POPC/CHAPS-solubilized pigment retained the potential for regeneration over 18 hours (Figure 3-2F), demonstrating the thermostabilizing property of POPC/CHAPS bicelles.

Figure 3-2. Photobleached Rho is more stable in POPC/CHAPS bicelle than in DM micelle. A) The structure of DM and the cartoon of Rho reconstituted in DM micelles. **B)** The structure of 1-palmitoyl-2-oleoylphosphatidylcholine (POPC) and 3-[(3-Cholamidopropyl) dimethylammonio]-1-propanesulfonate (CHAPS) and the cartoon of Rho reconstituted in POPC/CHAPS bicelles. **C)** The experimental procedures for assaying the thermal stability of photobleached Rho in either DM micelles or POPC/CHAPS bicelles. Rho purified from bovine ROS was reconstituted into DM micelles or POPC/CHAPS bicelles, photobleached by 505 nm-LED irradiation, and incubated in the dark at 28 °C for the indicated lengths of time. Then the samples were supplied with fresh 11-*cis*-retinal diluted in the POPC/CHAPS bicelle buffer (the molar ratio of 11-*cis*-retinal to opsin was 1.5:1). After complete regeneration (reaction time >15 h), the extent of regeneration was evaluated based on the 500-nm absorbance of the difference spectrum (the spectrum of the dark-state sample subtracted by the spectrum of the photobleached sample in the presence of NH_2OH). **D)** The end-point difference spectra of Rho in DM micelles showed a gradual loss of the 500-nm absorbance, indicating the formation of thermal denatured opsin that could not be regenerated with 11-*cis*-retinal. **E)** The end-point difference spectra of Rho in POPC/CHAPS bicelles showed that all the samples could be effectively regenerated. **F)** The time course of the thermal denaturation of Rho in DM micelles and in POPC/CHAPS bicelles at 28 °C. The 500-nm absorbance of the regenerated samples were normalized using the initial concentration of Rho measured before photobleaching. In DM, the time course was fitted into a mono-exponential model, with a half-life of 2.1 h. In POPC/CHAPS bicelle, photobleached Rho was essentially stable over 18 h.

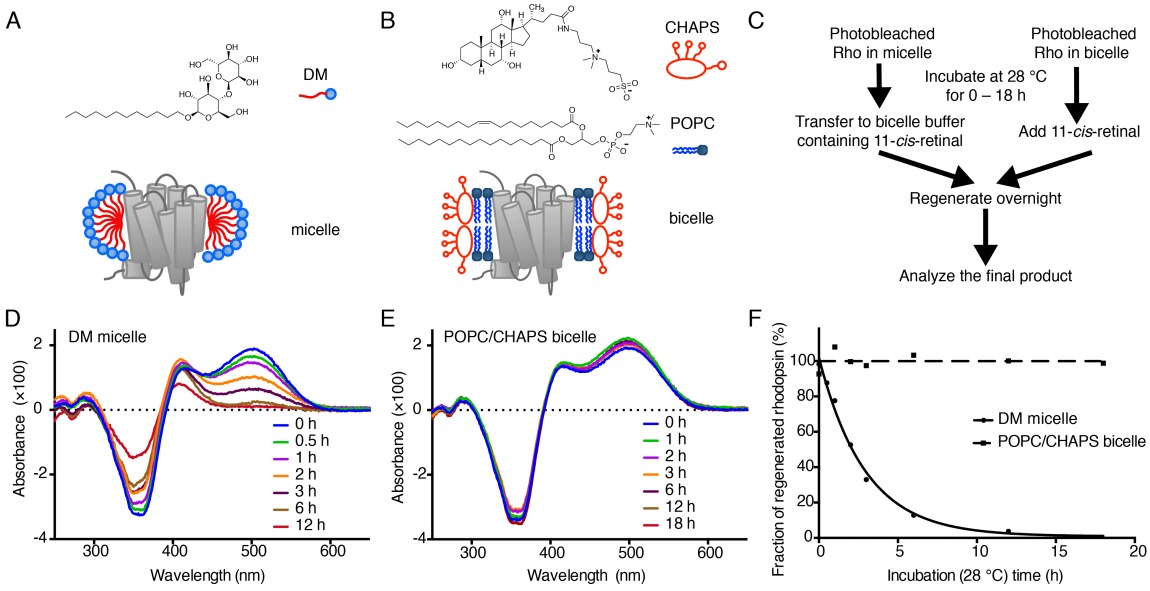
A
DM
micelle
B
CHAPS
POPC
bicelle
C
Photobleached Rho in micelle
Photobleached Rho in bicelle
Incubate at 28 °C for 0 – 18 h
Transfer to bicelle buffer containing 11-cis-retinal
Add 11-cis-retinal
Regenerate overnight
Analyze the final product
D
DM micelle
Absorbance (×100)
Wavelength (nm)
0 h
0.5 h
1 h
2 h
3 h
6 h
12 h
E
POPC/CHAPS bicelle
Absorbance (×100)
Wavelength (nm)
0 h
1 h
2 h
3 h
6 h
12 h
18 h
F
Fraction of regenerated rhodopsin (%)
Incubation (28 °C) time (h)
DM micelle
POPC/CHAPS bicelle

3.3.2 FRET-based assays to measure the kinetics of 11-*cis*-retinal binding to opsin

We established two FRET-based assays to measure regeneration kinetics, both of which involve a fluorescent reporter as the energy donor and retinal as the acceptor (Figure 3-3). The first assay utilizes intrinsic Trp fluorescence. Energy transfer between Trp residues and 11-*cis*-retinal results in approximately 80% quenching of the Trp fluorescence in the dark-state Rho. Upon photoactivation, 11-*cis*-retinal isomerizes to give all-*trans*-retinal, followed by the formation of the active Meta-II state characterized by a deprotonated Schiff base (SB). At Meta-II state, the retinal absorption peak shifts from 500 nm to 380 nm and the increased energy transfer further reduces the Trp fluorescence. The Meta-II species decays over time, and all-*trans*-retinal is released from its binding pocket, causing Trp fluorescence to increase (Farrens and Khorana, 1995). Therefore Trp fluorescence can be used in principle to measure the kinetics of retinal release through Meta-II decay and retinal entry.

The second assay utilizes an extrinsic fluorophore reporter Alexa488, which can be site-specifically attached to a receptor containing azF using a labeling protocol described in Chapter II. Approximately 50% of the Alexa488 fluorescence in S144-Alexa488 Rho is quenched by the bound 11-*cis*-retinal, due to the spectral overlap between the 500-nm absorption peak and Alexa488 emission. Once the Meta-II species is formed, the spectral shift results in the loss of this spectral overlap, and consequently a decrease in energy transfer between the donor and the acceptor. Thus Alexa488 fluorescence serves as an unambiguous indicator for the formation of the PSB, as it can be effectively quenched by the dark-state Rho alone. Previously, fluorescein has been attached to Rho as a reporter for retinal entry (Wu and Stryer, 1972).

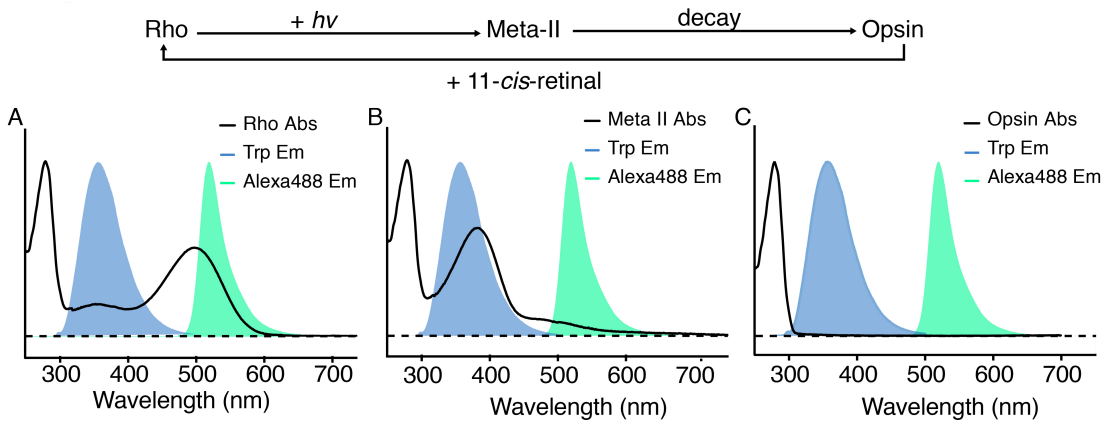

Figure 3-3. The energy transfer scheme for the Trp and Alexa488-based FRET assays. The assays employ an engineered Rho that harbors an Alexa488 fluorescent reporter covalently attached to the second intracellular loop of Rho (S144-Alexa488 Rho). The absorption spectra of Rho (**A**), Meta-II state Rho (**B**), and opsin (**C**) are overlaid with the fluorescence emission peak of Trp (*blue*, maximum at 330 nm) and Alexa488 (*green*, maximum at 520 nm). The scales of the peaks do not correspond to their actual intensities. **A**) At the dark-state, about 50% of Alexa488 fluorescence is quenched by the 500-nm absorption peak of Rho (1),(Tian et al., 2014) and about 80% of the fluorescence of Trp is quenched by the lower 380-nm peak (2) of Rho (Farrens and Khorana, 1995). **B**) Upon photoactivation, 11-*cis*-retinal isomerizes to form all-*trans*-retinal, followed by the formation of the active Meta-II state with a deprotonated Schiff base (SB). As a result, the retinal absorption peak shifts from 500 nm to 380 nm, and fluorescence emission of Alexa488 no longer overlaps with the 500-nm absorption peak (1), resulting in an increase of Alexa488 signal. Meanwhile, the energy transfer efficiency between Trp and the Meta-II Rho increases due to absorption peak of Meta-II Rho at 380 nm (3). Since the energy transfer efficiency is already high in Rho, this increased spectral overlap only slightly further reduces the Trp fluorescence. **C**) The deprotonated SB between opsin and all-*trans*-retinal hydrolyzes, causing retinal to dissociate from the binding pocket of opsin. This process is referred to as Meta-II decay. Neither Alexa488 nor Trp fluorescence is quenched in the apoprotein opsin, as the energy acceptor retinal is not within the physical proximity of the energy donor.

However, fluorescein exhibits dramatically reduced fluorescence at pH 6.0, as compared to neutral or basic pH. Compared to fluorescein, Alexa488, a fluorescein derivative, shows greater photostability and much less pH sensitivity. Moreover, Alexa488 fluorescence falls into a clean window of retinal absorbance so that the inner filter effect is negligible even for experiments involving a high retinal concentration.

We reconstituted Rho into POPC/CHAPS bicelle by simply adding Rho purified in DM micelles into the bicelle-containing assay buffer. We then photobleached the Rho and allowed the Meta-II decay to reach completion. Upon the addition of exogenous 11-*cis*-retinal, we observed a robust mono-exponential decrease in the Trp or Alexa488 fluorescence signal (Figure 3-4A, C). By contrast, we were not able to observe a similar extent of regeneration over a comparable time scale for Rho reconstituted in DM micelles (Figure 3-4B, D), suggesting that the presence of lipid bilayer environment was critical for regeneration.

We observed a small drop of fluorescence signal upon the addition of 11-*cis*-retinal for ROS Rho and S144-Alexa488 Rho in 1% POPC/CHAPS bicelle, and S144-Alexa488 Rho in 0.1% DM (Figure 3-4A, C, D). However, for ROS Rho reconstituted in 0.1% DM (Figure 3-4B), this initial drop was much larger. Moreover, in the experiments with Rho in POPC/CHAPS bicelle, where we observed effective regeneration, the fluorescence signal at the end of the reaction was also slightly smaller than the signal before photobleaching (Figure 3-4A, C).

In addition to the energy transfer, there are three plausible factors that may cause a reduction in the fluorescence signal. First, the dilution effect from adding 20 μL of

Figure 3-4. Comparison of Rho regeneration in bicelles and micelles. A) Purified ROS Rho reconstituted in 1% POPC/CHAPS bicelles; **B)** ROS Rho in 0.1% DM micelles (inset: ROS Rho in 2% DM micelles); **C)** Purified S144azF mutant Rho labeled with a Alexa488 fluorophore (S144-Alexa488 Rho) in 1% POPC/CHAPS bicelles; **D)** S144-Alexa488 Rho in 0.1% DM micelles. In all cases, dark-state ROS Rho or S144-Alexa488 Rho in 0.1% DM (30 μL) was added into the assay buffer (450 μL) containing either CHAPS/POPC bicelles or DM micelles (arrow a′). The sample was then photobleached by 505-nm LED light to form the active Meta-II state (arrow b′). After Meta-II decay was close to completion, ligand 11-*cis*-retinal diluted in the assay buffer (20 μL) was added to initiate pigment regeneration (arrow c′). In Panel **A)** and **B)**, the Trp fluorescence of ROS Rho was excited at 295 nm (bandpass 0.6 nm) and collected at 330 nm (bandpass 15 nm). In Panel **C)** and **D)**, the Alexa488 fluorescence of the mutant S144-Alexa488 Rho was excited at 488 nm (bandpass 0.2 nm) and collected at 520 nm (bandpass 15 nm). In the POPC/CHAPS bicelle system, both the Trp-based and Alexa488-based FRET assay showed a mono-exponential decrease of fluorescence signal upon the addition of exogenous 11-*cis*-retinal, indicating the formation of Rho. By contrast, such regeneration behavior was not observed for Rho in DM micelles.

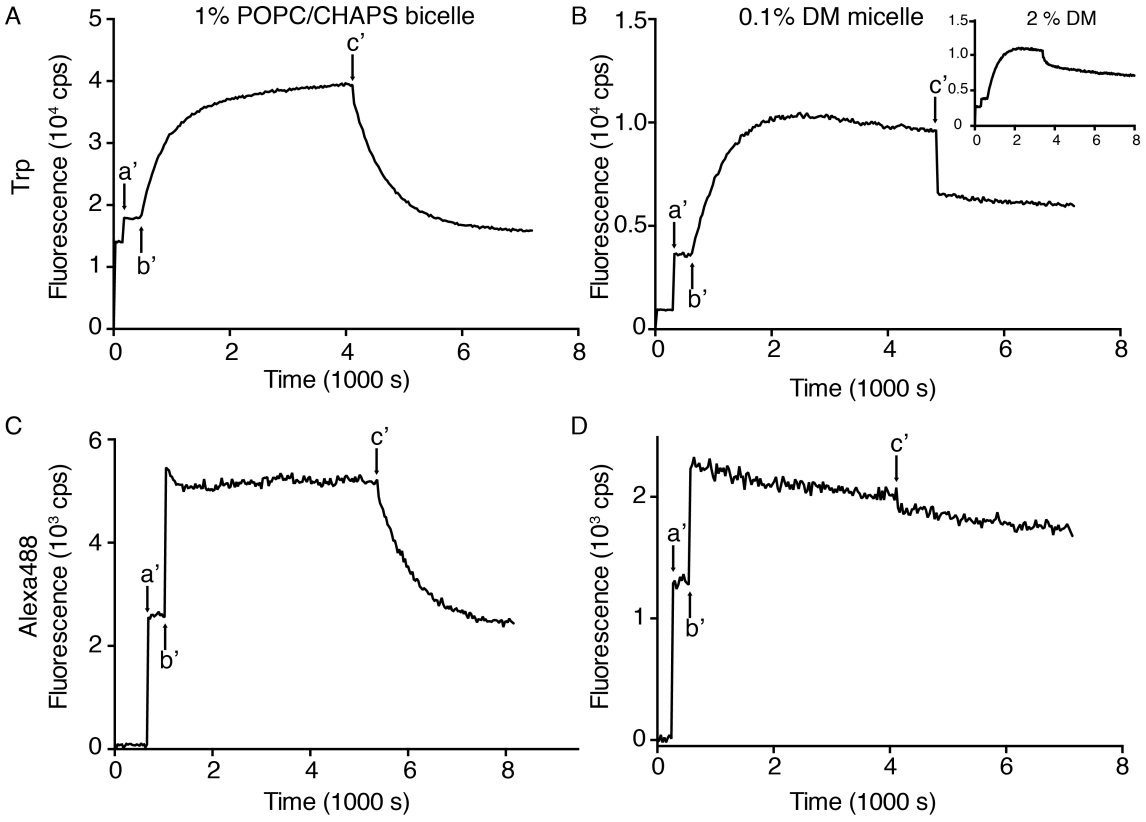
A
1% POPC/CHAPS bicelle
Trp
Fluorescence (10^4 cps)
a'
b'
c'
Time (1000 s)
B
0.1% DM micelle
2 % DM
Fluorescence (10^4 cps)
Time (1000 s)
C
Alexa488
Fluorescence (10^3 cps)
Time (1000 s)
D
Fluorescence (10^3 cps)
Time (1000 s)

retinal solution into the 480 μL-assay buffer can account for approximately 4% of the decrease in fluorescence signal. Second, the photons used to excite Trp residues as well as the photons emitted from them can be re-absorbed by the retinal molecules with a non-negligible extinction coefficient between 295 nm and 330 nm, which is referred to as the inner filter effect. Third, retinal tends to partition into the hydrophobic compartment of micelles or bicelles, and any retinal molecule surrounding the receptor can quench Trp fluorescence. The first is applicable for both the Trp-based and Alexa488-based assay, while the second and the third factors are more important only in the Trp-based assay. Thus, Alexa488-based assay has the advantage of circumventing the interference of retinal. At 28 °C, Alexa488-labeled Rho can be regenerated to 96 ± 4%, demonstrating that POPC/CHAPS bicelle enables essentially complete regeneration of Rho (Figure 3-4C).

For ROS Rho reconstituted in 0.1% DM (Figure 3-4B), the initial drop of signal upon addition of 11-*cis*-retinal was too pronounced be regarded as merely dilution and inner filter effect, but probably reflects some real energy transfer process. We propose that the initial fast quenching might indicate the partition of retinal into the hydrophobic compartment of DM micelles (Mccaslin and Tanford, 1981), which brings retinal and the receptor into physical proximity for energy transfer, but not necessarily requires retinal to enter the binding pocket for regeneration. The experiment with S144-Alexa488 Rho in DM provided a clear piece of evidence that no PSB was formed in the DM micelle system. We further reasoned that increasing the concentration of DM would reduce such non-specific quenching. In the experiment for ROS Rho in 2% DM (Figure 3-4B: inset),

the initial drop was only 1/3 of what was observed in 0.1% DM, thus qualitatively supporting our hypothesis.

Having established a robust assay for measuring the regeneration kinetics, we asked whether the DM-solubilized photobleached Rho, after transfer into POPC/CHAPS bicelle, has the same kinetics. We performed the fluorescence-quenching experiment for photobleached ROS Rho and incubated at 28 °C for 40 min, 60 min, and 13 h (Figure 3-5). No regeneration was observed for the sample that had been kept at 28 °C for 13 h, indicating complete loss of activity. For the 40-min and 60-min samples, the second-order rate constant (k_2) at 28 °C was 1.0 ± 0.2 $\times 10^3$ M^{-1} s^{-1}. This value is in good agreement with the regeneration kinetics obtained for Rho reconstituted in bicelle prior to photobleaching.

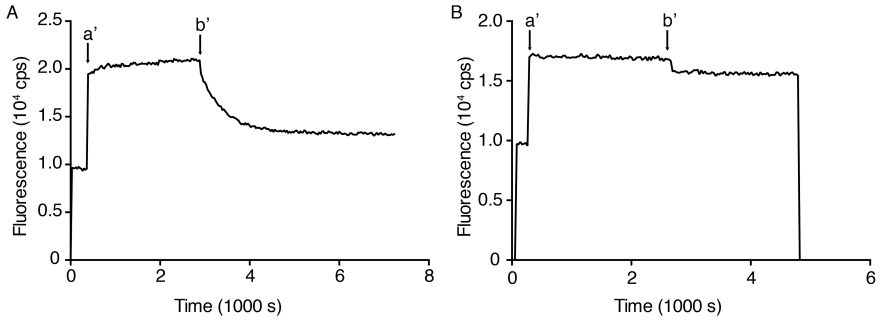

Figure 3-5. The regeneration of micelle-solubilized Rho after transfer into bicelles. Dark-state Rho solubilized in 0.1% DM (30 μL) was photobleached by 505-nm LED light (18 s, 495-nm cut-off filter) to form the active Meta-II state. The sample was incubated at 28 °C for **A)** 60 min and **B)** 13 hours. Then the sample was added into 450 μL of the assay buffer containing either CHAPS/POPC bicelles (arrow a′). Exogenous 11-*cis*-retinal solution (20 μL) was added more than 45 min later (arrow b′). No regeneration can be observed for the 13-hour sample, consistent with the results shown in Figure 3-2. For the 60-min sample and another 40-min sample (not shown), the second-order rate constant at 28 °C was 1.0 ± 0.2 $\times 10^3$ M^{-1} s^{-1}.

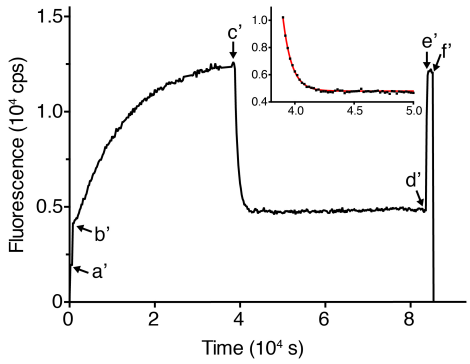

Figure 3-6. The regeneration of Rho in micelles at 4 °C. The Trp fluorescence was recorded as described in Figure 3-4. The sample compartment was cooled to 4 °C by water bath. Dry air was blown through the sample compartment to prevent condensation on the cuvette. Dark-state ROS Rho purified in 0.1% DM (30 μL) was added into the assay buffer (450 μL) containing 1% DM micelles (arrow a′). The sample was then photobleached by 505-nm LED light to form the active Meta-II state (arrow b′). After Meta-II decay was close to completion, 11-*cis*-retinal diluted in the assay buffer (20 μL) was added to initiate pigment regeneration (arrow c′). After overnight regeneration, NH_2OH was added to the sample (arrow d'). In the end, the regenerated pigment was photobleached again in the presence of NH_2OH (arrow e'), and the shutter was closed to record the dark count. Inset: the kinetics of regeneration was fitted with a mono-exponential model. The k_2 for Rho regeneration in 1% DM at 4 °C was 1.4×10^3 M^{-1} s^{-1}. In 0.1% DM, the initial quenching of Trp fluorescence masked real regeneration kinetics.

We also tested the regeneration of ROS Rho at 4 °C in DM micelles (Figure 3-6). We found that at a low temperature, it was possible to obtain fully regenerated pigment in both 0.1% DM and 1% DM. In 1% DM the k_2 is 1.4×10^3 M^{-1} s^{-1}.

3.3.3 The kinetics of the recombination reaction between opsin and 11-*cis*-retinal

To obtain the activation enthalpy and entropy of retinal binding to opsin, we first tested whether the recombination reaction between bicelle-solubilized Rho and 11-*cis*-retinal in POPC/CHAPS bicelles is bimolecular. We conducted the Trp-based fluorescence quenching assay for Rho purified from ROS using various retinal concentrations (molar ratio of retinal to receptor: 8.4 to 67), and derived the rate constant by assuming the regeneration kinetics was pseudo first-order. The linear relation between the pseudo first-order reaction rate and retinal concentration demonstrates that this reaction follows simple second-order rate law within the tested range of retinal concentrations (Figure 3-7A). Hence the second-order rate constant can be calculated by dividing the pseudo-first order rate constant with the concentration of retinal.

We further measured the temperature-dependence of Rho regeneration kinetics (Figure 3-7B and Table 3-1), and derived the activation enthalpy ($\Delta^{\neq}H_{on}$) and the activation entropy ($-T\Delta^{\neq}S_{on}$) from an Eyring plot (Figure 3-7B). For comparison with the existing literature, we also analyzed the data by Arrhenius plot to derive the activation energy ($E_{a,on}$) and the pre-exponential factor (A). These thermodynamic parameters are summarized in Table 3-2. These results showed that wild-type Rho purified from the natural source and the heterologously expressed Rho behaves the same with respect to regeneration. We also showed that the modification of Rho at position 144 in the second intracellular loop does not alter regeneration kinetics. This is expected from the Rho structure since the position 144 is located outside of and distant from the retinal-binding pocket.

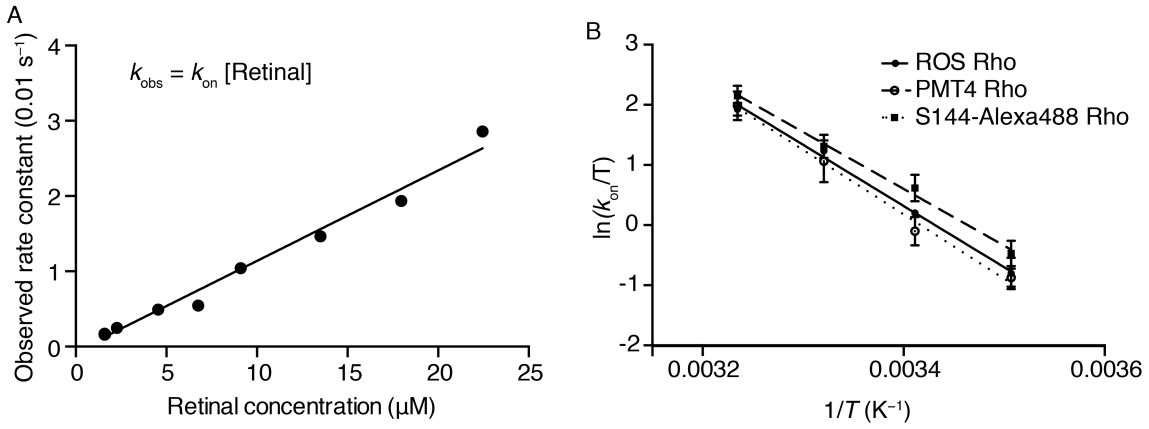

Figure 3-7. The kinetics of the recombination reaction between 11-*cis*-retinal and opsin. A) The regeneration kinetics of ROS Rho at 28 °C was measured at various concentrations of 11-*cis*-retinal (molar ratio of Rho to receptor: 8.4 to 67). The observed pseudo first-order rate constant (k_{obs}) was plotted against the retinal concentration, and shown to linearly correlate with the concentration of 11-*cis*-retinal ($R^2 > 0.98$). The slope of the plot corresponds to the second-order rate constant ($k_{on} = 1.20 \pm 0.05 \times 10^3$ M^{-1} s^{-1}). **B)** Eyring plot for the second-order rate constants of three Rho samples (Table 3-1): 1) purified wt Rho from bovine ROS Rho; 2) purified wt Rho heterologously expressed in HEK293T cells (PMT4 Rho); 3) purified S144azF mutant Rho labeled with a Alexa488 fluorophore (S144-Alexa488 Rho). The thermodynamic parameters derived from the Eyring plot ($\Delta^{\neq}G_{on}$, $\Delta^{\neq}H_{on}$, $-T\Delta^{\neq}S_{on}$) and the Arrhenius plot ($E_{a,on}$) are consistent for different Rho samples (Table 3-2).

Table 3-1 Second-order rate constants (k_2 , 10^3 M^{-1} s^{-1}) for retinal entry

	ROS Rho	PMT4 Rho	Rho S144-Alexa488
36 °C	2.1 ± 0.2	2.2 ± 0.5	2.7 ± 0.4
28 °C	1.03 ± 0.04	0.87 ± 0.30	1.1 ± 0.2
20 °C	0.36 ± 0.03	0.27 ± 0.06	0.54 ± 0.12
12 °C	0.13 ± 0.3	0.12 ± 0.2	0.18 ± 0.4

Table 3-2. The thermodynamic parameters for Rho regeneration at 28 °C

	ROS Rho	PMT4 Rho	S144-Alexa488 Rho
k_{on} (10^3 M^{-1} s^{-1})	1.03 ± 0.04	0.9 ± 0.3	1.1 ± 0.2
$\Delta^{\neq}H_{on}$ (kcal mol^{-1})	20.3 ± 0.9	21.3 ± 1.3	18.8 ± 1.0
$-T\Delta^{\neq}S_{on}$ (kcal mol^{-1})	6.6 ± 0.9	7.8 ± 1.2	5.4 ± 0.9
$\Delta^{\neq}G_{on}$ (kcal mol^{-1})	13.7 ± 0.5	13.6 ± 4.5	13.4 ± 2.4
$E_{a,on}$ (kcal mol^{-1})	20.8 ± 0.9	21.9 ± 1.3	19.4 ± 1.0
ln$A$	35.0 ± 1.6	36.6 ± 2.2	32.7 ± 1.7

We then considered the question of whether the observed kinetics reflects retinal entry into the receptor binding pocket, or retinal diffusion among bicelles. Based on the high partition coefficient of 11-*cis*-retinal between lipids and water, we reasoned that the k_2 for the recombination reaction should be inversely correlated to the concentration of bicelle. We measured the recombination reaction kinetics in 2% POPC/CHAPS bicelles, and found the k_2 was 45 ± 13% of that 1% POPC/CHAPS bicelles.

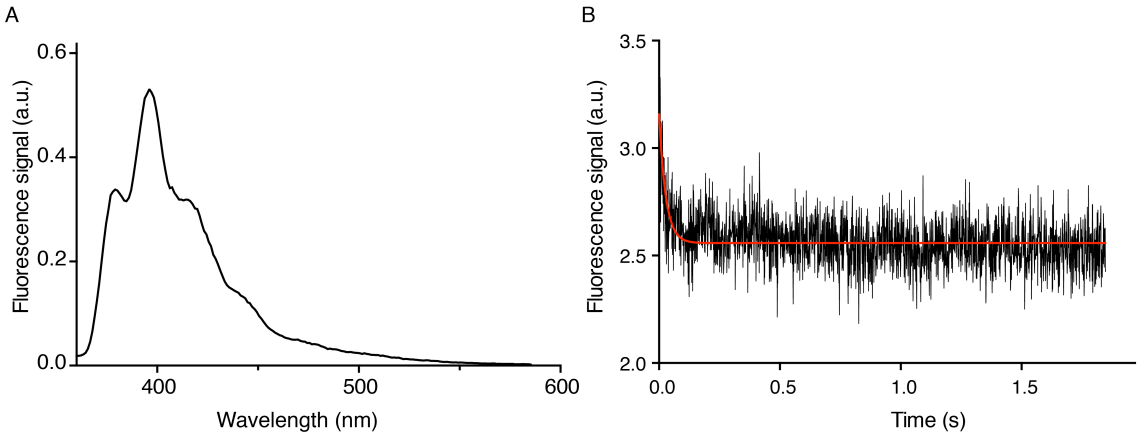

Figure 3-8. The stop-flow experiment for measuring the retinal diffusion kinetics among bicelles. A) The fluorescence emission spectrum of pyrene, obtained by principle component analysis. **B)**The kinetics of pyrene fluorescence quenching by retinal. The pyrene fluorescence signal was fitted with monoexponential decay model. The first-order time constant was 36 ± 3 s^{-1}.

We also designed a stop-flow experiment in which pyrene-lipid doped POPC/CHAPS bicelle was mixed with bicelles containing 11-*cis*-retinal (Figure 3-8). The proximity of retinal with pyrene would result in the partial quenching of pyrene fluorescence (Farrens and Khorana, 1995). The temporal resolution of stop-flow experiment enabled us to track the rapid diffusion of retinal among bicelles. We found

that the time constant for the diffusion of retinal among bicelles is three orders of magnitude higher than the observed retinal binding rate (the calculation is explained in Appendix II). Based on the pyrene-quenching experiment, we concluded that the diffusion of retinal among bicelles could be ruled out as a rate-limiting factor for the overall kinetics measured in the regeneration experiment.

3.3.4 The kinetics of the dissociation reaction between opsin and 11-*cis*-retinal

The SB linkage between 11-*cis*-retinal and K296 of opsin is known to extremely stable. Here we quantitatively assessed the stability of the SB bond by measuring the chromophore exchange rate of the bound 11-*cis*-retinal with exogenous 9-*cis*-retinal. The 9-*cis*-retinal can be admitted into the ligand-binding pocket only following the dissociation of 11-*cis*-retinal. The recombination product of opsin with 9-*cis*-retinal, isorhodopsin (isoRho), has its absorbance maximum shifted from 500 nm to 487 nm (Hubbard and Wald, 1952). Therefore, in a mixture of 11-*cis*-retinal bound Rho and 9-*cis*-retinal bound isoRho, the fraction of newly formed isoRho can be quantified by monitoring the decrease in 500-nm absorbance and the increase in the associated 487-nm. Because in this experiment the concentration of added 9-*cis*-retinal is much higher than that of 11-*cis*-retinal, we assume the fraction of newly formed Rho is negligible, and thus the fraction of newly formed isoRho can serve as a good approximation for 11-*cis*-retinal dissociation.

We first asked whether opsin in POPC/CHAPS bicelles effectively recombines with 9-*cis*-retinal (Figure 3-9). The addition of exogenous 9-*cis*-retinal resulted in robust regeneration of isoRho. The second-order rate constant for the recombination reaction

between opsin and 9-*cis*-retinal at 28 °C ((6.7 ± 0.3) $\times 10^2$ M^{-1} s^{-1}) was slightly slower than that between opsin and 11-*cis*-retinal ((1.03 ± 0.04) $\times 10^3$ M^{-1} s^{-1}).

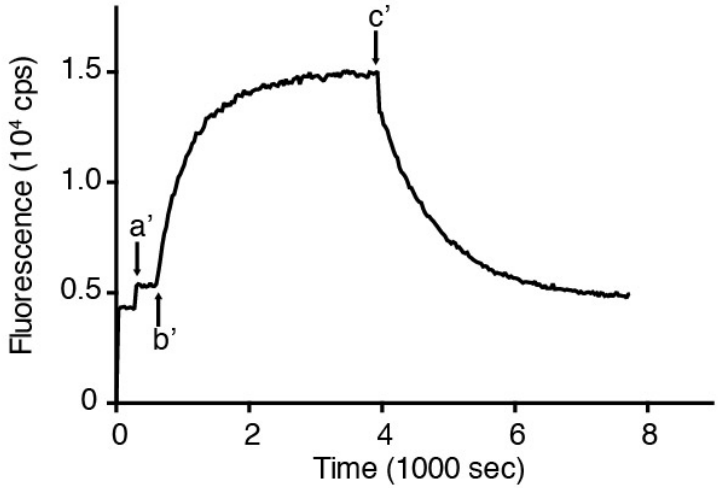

Figure 3-9. The regeneration of ROS Rho with 9-*cis*-retinal monitored by Trp fluorescence. Dark-state Rho solubilized in 0.1% DM (30 μL) was added to 450 μL of the assay buffer containing either CHAPS/POPC bicelles or DM (arrow a′). The sample was then photobleached by 505-nm LED light (18 s, 495-nm cut-off filter) to form the active Meta-II state (arrow b′). After Meta-II decay was close to completion, ligand 9-*cis*-retinal was added to initiate pigment regeneration (arrow c′). The Trp fluorescence was excited at 295 nm (bandpass 0.6 nm) and collected at 330 nm (bandpass 15 nm). The concentration of 9-*cis*-retinal working solution was determined from its 374-nm absorbance (extinction coefficient 36,000 M^{-1} cm^{-1}). The second-order rate constant (6.7 ± 0.3 $\times 10^2$ M^{-1} s^{-1}) was calculated by dividing the pseudo first-order rate constant with the 9-*cis*-retinal concentration.

We next tested whether 11-*cis*-retinal bound to Rho can be exchanged with 9-*cis*-retinal. ROS Rho was purified by lectin affinity chromatography and obtained in POPC/CHAPS bicelles. The thermostabilizing effect of POPC/CHAPS allowed us to choose prolonged reaction time (1×, 2× and 3×11.6 days; Figure 3-10). We conducted the chromophore-exchange experiment of Rho at 28 °C, 36 °C, and 44 °C, with a 9-fold

Figure 3-10. Measurement of slow chromophore exchange rate in ROS Rho reconstituted in bicelles. A) The scheme of chromophore exchange in Rho. After the spontaneous dissociation of 11-*cis*-retinal, opsin either recombines with 9-*cis*-retinal, or proceed through the thermal denaturation pathway. **B)** Rho was slowly converted to isorhodopsin (isoRho) in the presence of 9-*cis*-retinal. The formation of isoRho was measured at different temperatures (28 °C, 36 °C, and 44 °C) as a function of time. UV-Vis spectra were recorded at 10^6 s (11.6 days), 2×10^6 s (23.2 days), and 3×10^6 s (34.8 days). The spectra were normalized based on the λ_{max}. **C)** The difference spectra of the Rho-isoRho mixtures were subtracted from the spectrum of pure Rho to reveal the decrease in the 500-nm absorbance of Rho and increase in the 487-nm absorbance of isoRho. **D)** The fraction of isoRho formed by chromophore exchange was plotted versus the incubation time at 28 °C (square), 36 °C (circle), and 44 °C (diamond). The data after correcting for the effect of opsin thermal denaturation were fitted using a mono-exponential model to derive the first-order rate constant. Inset: the Eyring plot for the rate constants at different temperatures ($R^2 = 0.99$). The calculated $\Delta^{\neq} H_{off}$ is 38.4 ± 4.4 kcal mol^{-1}. At 28 °C we also obtained from the Arrhenius plot (not shown) an $E_{a,off}$ of 38.9 ± 4.4 kcal mol^{-1} and a pre-exponential factor A of 5.7×10^{20}.

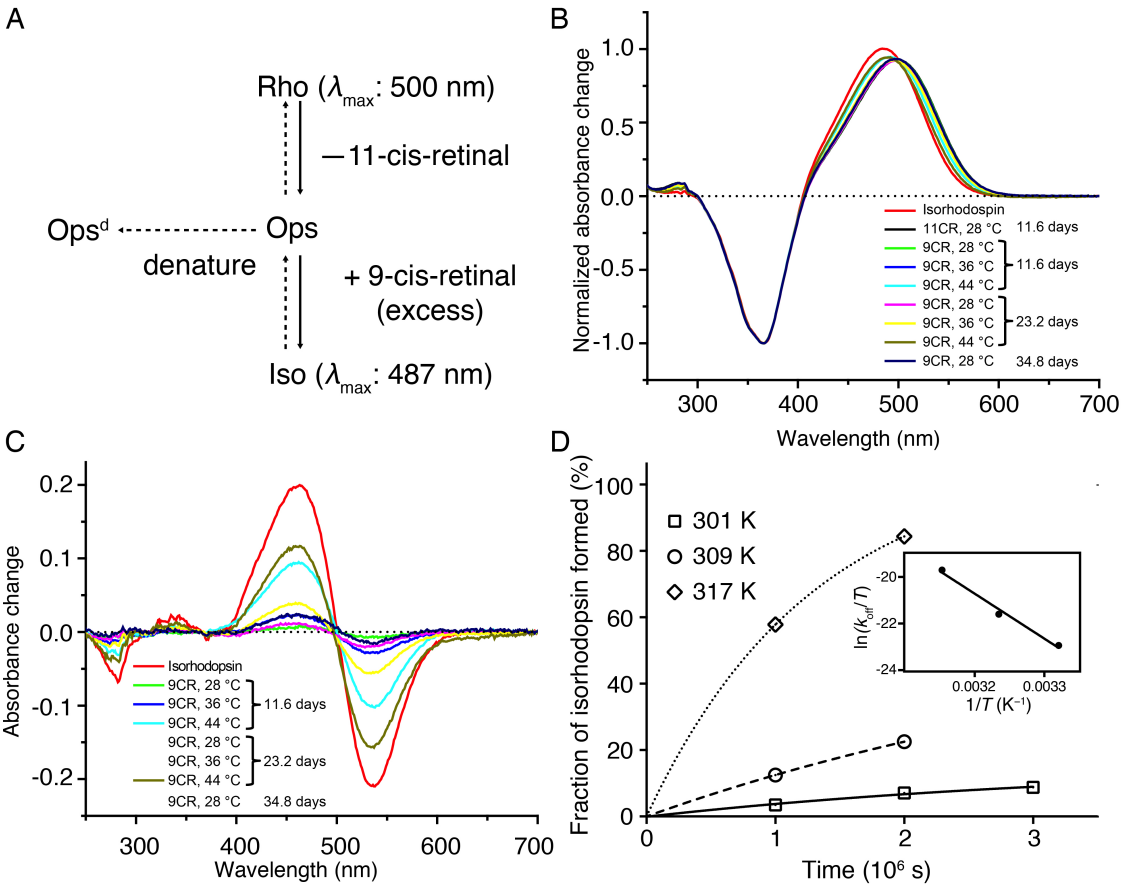
A
Rho (λ_{max}: 500 nm)
—11-cis-retinal
Ops^d
Ops
denature
+ 9-cis-retinal
(excess)
Iso (λ_{max}: 487 nm)
B
Normalized absorbance change
Wavelength (nm)
Isorhodospin
11CR, 28 °C 11.6 days
9CR, 28 °C
9CR, 36 °C
9CR, 44 °C
11.6 days
9CR, 28 °C
9CR, 36 °C
9CR, 44 °C
23.2 days
9CR, 28 °C 34.8 days
C
Absorbance change
Wavelength (nm)
Isorhodopsin
9CR, 28 °C
9CR, 36 °C
9CR, 44 °C
11.6 days
9CR, 28 °C
9CR, 36 °C
9CR, 44 °C
23.2 days
9CR, 28 °C 34.8 days
D
Fraction of isorhodopsin formed (%)
Time (10^6 s)
301 K
309 K
317 K
ln(k_{off}/T)
1/T (K^{-1})

excess of 9-*cis*-retinal. Then the samples were immunopurified to remove the excess retinal and analyzed by UV-Vis spectroscopy. We observed a gradual increase in the 487-nm absorbance and a decrease in the 500-nm absorbance, indicating the conversion of the 11-*cis*-retinal-bound Rho to 9-*cis*-retinal-bound isoRho (Figure 3-10 B,C).

During the unusually long reaction time of the chromophore exchange experiment, opsin denaturation could compete with 9-*cis*-retinal, causing a greater underestimation for the exchange kinetics, particularly at high temperatures. Therefore, we performed a correction for the effect of opsin thermal denaturation. We assume that retinal dissociation was the rate-limiting step, and the resulting opsin either followed the thermal denaturation pathway, or recombined with 9-*cis*-retinal. The amount of the denatured opsin could be quantified by UV-Vis spectroscopy. Based on the absorption spectra, significant opsin denaturation was found only for the samples incubated at 44 °C (Figure 3-11 and Table 3-3). The correction procedure is described in the experimental section.

We plotted the fraction of isoRho against time and analyzed the kinetics based on the assumption that this reaction follows first-order kinetics (Figure 3-10D and Figure 3-11). We derived the Eyring plot (Figure 3-10D, inset) and Arrhenius plot (not shown) for the dissociation reaction, as well as $\Delta G_{off}^{\neq}$, $\Delta^{\neq}H_{off}$, and $-T\Delta^{\neq}S_{off}$ and $E_{a,off}$. We found that Without the correction, dissociation kinetics at high temperatures and consequently the activation enthalpy for the reverse reaction (shown by the slope of the Eyring plot) would be underestimated (uncorrected: 33.5 ± 1.4 kcal mol^{-1}; corrected: 38.4 ± 4.4 kcal mol^{-1})

Table 3-3. The fraction of retinal dissociation and the rate constant

Temperature (°C)	28	36	44 (uncorrected)	44 (corrected)
$t = 1\times10^6$ s	0.0345	0.125	0.475	0.578
$t = 2\times10^6$ s	0.0708	0.225	0.658	0.844
$t = 3\times10^6$ s	0.0880	NA	NA	NA
$k_{off}(10^{-7}\ s^{-1})$	0.328 ± 0.016	1.29 ± 0.02	5.82 ± 0.38	8.89 ± 0.22

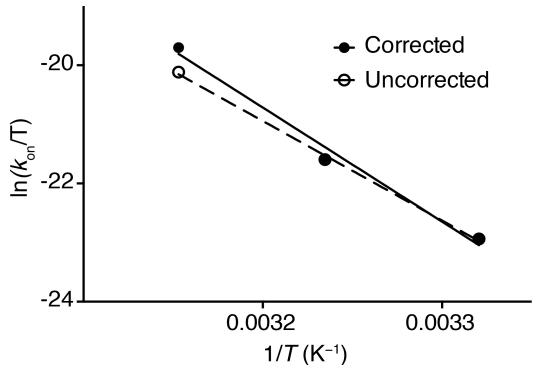

Figure 3-11. The retinal dissociation rates in Rho. The solid line represents the Eyring plot for rates corrected for opsin denaturation, the dash line for rates uncorrected for opsin denaturation.

3.3.5 The reaction enthalpy of the recombination reaction between opsin and 11-*cis*-retinal

Having characterized the transition state energy change of the forward and the reverse reaction, we further conducted an ITC experiment to measure the overall enthalpy change. Opsin was purified and reconstituted in POPC/CHAPS bicelles to provide a thermostabilizing lipid bilayer environment. The opsin samples in the titration chamber were mixed with 11-*cis*-retinal solutions prepared in the same POPC/CHAPS bicelle buffer. Three independent experiments were performed (Figure 3-12). In the raw data plots, the differential powers first decreased, then increased after the titration point (Figure 3-12A-C). The two types of peaks showed different kinetics (Figure 3-12E). Thpeaks occurring before the titration points have significantly longer decay time, and consequently correspond to larger integrated reaction heat. We speculate the peaks after the titration point reflected the mixing heat. We observed the reaction enthalpy in the range of −20 to −25 kcal mol^{-1}, giving an average $\Delta H°$' of – 21.6 ± 1.6 kcal mol^{-1}. Nonetheless, the stoichiometry of retinal binding to opsin was 1.15 ± 0.14, slightly greater than the expected value 1.0. We performed careful titrations to determine the extinction coefficient of opsin and retinal in the POPC/CHAPS bicelle buffer (Figure 3-13 and Table 3-4). Due to the limitations of the sensitivity of the ITC instrument and corresponding high concentrations necessary to give a measurable signal, we could not determine K_d from the shape of the titration curve (Pierce et al., 1999).

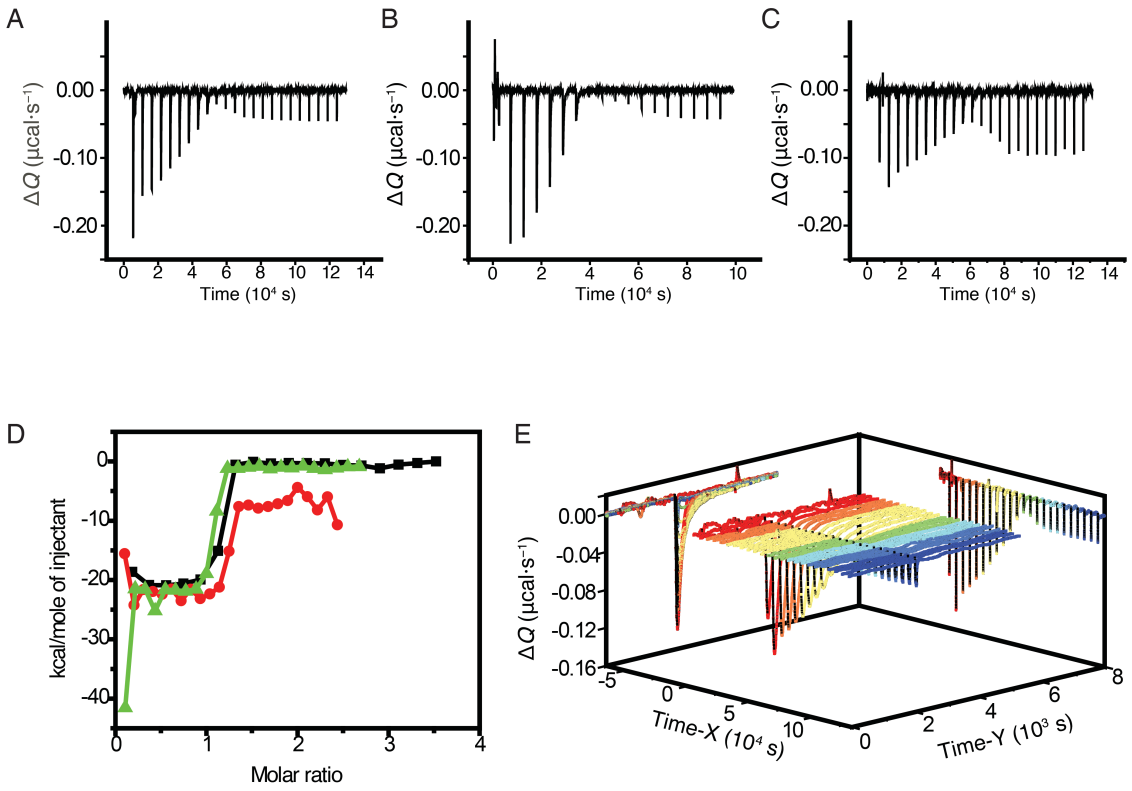

Figure 3-12. Reaction enthalpy for the binding of 11-*cis*-retinal to opsin determined by ITC experiments. A-C) Raw ITC data plots from three independent experiments. In each panel, the differential power was plotted versus time. The baseline curve was generated by sampling the intermediate time points between each injection. In these plots, the signals were corrected by subtracting the baseline. **D)** The integrated reaction heat per mole of injectant versus the stoichiometry for three independent experiments (dots, squares, and triangles). Note that due to the very slow binding kinetics the experiments are about 10 times longer and the corresponding differential power signals are several-fold smaller than in typical ITC studies of a ligand binding to a protein. The calculated $\Delta H°$' were -24.2 ± 1.5 kcal mol^{-1}, -19.4 ± 0.5 kcal mol^{-1}, and -21.2 ± 1.6 kcal mol^{-1}, respectively, giving an average $\Delta H°$' of -21.6 ± 1.3 kcal mol^{-1}. **E)** 3-dimensional projection of a representative ITC experiment (Panel **C**). Time-X represents the entire time course of the experiment; Time-Y represents the time course of each injectant.

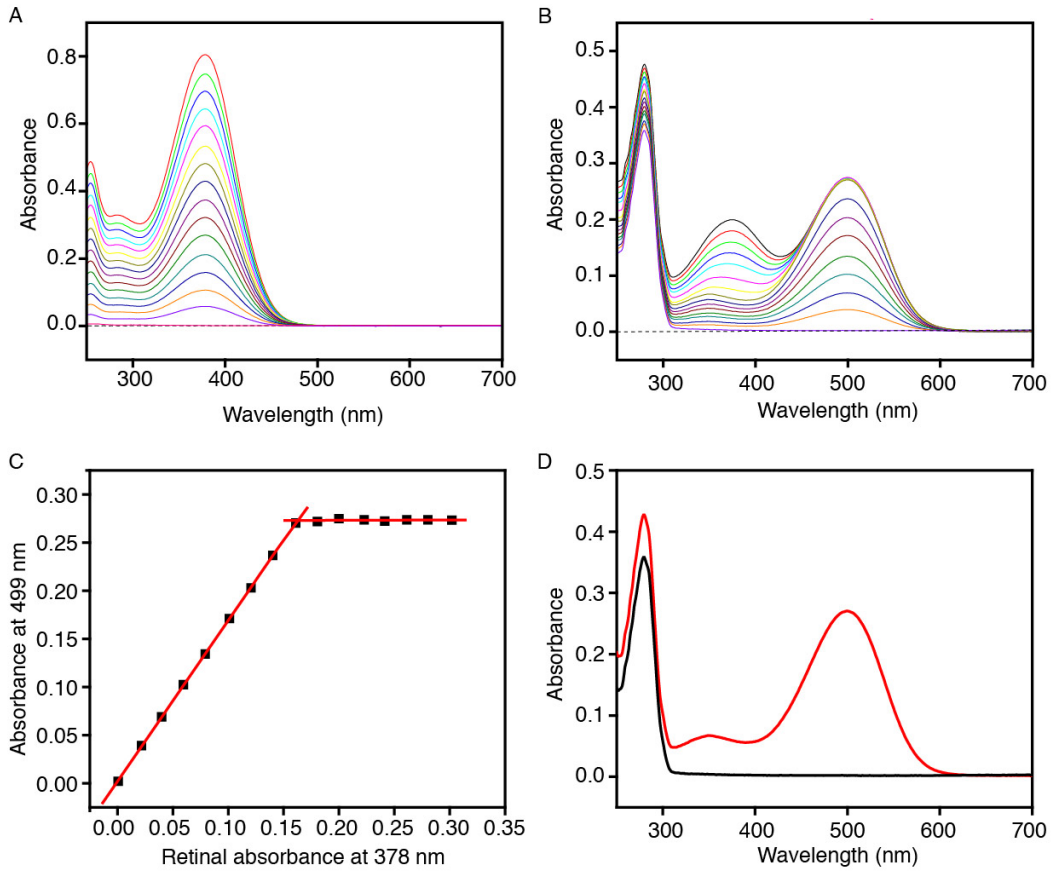

Figure 3-13. Determination of molar extinction coefficients of 11-*cis*-retinal, opsin, and Rho. A) The UV-Vis spectra of Dilution series of 11-*cis*-retinal in the POPC/CHAPS bicelle buffer. **B)** An aliquots of 11-*cis*-retinal (120 µL; linear dilution series with 16 concentrations in the range from 0 to 31.5 µM) was mixed with aliquots of purified opsin (120 µL, 10.2 µM). After complete regeneration, the UV-Vis spectrum of each sample was recorded. **C)** The correlation of the absorption of 11-*cis*-retinal in POPC/CHAPS bicelle buffer at 378 nm (corrected for a dilution factor of 0.375) was plotted against the 499-nm absorbance of Rho in the opsin samples. The perfect linear correlation before the saturation of the retinal binding site yielded a molar extinction coefficient of Rho $\varepsilon_{499\ nm}$ = 42,742 M^{-1} cm^{-1}. **D)** The absorption spectra of opsin (*black*) and Rho (*red*) are compared. The corresponding extinction coefficients are shown in Table 3-4. The resulting A279/A499 ratio of Rho at the equivalence point is 1.58 ± 0.01, indicating a slightly higher purity than previously best results obtained by column chromatography 1.65–1.75 (Litman, 1982) and 1.60 –1.70(Degrip, 1982b), suggesting that the opsin sample is fully regenerable.

Table 3-4. Molar extinction coefficient of opsin and Rho in POPC/CHAPS bicelles

	$\varepsilon_{279\ nm}$ / M^{-1} cm^{-1}	$\varepsilon_{499\ nm}$ / M^{-1} cm^{-1}
Opsin	56,057 ± 184	–
Rho	67,532 ± 221	42,742

3.3.6 The energy landscape of Rho regeneration

We sought to integrate the information gleaned from the above experiments into a single energy diagram, based on the assumption that the partial reactions for ligand binding and unbinding proceed over the same transition state, *i.e.*, the dissociation of 11-*cis*-retinal represents the reverse reaction for the recombination reaction on the microscopic level. We assumed a modified biochemical standard state, with Rho reconstituted into POPC/CHAPS bicelles in aqueous solution, at 28 °C, pH 6.0, under ambient atmospheric pressure, and all other conditions at 1 M.

The values in the energy diagram were derived as follows:

The free energy (ΔG)

1. The activation energy of the forward reaction ($\Delta^{\neq}G_{on}$ = 13.7 ± 0.5 kcal mol^{-1}) was obtained from the retinal binding kinetics (k_{on} = (1.03 ± 0.04)×10^3 M^{-1} s^{-1})

$$\Delta^{\neq}G_{on} = -RT\ln\frac{k_{on}h}{k_BT}$$

The error was given by:

$$\sigma\left(\Delta^{\neq}G_{on}\right) \approx RT\frac{\sigma\left(k_{on}\right)}{k_{on}}$$

2. The activation energy of the reverse reaction ($\Delta^{\neq}G_{\text{off}}$ = 27.9 ± 1.4 kcal mol^{-1}) was obtained from the chromophore exchange kinetics (k_{off} = (0.328 ± 0.016)×10^{-7} s^{-1})

$$\Delta^{\neq}G_{\text{off}} = -RT\ln\frac{k_{\text{off}}h}{k_BT}$$

The error was given by:

$$\sigma\left(\Delta^{\neq}G_{\text{off}}\right) \approx RT\frac{\sigma\left(k_{\text{off}}\right)}{k_{\text{off}}}$$

3. The energy difference between the reactants and the products under a particular state ($\Delta G°'$ = 14.5 ± 0.9 kcal mol^{-1}) was obtained by dissociation constant:

$$\Delta G°' = -RT\ln K_{\text{d}}$$

With both the binding and unbinding rates known, the equilibrium dissociation constant (K_{d} = 40 ± 2 pM) between retinal and opsin can be derived by:

$$K_{\text{d}} = k_{\text{off}} / k_{\text{on}}$$

The error is given by:

$$\sigma\left(K_{\text{d}}\right) = K_{\text{d}}\left\{\left[\frac{\sigma\left(k_{\text{off}}\right)}{k_{\text{off}}}\right]^2 + \left[\frac{\sigma\left(k_{\text{on}}\right)}{k_{\text{on}}}\right]^2\right\}^{1/2}$$

$$\sigma\left(\Delta G°'\right) \approx RT\frac{\sigma\left(K_{\text{d}}\right)}{K_{\text{d}}}$$

In the energy diagram (*cf.* Figure 7) we only indicated $\Delta^{\neq}G_{\text{on}}$ and $\Delta G°'$.

The enthalpic term (ΔH)

4. The activation enthalpy of the forward reaction ($\Delta^{\neq}H_{\text{on}}$ = 20.3 ± 0.9 kcal mol^{-1}) was obtained from the Eyring plot of the retinal binding kinetics (*cf.* Table 1). The error was derived from the fitting error.

$$\frac{k_{on}}{T} = -\frac{\Delta^{\neq}H_{on}}{R}\cdot\frac{1}{T} + \ln\frac{k_B}{h} + \frac{\Delta^{\neq}S_{on}}{R}$$

5. The activation enthalpy of the reverse reaction ($\Delta^{\neq}H_{off}$ = 38.4 ± 4.4 kcal mol^{-1}) was obtained from the Eyring plot of the chromophore exchange kinetics (*cf*. Figure 5B, inset). The error was derived from the fitting error.

$$\frac{k_{off}}{T} = -\frac{\Delta^{\neq}H_{off}}{R}\cdot\frac{1}{T} + \ln\frac{k_B}{h} + \frac{\Delta^{\neq}S_{off}}{R}$$

6. The reaction enthalpy ($\Delta H^{\circ\prime}$ = –21.6 ± 1.3 kcal mol^{-1}) was directly measured by the ITC experiment (*cf*. Figure 6). The error for the reaction enthalpy was obtained based on three independent measurements.

Ideally the difference between the activation enthalpy of the forward and reverse reactions should have the same value as the enthalpy of formation:

$$\Delta^{\neq}H_{on} - \Delta^{\neq}H_{off} - \Delta H^{\circ\prime} = 0$$

Insert the values above, we have:

$$\Delta^{\neq}H_{on} - \Delta^{\neq}H_{off} - \Delta H^{\circ\prime} = 3.5 \pm 4.7 \text{ kcal mol}^{-1}$$

Therefore, the apparent discrepancy of 3.5 kcal mol^{-1} can be explained by the experimental errors.

The entropic term (−TΔS)

7. The activation entropy of the forward reaction ($\Delta^{\neq}S_{on}$ = 22 ± 3 cal mol^{-1}) was obtained from the Eyring plot of the retinal binding kinetics. The entropic term was calculated for 28 °C ($-T\Delta^{\neq}S_{on}$ = 6.7 ± 0.94 kcal mol^{-1}). The error was derived from the fitting error.

$$\frac{k_{on}}{T} = -\frac{\Delta^{\neq}H_{on}}{R}\cdot\frac{1}{T} + \ln\frac{k_B}{h} + \frac{\Delta^{\neq}S_{on}}{R}$$

8. The activation entropy of the reverse reaction ($\Delta^{\neq}S_{off}$ = 34 ± 14 cal mol^{-1}) was obtained from the Eyring plot of the chromophore exchange kinetics. The entropic term was calculated for 28 °C ($-T\Delta^{\neq}S_{off}$ = 10.4 ± 4.3 kcal mol^{-1}). The error was derived from the fitting error.

$$\frac{k_{off}}{T} = -\frac{\Delta^{\neq}H_{off}}{R}\cdot\frac{1}{T} + \ln\frac{k_B}{h} + \frac{\Delta^{\neq}S_{off}}{R}$$

9. The reaction entropy was calculated by ($-T\Delta S°' = \Delta G°' - \Delta H°' = -7.1 \pm 1.6$ kcal mol^{-1}). The error was derived by:

$$\sigma(T\Delta S°') = \left[\sigma(\Delta G°')^2 + \sigma(\Delta H°')^2\right]^{1/2}$$

Based on these results, we present here the energy diagram for the regeneration of Rho (Figure 3-14). The approaches used to derive these values are indicated in the figure. The ITC experiment of the ligand binding reaction of R and L showed that the enthalpy of formation ($\Delta H°'$) was – 21.6 ± 1.3 kcal mol^{-1}. Therefore, the recombination reaction between 11-*cis*-retinal and opsin is enthalpy-driven.

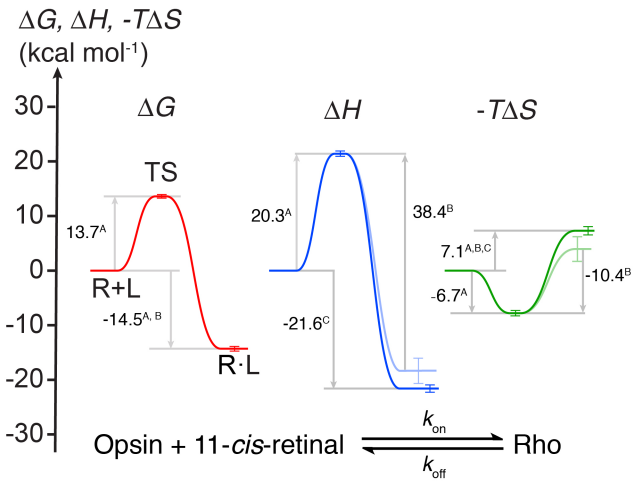

Figure 3-14. Energy diagram for the recombination reaction between opsin and retinal. All the values were obtained for Rho reconstituted into POPC/CHAPS bicelles, at 28 °C, pH 6.0, under ambient atmospheric pressure. The changes in free energy (ΔG, *red*), enthalpy (ΔH, *blue*) and entropy ($-T\Delta S$, *green*) are indicated in the diagram. The superscript letter next to each value indicates the experimental approach used to derive the value: (A) The kinetics of retinal entry; (B) the chromophore exchange experiment; (C) the ITC experiment. The chromophore exchange experiment (light line) and ITC experiment (dark line) yielded essentially consistent results on the activation enthalpy ($\Delta^{\neq}H_{off}$) and the activation entropy ($-T\Delta^{\neq}S_{off}$) for the reverse reaction.

3.4 Discussion

3.4.1 Identifying POPC/CHAPS bicelles as a suitable model lipid bilayer system to study Rho regeneration

The ability of G protein-coupled receptors (GPCRs) to bind with ligand has been one of the best criteria for assessing their thermostability in various reconstitution systems, and ligand binding generally enhances the thermostability of the receptor (Rosenbaum et al., 2007; Degrip, 1982a). It is well known that the stability of Rho and opsin in detergent differ strikingly. While DM-solubilized Rho denatures at approximately 60 °C, the half-life of opsin at 30 °C is only 2 h (Degrip, 1982a). Similarly, ligand-free β_2 adrenergic receptor has a half-life of less than 1 hour at 37 °C (Rosenbaum et al., 2007). The inefficiency of opsin to recombine with 11-*cis*-retinal in DM has been a major obstacle for studying pigment regeneration (Sanchez-Martin et al., 2013; Sakamoto and Khorana, 1995; Srinivasan et al., 2014). Successful examples to study the recombination between opsin and 11-*cis*-retinal in DM system either involved a low concentration of lipids (Schadel et al., 2003), or engineering a thermostabilized receptor (Xie et al., 2003).

Previous biochemical studies have yielded the insight that addition of lipids into the detergent system improves the stability of opsin and other GPCRs (Sakamoto and Khorana, 1995; Navratilova et al., 2005). Here we employed a POPC/CHAPS bicelle system to mimic the native membrane environment. We showed that photobleached Rho reconstituted into POPC/CHAPS bicelles retained its ability to recombine with 11-*cis*-retinal over a significantly longer period of time micelles (>98% regenerated after 18 h at 28 °C, *cf*. Figure 3-2E, F) as compared with receptors in DM micelles (half-life 2.1 hours

at 28 °C, *cf*. Figure 3-2D, F). In the experiment testing opsin stability in DM, samples were transferred into POPC/CHAPS bicelles to "quench" the denaturation process, as well as to facilitate the regeneration of the remaining functional opsin. In this way, we were able to capture the exact fraction of functional component at a particular time point. Our results support the idea that the interaction between opsin and lipids play an important role in stabilizing the ligand-free receptor (Oates and Watts, 2011).

Next we showed that using two FRET-based assays, we were able to monitor the regeneration of ROS Rho and S144-Alexa488 Rho in POPC/CHAPS bicelles at 28 °C, and the time-course of the regeneration was characterized by an apparent mono-exponential process (*cf*. Figure 3-4A and 3-4C). By contrast, the experiment with ROS Rho and S144-Alexa488 Rho in DM micelles showed a monotonic decrease with distinct kinetics from the experiment involving POPC/CHAPS bicelles, both before and after the addition of 11-*cis*-retinal (*cf*. Figure 3-4B and 3-4D). It is possible that this decrease is caused by denaturation and subsequent precipitation of opsin in DM rather than real regeneration.

Several studies on Rho regeneration in DM have reported a large decrease in Trp fluorescence upon the addition of 11-*cis*-retinal (Sanchez-Martin et al., 2013; Srinivasan et al., 2014). An alternate theory proposed that this may indicate a two-step regeneration mechanism: the initial drop represents the fast entry of retinal into the ligand binding channel, possibly as a non-covalent retinal-opsin complex, and the following decay corresponds to the formation of the pigment with the PSB bond (Srinivasan et al., 2014). However, this theory cannot explain the much smaller initial drop observed for bicelle-reconstituted receptor, unless we assume that in POPC/CHAPS bicelle, retinal entry

operates in a distinct one-step mechanism. Furthermore, it is counterintuitive to assume the initial entry of retinal into the binding pocket is faster in DM than in the POPC/CHAPS, but the formation of the SB turned out to be rate limiting. The fast retinal entry should position the aldehyde group of 11-*cis*-retinal to react with the ε-amino group of K296, and accelerate the overall reaction. Our experiments using high (2%) and low (0.1%) concentration of DM suggested that this initial quenching was due to retinal partitioning into DM micelles, and did not involve any regeneration. The absence of the initial drop of Trp fluorescence in POPC/CHAPS bicelles can be explained by the higher concentration of bicelles (1%) than micelles (0.1%).

Rho regeneration in DM micelles could barely proceed at 28 °C, but reached completion at 4 °C (*cf*. Figure3-6). Based on the denaturation kinetics at 28 °C (*cf*. Figure 3-2F), within two hours after photobleaching, there was substantial fraction of functional opsin that would manifest its potential for regeneration once transferred into suitable lipid bilayer environment. Therefore, it seems that the problem with the detergent system was not simply opsin denaturation as McCaslin *et al.* proposed. We hypothesize that DM may inhibit the ability of opsin to bind with retinal by modulating its conformation and energetics.

Take together, these results demonstrated the utility of POPC/CHAPS bicelle as a valuable tool for studying the regeneration of Rho, and possibly to study GPCRs in general. The role of bicelle is two-fold: 1) it thermostabilizes the conformation of opsin, and 2) it modulates the activity of opsin with respect to regeneration. By comparison, DM-solubilized photobleached Rho can be divided into two fractions based on its ability to recombine with retinal. The first fraction has undergone an irreversible denaturing

pathway that follows first-order kinetics. The second fraction, although it retains its potential of regeneration, cannot be as efficiently regenerated in DM as it is in POPC/CHAPS bicelle. These findings should prompt a rethink on the activity of GPCRs in detergent systems.

Typically, the FRET experiment for measuring regeneration kinetics lasted less than 6 hours. The longest ITC measurement took approximately 35 hours. Yet ligand binding was complete within 14 hours. While the chromophore exchange spanned weeks, except at 44 °C, the dominating species during this process were retinal-bound Rho or isoRho rather than ligand-free opsin. Therefore we believe that in the experiments of this study we were able to maintain Rho and opsin at the functional state.

3.4.2 The kinetics of Rho regeneration

In the fluorescence-quenching assay, the concentration of 11-*cis*-retinal is typically 1.5-2.0 μM. The concentration of ROS Rho in the Trp-based assay is approximately 0.25 μM and Alexa488-Rho in the Alexa488-based assay is 5–50 nM. The estimated concentration of bicelles is 17 μM (for the detailed calculation see Appendix II). Considering that the partition coefficient of retinal between lipid and water is very high, retinal is predominately found in bicelles. Thus, the ratio of empty bicelles, retinal-containing bicelles and Rho-containing bicelles is 10: 1: (0.003~ 0.16). At any particular time point, a Rho molecule does not necessarily have a retinal molecule in the same bicelle, and before any recombination can occur, a retinal molecule needs to diffuse into a Rho-containing bicelle. We asked whether in our bicelle bilayer system the diffusion of 11-*cis*-retinal among the bicelles could be rate limiting. If so, varying the concentrations of 11-*cis*-retinal and Rho should greatly affect the observed kinetics. We showed that the

concentration of 11-*cis*-retinal exhibited a simple linear correlation with the pseudo-first order rate constants (Figure 3-7A). Moreover, the concentrations of ROS Rho (~0.25 μM) in the Trp-based assay and Alexa488-Rho (5-50 nM) in the Alexa488-based assay differ by at least 5-fold, but the reactions rates are not statistically different (Figure 3-7B).

We were looking for an independent test that could show rapid exchange of retinal among bicelles. It was known that pyrene fluorescence could be quenched by retinal (Farrens and Khorana, 1995). Therefore it is possible to monitor retinal diffusion into pyrene-labeled bicelle based on the decrease of pyrene fluorescence. Using the same experimental setup for monitoring Rho regeneration, we observed rapid quenching of pyrene fluorescence upon the addition of 11-*cis*-retinal. However, we could not resolve the kinetics of retinal diffusion, as mixing in the magnetically stirred cuvette was not fast enough. To address this question, we carried out a stop-flow experiment (Figure 3-8). Based on the results from the stop-flow experiment, we estimated that the average lifetime of a retinal free bicelles is ~3 orders of magnitude faster than the recombination reaction. Therefore, we ruled out the diffusion of retinal among bicelles as a rate-limiting step in the entire regeneration process.

We tested three different Rho samples, Rho purified, recombinant expressed Rho, and S144-Alexa488 Rho, based on either the intrinsic Trp fluorescence or the extrinsic Alexa488 fluorescence. All of the samples showed consistent kinetics and temperature-dependence (Table 3-2). The absolute value of Rho regeneration kinetics is dependent on the type and concentration of micelles (Matsumoto et al., 1978) and bicelles, probably due to the partitioning of retinal into micelles and bicelles (Mccaslin and Tanford, 1981). Therefore it is not informative to compare the absolute values unless the reconstitution

conditions were identical. Nonetheless, we found the Arrhenius activation energy ($E_{a,on}$: 19.4 ± 1.0 ~ 21.9 ± 1.3 kcal mol^{-1}, Table 3-2) is in good agreement with value previously reported for Rho regeneration in ROS membrane (18.7 kcal·mol^{-1}) (Kawaguchi et al., 1986) and in 1% digitonin (22 kcal mol^{-1}) (Matsumoto et al., 1978). This suggests that regeneration in the POPC/CHAPS bicelle environment is close to the native ROS membrane environment in photoreceptor cells.

Electrophysiological studies suggested that the pigment regeneration process likely involves a transient non-covalent complex between retinal and opsin that precedes the formation of the mature pigment with the PSB bond (Kefalov et al., 2001). The tryptophan fluorescence assay reflects whether retinal resides in the binding pocket, whereas the Alexa488 fluorescence assay indicates the formation of PSB bond. As the retinal binding curves and thermodynamic parameters (Table 3-2) in both assays are very similar in POPC/CHAPS bicelles, the formation of any non-covalent intermediate and the formation of PSB bond is likely to be tightly coupled, and the retinal entry into its binding pocket is likely to be the rate-limiting step.

We also demonstrated that the incorporation of an unnatural amino acid at position S144, and the subsequent conjugation of a fluorophore to it, does not alter the receptor's behavior with respect to retinal entry. Alexa488 fluorescence is compatible with a high concentration of retinal and thus valuable for studying mutants with slow retinal entry kinetics. Based on these results, we anticipate S144-Alexa488 Rho to be used as the background construct for kinetic and mechanistic studies of mutations regulating retinal entry.

3.4.3 The chromophore exchange experiment indicates that the PSB of Rho is less stable than previously thought

Rho is stabilized in its inactive conformation by the inverse agonist 11-*cis*-retinal. A unique feature of 11-*cis*-retinal as the native ligand is that it utilizes a covalent PSB bond, in addition to a series of non-covalent weak interactions, to remain tethered to the protein. A sufficiently long lifetime of this covalent bond is critical, as both the non-covalent retinal-opsin complex (Kefalov et al., 2001), and the apoprotein opsin (Cornwall and Fain, 1994; Cornwall et al., 1995; Surya et al., 1995) activates the signal transduction cascade to some extent. Spontaneous dissociation of 11-*cis*-retinal from cone receptor binding pocket has been well described by biochemical and electrophysiological methods (Matsumoto et al., 1975; Crescitelli, 1984; Kefalov et al., 2005).

An *in vivo* radioactive labeling study on dark-adapted mouse reported that chromophore turnover occurs in rod receptor at a rate of 1.8×10^{-7} s^{-1} (Defoe and Bok, 1983). However, this study could not distinguish between *de novo* pigment synthesis and chromophore exchange within the existing pigment. Here we utilized the difference in the absorption maxima of 11-*cis*-retinal-bound Rho and 9-*cis*-retinal-bound isoRho to assess the rate of retinal dissociation from opsin. A recent study reported that purified opsin in DM micelles (0.05% w/v) showed a marked preference for 9-*cis*-retinal over 11-*cis*-retinal in regeneration experiments, suggesting that the binding pocket of opsin is more accessible to 9-*cis*-retinal than to 11-*cis*-retinal (Srinivasan et al., 2014). By contrast, our results showed that Rho in POPC/CHAPS bicelles can be readily regenerated with either, and the recombination reaction for 11-*cis*-retinal is even 50% faster than that for 9-*cis*-retinal. This is in line with the idea that the retinal-binding pocket was evolved to utilize

11-*cis*-retinal. It provides further evidence that the presence of lipid bilayer environment may modulate the conformation of receptor in a distinct mode from detergent systems. In our experiments, we found at 36 °C a k_{off} of (1.29 ± 0.02) $\times 10^{-7}$ s^{-1}. To our knowledge, this study is the first *in vitro* demonstration of chromophore exchange for a rod receptor.

In a classic electrophysiological study on the physiological noises of a single rod cell from toad retina, it was estimated that at 37 °C, in rod cells a Rho molecule "turns on" once every 400 years (Baylor et al., 1980). The chemical nature of this spontaneous activation of Rho remains obscure. Plausible mechanisms include 1) 11-*cis*-retinal may thermo isomerize to all-*trans*-retinal without any photoactivation, triggering the Meta-II pathway (Liu et al., 2009; Liu et al., 2011); 2) the breaking of the SB bond results in a active retinal-opsin non-covalent complex (Kefalov et al., 2001); and 3) regardless of retinal isomerization, the dissociation of retinal from the binding pocket produces opsin with basal activity (Cornwall and Fain, 1994; Cornwall et al., 1995; Surya et al., 1995). Previously, the rate of the thermal isomerization of 11-*cis*-retinal to all-*trans*-retinal in 1% digitonin was measured at temperatures above 70 °C, with an E_a of 24.5 kcal mol^{-1} (Hubbard, 1966). If we assume the Arrhenius plot for this reaction at high temperatures extended its linearity to physiological temperature, the corresponding thermal isomerization rate of 11-*cis*-retinal would be 1.9 $\times 10^{-7}$ s^{-1} at 36 °C. Nonetheless, the thermal isomerization of bound 11-*cis*-retinal is likely to be different from that of free retinal in solution. We could not determine whether thermal isomerization of 11-*cis*-retinal to all-*trans*-retinal was involved in our experiment, as the large excess of 9-*cis*-retinal to Rho imposed substantial technical challenge for quantifying the presence of all-*trans*-retinal. However, we obtained an $E_{a,\,off}$ of 38.9 ± 4.4 kcal mol^{-1}, which is clearly

higher than the E_a of 22 kcal mol^{-1} for thermal activation (Baylor et al., 1980). This indicates that the chromophore exchange observed here is at least not entirely due to thermal isomerization of retinal; it primarily involved direct breaking of the PSB and perhaps as well as thermal isomerization.

The apparent rate for the spontaneous dissociation of retinal from opsin (half-life 220 days at 28 °C, and 62 days at 36 °C) is in general three orders of magnitude higher than the spontaneous activation of Rho (Baylor et al., 1980). The spontaneous dissociation of 11-*cis*-retinal from cone opsin contributes to elevated noise and reduced sensitivity of cone photoreceptor cells compared to rod photoreceptor cells (Kefalov et al., 2005). This question is how much the spontaneous dissociation of retinal from opsin contributes to the two components of electrical dark noise in photoreceptor cells (Baylor et al., 1980).

3.4.4 ITC provided direct information on the reaction enthalpy of Rho regeneration

ITC is a powerful tool for studying binding events between molecules, as it yields information on the dissociation constant and binding enthalpy. However, examples of using ITC to investigate ligand-binding enthalpy of GPCRs remain rare, largely because of the difficulty of obtaining high-purity receptor samples in large quantity. To date, only a few GPCR domains have been studied by ITC (Fernando et al., 2007; Nisius et al., 2008; Rajarathnam and Rosgen, 2014). Here we presented the first ITC measurement of the binding enthalpy between a full-length GPCR and its native ligand. In contrast to photocalorimetry, our experiments are a direct measurement of the binding enthalpy and do not rely on complicated thermodynamic cycles involving error-prone calculations of

hydroxylamine dependent reaction steps (Cooper and Converse, 1976; Cooper, 1979). Interestingly, the value of $\Delta H°'$ of Rho is close to the difference between the E_a of Rho denaturation (100 kcal mol^{-1}) and opsin denaturation (73 kcal mol^{-1}), suggesting that $\Delta H°'$ contributes substantially to the thermostabilizing effect of retinal binding to opsin (Hubbard, 1958).

3.4.5 The energy landscape of Rho regeneration

We present a complete energy diagram based on the results of the two kinetic studies and the calorimetry experiment. The energy diagram assumes that the dissociation reaction of retinal from Rho is the reverse reaction of the recombination reaction of retinal and opsin, and that the reactions proceed through a common transition state but in opposite directions. The kinetics of the forward (k_{on}) and reverse reaction (k_{off}) enabled us to calculate the change of free energy from the ground state to the transition state ($\Delta^{\neq}G_{on}$ and $\Delta^{\neq}G_{off}$).

We also determined the K_d of the reaction of 11-*cis*-retinal and opsin to be 40 ± 2 pM at 28 °C (32 ± 2 pM at 25 °C). This value is similar to that of three high-affinity ligands for β_2 adrenergic receptor, carazolol (antagonist), iodopindolol (antagonist), BI-167107 (agonist), which have a K_d of less than 100 pM (Rasmussen et al., 2011a; Manalan et al., 1981; Contreras et al., 1986). We compared the kinetics and thermodynamic properties of β_2 adrenergic receptor and Rho binding with their ligands (Table 3-5). Despite similar K_d and $\Delta G°'$, the energy barriers for the association reaction between opsin and 11-*cis*-retinal ($\Delta^{\neq}G_{on}$), as well as for dissociation reaction ($\Delta^{\neq}G_{off}$), are

Table 3-5. The kinetic and thermodynamic parameters for β_2AR and Rho with their ligands at 25 °C

Receptor	β_2AR			Rho
Ligand	BI-167107 (Rasmussen et al., 2011a)	Carazolol (Rosenbaum et al., 2007)	Iodopindolol (Contreras et al., 1986)	11-*cis*-retinal**
k_{on} (M^{-1} s^{-1})	7.6×10^4 *	$> 6.3\times10^4$ *	8.0×10^6	6.6×10^2
k_{off} (s^{-1})	6.4×10^{-6}	6.3×10^{-6}	4.2×10^{-4}	2.1×10^{-8}
K_d (pM)	84	<100	53	32
$\Delta G°'$ (kcal mol^{-1})	-13.7	< -13.6	-14.0	-14.3
$\Delta G_{on}^{\neq}$ (kcal mol^{-1})	10.8	> 10.9	8.0	13.6
$\Delta G_{off}^{\neq}$ (kcal mol^{-1})	24.5	24.5	22.0	27.9

* Calculated based on the transition state theory, using K_d and k_{off} reported in the reference.

* * Calculated from the Arrhenius plot based on the kinetic data in this study

particularly high. For comparison, if the ligand-receptor binding process would be diffusion-limited (k_{on}: $10^8 \sim 10^{10}$ M^{-1} s^{-1}) (Alberty and Hammes, 1958), the $\Delta^{\neq}G_{on}$ is about 3.8 ~ 6.6 kcal mol^{-1}. Thus the relatively slow retinal binding rate is advantageous for the design of a photoreceptor, as it confers slow dissociation rate of retinal from opsin, and hence longer lifetime for the dark-state photoreceptor.

We further utilized the temperature dependence of the binding and unbinding kinetics to separate the enthalpic and entropic contribution to the free energy of activation. Ideally the difference between the activation enthalpy of the forward and reverse reactions should have the same value as the enthalpy of formation ($\Delta^{\neq}H_{on}$ - $\Delta^{\neq}H_{off}$ = $\Delta H^{o'}$). The results from the chromophore exchange experiment (*light blue*) and the ITC experiment (*dark blue*) are within the error estimation, supporting our assumption that the recombination reaction and the dissociation reaction measured here represent the reverse process of each other.

The activation energy ($E_{a,\,on}$) for the recombination reaction in bicelles is 20.8 ± 0.9 kcal mol^{-1}. Recently it was reported that the ($E_{a,\,on}$) in DM micelles is ~13 kcal mol^{-1}, lower by ~7 kcal mol^{-1}. One possible explanation is that a receptor conformation is more flexible in micelles than in bilayer(Kusnetzow et al., 2006), which reduces the energy barrier for opsin to reach the conformation competent for retinal binding. Another possible source of the difference is the viscosity of lipid bilayer, which has been reported to contribute to the energy barrier of ligand binding in GPCRs (Lee, 2004). Retinal binding with opsin proceeds through an intramembranous pathway (Wang and Duan, 2007), while for β_2 adrenergic receptor ligand binding is more likely to occur through the exposed extracellular surface (Wang and Duan, 2009). Therefore, the difference in $\Delta^{\neq}G_{on}$

for opsin and β_2 adrenergic receptor may be partially explained the different modes of ligand binding utilized by the two receptors.

3.5 Materials and Methods

3.5.1 Materials

E. coli TOP10 cells (Invitrogen) were used for plasmid propagation and isolation. 1D4-Sepharose 2B was prepared as described in Chapter II (Oprian et al., 1987; Knepp et al., 2011). Alexa488-DIBO was obtained from Molecular Probes/Thermo Fisher Scientific as a dry powder, dissolved in DMSO (5 mM), and stored at −20 °C. *n*-dodecyl-*β*-D-maltoside (DM) was obtained from Anatrace. 1-palmitoyl-2-oleoyl-*sn*-glycero-3-phosphocholine (POPC) was obtained from Avanti. 1-hexadecanoyl-2-(1-pyrenedecanoyl)-*sn*-glycero-3-phosphocholine (*β*-pyrene-C10-HPC) was obtained from Molecular Probes, Invitrogen.

3.5.2 Preparation of the POPC/CHAPS bicelles buffer

The POPC lipids were stored at −20 °C prior to use. The POPC lipids were dissolved in 20% (w/v) CHAPS solution at a 1: 1 ratio (w:w) to make a 10% (w/v) stock bicelle solution. The solution was frozen in liquid nitrogen and then thawed repeatedly to facilitate the dissolution of POPC. The POPC/CHAPS stock solution was diluted with Buffer A (25 mM MES, 25 mM HEPES, pH 6.0, 125 mM KCl) to make 1% (w/v) bicelle. To prepare pyrene-labeled bicelle, appropriate amount of *β*-pyrene-C10-HPC (1mg/mL DMSO solution) was directly added into 1% POPC/CHAPS bicelle solution.

3.5.3 Isolation of ROS membranes

Native rod outer segment (ROS) membranes were isolated under dim red light from frozen bovine retinas (W. L. Lawson Co., Lincoln, NE) by gentle homogenization, differential centrifugation and density gradient centrifugation as described (Papermaster

and Dreyer, 1974; Botelho et al., 2002). Aliquots of the membranes with a Rho concentration in the range 140–180 μM in 67 μM potassium phosphate buffer, pH 7.0, were stored under argon at −80 °C.

3.5.4 Immunopurification of ROS Rho or mutant Rho using 1D4-sepharose resin for the pigment regeneration studies

Bovine ROS or heterologously expressed mutant Rho were lysed with the solubilization buffer (1% (w/v) DM, 50 mM HEPES or Tris-HCl, pH 6.8, 100 mM NaCl, 1 mM $CaCl_2$ with complete EDTA-free Protease Inhibitor Cocktail, Roche) for at least 1 h at 4°C. To lyse cells, 1 mL of solubilization buffer was used for 10^7 cells. For ROS membranes, the volume of solubilization buffer was not critical, as long as the final solubilization buffer contains 1% DM. The lysate was cleared by centrifugation at 100,000 × g for 30 min. The supernatant fraction was mixed with 1D4-Sepharose-2B resin (binding capacity for Rho determined by UV-Vis spectroscopy: 600 μg/mL) and incubated overnight at 4°C. The resin was transferred in a centrifugal filter unit with a 0.45-μm microporous hydrophilic surface modified PVDF membrane (Ultrafree-CL; Millipore), which enables efficient removal of washing buffer. The resin was first washed with 1× DPBS containing 0.1% (w/v) DM for three times (30 min incubation each time), and then with a low-salt buffer (0.1% (w/v) DM in 2 mM phosphate buffer, pH 6.0). Eventually, the receptor was eluted with the elution buffer (100 μL, no less than the volume of the resin; 0.1% (w/v) DM and 0.33 mg/mL 1D5 nonapeptide TETSQVAPA peptide in 2 mM phosphate buffer, pH 6.0). The resin was incubated with the elution buffer on ice for at least 1 h. The purified receptor was collected in a clean 1.5 mL Eppendorf tube.

3.5.5 Immunoaffinity purification of opsin using1D4-sepharose resin for the ITC experiment

In a typical experiment, 0.25 mL aliquot of ROS membranes (~1.4 mg Rho) was solubilized using the wash buffer (2.5 mL; 7.5 mg/mL CHAPS, 1 mg/mL POPC, 137.5 mM NaCl, 25 mM MES, 25 mM hemisodium HEPES, 0.25 mM disodium EDTA, pH 6.0, supplemented with 0.14 mL 10% (w/v) CHAPS in water). The mixture was gently agitated for 30 min at 4°C. The insoluble material was removed by centrifugation for 10 min at 2,200 × g in a clinical desktop centrifuge. The supernatant fraction was incubated at 4°C for 3 h under gentle agitation with 1.6 mL packed 1D4-Sepharose 2B resin pre-equilibrated with wash buffer. The matrix was washed 4 times for 20 min each time with 6 mL wash buffer. The resin was then transferred into a 0.45-μm microporous centrifugal filtering unit (Ultrafree-CL; Millipore), washed once (1.0 mL; 10 mg/mL CHAPS, 10 mg/mL POPC, 137.5 mM NaCl, 25 mM MES, 25 mM hemisodium HEPES, 0.25 mM disodium EDTA, pH 6.0) and re-hydrated with POPC/CHAPS bicelle buffer supplemented with 50 mM hydroxylamine (1.0 mL). The sample in the filtration unit was illuminated with a 500 nm long-pass filter equipped fiber optics coupled microscope illuminator (Dolan) for one hour with gentle head-over-head mixing. The resin was washed 15 times with 1.0 mL POPC/CHAPS bicelle buffer. The large number of washing cycles is sufficient to ensure that the concentration of hydroxylamine is reduced below a level that might interfere with the ITC experiments. The washing buffer was removed by centrifugation and opsin was eluted twice with 1 mL of POPC/CHAPS bicelle buffer supplemented with 0.33 mg/mL nonapeptide TETSQVAPA. Typically, the

protein concentration was in the range 4.7 ± 0.2 μM (corresponding to 0.18 ± 0.02 mg/mL protein)

3.5.6 Lectin affinity purification of Rho for chromophore exchange experiment

As an alternate method to immunoaffinity purification, concanavalin A (ConA) bound to a gel matrix was employed to purify Rho from ROS membranes. The advantage is that the α-methylmannoside used for elution does not interfere with a potential second purification step using the 1D4 sepharose 2B resin. Briefly, an aliquot of ROS membranes (0.75 mL; ~4 mg Rho) was solubilized using a solubilization buffer containing phospholipids (7.5 mL; 12.2 mg/mL CHAPS, 1 mg/mL POPC, 137.5 mM NaCl, 25 mM MES, 25 mM hemisodium HEPES, 0.25 mM disodium EDTA, 1 mM $MnCl_2$ and 1 mM $CaCl_2$, pH 6.0). The mixture was gently agitated for 1 hour at 4°C. The insoluble material was removed by centrifugation for 10 min at 2,200 × g in a clinical desktop centrifuge. The supernatant was incubated at 4°C for 3 hours under gentle agitation with concanavalin A Sepharose conjugate affinity matrix (1.7 mL packed volume; Sigma). The concanavalin molecules of the affinity matrix were cross-linked by glutaraldehyde treatment to reduce leakage (Degrip, 1982b). The matrix was washed for 4 times, 20 min each time, with buffer OG (12.5 mL; 15 mg/mL *β*-octylglucoside, 137.5 mM NaCl, 25 mM MES, 25 mM hemisodium HEPES, 0.25 mM disodium EDTA, pH 6.0). The resin was transferred in a centrifugal filter unit with a 0.45-μm microporous hydrophilic surface modified PVDF membrane (Ultrafree-CL; Millipore). The washing buffer was removed by centrifugation and Rho was eluted with buffer OG supplemented with 100 mM *α*-methyl-D-mannoside (1 mL) for 3 times. The combined elution was concentrated to a volume of approximately 200 μL using an Amicon Ultra-4 centrifugal

ultrafiltration device with a regenerated cellulose membrane (Millipore). The concentrated sample was applied to a small Sephadex G-50 column (5 cm × 0.7 cm) equilibrated with buffer A (10 mL; 150 mM NaCl and 50 mM sodium acetate adjusted with hydrochloric acid to pH 5.5), followed by buffer A containing 1% CHAPS (10 mL), and 4 times 0.5 mL POPC/CHAPS bicelle buffer. The sample was eluted with the POPC/CHAPS bicelle buffer for 5 times (200 μL each). The main Rho-containing fractions were identified by UV-Vis spectroscopy, pooled and diluted with the POPC/CHAPS bicelle buffer to 10 mL.

3.5.7 Determination of molar extinction coefficient of 11-*cis*-retinal in the POPC/CHAPS bicelle buffer

The analysis of the results from titration calorimetry experiments in terms of molar binding enthalpies is critically dependent on a precise knowledge of the concentrations of ligand and protein solutions. Therefore it is necessary to determine the molar extinction coefficients under the experimental buffer conditions. The strategy is to utilize the know literature value for the molar extinction of 11-*cis*-retinal in ethanol, $\varepsilon_{376.5\ nm}$ = 24,935 M^{-1} cm^{-1} (Hubbard and Wald, 1952; Dieterle and Robeson, 1954; Brown and Wald, 1956). The buffer effects on the 11-*cis*-retinal spectrum were determined by a dilution assay. Briefly, an aliquot of ethanolic 11-*cis*-retinal solution (10 μL) was added to ethanol or POPC/CHAPS bicelle buffer (1 mL) using a micro syringe (10 μL gas-tight model RN, Hamilton Co., Reno, NV). The exact volume was gravimetrically determined and used in the calculation of the dilution factor. UV-Vis spectra were recorded over the range from 750 to 250 nm with 1-nm step size, 0.2-s integration time, and 1-nm slit width. The experiment was performed in triplicate, resulting in 2.6% increased absorption of the

spectral maximum in POPC/CHAPS bicelle buffer as compared with ethanol. The observed absorption maximum of 11-*cis*-retinal in ethanol was at 378.5 nm, identical to the maximum observed in POPC/CHAPS bicelle buffer. This corresponds to a molar extinction coefficient for 11-*cis*-retinal in POPC/CHAPS bicelle buffer of $\varepsilon_{378\ nm}$ = 25,574 M^{-1} cm^{-1}. The A254/A378.5 ratio is 0.73, slightly higher than the literature value of 0.70 (Brown and Wald, 1956). This indicates a high isomeric purity if the sample, as contamination other isomers, such as all-*trans*-retinal or and 9-*cis*-retinal will result in lower values of this ratio. The isomeric purity is confirmed by reverse phase high performance liquid chromatography (HPLC) using an analytical C18 column and acetonitrile mixtures with ammonium acetate buffer (pH 4.5) shows 2.4% impurities at longer retention time for a different sample from the same master stock solution (Dr. Shixin Ye, personal communication). In comparison, dilution in the same buffer containing 2% digitonin instead of 1% POPC and 1% CHAPS, the absorption maximum is red-shifted to 383.5 nm with a reduction of the absorbance of just 0.5% compared to ethanol. In light of these findings, it is unlikely that the extinction coefficient in POPC/CHAPS bicelle buffer is significantly different compared with ethanol solutions, in contrast to the earlier observations that in digitonin the extinction coefficient of 11-*cis*-retinal is about 13% reduced as compared to ethanol(Brown and Wald, 1956).

3.5.8 Determination of molar extinction coefficients of opsin and Rho

Knowledge of the molar extinction coefficient for 11-*cis*-retinal allows titration of the binding site for determination of the extinction coefficients for opsin and Rho in POPC/CHAPS bicelle buffer. From a linear dilution series of 11-*cis*-retinal with 16 concentrations in the range from 0 to 31.5 μM, 120 μL aliquots were mixed with 200 μL

aliquots of purified opsin (10.2 μM). The samples were incubated at room temperature for 4 h in the dark. The correlation of the absorption of 11-*cis*-retinal in buffer at 378 nm, corrected for a dilution factor *df* = 0.375, and of Rho in the opsin samples at 499 nm yields a perfectly linear correlation at sub-stoichiometric ratios, corresponding to a molar extinction coefficient of Rho $\varepsilon_{499\ nm}$ = 42,742 M^{-1} cm^{-1}.

3.5.9 Assessing the stability of opsin solubilized in DM micelles

The purified opsin (15 μL, 2.7 μM, solubilized in 0.1% DM) was aliquoted into 1.5-mL Eppendorf tubes and photobleached by irradiating with a 505-nm LED light source (Thorlabs) for 30 s. After photobleaching, the samples were kept in the dark at 28 °C for varied durations. Then 135 μL of POPC/CHAPS bicelle buffer supplemented with 11-*cis*-retinal. The final concentration of opsin was 0.27 μM, and the molar ratio of 11-*cis*-retinal to opsin was 1.5:1. The regeneration reaction was allowed to proceed overnight (>15 h) to reach completion. The dark and the photobleached spectrum of the regenerated samples were recorded as described above. In the presence of 11-*cis*-retinal, longer exposure to 505-nm LED light source (1 min) were required to fully photo bleach the photoreceptor. The extent of regeneration was evaluated based on the 500-nm absorbance of the difference spectrum.

3.5.10 Assessing the stability of opsin solubilized in POPC/CHAPS bicelles

The purified opsin (15 μL, 2.7 μM, solubilized in 0.1% DM) was added to 120 μL of POPC/CHAPS bicelle buffer. The samples were photobleached by irradiating with a 505-nm LED light source (Thorlabs) for 30 seconds. After photobleaching, the samples were incubated in the dark at 28 °C for varied durations. Then 11-*cis*-retinal diluted in POPC/CHAPS bicelle buffer (15 μL) was added into the opsin samples. The final

concentration of opsin was 0.27 μM, and the molar ratio of 11-*cis*-retinal to opsin was 1.5:1. The regeneration reaction was allowed to proceed overnight (>15 h) to reach completion. The dark and photobleached spectrum of the regenerated samples were recorded as described above. In the presence of 11-*cis*-retinal, longer exposure to 505-nm LED light source (1 min) were required to fully photo bleach the photoreceptor. The extent of regeneration was evaluated based on the 500-nm absorbance of the difference spectrum.

3.5.11 Measuring retinal entry and release kinetics based on quenching of Trp fluorescence

Fluorescence spectroscopy was performed at 28 °C on a SPEX Fluorolog Tau-3 spectrofluorometer (Horiba) in photon-counting mode. The time-course experiments were done by adding aliquots of the elution samples from receptors (30 μL) to the POPC/CHAPS bicelle buffer to give a final concentration of 0.25-0.30 μM under constant stirring. The excitation wavelength was 295 nm with a 0.6-nm band-pass, and the emission was measured at a wavelength of 330 nm with a 15-nm band-pass. The 11-*cis*-retinal or 9-*cis*-retinal stock solution in ethanol was diluted in the POPC/CHAPS bicelle buffer, and 20 μL of this working dilution was added to the cuvette to give a desired final concentration. For each measurement, the concentration of freshly diluted retinal was determined from its 378-nm absorbance (extinction coefficient 24,400 M^{-1} s^{-1}). The reaction rate constant for retinal release was obtained by fitting the fluorescence signal corresponding to Meta-II decay with monoexponential decay model. The pseudo-first order rate constant (k_1) was obtained by fitting the fluorescence signal corresponding to

pigment regeneration with monoexponential decay model. The second-order recombination reaction rate constant (k_2) was calculated as k_1/c_{retinal}.

The procedure for preparing Alexa488-labeled Rho has been described in Section 2.4.7. Measurement of retinal entry kinetics based on quenching of Alexa488 fluorescence has been described in Section 2.4.13.

3.5.12 The chromophore exchange of ROS Rho

Retinoid solution in benzene (approximately 0.3 mL 30 mM) was transferred to nitric acid washed 4-mL glass vial. The solvent was evaporated under a stream of argon under red light. The sample was kept at high vacuum for 15 min. Then the retinoids was dissolved in pure ethanol (0.5 mL). The stock solution was diluted by 20-fold (0.1 mL of stock solution in 1.9 mL ethanol), and a UV-Vis spectrum of a 1:100 dilution in ethanol was measured. Concentrations were normalized to about 2mM for the diluted stock. Lectin-affinity purified ROS Rho was obtained in the POPC/CHAPS bicelle buffer and diluted with the bicelle buffer to give a total volume of 6.74 mL (0.21 mg mL^{-1}, 5.2 μM). The sample was divided into five volumes and supplemented with the following: A) ethanol; B) 11-*cis*-retinal; C) 9-*cis* retinal (concentration); D) all-*trans*-retinal E) 50 mM NH_2OH. Each combination of Rho with retinal were incubated under five different conditions: 1) 28 °C for 11.6 days (10^6 s); 2) 36 °C for 11.6 days (10^6 s); 3) 44 °C for 11.6 days (10^6 s); 4) 28 °C for 2×11.6 days (2×10^6 s); 5) 36 °C for 2×11.6 days (2×10^6 s); 6) 44 °C for 2×11.6 days (2×10^6 s); 7) 28 °C for 3×11.6 days (3×10^6 s). The samples were denoted as A1, A2, … A6, A7….E6, E7. Each sample contained a total volume of 150 μL (32 μg of Rho), and supplemented with retinals (3.75 μL of 2 mM ethanolic solution, final concentration 49 μM). The samples were kept in 200-μL PCR tubes inside

1.5-mL brown micro centrifuge tubes. Each set of 5 tubes was kept in large UZ tubes and wrapped in aluminum foil and incubated in a large brown screw cap glass in a water bath. To overcome buoyancy, large steel rods were added into the UZ tubes as weights. At the end of incubation, the samples were checked for their volume, and no loss was observed. The samples were then purified using 1D4-sepharose resin. The slurry of 1D4-Sepharose-2B (100 μL) was loaded in Microcon-MC 0.2-μm PVDF filter and spun to remove the storage buffer. Then the samples were added to resin and mixed at 4 °C for 4 h on the wheel. The unbound fraction was checked with UV-Vis to confirm complete immunoprecipitation. The resin was washed 5 times with 400-μL wash buffer (Buffer A + 0.75% CHAPS + 0.1% POPC). The mixture of Rho and isorhodopsin) was eluted with the elution buffer (wash buffer + 0.33 mg mL^{-1} 1D5 peptide, 3×30 μL, 20 min each time). The purified receptor was characterized using UV-Vis spectroscopy.

We found that at 44 °C, there is significant opsin denaturation, which needs to be corrected for. Let the total recovery of isoRho and rhodopsin be *a,* and the fraction of isoRho exchanged from rhodopsin be *b*:

$$a = \frac{[\text{isoRho}]_{\text{recovered}} + [\text{Rho}]_{\text{recovered}}}{[\text{Rho}]_{\text{initial}}}$$

$$b = \frac{[\text{isoRho}]_{\text{recovered}}}{[\text{isoRho}]_{\text{recovered}} + [\text{Rho}]_{\text{recovered}}}$$

The fraction of retinal spontaneous dissociation is $(1-a+ab)$.

3.5.13 Determination of the binding enthalpy of 11-*cis*-retinal and opsin using ITC

For each measurement, opsin and 11-*cis*-retinal bicelle solution were prepared fresh. Purified opsin was obtained in the POPC/CHAPS bicelle buffer. The concentration

of the opsin sample was determined to by UV-Vis spectroscopy (4.7 ± 0.2 μM). To avoid the dilution heat of ethanol in water, the ethanolic solution of 11-*cis*-retinal was evaporated with argon under red light, and re-dissolved in POPC/CHAPS bicelle buffer. The solution was centrifuged (14, 000 × g, 10 min) to remove any the insoluble fraction. The concentration of 11-*cis*-retinal solution was determined by UV-Vis spectroscopy.

3.5.14 Determination of retinal diffusion kinetics among bicelles

In the stop-flow apparatus, the donor POPC/CHAPS bicelle contains 100 μM 11-*cis*-retinal, and the acceptor POPC/CHAPS bicelle are doped with 0.1% *β*-pyrene-C10-HPC (w/w). The experiment was carried out under dim red light. The temperature of solutions was maintained at 28 °C by pumping water from water bath with temperature controller into the sample chamber. The two solutions were simultaneously injected into the mixing chamber. After rapid mixing, the transfer of retinal was monitored by the decrease of pyrene fluorescence. The fluorescence signal was acquired from 360 nm to 585 nm, at a rate of 60 scans s^{-1}. The spectrum of pyrene was extracted by principle component analysis. The component corresponding pyrene fluorescence was fitted using monoexponential model with background.

Chapter Four: Mutagenesis study to identify the retinal entry pathway in opsin

4.1 Summary

The visual photoreceptor rhodopsin (Rho) consists of a chromophore 11-*cis*-retinal bound inside a heptahelical polypeptide backbone. However, the molecular mechanism for retinal to enter the ligand binding channel is not well understood. Here we approached this question by assessing how mutations affect retinal entry and release kinetics. We measured the entry kinetics by two FRET-based assays utilizing intrinsic tryptophan fluorescence and extrinsic Alexa488 fluorescence of a bioorthogonally-labeled Rho mutant. We identified a set of residues at the fifth and sixth transmembrane (TM) helices where mutations exert a much greater influence on the retinal entry kinetics than on the retinal release kinetics. We employed three criteria to evaluate the relative influence of these mutations: 1) the correlation between side-chain size and entry kinetics; 2) the change in the activation energy for retinal entry; 3) the effect of increasing polarity at these sites. We found that three sites, F208, F212 and A269, are particularly important in regulating retinal entry. Based on these findings, we propose a model for retinal entry.

4.2. Introduction

The visual photoreceptor Rho consists of an apoprotein opsin and its native ligand 11-*cis*-retinal that is covalently linked to K296 of opsin via a protonated Schiff base (PSB) bond (Wald, 1968). 11-*cis*-retinal is a strong inverse agonist that stabilizes Rho at its inactive state with minimal basal activity. Upon photobleaching, 11-*cis*-retinal absorbs a photo to isomerize to all-*trans*-retinal, triggering a series of conformational changes to reach the active Meta-II Rho, the state capable of activating transducin. Meta-II Rho signaling is shut off by phosphorylation of the receptor and subsequent binding with arrestin (Wilden et al., 1986; Kühn and Wilden, 1987), a process called desensitization that occurs within tens of milliseconds to one second in photoreceptor cells (Richard and Lisman, 1992; Ranganathan and Stevens, 1995). The hallmark of GPCR activation is the relative rotation of TM3, TM5, and particular the outward tilt of TM6, which opens the cytoplasmic cavity for G protein binding. Biochemical and structural studies have firmly established the correlation between this particular conformation and the receptor's capacity to activate G protein (Farrens et al., 1996; Sheikh et al., 1996; Park et al., 2008; Deupi et al., 2012a; Rasmussen et al., 2011b).

The docking mode of 11-*cis*-retinal in the ligand binding channel of dark-state Rho has been defined first through biochemical studies (Nakayama and Khorana, 1990b) and structural studies (Palczewski et al., 2000; Okada et al., 2004). Nonetheless, the mechanism for 11-*cis*-retinal to enter and exit the binding pocket remains obscure. A bewildering feature about the crystal structure of the dark-state Rho is that it reveals no obvious ligand entry or exit site on the protein surface, while other GPCRs invariably exhibit a ligand binding channel accessible to the extracellular environment (Katritch et

al., 2012). By comparison, in the structures of opsin (Park et al., 2008) and Meta-II Rho (Choe et al., 2011), two openings are found in proximity of the two ends of retinal (Choe et al., 2011; Hildebrand et al., 2009), one between TM1 and TM7 close to the PSB linkage (Opening A) as a result of the rotamer change of F293, the other between TM5 and TM6 close to the *β*-ionone ring (Opening B) due to the outward movement of F208, F212 and F273. Based on the structural studies, it was inferred that retinal entry and release proceed through an intramembraneous pathway, utilizing these two openings to enter and exit the ligand binding pocket (Piechnick et al., 2012; Hildebrand et al., 2009). The second inference was that retinal entry requires the active conformation, as the two openings are not found in the inactive state. This "active conformation" theory seems appealing because it is in line with the high partition coefficient of retinal between lipid bilayer and water (Frederiksen et al., 2012), and consistent with the sequence of events in Rho activation and signaling.

For the two openings, there are in principle five possible scenarios for retinal entry and release: 1) Opening A for both entry and release; 2) Opening B for both entry and release; 3) Opening A for entry and B for release; 4) A for release and B for entry; and 5) retinal entry and release promiscuously use Opening A and B. The molecular dynamics simulation alone could not distinguish the specific roles of these two openings (Hildebrand et al., 2009).

To answer this question with experimental evidence, Piechnick *et al.* generated a series of mutations at the putative entry and exit site and the middle of the ligand-binding channel, and measured the effect of these mutations on retinal entry and release kinetics. Their rationale was straightforward: if a particular opening is used for retinal entry, then a

mutation at this site is expected to alter the entry kinetics but have little effect on the exit rate, and vice versa. However, the results did not fall into the predicted pattern: a number of mutations simultaneously changed the entry and exit kinetics (Piechnick et al., 2012).

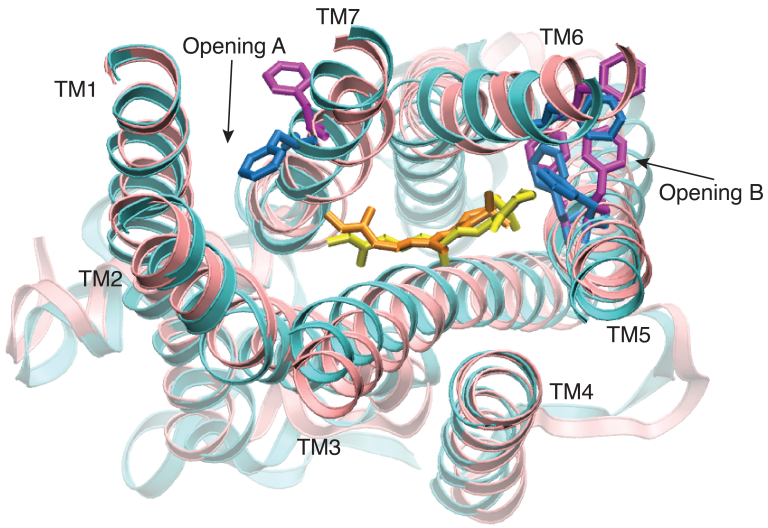

Figure 4-1. Comparison of the crystal structure of dark-state Rho (PDB accession code 1U19) and Meta-II Rho (3XPO). The polypeptide backbones (view from the EC side) of Rho are shown in *cyan*, and that of Meta-II Rho in *pink*. The residues are highlighted as sticks (dark state: *blue*; Meta-II: *magenta*). 11-*cis*-retinal is shown in *yellow* and all-*trans*-retinal in *orange*. The N-terminus and EC loops are removed to reveal the retinal. The transition from inactive conformation to active conformation exposed two openings (Opening A and B) at the two ends of the bound retinal. Four residues (Opening A: F208, F212, F273; Opening B: F293) at the two openings have undergone major structural changes, rotating outward from the inactive state.

It was reported that the constitutively active mutant M257Y (Han et al., 1998) exhibits slower rather than faster retinal entry kinetics, and fusing a transducin-mimic peptide known to stabilize the active conformation to the C-terminus of Rho also reduces the binding rate {Schafer, 2015 #1428}. These observations constitute a greater attack on the active conformation theory, because both M257Y mutation and transducin peptide fusion are expected to shifts the equilibrium to the active conformation (Deupi et al., 2012a; Tsukamoto and Farrens, 2013). Therefore, the Meta-II Rho and opsin structure characterized by the outwardly tilted TM6 may not represent the conformation competent for retinal uptake. Retinal entry obviously cannot occur at Meta-II state while the binding pocket is still being occupied. Yet it remains unclear whether after all-*trans*-retinal dissociation, opsin would spontaneously "collapse" to the inactive conformation, or retain the active-state-like conformation until retinal entry "reset" it. The specific location of the aforementioned Opening A and B were assigned based on the active conformation, which may underlie the ambiguous results in the earlier retinal entry kinetics study (Piechnick et al., 2012).

Here we present results on retinal entry and release in Rho mutants. We adopted a similar approach based on site-directed mutagenesis combined with retinal entry and exit kinetics. We improved the experimental design in several important ways. First, we reconstituted the receptor into POPC/CHAPS bicelles, which thermostabilizes the ligand-free opsin more effectively than DM micelle. Second, we used two complementary FRET-based assays to measure the retinal entry kinetics. The Trp-based assay detects retinal uptake by the ligand-binding channel, and the Alexa488-based assay reflects the formation of PSB.

4.3 Results

4.3.1 The mutations at TM5 and TM6 primarily alter the retinal entry kinetics but not the exit kinetics

We generated a series of mutations at five sites close to Opening B (between TM5 and TM6): F208, F212, A269, G270, F273. The side chains of F208, F212 and F273 exhibited major translocations in the structure of Meta-II Rho. A269 is situated on the opposite side of F212, and we reasoned that increasing the size of the side chain might contribute to the sterical hindrance. In both dark-state Rho and Meta-II Rho, these residues point outward from, rather than protrude into the ligand binding channel. G270 was added as reference. We utilized the Trp fluorescence quenching assay (the details of the assay has been described in Chapter 2 and Chapter 3) to measure the retinal entry and exit kinetics. We found that these mutations have a much more pronounced effect on the retinal entry rates than the retinal exit rate. The mutant with the fastest retinal entry kinetics was G270 L (4.2 ± 0.4 as compared with wt), the slowest F212 W (0.043 ± 0.022), spanning two orders of magnitude. By comparison, the release kinetics ranged from 2.4 ± 1.0 (F212A) to 0.78 (A269F). Therefore, the mutations at Opening B (Figure 4-2) exert a much greater effect on the kinetics retinal entry than release.

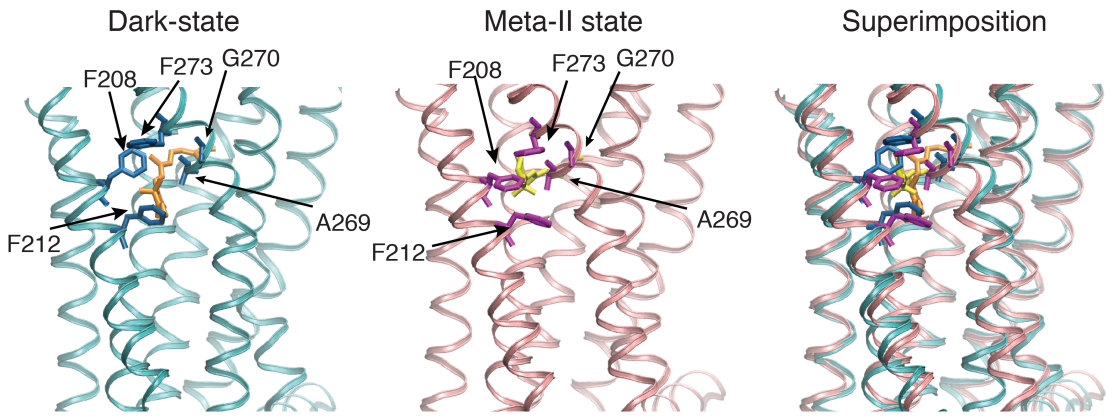

Figure 4-2. The tested TM5/6 mutations. The side view of polypeptide backbones of Rho (1U19) and Meta-II Rho (3XPO) are shown in *cyan*, and that of Meta-II Rho in *pink*. The five residues tested in the present study (F208, A269, G270, F273, F273) are shown as sticks (dark state: *blue*; Meta-II: *magenta*), 11-*cis*-retinal in *yellow* and all-*trans*-retinal in *orange*.

4.3.2 The effect of side-chain size is dependent on the site

We assessed how varying the side-chain size will alter the retinal entry kinetics. We chose a series of hydrophobic residues A, L, F, W, with increasing sterical hindrance. In this way we avoided dramatic alteration in their electrostatic, hydrogen bonding and hydrophilicity properties. For A269 and G270, we did not have the W mutation, or the L mutation for F273. For the F208, F212, A269, F273 mutants, we utilized both the Trp-based assay and Alexa488-based assay to ascertain the proper formation of a mature pigment as indicated by the PSB. The entry kinetics measured by the two different assays is generally consistent, as we have observed for the wt Rho. Therefore, we concluded that these mutations do not affect PSB formation; their primary role is to modulate the property of ligand entry site.

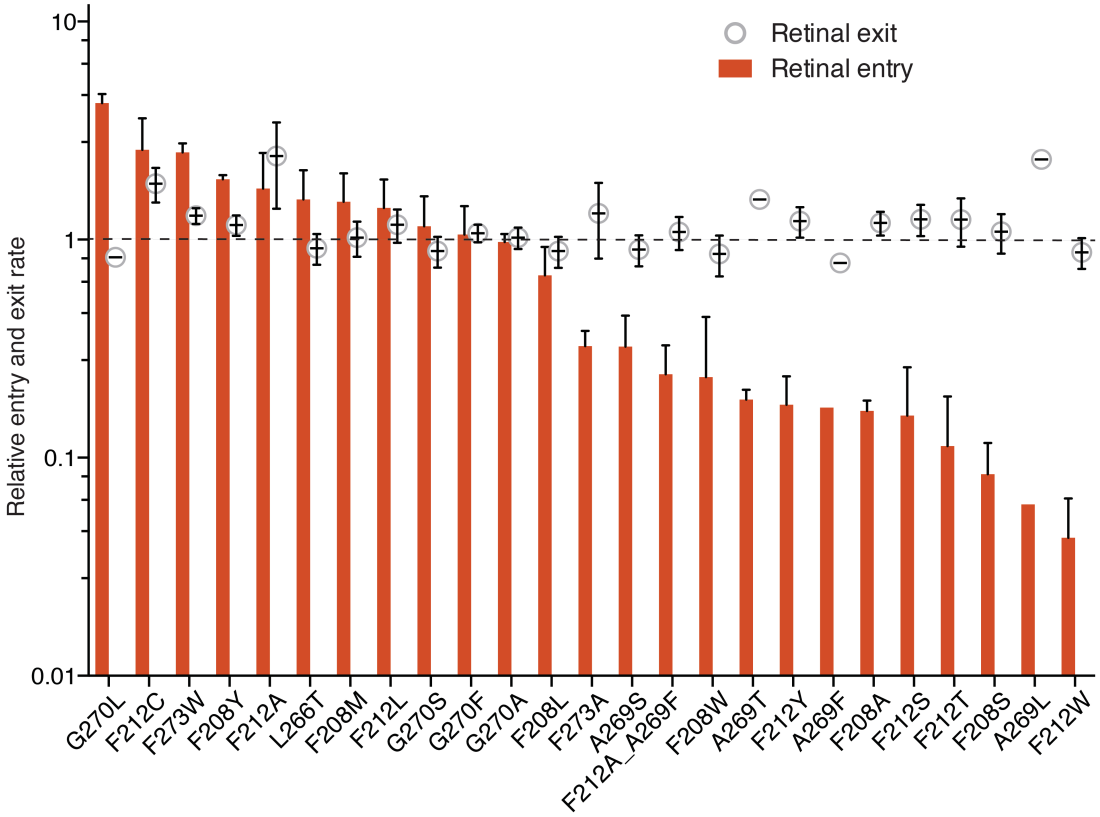

Figure 4-3. The retinal entry and release kinetics. All the values are normalized against that of wt Rho (dash line). The entry kinetics are shown as red bar, and the release kinetics as grey empty circle. The mutants are arranged based on their entry kinetics. For the tested mutants, the variation in retinal entry kinetics is much greater than that of the release kinetics.

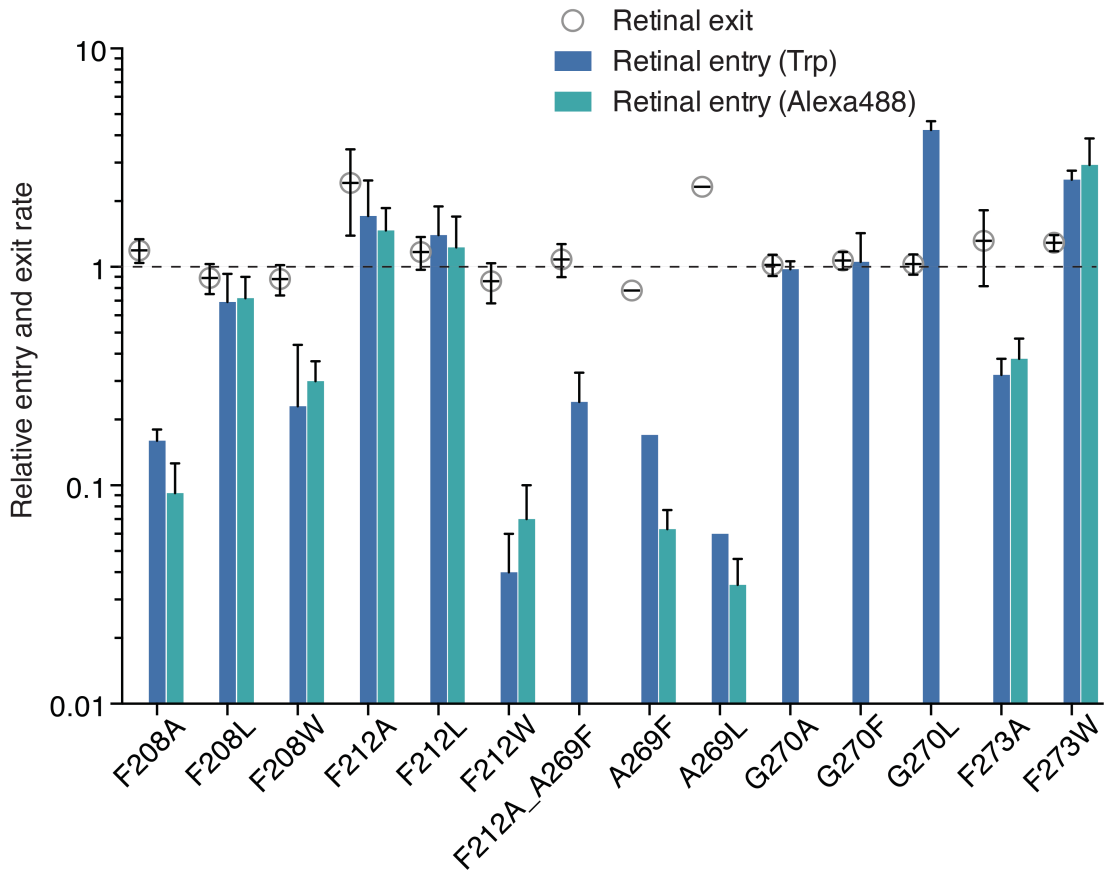

Figure 4-4. The effect of changing the side-chain size. All the values are normalized against that of wt Rho. The entry kinetics are shown as blue (measured by the change in Trp fluorescence) and turquoise (measured by Alexa488 fluorescence) bars, and the release kinetics as grey empty circle.

To our surprise, we found that increasing the side-chain size did not necessarily slow down the entry kinetics, and reducing the side-chain size may not always accelerate it: the behaviors of these mutations are site-dependent. For F208, increasing the side-chain size (F208W) or decreasing it (F208A) both resulted in slower retinal entry kinetics. For F212 and A269, the consequences of the mutations are more straightforward: retinal entry kinetics is negatively correlated with the side-chain size. We also tested the double mutant F212A/A269F, whose effect is the energetic

combination of the two individual mutations. The mutations at G270 are relatively minor compared with other sites, although G270L caused significantly faster entry kinetics. The effect of F273 mutations is the opposite of that of F212 and A269: decreasing the side-chain size led to slower retinal uptake.

4.3.3 The mutations affect both the activation enthalpy and entropy of retinal entry reaction

We measured the temperature-dependent retinal entry kinetics for five mutants, F208W, F212A, F212W, F273A, and F273W by Alexa488-based retinal entry assay. The fluorescence of Alexa488 falls into a clean window of retinal absorbance. As a result, this assay is compatible with a wide range of retinal concentrations and enabled us to measure retinal entry kinetics over three-orders of magnitude (k_2 10 ~10^4 M^{-1} s^{-1}). This dynamic range is superior that that of the Trp-based assay, as the Trp fluorescence signal is significantly quenched by a high concentration of retinal, which would impose a great technical difficulty for measurements in "slow" mutants. We have previously benchmarked the Alexa488-based assay against the Trp-based assay, and demonstrated that the engineered S144-Alexa488 Rho exhibited similar thermodynamic parameters compared with wt Rho (Chapter Three).

We calculated the change in the activation free energy, enthalpy and entropic term for these mutants. We found that two mutations, F208W and F212A, caused significant change in the activation enthalpy. F208W increased the activation enthalpy (ΔH) by 4.8 ± 3.1 kcal mol^{-1} while F212A reduced it by −3.7 ± 1.6 kcal mol^{-1}. We also found that F208W, F212A and F212W changed the entropic term ($-T\Delta S$, calculated for 28 °C) by 3.9 ± 3.1 kcal mol^{-1}, −3.5 ± 1.6 kcal mol^{-1}, and −3.0 ± 1.8 kcal mol^{-1}, respectively. The

thermodynamic effects of F273A/W are less significant compared to the mutations at F208 and F212.

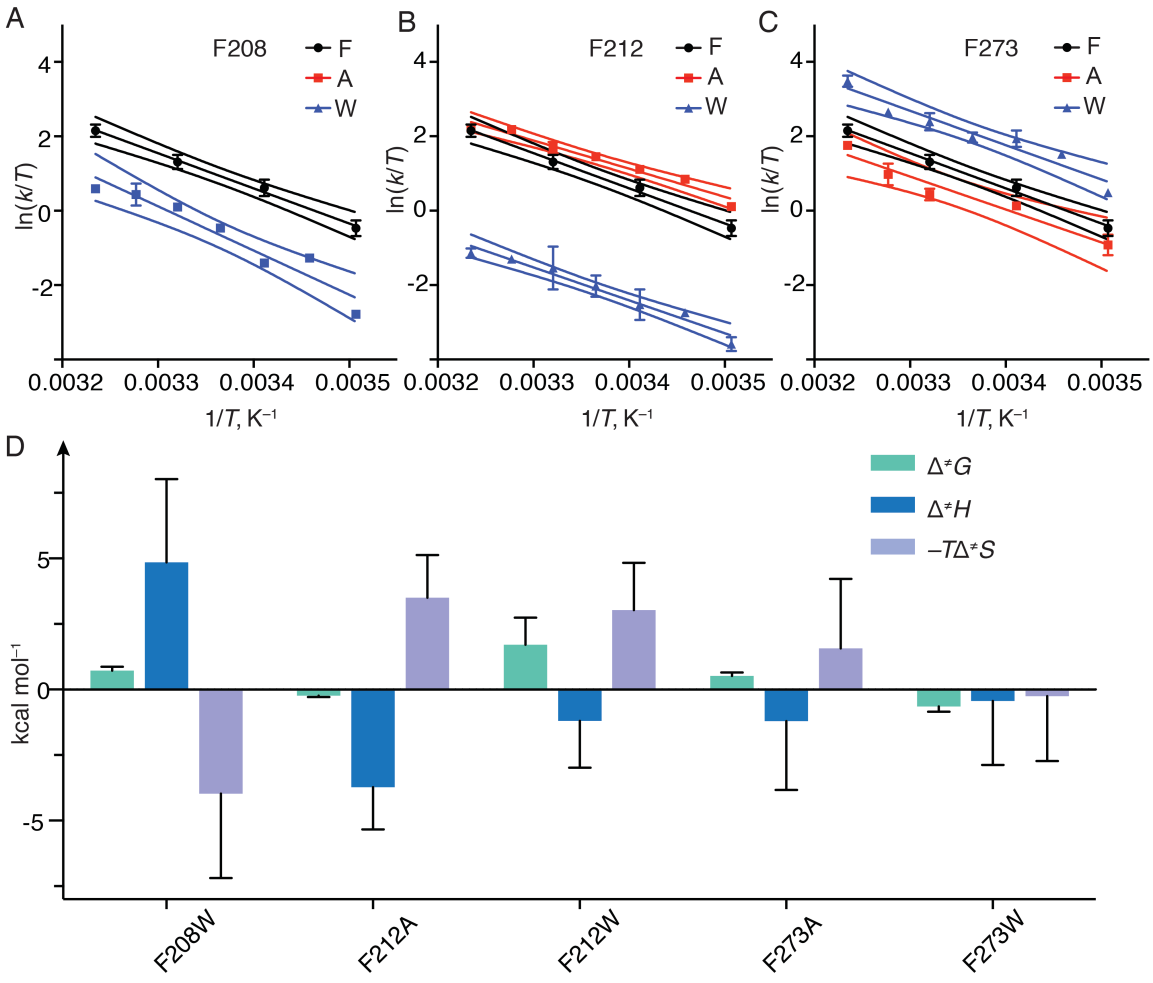

Figure 4-5. The activation energy of F208, F212 and F273 mutants. A-C) The thermodynamic effect of increasing the side-chain size (W) and decreasing it (A) at position 208, 212 and 273 are assessed by Eyring plot. The entry kinetics are measured by Alexa488 fluorescence quenching on S144-Alexa488 Rho background. **D**) The changes in activation free energy ($\Delta^{\neq}G$, *green*), enthalpy ($\Delta^{\neq}H$, *blue*), and entropy ($-T\Delta^{\neq}S$, *violet*) are shown as bar graphs.

4.3.4 Polar residues at TM5 and TM6 slows down retinal entry

We also tested the effect of adding polar residues at position 208, 212, 269, and 270. Compared with alanine and phenylalanine, serine and tyrosine only differ from them in having an additional hydroxyl group, the comparison of S/A and Y/F pairs are particularly meaningful as it minimizes the influence on the sterical factor. We found that substitution of A for S at position 212 and 269 caused a sharp decrease in retinal entry kinetics. Similar effect was observed for F212Y. We could not measure the retinal entry kinetics for A269Y because this mutant simply could not be regenerated after prolonged incubation with a high concentration of retinal (15 μM, over 48 h). Thus compared with A269F, A269Y further slowed down retinal entry kinetics. F212T and A269T also impeded retinal entry. The behavior of site 208 was different from 212 and 269. Two mutants, F208S and F208T, exhibited slower retinal entry kinetics, while F208Y accelerated retinal uptake. Different from 208, 212 and 269, G270S does not cause a significant change compared to wt or G270A.

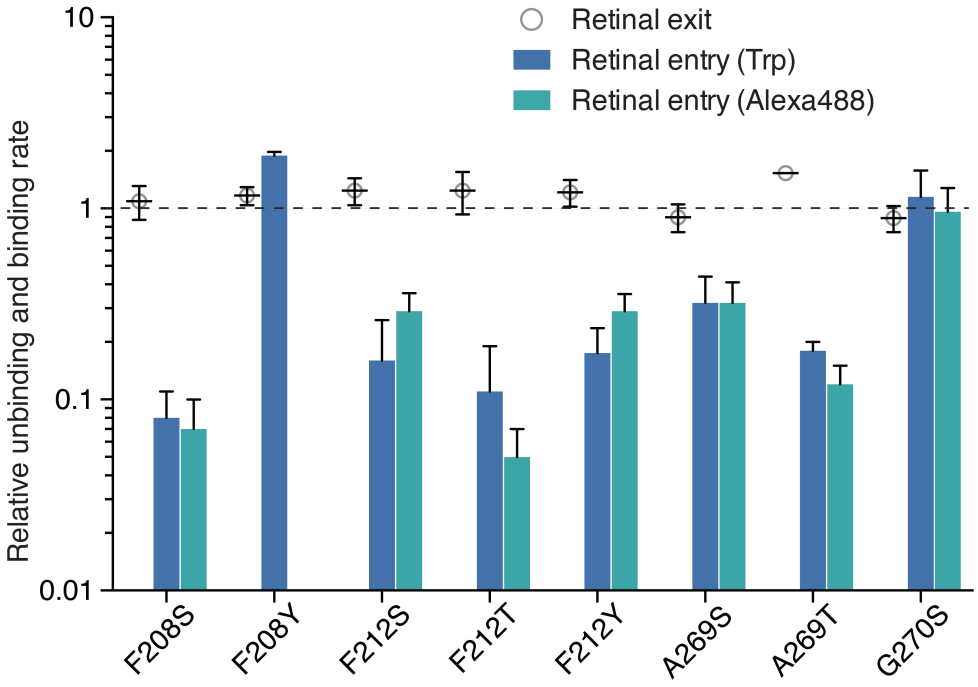

Figure 4-6. The effect of polar mutations at position 208, 212, 269 and 270. All the values are normalized against that of wt Rho. The entry kinetics are shown as blue (measured by the change in Trp fluorescence) and turquoise (measured by Alexa488 fluorescence) bars, and the release kinetics as grey empty circles. With the exception of F208Y, increasing the polarity at position 208, 212 and 269 reduced the retinal entry kinetics.

4.4 Discussion

4.4.1 A model for retinal uptake by the ligand binding pocket

Based on the retinal entry and release kinetics for the tested mutants, we propose the following model for retinal entry and release in Rho, whose key points are summarized as follows: 1) the crystal structure of Meta-II Rho represents the Rho conformation when all-*trans*-retinal dissociates from the ligand binding channel (*i.e.* Meta-II decay); 2) after retinal release, active-state-like opsin (Ops∗) collapses to a conformation resembling the inactive state (Ops); 3) the population of ligand-free opsin exists in an equilibrium of different conformations, one of which is competent for retinal uptake (Ops∗∗); 4) retinal entry occurs at the Opening A of Ops∗∗ between TM5 and TM6, with F208, F212, and A269 as the gating residues; 5) the rate-determining step for the recombination reaction between opsin and 11-*cis*-retinal is the initial binding between opsin and retinal to form a non-covalent complex, rather than Schiff base formation, while the rate-determining step for the retinal release is Schiff base hydrolysis rather than its dissociation from the ligand-binding channel.

4.4.2 The active conformation is for retinal release, not for retinal entry

In our attempt to derive the model for retinal entry and release, we first rejected the theory that retinal entry requires the active conformation (Piechnick et al., 2012). In the introduction we have discussed the implication of the slower retinal entry kinetics observed for opsin carrying the activating mutation M257Y and the transducin-peptide fusion(Schafer and Farrens, 2015). More importantly, the active conformation theory contradicts the fact that opsin has a marked preference for 11-*cis*-retinal over all-*trans*-

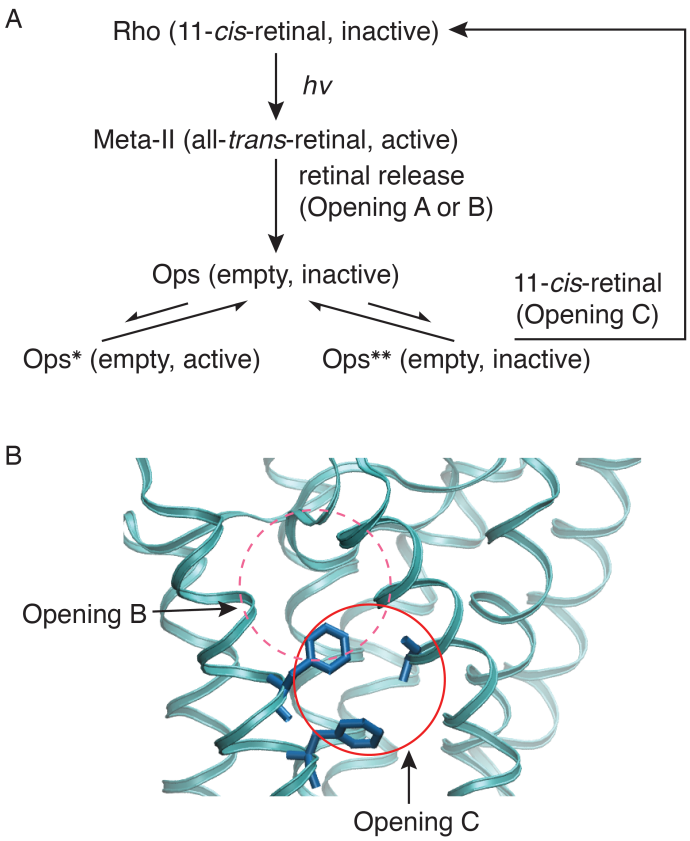

Figure 4-7. The model for retinal entry and release. A) The scheme of retinal entry and release. All-*trans*-retinal in the photoactivated Meta-II Rho was released through either Opening A between TM1 and TM7, or Opening B between TM5 and TM6. The ligand-free, inactive opsin exists in an equilibrium between different conformations. Opsin∗ resembles the active conformation and is capable of activating transducin. Opsin∗∗ is the conformation for retinal entry. We postulate that the overall backbone of Opsin∗∗ is closer to the inactive conformation than to the active conformation. **B)** The location of retinal entry site Opening C (*red circle*) are shown on the polypeptide backbone of dark-state Rho. The key residues F208, F212 and A269 are shown as sticks in *blue*. Opening B (*red dash circle*) found in the active conformation are one turn of helix above Opening C.

retinal, into the ligand binding channel. Various lines of evidence have demonstrated that the active conformation makes the ligand binding channel more accessible to all-*trans*-retinal. It was also known that a lower pH promotes the active conformation (Vogel and Siebert, 2001) and that all-*trans*-retinal stimulates opsin's ability to activate transducin only at weakly acidic pH (Sachs et al., 2000), indicating a correlation between active conformation and all-*trans*-retinal binding. Two activating mutations, E113Q (Sakmar et al., 1989) and M257Y (Schafer and Farrens, 2015) have been shown to enable opsin to bind with all-*trans* retinal. Mutant opsin stabilized towards active conformation was shown to have higher affinity for all-*trans*-retinal binding than for 11-*cis*-retinal (Schafer and Farrens, 2015). Thus if the active conformation theory is true, opsin's affinity with all-*trans*-retinal should have been much higher than what has been observed. In fact, the ligand-free opsin with the active conformation was obtained at pH 6.0 (Park et al., 2008). Thus we contend that this structure is not the suitable basis for understanding retinal entry.

However, we agree that the Meta-II Rho structure (Choe et al., 2011) reflects the conformation when retinal release occurs. The susceptibility of the Schiff base to hydroxylamine (Wald and Brown, 1953) and sodium borohydride (Bownds and Wald, 1965) indicates the receptor maintains until the hydrolysis of Schiff base. Also, it has been shown that TM3 resetting and retinal release as measured by the increase in Trp fluorescence are tightly coupled (Farrens and Khorana, 1995). The two openings provides ready egresses for retinal to dissociate from the binding channel.

4.4.3 The retinal entry site is located between TM5 and TM6

We next came to the conclusion that the entry site is located between TM5 and TM6. First, we have identified a cluster of mutations on TM5 and TM6 that exert a significant impact on the entry kinetics, but not the release kinetics. The TM5/6 mutations are distal from the PSB and are unlikely to perturb the formation or hydrolysis of imine. Moreover, in Chapter 3 we have shown that the energy barrier for retinal binding measured by the Trp-based fluorescence quenching assay and the Alexa488-based assay are essentially the same, which suggests that in the process of pigment regeneration, it is the first step (*i.e.* retinal entering into the ligand binding channel, rather than the formation of Schiff base bond) that determines the overall reaction rate. Therefore, these mutations can have such a pronounced effect only by modulating the accessibility of the retinal-binding channel. Second, we found that two mutations, F208W and F212A, changed the activation enthalpy of retinal entry, suggesting these two sites may directly interact with the incoming retinal. If an opening between TM5 and TM6 do mediate retinal entry, then the aldehyde group should precede the polyene chain and the *β*-ionone ring to gain access to the binding channel. This scenario would explain our observation that polar residues would reduce the entry kinetics, as the hydroxyl group may interact with the carbonyl group of retinal through dipole-dipole interaction or hydrogen bonding. Furthermore, the entry kinetics is insensitive to mutations at F293 (Piechnick et al., 2012), which is a key gating residue at Opening A.

4.4.4 F208, F212 and A269 are likely to be part of the entry site

Then which residues in TM5 and TM6 constitute the entry site? The emergence of Opening B requires the rotation of TM5 and TM6. However, we have excluded this

conformation to be responsible for retinal entry. We postulate that the actual opening is comprised of three residues, F208, F212 and A269 (Opening C), which are situated one turn of helix lower than Opening B exposed in the Meta-II structure. The electron density at Opening C in dark-state Rho is lower than what is generally found between other helices (Okada, 2004). The ligand-free opsin is flexible and dynamic than dark-state Rho, and a sufficiently large opening may be created by the motion of TM5 and TM6 and the rotation of the side chains. Our mutagenesis data support the presence of Opening C. F212 is a conserved residue in Rho and short-wavelength sensitive cone receptor. A series of F212 mutations (F212A/C/S/T/W) have a significant impact on the retinal entry kinetics, supporting its essential role in retinal entry. The behavior of site 269 resembles that of site 212: increasing side-chain size or polarity at site 212 and 269 invariably impeded retinal entry. By comparison, increasing side-chain size (G270F) and polarity (G270S) at site 270 barely affected the entry kinetics, suggesting these effects are specific to the sites located on the trajectory of incoming retinal.

The behaviors of F208 and F273 mutants are different from F212 and A269 mutants. The effect of F208W is to decrease entry kinetics and increase the activation enthalpy. However, the slower entry kinetics for F208A is counterintuitive, as this mutation is expected to make Opening C larger. The finding that F273A reduced entry kinetics and F273W accelerated it is also puzzling. Similar observations have been reported for F208A and F273A (Schafer *et al*., 2015). It should be kept in mind that the effect of these hydrophobic mutations can be multi-fold: 1) it may change the sterical hindrance at Opening C; 2) it may alter the residue's interaction with its neighboring residues; 3) it may affect the dynamics of helix motion; 4) it may disrupt the overall

folding. The first effect regarding sterical hindrance is relevant only to those sites that are part of Opening C. The second and the third effect are not so critically dependent on the mutation's closeness to Opening C, but are likely to diminish at the distance increases. We tried to avoid the fourth effect by judicious choice of mutation. One plausible cause for the unexpected entry kinetics of F208A, F273A and F273W is the π-π stacking interaction between F212-F208 and F208-F273. In both inactive conformation and active conformation, the T-shaped or parallel-displaced orientation of these three phenylalanines are for adequate for π-π stacking to occur (McGaughey et al., 1998). Therefore, F212, F208 and F273 are possibly coupled to fine-tune the dynamics of Opening C. Consistent with this idea, the F273A/W mutations exert a less significant effect than F208 and F212 mutation the activation enthalpy and entropy of retinal entry kinetics. Furthermore, the phenyl group of F208 may serve as the spacer for the upper rim of Opening C, and removing the side chain of F208 caused the opening to partially collapse. It has been reported that F208 and A269 are functionally complementary; they together act as a pivot between TM5 and TM6 (Tsukamoto et al., 2010). We do not rule out the possibility that F208A has produced some unpredictable consequence.

4.4.5 The retinal exit site

In the end we asked in which direction retinal moves out of the ligand-binding channel. Addition of hydroxylamine accelerates retinal release by more than 10^2 fold, thus the rate-limiting step in retinal release is likely to be Schiff base hydrolysis rather than retinal egress from the binding pocket. The implication of this rate-limiting step is that we cannot exclude Opening B as the exit site simply because most TM5/TM6 mutations do not significantly alter the release kinetics. It is possible that retinal

promiscuously uses Opening A and B for exit. Molecular dynamic simulation using the ligand-free opsin structure suggested that TM5-TM6 opening is more frequently utilized than the TM1-TM7 opening for exit (Wang and Duan, 2011). However, we noticed that increasing the side-chain size at A272 (A272V/I/F) greatly accelerated retinal releases (Piechnick et al., 2012). In the Meta-II state, the side chain of A272 directly interacts with the *β*-ionone ring of all-*trans*-retinal. Thus, a straightforward explanation is that A272V/I/F may "push" the retinal out of the binding channel once Opening A becomes available. These data suggest that exit through Opening A is a possible scenario.

4.4.6 Comparison with the previously published mutagenesis data on retinal entry and release

In an earlier study, Piechnick *et al.* characterized the retinal entry and release kinetics for mutations in the middle of ligand binding channel, close to Opening A, and close to Opening B (Figure 4-8) (Piechnick et al., 2012). For retinal entry, Piechnick *et a.l* used UV-Vis spectroscopy to monitor retinal entry, in reality the formation of PSB (although these kinetics of the two processes are often numerically close). Retinal release was measured by change in Trp fluorescence.

Not surprisingly, drastic changes in retinal entry and release kinetics were observed for mutations in the middle of ligand binding pocket (E181, S186, Y268, A292). E181 has been suggested to act together with S186 as a counterion to stabilize the PSB in Meta-I state (Ludeke et al., 2005; Sekharan and Buss, 2008). The observation that E181Q on Meta-II decay has been described (Lewis et al., 2004). E181, S186 and Y268 have been identified as part of the hydrogen bonding network for maintaining PSB stability in the dark-state and regulating its hydrolysis in the photoactivated state (Choe et

al., 2011; Janz and Farrens, 2004). A292 has been found to make contact the C14 of 11-*cis*-retinal with E181 (Okada et al., 2004). Increasing its side-chain size (A292V/L/F) is retinal with E181 (Okada et al., 2004). Increasing its side-chain size (A292V/L/F) is expected to add a constriction site for retinal to move through the binding channel, hence explaining the simultaneously reduced entry and release kinetics.

Among the mutations close to Opening A (M39, L40, Y43, M44, F91, T94, T289, F293), M39, as the structure and kinetic data suggested, may be too distal from Opening A to have a significant effect. L40, M44 and F91 are situated on the trajectory of retinal if it would move through Opening A, and mutating these residues is expected to be consequential. However, any mutation inside the helix bundle has a theoretical possibility of disrupting the native folding of ligand binding channel and consequently alter the retinal entry or release kinetics. Replacing a non-polar residue to a polar or charged one (*e.g.* L40D) may cause a rearrangement of the internal hydrogen-bonding network. Moreover, switching between aliphatic and aromatic residue can make a significant difference by creating or abolishing cation-π or π-π interaction (note that the protonated Schiff base is positively charged). Y43 has been found make hydrogen bonding with the carbonyl oxygen of F293 in dark-state Rho, whose breaking is required for transition to Meta-II state (Adamian and Liang, 2002; Tikhonova et al., 2008). T94 and T289 participate in a conserved internal hydrogen bonding network that also involves E181, S186 (Choe et al., 2011; Janz and Farrens, 2004). Therefore, the observed slower retinal

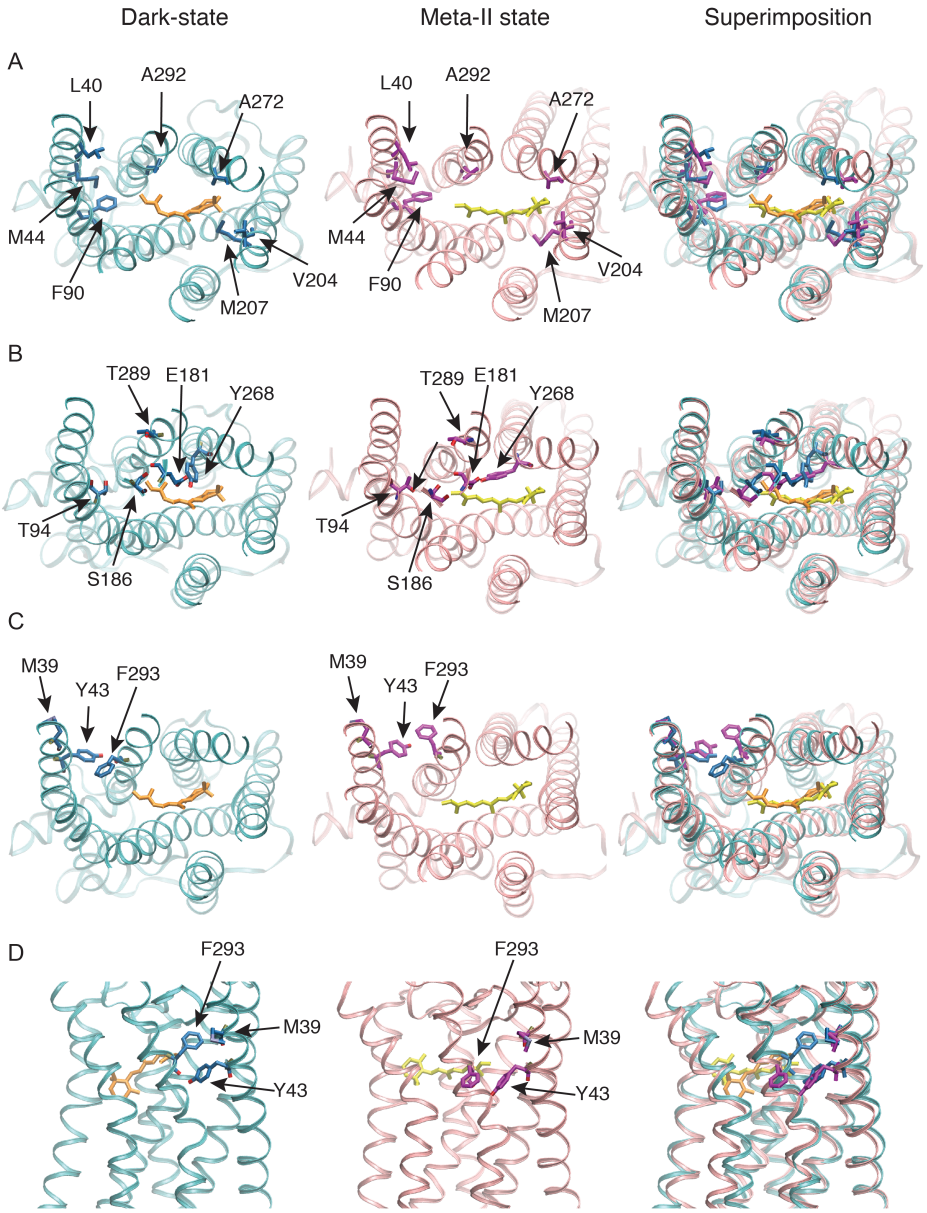

Figure 4-8. The sites studied in the previous report (Piechnick et al., 2012). A) The sites whose side chains point into the helix bundle (top view). **B)** The sites are participate in the internal hydrogen bonding network (top view). **C)** The sites at Opening A (top view). **D)** The sites at Opening A (side view). The N-terminus and EC loops are removed in the top view to reveal the retinal and highlighted residues.

entry for T289A/D/R/F and T94I mutants might arise from alteration in Schiff base chemistry. The slower Meta-II decay rate for T94I has been described previously (Gross et al., 2003a). Among all residues close to Opening A, F293 exhibits the greatest structural change in photoactivation. The essentially unchanged retinal entry kinetics for F293 mutations fits into our model, *i.e.*, the conformation for retinal uptake resembles that of the inactive state, and Opening C between TM5 and TM6 is used for retinal entry. For retinal release, since the phenyl group of F293 has been completely displaced from the exit site, F293A/L mutations would not make a great difference with respect to sterical hindrance.

In agreement with our observation that mutations at TM5/6 generally do not perturb the retinal release, in the set of mutations chosen by Piechnick *et al.* (V204, I205, M207, F208, F273, F276), I205Q, F208L/Q, F273L/Q and F276L/Q exhibited retinal release kinetics similar to that of wt Rho. However, a confounding finding was that mutations M207A, A272V/I, and V204F significantly increased retinal release kinetics. A scrutiny of the structure reveals that the side chains of A272 and V204 protrude into the helix bundle, particularly A272, which makes direct contacts with the β-ionone ring of all *trans*-retinal in Meta-II state (Choe et al., 2011). Thus apart from the possibility to disrupt the overall folding of ligand binding channel, substituting A272 for larger residues may result in clashes between the β-ionone ring and site 272, thus explaining the highly accelerated retinal release rate for A272I. M207 has been predicted a key residue for the formation of retinal binding pocket (Moitra et al., 2012) and the mutation M207A possibly makes the binding pocket less adequate for retinal to dock, resulting in the reduced entry kinetics and increased release kinetics. F208L was also tested in our study,

for which we obtained a retinal entry rate close to that of wt, while Piechnick *et al.* found it slowed down entry kinetics. Interestingly, Piechnick *et al.* also observed that adding polar groups to TM5/6 residues (L→Q) slowed down retinal entry.

Overall, the observed effects for most of the mutations reported in this earlier study could be explained by existing structural, biochemical and spectroscopical data on Rho. However, many of these mutations are incapable of providing clear evidence on the question addressed in the present study, as they are likely to cause rearrangement of hydrogen bonding network or abnormal folding of ligand binding channel. Based on the above analysis, we reasoned that it is crucial to test the residues that primarily act as the "gate" of the retinal entry or exit site.

4.4.6 Perspective and future direction

Several additional mutants or experiments may be considered to help clarify the mechanism for retinal entry in opsin. First, the Eyring plot of F208A and an A269 mutant (A269L or A269F) may provide insights into the role of F208 and A269 in regulating Opening C. Second, the double mutant F208A/A269F may answer whether F208 and A269 are functionally complementary with respect to retinal entry. Third, F293W mutant can be used to assess the role of Opening A in retinal release.

4.5 Materials and Methods

The methods for heterologous expression of wt and mutant Rho, site-specific fluorescent labeling of azF-Rho, and measurement of the retinal entry and release kinetics have been described in Chapter 2 and Chapter 3.

4.5.1 Site-directed mutagenesis

Rho mutants are created on the wt background or S144amb background. The primers used to generate these mutations are listed in Table 4-1.

Table 4-1 The primers for site-directed mutagenesis

Mutation	Forward (5'→3')	Reverse (5'→3')
F208A	catctacatggccgtggtccacttcatc	gatgaagtggaccacggccatgtagatg
F028S	catctacatgtccgtggtccacttcatc	gatgaagtggaccacggacatgtagatg
F208L	catctacatgctggtggtccacttcatc	gatgaagtggaccaccagcatgtagatg
F208M	catctacatgatggtggtccacttcatc	gatgaagtggaccaccatcatgtagatg
F208Y	catctacatgtacgtggtccacttcatc	gatgaagtggaccacgtacatgtagatg
F208W	catctacatgtgggtggtccacttcatc	gatgaagtggaccacccacatgtagatg
F212A	gttcgtggtccacgccatcatcccgctg	cagcgggatgatggcgtggaccacgaac
F212C	gttcgtggtccactgcatcatcccgctg	cagcgggatgatgcagtggaccacgaac
F212T	gttcgtggtccacaccatcatcccgctg	cagcgggatgatggtgtggaccacgaac
F212S	gttcgtggtccactccatcatcccgctg	cagcgggatgatggagtggaccacgaac
F212L	gttcgtggtccacctgatcatcccgctg	cagcgggatgatcaggtggaccacgaac
F212W	cgtggtccactggatcatcccgctgattg	caatcagcgggatgatccagtggaccacg
A269T	gctgccatataccggtgtggcgttctac	gtagaacgccacaccgtaatatggcagc
A269S	ctgccatatagcggtgtggcgttctacatc	gatgtagaacgccacaccgctatatggcag
A269F	ctgccatatttcggtgtggcgttctacatc	gatgtagaacgccacaccgaaatatggcag
A269Y	gctgccatattacggtgtggcgttctac	gtagaacgccacaccgtaatatggcagc
G270A	ctgccatatgctgccgtggcgttctacatc	gatgtagaacgccacggcagcatatggcag
G270L	ctgccatatgctctggtggcgttctacatc	gatgtagaacgccaccagagcatatggcag
G270F	ctgccatatgctttcgtggcgttctacatc	gatgtagaacgccacgaaagcatatggcag
F273A	ctggtgtggcggcctacatcttcacccatc	gatgggtgaagatgtaggccgccacaccag
F273W	ctggtgtggcgtggtacatcttcacccatc	gatgggtgaagatgtaccacgccacaccag

Chapter Five: Conclusion and Perspective

5.1 Developing novel chemical biology tools for studying GPCRs

This thesis presents a general approach for the labeling of GPCRs with useful chemical probes or chemically reactive handles at defined sites by combining unnatural amino acid (uaa) mutagenesis and bioorthogonal chemistry. A comparative study was conducted to assess several different strategies for labeling uaa residues genetically encoded into GPCRs expressed in mammalian cells in culture. Using the visual pigment Rho as a model GPCR, the strain-promoted [3+2] azide-alkyne reaction (SpAAC) between dibenzocyclooctyne (DIBO) and *p*-azido-L-phenylalanine (azF) was shown to be a suitable strategy for attaching labels to GPCRs. Then the specificity, kinetics, and topology-dependent reactivity of the labeling chemistry were characterized for Rho. The reaction rate of SpAAC with azF situated in the transmembrane region of the receptor was found to exhibit up to 1000-fold enhancement, which was attributed to DIBO partitioning into the hydrophobic core of micelles. The capability of labeling residues embedded in hydrophobic environment makes the combination of SpAAC with azF a promising approach for studying membrane proteins. In conclusion, the methods described in this thesis add to the chemical biology tool kit for probing the structure-function relationship in GPCRs.

5.2 The applications of the bioorthogonal labeling strategy

5.2.1 A FRET-based assay for measuring ligand binding kinetics of GPCRs

The possibility of attaching extrinsic fluorescent reporters to GPCRs enabled a general scheme for measuring ligand-binding kinetics based on the FRET between the ligand and the fluorescent reporter. The ligand can be chemically modified to make a FRET pair with the fluorescent label. In the case of Alexa488-labeled Rho, the ligand 11-*cis*-retinal is natural chromophore, which is capable of quenching the fluorescence of Alexa488. Thus the kinetics of the recombination reaction between the ligand-free opsin and 11-*cis*-retinal can be monitored by the decrease of Alexa488 signal. Compared with the assays based on the intrinsic tryptophan fluorescence, the extrinsic fluorescent reporters can be tailored to have optimal photophysical properties so as to enhance the sensitivity and dynamic range of the ligand-binding assay.

This assay was first utilized to address the energetics of the recombination reaction between opsin and 11-*cis*-retinal. The activation energy for retinal binding was obtained from the temperature-dependent retinal entry kinetics. The activation energy for the reverse reaction was measured by chromophore exchange of the bound 11-*cis*-retinal with exogenous 9-*cis*-retinal. The reaction enthalpy was measured by ITC. Based on these results, the complete energy diagram was derived for the binding between 11-*cis*-retinal and opsin.

Next this ligand-binding assay was applied to study the mutations of highly conserved amino acid residues putatively involved in the pathway for retinal entry and/or release. A set of mutations located at the fifth and sixth transmembrane (TM) helices was found to exert a much greater influence on the retinal entry kinetics than on the retinal

release kinetics. Three criteria were used to evaluate the influence of these mutations: 1) the correlation between side-chain size and entry kinetics; 2) the change in the activation energy for retinal entry; 3) the effect of increasing polarity at these sites. Based on these findings, a model was proposed to describe the retinal entry pathway leading from the membrane-embedded receptor surface to the ligand-biding site in the transmembrane core.

5.2.2 Single-molecule fluorescence study of fluorescently labeled GPCRs

The temporal resolution and the capability of multi-color tracking make single-molecule fluorescence ideally suited for probing the signaling complex of GPCRs. We developed a single-molecule total internal reflection fluorescence (smTIRF) platform to image fluorescently labeled receptors and the dynamic assembly of the signaling complex (Huber and Sakmar, 2011). TIRF methods enable selective excitation of fluorophores by the evanescent wave immediately adjacent to the glass-water interface. The fluorescent labeled receptors are captured to the TIRF surface via antigen-antibody interaction to facilitate long-term visualization of the ligand-receptor binding dynamics. The brightness and photostability of organic dyes make them better choices than fluorescent proteins for tracking the binding events at time scales of hours.

We tested Rho labeled with three different Alexa fluorophores at position 144 on the single-molecule TIRF set-up (Figure 5-1) (Tian et al., 2013a). We were able to distinguish the signals from different fluorophores in the QuadView detection scheme, and register the position of labeled receptors in the TIRF image. In principle, receptor demonization and receptor-ligand binding can be determined from the co-localization of different fluorescent labels. However, co-localization is limited by the axial and lateral

resolution of the TIRF microscope, which are one or two orders of magnitude larger than the dimension of receptors (< 5 nm). Thus co-localization of fluorophores is a necessary, but not sufficient criterion for identifying intermolecular interaction.

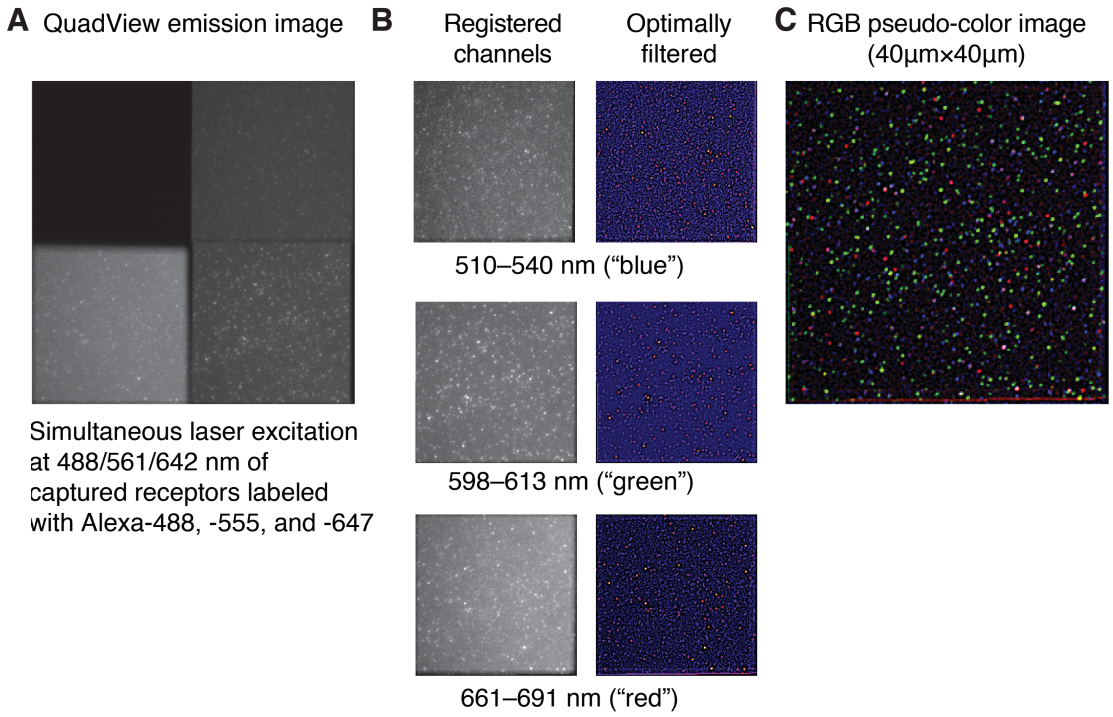

Figure 5-1. Images of single-fluorophore spots. One side of the quadratic image corresponds to 40 µm in the sample plane. **A)** The QuadView image of Alexa488 Rho, Alexa555-Rho and Alexa647-Rho. **B)** A false color image of the same data after subtraction of static background from "hot" pixels of the CCD sensor and after application of a 2D convolution with a spot-enhancing filter that was shown to be the optimal detector of a Gaussian-like spot in $1/\omega^2$ noise (Sage et al., 2005). **C)** The merged pseudo-color image of the three detection channels. Figure taken from (Tian et al., 2013b).

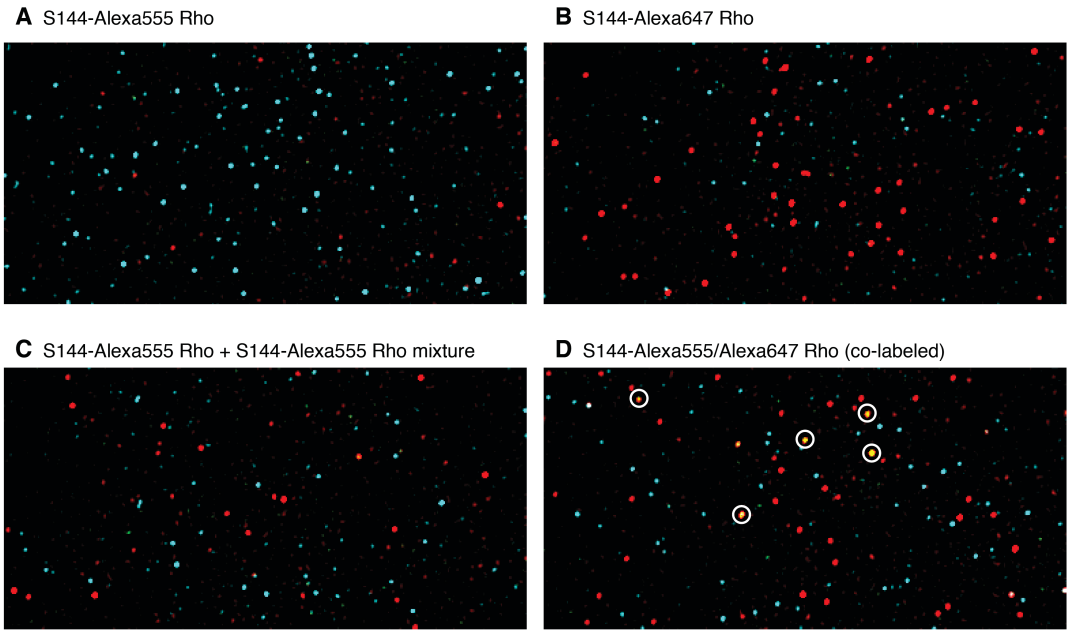

Figure 5-2. The smTIRF images for Alexa555-labeled and Alexa647-labeled Rho. Three channels were recorded at the same time: 1) excitation: 532 nm; emission: 555 nm-595 nm (*cyan*, donor channel); 2) excitation: 642 nm; emission: 655 nm-705 nm (*red*, acceptor channel); 3) excitation: 532 nm; emission: 655 nm-705 nm (*green*, FRET channel). Each image contains the following samples: **A)** S144-Alexa555 Rho (*cyan*). **B)** S144-Alexa647 Rho (*red*). **C)** The mixture of S144-Alexa555 Rho and S144-Alexa647 Rho (*cyan* + *red*). **D)** S144azF Rho co-labeled with Alexa555-DIBO and Alexa647-DIBO, *i.e.*, one sample was treated simultaneously with two labeling reagents and then purified together. In this particular sample, a number of FRET signal could be detected. Because the FRET signal (*green*) overlaps with the acceptor signal (*red*), the merged signals are represented as *yellow* dots (circled).

Another approach for detecting intermolecular interaction is to monitor the FRET signal between donor and acceptor fluorophores. The energy transfer is sensitive to small changes of the distance on the nanoscale (Holden et al., 2014). We used Alexa555-Rho and Alexa647-Rho to test the capability of the smTIRF platform for FRET detection. We made an interesting observation for S144azF Rho simultaneously reacted with Alexa555-

DIBO and Alexa647-DIBO. When S144-Alexa555 Rho and S144-Alexa647 Rho were mixed together, few FRET signals were observed. By comparison, FRET spots were readily detected for Rho co-labeled with two fluorophores (Figure 5-2, *white* circle). Because each azF-tagged receptor only possesses one reactive handle, the FRET signals suggest the presence of constitutive dimers in heterologously expressed Rho.

5.2.3 Site-specific bioorthogonal labeling of the chemokine CCR5 receptor

The C-C chemokine receptor 5 (CCR5) is a Class A GPCR. It is expressed on the cell surface of leukocytes and activated by the chemotactic cytokines (chemokines), such as macrophage inflammatory protein-1α (MIP-1α, also known as CCL3), MIP-1β (CCL4), and regulated-and-normal-T cell-expressed and secreted (RANTES, or CCL5). CCR5 receptor is implicated in inflammatory response. More importantly, CCR5 is hijacked by the human immunodeficiency virus (HIV) to facilitate viral entry. The viral envelope protein gp120 forms a tertiary complex with CCR5 and another cell-surface glycoprotein CD4, which attaches the virus to the outer surface of host cell and subsequently induces membrane fusion. The finding that a deletion mutation CCR5Δ32 confers resistance to macrophage-tropic HIV-1 strain has substantiated the essential role of CCR5 in HIV infection. Therefore, molecules that block the CCR5 receptor are potentially useful for inhibiting HIV entry. In 2007, Maraviroc, a small molecule that binds to a cavity of CCR5, became the first FDA-approved CCR5-specific HIV entry blocker.

We are interested in utilizing our smTIRF capability to understand the dynamic assembly of CCR5 signaling complex. However, the CCR5 receptor bears multiple cysteines and cannot be site-specifically labeled using maleimide or sulfonate chemistry.

Figure 5-3. The multiplex detection scheme for FLAG-tagged CCR5 receptor using a sandwich fluorophore-linked immunosorbent assay. **A)** The uaa azF genetically encoded at a target site. SpAAC reaction is used to site-specifically attach the FLAG peptide-epitope (*green*) conjugated to a DBCO (*red*) via a maleimide crosslinker (DBCO-FLAG). **B)** Upper panel: the schematic diagram of the immunosorbent assay (ISA) to detect the expression levels of wt and F96azF-CCR5. The receptor is captured to the plate surface using the C-terminal-specific 1D4 mAb. The N-terminal epitope of CCR5 is probed using anti-CCR5 T21/8-biotin mAb followed by streptavidin coupled to IRDye 680RD (SA-680RD). Lower panel: the corresponding fluorescence image of the triplicate wells (pseudo color: *red*, detected in the 700-nm channel). **C)** Upper panel: the schematic diagram for detecting the labeling efficiencies of wt and F96azF-CCR5 with DBCO-FLAG. With the receptor immobilized to the plate surface with the C-terminal-specific 1D4 mAb, the FLAG tag epitope of CCR5 is probed with anti-FLAG pAb followed by anti-rabbit Gig conjugated to IRDye 800CW (anti-R800CW). Lower panel: the corresponding fluorescence image of the triplicate wells (pseudo color: green, detected in the 800 nm-channel). **D)** Upper panel: the schematic diagram of ISA experiment for FLAG-labeled CCR5. The dual-color detection enabled simultaneous quantification of the receptor expression level and the labeling efficiency by DBCO-FLAG. Lower panel: the corresponding fluorescence image of the triplicate wells shown for both the N-terminal epitope signal (*red*, 700-nm channel) and FLAG signal (*green*, 800-nm channel). Wells containing wt CCR5 treated with DBCO-FLAG shows a strong N-terminal epitope signal, but much weaker FLAG signal. Wells containing F96azF-CCR5 treated under the same reaction condition yielded strongly both the N-terminal epitope signal and FLAG signal, indicating the presence of expressed full-length receptor tagging with a FLAG epitope (merged, *yellow*). **E)** The integrated intensities of the wells shown in **B-D**, plotted in arbitrary units (a.u.). The expression of wt CCR5 and F96azF-CCR5 (*red* bars) and the level of FLAG signal indicate specific labeling of F96azF-CCR5 (*green* bars). The data are presented from a representative experiment and error bars represent the standard error of the mean of triplicate measurements. Figure taken from (Naganathan et al., 2015).

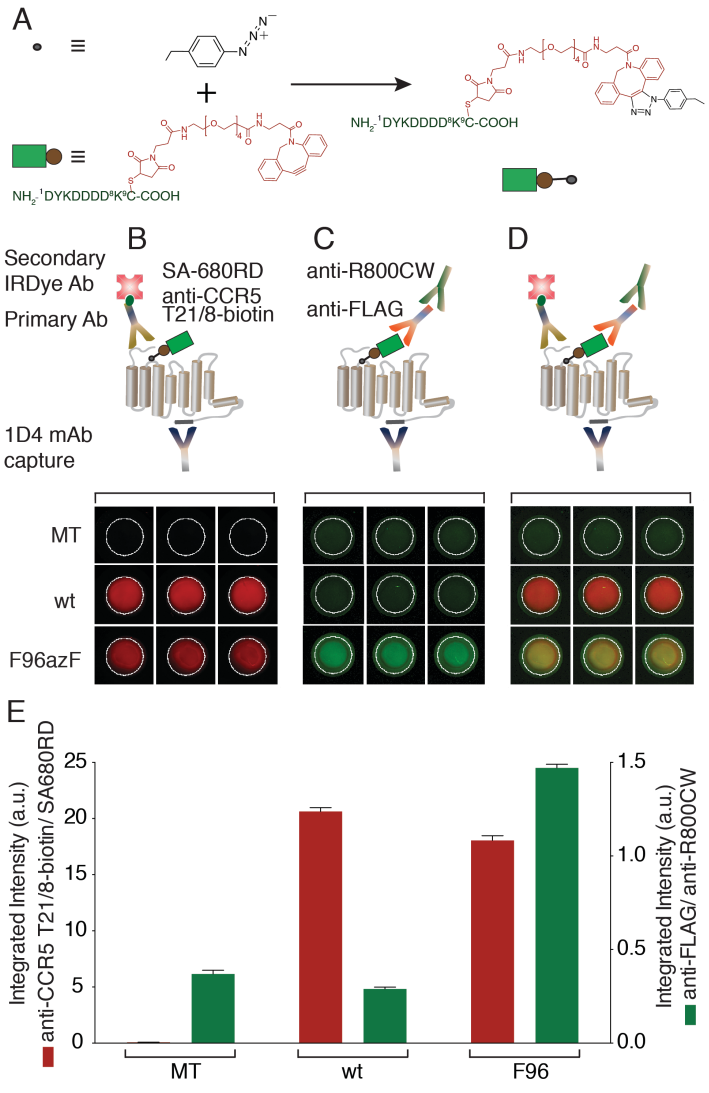
A
NH2-1DYKDDDD8K9C-COOH
NH2-1DYKDDDD8K9C-COOH
B
C
D
Secondary IRDye Ab
Primary Ab
1D4 mAb capture
SA-680RD
anti-CCR5 T21/8-biotin
anti-R800CW
anti-FLAG
MT
wt
F96azF
E
Integrated Intensity (a.u.) anti-CCR5 T21/8-biotin/ SA680RD
Integrated Intensity (a.u.) anti-FLAG/ anti-R800CW
25
20
15
10
5
0
1.5
1.0
0.5
0.0
MT
wt
F96

Thus, we would like to apply SpAAC to generate fluorescently labeled CCR5 receptor. However, the expression level of azF-CCR5 is one order of magnitude lower than that of azF-Rho, making in-gel fluorescence and UV-Vis spectroscopy inadequate for quantifying the extent of labeling. To efficiently identify sites that are amenable for covalent modification, we designed a sandwich fluorophore-linked immunosorbent assay to enable semi-high throughput microtiter plate-based detection of labeled CCR5 receptor (Figure 5-3A) (Naganathan et al., 2015). We chose FLAG-DBCO, a dibenzocyclooctyne reagent carrying a FLAG detection handle, to modify a set of 32 azF-CCR5 variant. The labeled receptors are immobilized to the surface of microtiter plate using the C-terminal specific 1D4 mAb. The N-terminus was probed with the N-terminal specific mAb, and the FLAG tag with the anti-FLAG polyclonal antibody. The secondary antibodies each carry two different IR fluorophores, which can be quantified independently in two IR channels. This multiplex detection scheme enables simultaneous quantification of receptor expression and label incorporation.

We found that F109, a site located in the hydrophobic cavity of CCR5, to be particularly reactive with FLAG-DBCO (Figure 5-3B). In the crystal structure of CCR5 in complex with Maraviroc, F109 makes hydrophobic contacts with a phenyl ring of Maraviroc (Tan et al., 2013). We propose to exploit the high reactivity between site F109azF and DBCO to engineer tethered ligand that modulates the biological activity of CCR5. While small molecule is a popular tool for probing protein function, the affinity between the candidate small molecules and the target protein can be too low to be practical. Creating a covalent linkage between ligand and target protein can circumvent this issue. The high reactivity of F109azF is also in line with the earlier observations from

labeling Rho that dibenzocyclooctyne reagents preferably label the hydrophobic transmembrane region of the receptor.

In the next stage of work to interrogate the GPCR "signalosome," we would like to carry out smTIRF studies on the binding events between CCR5 receptor and various ligands. The knowledge obtained from the labeling studies of the TM region of Rho will be useful to design and prepare fluorescently labeled CCR5 receptor variants suitable for FRET analysis. We would also like to generate dual-color labeled CCR5 receptor by combining SpAAC with self-labeling SNAP/CLIP tags. This doubly labeled receptor may yield further insights into the conformational dynamics of the CCR5 receptor in the presence of ligands with various pharmacological characteristics. Progress along these lines has already been achieved. In the longer term, we anticipate that the smTIRF approach enabled by the chemical biology methods described here will shed light on the allosteric regulation of the GPCR signaling complex and may lead to new approaches to drug discovery.

Appendix One: Analysis of the filtration of Alexa488-DIBO in DM

- *Symbols*: c, concentration; n, amount of substance; V, volume; P, partition coefficient; f, weight/volume percent of DM.
- *Superscript*: B, bound; F, free; mic, micelle; buf, buffer.
- *Subscripts*: 0, the initial condition; t, the condition at time point t; 1, filtrate; 2, retentate.

The concentration of DM-micelle bound and free Alexa488-DIBO

The partition coefficient of Alexa488-DIBO between DM micelles and buffer is defined as:

$$P = \frac{c^{\mathrm{B}}}{c^{\mathrm{F}}} \qquad \text{Eq. (1)}$$

Here "bound" denotes the Alexa488-DIBO molecules in the DM micelle, and "free" the molecules in the buffer. It can be re-written as:

$$P = \frac{n^{\mathrm{B}} / V^{\mathrm{mic}}}{n^{\mathrm{F}} / V^{\mathrm{buf}}} \qquad \text{Eq.(2)}$$

The total volume of the solution equals the addition of the volume of DM micelle and the volume of buffer.

$$V = V^{\mathrm{mic}} + V^{\mathrm{buf}} \qquad \text{Eq.(3)}$$

Assuming the density of DM micelles is very close to that of water, the ratio of the volume of DM and the volume of buffer numerically equals the weight/volume percent (f) of DM:

$$V^{\mathrm{mic}} / V = f \qquad \text{Eq.(4)}$$

Because f is generally below 0.01, V^{mic} is neglegible compared to V^{buf}.

$$V^{\text{buf}} \approx V \qquad \text{Eq.(5)}$$

The total moles of DM (n) is:

$$n = n^{\text{B}} + n^{\text{F}} \qquad \text{Eq.(6)}$$

The amount of Alexa488-DIBO in the micelles is:

$$n^{\text{B}} = \frac{Pf}{1+Pf} n \qquad \text{Eq.(7)}$$

and

$$n^{\text{F}} = \frac{1}{1+Pf} n \qquad \text{Eq.(8)}$$

The molar concentrations of Alexa488-DIBO bound in DM micelles and free in the buffer are:

$$c^{\text{B}} = \frac{n^{\text{B}}}{V^{\text{mic}}} = \frac{Pf}{1+Pf} \frac{n}{V^{\text{buf}}} \qquad \text{Eq.(9)}$$

and

$$c^{\text{F}} = \frac{n^{\text{F}}}{V^{\text{buf}}} = \frac{1}{1+Pf} \frac{n}{V^{\text{buf}}} \qquad \text{Eq.(10)}$$

Substitute Eq. (4) into Eq.(9), and Eq.(5) into Eq.(10) we have

$$c^{\text{B}} = \frac{P}{1+Pf} \frac{n}{V} = \frac{P}{1+Pf} c \quad \text{Eq.(11)} \quad \text{and} \quad c^{\text{F}} = \frac{1}{1+Pf} \frac{n}{V} \qquad \text{Eq.(12)}$$

Because the apparent concentration (c) was used to calculate the reaction rate (k_2), the rate enhancement factor is $P/(1+Pf)$. It can be seen that for a given P, using lower concentration of DM (smaller f) gives higher effective concentration. Practically the concentration of DM must be above its critical micelle concentration (CMC), which is 0.17 mM, corresponding to 0.009% (w/v) to prevent precipitation of Rho. In our labeling and kinetics study we used 0.1% (w/v).

De*rivation *of the partition coefficient (P) from the filtration experiment

As the volume of the retentate decreases during centrifugation, the weight/volume percent of DM is:

$$f = \frac{V_{2,0}}{V_{2,t}} f_0 \qquad \text{Eq.(13)}$$

The amount of free Alexa488-DIBO in the retentate is:

$$n_2^F = \frac{1}{1+Pf} n_2 \qquad \text{Eq.(14)}$$

Substitute Eq.(13) into Eq.(14)

$$n_2^F = \frac{1}{1+Pf_0 V_{2,0}/V_{2,t}} n_2 \qquad \text{Eq.(15)}$$

The concentration of free Alexa488-DIBO is:

$$c_2^F = \frac{n_2^F}{V_{2,t}} = \frac{n_2}{V_{2,t}+Pf_0 V_{2,0}} \qquad \text{Eq.(16)}$$

Assuming fast equlibrium of Alexa488-DIBO between DM micelles and buffer, and only the Alexa488-DIBO in the buffer can flow through the membrane, thus the concentration of Alexa488-DIBO in the filtrate is equal to that of the free Alexa488-DIBO in the retentate:

$$c_{1,t} = c_2^F \qquad \text{Eq.(17)}$$

Substitute Eq.(17) into Eq. (18), we have:

$$c_{1,t} = \frac{c_{2,t} V_{2,t}}{V_{2,t}+Pf_0 V_{2,0}} \qquad \text{Eq.(18)}$$

Notice that $V_{2,0} = V_0 = V_{1,t} + V_{2,t}$

Eq.(19) Substitute Eq. (19) into Eq.(18) and rearrange, we have:

$$P = \frac{\left(c_{2,\mathrm{t}} - c_{1,\mathrm{t}}\right) V_{2,t}}{c_{1,\mathrm{t}}\left(V_{1,t} + V_{2,t}\right) f_0} \qquad \text{Eq.(20)}$$

Appendix Two: the diffusion of retinal among bicelles

Estimation of the numbers of POPC and CHAPS molecules in one bicelle

Bicelles of different compositions are characterized by the molar ratio of long-chain to short-chain component, denoted as q value. Here q = [POPC]/[CHAPS]. We assume the simplest scenario where the bicelle appears to be a disc with Rho at the center (Figure A-1, Panel B).

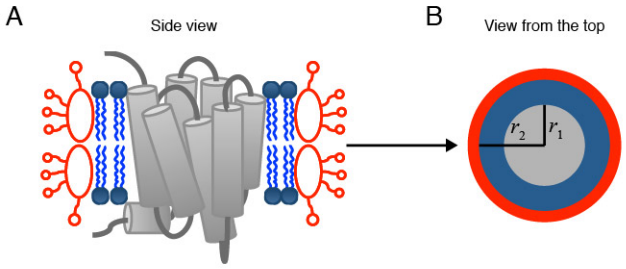

Figure A-1. The schematic representation of Rho reconstituted into bicelles. A) Side view. **B)** Schematic view from the top.

In our bicelle buffer, the concentrations of POPC and CHAPS are both 1 mg mL^{-1}, and their molar concentrations are 1.3 mM and 1.6 mM, respectively, and the q value is 0.81. The headgroup area of phosphatidylcholine is 0.71 nm^2. CHAPS have a high critical micelle concentration (CMC) of 8 to 10 mM. Thus we can assume that there is no CHAPS micelle in the solution. We further assume that the CHAPS layer around the rim of POPC has only one molecule, and the percentage of CHAPS dispersed in solution is negligible. CHAPS is a bean-like detergent and it is difficult to estimate their geometrical dimension. Here we assume that each CHAPS molecule stretches a length of 0.5 nm along the circumference of the bicelle.

The dimension of Rho has been determined by X-ray crystallography. If described by an ellipsoid, Rho is approximately 75 Å in height (perpendicular to the membrane), 48 Å wide in the standard view, and 35Å thick (Palczewski et al., 2000). To simplify the issue, we assume Rho is cylindrical with a height of 75 Å and a radius of 23 Å, so that the area of cross section remains the same.

The relationship between the numbers of POPC and CHAPS molecules are given by the following equation:

$$q = \frac{\pi\left(r_2^2 - r_1^2\right) / A_{\text{POPC}}}{2\pi r_2 / d_{\text{CHAPS}}} = 0.81 \quad A_{\text{POPC}} = 0.71 \text{ nm}^2 \quad r_1 = 2.3 \text{ nm} \quad d_{\text{CHAPS}} = 0.5 \text{ nm}$$

$r_2 = 3.72$ nm

In each bicelle, the number of POPC is given by:

$$\pi\left(r_2^2 - r_1^2\right) / A_{\text{POPC}}$$

The calculation shows that there are 38 molecules of POPC in each lipid layer of the bicelle. A bicelle has two layers of lipids. So there are approximately 76 POPC molecules and 94 CHAPS molecules. The molar concentration of POPC/CHAPS bicelles is 17 μM.

The kinetics of retinal diffusion among bicelles

In the experiment for measuring Rho regeneration kinetics, we added 20 μL of POPC/CHAPS bicelle buffer containing 25~50 μM retinal into 480 μL of sample. The resulting total concentration of 11-*cis*-retinal normally ranged from 1 μM to 2 μM. The molar concentration of POPC/CHAPS bicelles is 17 μM, which means each bicelle has on

average of 0.06 ~ 0.12 retinal molecule. The concentration of Rho is 0. 25-0.30 μM. Therefore, not every bicelle necessarily contains one molecule of Rho and at least one molecule of retinal at the same time, and the diffusion of retinal among bicelles is potentially a rate-limiting step. Therefore, we would like to find out what is the reaction rate for the association reaction between Rho^+ bicelles and retinal.

Let A represent bicelle, B represent retinal. The diffusion of retinal from one retinal to another consists of two steps. First, a retinal dissociates from a bicelle. Assume that process follows the first-order kinetics, with a time constant k_1. k_1 is related to the size, shape and composition of bicelle. The rate of dissociation is:

$$r_1 = k_1[\mathrm{AB}]$$

Second, retinal collides with a bicelle and partitions into it. This process follows bimolecular kinetics, with a time constant k_2. The rate of association is

$$r_2 = k_2[\mathrm{A}][\mathrm{B}]$$

Note that here [A] and [B] are the concentration of bicelles and retinal in the aqueous phase. At equilibrium, the rate of association equals the rate of dissociation:

$$k_1[\mathrm{AB}] = k_2[\mathrm{A}][\mathrm{B}]$$

The equilibrium constant is:

$$K_{\mathrm{eq}} = \frac{[\mathrm{AB}]}{[\mathrm{A}][\mathrm{B}]} = \frac{k_2}{k_1}$$

Although the partition coefficient of retinal among bicelles (K_{eq}) has not been measured, it is known to be very high. A previous study on the partition of retinal

between salamander rod cell membranes reported a partition coefficient of (1.6 ± 0.5) × 10^8 (Frederiksen et al., 2012). Therefore, $k_2 >> k_1$, and the rate-limiting step for retinal diffusion among bicelles is the time required for a free retinal in water to collide with a bicelle.

The concentration of free retinals in the aqueous phase is proportional to the apparent concentration of retinal in the entire system (c_B).

$$[B] = \frac{1}{1+Pf} c_B = \alpha c_B \qquad \frac{1}{1+Pf} = \alpha$$

Here P is the partition coefficient of retinal between bicelle and water, and f is the weight/volume percent. Let the apparent concentration of bicelle be c_A.

$$r_2 = \alpha k_2 c_A c_B = k_2^{'} c_A c_B$$

Therefore, the rate of diffusion is proportional to the apparent concentration of retinal and bicelles. If the concentration of retinal is in large excess, then the observed psuedo first order rate constant for bicelle is

$$k_{obs} = k_2^{'} c_B$$

In the stop-flow experiment, we could not reliably measure the quenching of pyrene fluorescence at a low concentration of retinal (*e.g.* 1.5 μM) on our stop-flow apparatus. Therefore, we used bicelles containing 100 μM 11-*cis*-retinal and retinal-free bicelles doped with 0.1% *β*-pyrene-C10-HPC (w/w) at a 1:1 (v/v) ratio. After rapid mixing, the apparent concentration of 11-*cis*-retinal was 50 μM, and the concentration of pyrene$^+$ bicelles was 8.5 μM. For the decay of pyrene fluorescence we obtained a first-order rate constant of 36 ± 3 s^{-1}.

$$k_2^{'} = 36 \pm 3 \text{ s}^{-1} / (50\ \mu\text{M}) = (7.2 \pm 0.6) \times 10^5 \text{ M}^{-1} \text{ s}^{-1}$$

In a typical retinal regeneration experiment, the concentration of retinal was typically 1~2 μM, the rate constant of retinal diffusion into bicelles is

$$r_2 = (7.2 \pm 0.6) \times 10^5 \text{ M}^{-1} \text{ s}^{-1} \times 1.5\ \mu\text{M} \approx 1.0 \pm 0.1 \text{ s}^{-1}$$

By comparison, the observed first-order rate constant for Rho regeneration normally falls into the range of $1\sim2 \times 10^{-3}$ s^{-1}, three order of magnitude lower than the retinal diffusion rate. Therefore, we ruled out retinal diffusion among bicelles as the rate-limiting step in the POPC/CHAPS bicelle system, and what we measured reflects the kinetics of the recombination between retinal and opsin.

References

(1) Overington, J.P., Al-Lazikani, B., and Hopkins, A.L. (2006). How Many Drug Targets Are There? Nat Rev Drug Discov *5*, 993-996.

(2) Bockaert, J., and Pin, J.P. (1999). Molecular Tinkering of G Protein-Coupled Receptors: an Evolutionary Success. EMBO J *18*, 1723-1729.

(3) Lagerstrom, M.C., and Schioth, H.B. (2008). Structural Diversity of G Protein-Coupled Receptors and Significance for Drug Discovery. Nat Rev Drug Discov *7*, 339-357.

(4) Dorsam, R.T., and Gutkind, J.S. (2007). G Protein-Coupled Receptors and Cancer. Nat Rev Cancer *7*, 79-94.

(5) Oldham, W.M., and Hamm, H.E. (2008). Heterotrimeric G Protein Activation by G Protein-Coupled Receptors. Nat Rev Mol Cell Biol *9*, 60-71.

(6) Nobles, M., Benians, A., and Tinker, A. (2005). Heterotrimeric G Proteins Precouple with G Protein-Coupled Receptors in Living Cells. Proc Natl Acad Sci USA *102*, 18706-18711.

(7) Violin, J.D., and Lefkowitz, R.J. (2007). *β*-Arrestin-Biased Ligands at Seven-Transmembrane Receptors. Trends Pharmacol Sci *28*, 416-422.

(8) Schickore, J. (2000). Locating Rods and Cones: Microscopic Investigations of the Retina in Mid-Nineteenth-Century Berlin and Wurzburg. Sci Context *13*, 137-152.

(9) Boll, F. (1876). Monaster Berlin Akad, 783-788.

(10) Gamgee, A. (1877). Kühne's Research on the Photochemical Process in the Retina. Nature *15*, 296.

(11) Kühne, W. (1878). On the Photochemistry in the Retina and on Visual Purple (London: Macmillan and Co.).

(12) Wolf, G. (2001). The Discovery of the Visual Function of Vitamin A. J Nutr *131*, 1647-1650.

(13) Wald, G. (1968). Molecular Basis of Visual Excitation. Science *162*, 230-239.

(14) Hecht, S., Shlaer, S., and Pirenne, M.H. (1942). Energy, Quanta, and Vision. J Gen Physiol *25*, 819-840.

(15) Hecht, S. (1942). The Chemistry of Visual Substances. Annu Rev Biochem *11*, 465-496.

(16) Wald, G. (1933). Vitamin A in the Retina. Nature *132*, 316-317.

(17) Wald, G. (1934). Carotenoids and the Vitamin A Cycle in Vision. Nature *134*, 65-65.

(18) Wald, G. (1953). The Biochemistry of Vision. Annu Rev Biochem *22*, 497-526.

(19) Wald, G. (1964). Receptors of Human Color Vision. Science *145*, 1007-1016.

(20) Wald, G., Durell, J., and St George, C.C. (1950). The Light Reaction in the Bleaching of Rhodopsin. Science *111*, 179-181.

(21) Wald, G., and Brown, P.K. (1950). The Synthesis of Rhodopsin from Retinene (1). Proc Natl Acad Sci USA *36*, 84-92.

(22) Hubbard, R., and Wald, G. (1952). Cis-Trans Isomers of Vitamin A and Retinene in the Rhodopsin System. J Gen Physiol *36*, 269-315.

(23) Bownds, D., and Wald, G. (1965). Reaction of the Rhodopsin Chromophore with Sodium Borohydride. Nature *205*, 254-257.

(24) Bownds, D. (1967). Site of Attachment of Retinal in Rhodopsin. Nature *216*, 1178-1181.

(25) Hargrave, P.A., and Fong, S.L. (1977). Amino-Terminal and Carboxyl-Terminal Sequence of Bovine Rhodopsin. J Supramol Str Cell *6*, 559-570.

(26) Hargrave, P.A., Mcdowell, J.H., Siemiatkowskijuszczak, E.C., Fong, S.L., Kühn, H., Wang, J.K., Curtis, D.R., Rao, J.K.M., Argos, P., and Feldmann, R.J. (1982a). The Carboxyl-Terminal One Third of Bovine Rhodopsin - Its Structure and Function. Vision Res *22*, 1429-1438.

(27) Wang, J.K., McDowell, J.H., and Hargrave, P.A. (1980). Site of Attachment of 11-*Cis*-Retinal in Bovine Rhodopsin. Biochemistry *19*, 5111-5117.

(28) Hargrave, P.A., Bownds, D., Wang, J.K., and Mcdowell, J.H. (1982b). Retinyl Peptide Isolation and Characterization. Methods Enzymol *81*, 211-214.

(29) Fukuda, M.N., Papermaster, D.S., and Hargrave, P.A. (1979). Rhodopsin Carbohydrate - Structure of Small Oligosaccharides Attached at 2 Sites near the NH_2 Terminus. J Biol Chem *254*, 8201-8207.

(30) Fukuda, M.N., Papermaster, D.S., and Hargrave, P.A. (1982). Structural-Analysis of Carbohydrate Moiety of Bovine Rhodopsin. Methods Enzymol *81*, 214-223.

(31) Ovchinnikov, Y.A. (1982). Rhodopsin and Bacteriorhodopsin: Structure-Function Relationships. FEBS Lett *148*, 179-191.

(32) Hargrave, P.A., Mcdowell, J.H., Curtis, D.R., Wang, J.K., Juszczak, E., Fong, S.L., Rao, J.K.M., and Argos, P. (1983). The Structure of Bovine Rhodopsin. Biophys Struct Mech *9*, 235-244.

(33) Rattner, A., Smallwood, P.M., and Nathans, J. (2000). Identification and Characterization of All-Trans-Retinol Dehydrogenase from Photoreceptor Outer Segments, the Visual Cycle Enzyme That Reduces All-*Trans*-Retinal to All-*Trans*-Retinol. J Biol Chem *275*, 11034-11043.

(34) Koen, A.L., and Shaw, C.R. (1966). Retinol and Alcohol Dehydrogenases in Retina and Liver. Biochim Biophys Acta *128*, 48-54.

(35) Saari, J.C., and Bredberg, D.L. (1989). Lecithin-Retinol Acyltransferase in Retinal-Pigment Epithelial Microsomes. J Biol Chem *264*, 8636-8640.

(36) Ruiz, A., Winston, A., Lim, Y.H., Gilbert, B.A., Rando, R.R., and Bok, D. (1999). Molecular and Biochemical Characterization of Lecithin Retinol Acyltransferase. J Biol Chem *274*, 3834-3841.

(37) Redmond, T.M., Yu, S., Lee, E., Bok, D., Hamasaki, D., Chen, N., Goletz, P., Ma, J.X., Crouch, R.K., and Pfeifer, K. (1998). Rpe65 Is Necessary for Production of 11-*Cis*-Vitamin A in the Retinal Visual Cycle. Nat Genet *20*, 344-351.

(38) Jin, M.H., Li, S.H., Moghrabi, W.N., Sun, H., and Travis, G.H. (2005). Rpe65 Is the Retinoid Isomerase in Bovine Retinal Pigment Epithelium. Cell *122*, 449-459.

(39) Moiseyev, G., Chen, Y., Takahashi, Y., Wu, B.X., and Ma, J.X. (2005). Rpe65 Is the Isomerohydrolase in the Retinoid Visual Cycle. Proc Natl Acad Sci USA *102*, 12413-12418.

(40) Moiseyev, G., Takahashi, Y., Chen, Y., Gentleman, S., Redmond, T.M., Crouch, R.K., and Ma, J.X. (2006). Rpe65 Is an Iron(II)-Dependent Isomerohydrolase in the Retinoid Visual Cycle. J Biol Chem *281*, 2835-2840.

(41) Simon, A., Hellman, U., Wernstedt, C., and Eriksson, U. (1995). The Retinal-Pigment Epithelial-Specific 11-*Cis*-Retinol Dehydrogenase Belongs to the Family of Short-Chain Alcohol Dehydrogenases. J Biol Chem *270*, 1107-1112.

(42) Simon, A., Lagercrantz, J., BajalicaLagercrantz, S., and Eriksson, U. (1996). Primary Structure of Human 11-*Cis*-Retinol Dehydrogenase and Organization and Chromosomal Localization of the Corresponding Gene. Genomics *36*, 424-430.

(43) Wald, G., and Brown, P.K. (1953). The Molar Extinction of Rhodopsin. J Gen Physiol *37*, 189-200.

(44) Thomas, D.D., and Stryer, L. (1982). Transverse Location of the Retinal Chromophore of Rhodopsin in Rod Outer Segment Disc Membranes. J Mol Biol *154*, 145-157.

(45) Karnik, S.S., Sakmar, T.P., Chen, H.B., and Khorana, H.G. (1988). Cysteine Residues 110 and 187 Are Essential for the Formation of Correct Structure in Bovine Rhodopsin. Proc Natl Acad Sci USA *85*, 8459-8463.

(46) Franke, R.R., Sakmar, T.P., Oprian, D.D., and Khorana, H.G. (1988). A Single Amino Acid Substitution in Rhodopsin (Lysine 248-Leucine) Prevents Activation of Transducin. J Biol Chem *263*, 2119-2122.

(47) Franke, R.R., Konig, B., Sakmar, T.P., Khorana, H.G., and Hofmann, K.P. (1990). Rhodopsin Mutants That Bind but Fail to Activate Transducin. Science *250*, 123-125.

(48) Hargrave, P.A., and Mcdowell, J.H. (1992). Rhodopsin and Phototransduction - a Model System for G Protein-Linked Receptors. FASEB J *6*, 2323-2331.

(49) Nathans, J., and Hogness, D.S. (1983). Isolation, Sequence-Analysis, and Intron Exon Arrangement of the Gene Encoding Bovine Rhodopsin. Cell *34*, 807-814.

(50) Nathans, J., and Hogness, D.S. (1984). Isolation and Nucleotide-Sequence of the Gene Encoding Human Rhodopsin. Proc Natl Acad Sci USA *81*, 4851-4855.

(51) Zuker, C.S., Cowman, A.F., and Rubin, G.M. (1985). Isolation and Structure of a Rhodopsin Gene from Drosophila-Melanogaster. Cell *40*, 851-858.

(52) Nathans, J., Thomas, D., and Hogness, D.S. (1986). Molecular-Genetics of Human Color-Vision - the Genes Encoding Blue, Green, and Red Pigments. Science *232*, 193-202.

(53) Dixon, R.A.F., Kobilka, B.K., Strader, D.J., Benovic, J.L., Dohlman, H.G., Frielle, T., Bolanowski, M.A., Bennett, C.D., Rands, E., Diehl, R.E., Mumford, R.A., Slater, E.E., Sigal, I.S., Caron, M.G., Lefkowitz, R.J., and Strader, C.D. (1986). Cloning of the Gene and cDNA for Mammalian β-Adrenergic Receptor and Homology with Rhodopsin. Nature *321*, 75-79.

(54) Frielle, T., Collins, S., Daniel, K.W., Caron, M.G., Lefkowitz, R.J., and Kobilka, B.K. (1987). Cloning of the cDNA for the Human β_1-Adrenergic Receptor. Proc Natl Acad Sci USA *84*, 7920-7924.

(55) Kobilka, B.K., Matsui, H., Kobilka, T.S., Yang-Feng, T.L., Francke, U., Caron, M.G., Lefkowitz, R.J., and Regan, J.W. (1987). Cloning, Sequencing, and Expression of the Gene Coding for the Human Platelet α_2-Adrenergic Receptor. Science *238*, 650-656.

(56) Rall, T.W., Sutherland, E.W., and Berthet, J. (1957). The Relationship of Epinephrine and Glucagon to Liver Phosphorylase. IV: Effect of Epinephrine and Glucagon on the Reactivation of Phosphorylase in Liver Homogenates. J Biol Chem *224*, 463-475.

(57) Rall, T.W., and Sutherland, E.W. (1958). Formation of a Cyclic Adenine Ribonucleotide by Tissue Particles. J Biol Chem *232*, 1065-1076.

(58) Sutherland, E.W., Rall, T.W., and Menon, T. (1962). Adenyl Cylase. I: Distribution, Preparation, and Properties. J Biol Chem *237*, 1220-1227.

(59) Butcher, R.W., and Sutherland, E.W. (1962). Adenosine 3',5'-Phosphate in Biological Materials. I: Purification and Properties of Cyclic 3',5'-Nucleotide Phosphodiesterase and Use of this Enzyme to Characterize Adenosine 3',5'-Phosphate in Human Urine. J Biol Chem *237*, 1244-1250.

(60) Ashman, D.F., Lipton, R., Melicow, M.M., and Price, T.D. (1963). Isolation of Adenosine 3', 5'-Monophosphate and Guanosine 3', 5'-Monophosphate from Rat Urine. Biochem Bioph Res Co *11*, 330-334.

(61) Rodbell, M., Krans, H.M., Pohl, S.L., and Birnbaumer, L. (1971a). The Glucagon-Sensitive Adenyl Cyclase System in Plasma Membranes of Rat Liver. IV: Effects of Guanylnucleotides on Binding of ^{125}I-Glucagon. J Biol Chem *246*, 1872-1876.

(62) Rodbell, M., Birnbaumer, L., Pohl, S.L., and Krans, H.M. (1971b). The Glucagon-Sensitive Adenyl Cyclase System in Plasma Membranes of Rat Liver. V: an Obligatory Role of Guanylnucleotides in Glucagon Action. J Biol Chem *246*, 1877-1882.

(63) Ross, E.M., and Gilman, A.G. (1977a). Resolution of Some Components of Adenylate-Cyclase Necessary for Catalytic Activity. J Biol Chem *252*, 6966-6969.

(64) Ross, E.M., and Gilman, A.G. (1977b). Reconstitution of Catecholamine-Sensitive Adenylate-Cyclase Activity-Interaction of Solubilized Components with Receptor-Replete Membranes - (S49 Lymphoma-L-Cell-Complementation *In Vitro* Somatic Cell Variants). Proc Natl Acad Sci USA *74*, 3715-3719.

(65) Woodruff, M.L., and Bownds, M.D. (1979). Amplitude, Kinetics, and Reversibility of a Light-Induced Decrease in Guanosine 3',5'-Cyclic Monophosphate in Frog Photoreceptor Membranes. J Gen Physiol *73*, 629-653.

(66) Yee, R., and Liebman, P.A. (1978). Light-Activated Phosphodiesterase of the Rod Outer Segment. Kinetics and Parameters of Activation and Deactivation. J Biol Chem *253*, 8902-8909.

(67) Miller, W.H., and Nicol, G.D. (1979). Evidence that Cyclic-GMP Regulates Membrane-Potential in Rod Photoreceptors. Nature *280*, 64-66.

(68) Bitensky, M.W., Miki, N., Keirns, J.J., Keirns, M., Baraban, J.M., Freeman, J., Wheeler, M.A., Lacy, J., and Marcus, F.R. (1975). Activation of Photoreceptor Disk Membrane Phosphodiesterase by Light and ATP. Adv Cyclic Nucleotide Res *5*, 213-240.

(69) Miki, N., Baraban, J.M., Keirns, J.J., Boyce, J.J., and Bitensky, M.W. (1975). Purification and Properties of the Light-Activated Cyclic Nucleotide Phosphodiesterase of Rod Outer Segments. J Biol Chem *250*, 6320-6327.

(70) Keirns, J.J., Miki, N., Bitensky, M.W., and Keirns, M. (1975). A Link between Rhodopsin and Disc Membrane Cyclic Nucleotide Phosphodiesterase. Action Spectrum and Sensitivity to Illumination. Biochemistry *14*, 2760-2766.

(71) Wheeler, G.L., and Bitensky, M.W. (1977). Light-Activated Gtpase in Vertebrate Photoreceptors - Regulation of Light-Activated Cyclic-GMP Phosphodiesterase. Proc Natl Acad Sci USA *74*, 4238-4242.

(72) Fung, B.K., Hurley, J.B., and Stryer, L. (1981). Flow of Information in the Light-Triggered Cyclic Nucleotide Cascade of Vision. Proc Natl Acad Sci USA *78*, 152-156.

(73) Kühn, H. (1980). Light- and GTP-Regulated Interaction of GTPase and Other Proteins with Bovine Photoreceptor Membranes. Nature *283*, 587-589.

(74) Shinozawa, T., Sen, I., Wheeler, G., and Bitensky, M. (1979). Predictive Value of the Analogy between Hormone-Sensitive Adenylate-Cyclase and Light-Sensitive Photoreceptor Cyclic-GMP Phosphodiesterase - Specific Role for a Light-Sensitive GTPase as a Component in the Activation Sequence. J Supramol Str Cell *10*, 185-190.

(75) Bitensky, M.W., Wheeler, G.L., Yamazaki, A., Rasenick, M.M., and Stein, P.J. (1981). Chapter 14 Cyclic-Nucleotide Metabolism in Vertebrate Photoreceptors: A Remarkable Analogy and an Unraveling Enigma. Curr Top Membr Trans *15*, 237-271.

(76) Stein, P.J., Rasenick, M.M., and Bitensky, M.W. (1982). Chapter 8 Biochemistry of the Cyclic Nucleotide-Related Enzymes in Rod Photoreceptors. Prog Retin Res *1*, 227-243.

(77) Bitensky, M.W., Wheeler, M.A., Rasenick, M.M., Yamazaki, A., Stein, P.J., Halliday, K.R., and Wheeler, G.L. (1982). Functional Exchange of Components between Light-Activated Photoreceptor Phosphodiesterase and Hormone-Activated Adenylate-Cyclase Systems. Proc Natl Acad Sci USA *79*, 3408-3412.

(78) Stryer, L. (1983). Transducin and the Cyclic-GMP Phosphodiesterase - Amplifier Proteins in Vision. Cold Spring Harb Sym *48*, 841-852.

(79) Stryer, L. (1986). Cyclic-GMP Cascade of Vision. Annu Rev Neurosci *9*, 87-119.

(80) Dohlman, H.G., Caron, M.G., and Lefkowitz, R.J. (1987). A Family of Receptors Coupled to Guanine-Nucleotide Regulatory Proteins. Biochemistry *26*, 2657-2664.

(81) Stadel, J.M., Nambi, P., Shorr, R.G.L., Sawyer, D.F., Caron, M.G., and Lefkowitz, R.J. (1983). Catecholamine-Induced Desensitization of Turkey Erythrocyte Adenylate-

Cyclase Is Associated with Phosphorylation of the β-Adrenergic Receptor. Proc Natl Acad Sci USA *80*, 3173-3177.

(82) Lefkowitz, R.J., Stadel, J.M., and Caron, M.G. (1983). Adenylate Cyclase-Coupled Beta-Adrenergic Receptors - Structure and Mechanisms of Activation and Desensitization. Annu Rev Biochem *52*, 159-186.

(83) Benovic, J.L., Mayor, F., Staniszewski, C., Lefkowitz, R.J., and Caron, M.G. (1987a). Purification and Characterization of the β-Adrenergic Receptor Kinase. J Biol Chem *262*, 9026-9032.

(84) Pfister, C., Chabre, M., Plouet, J., Tuyen, V.V., Dekozak, Y., Faure, J.P., and Kühn, H. (1985). Retinal-S Antigen Identified as the 48k-Protein Regulating Light-Dependent Phosphodiesterase in Rods. Science *228*, 891-893.

(85) Wilden, U., Hall, S.W., and Kühn, H. (1986). Phosphodiesterase Activation by Photoexcited Rhodopsin Is Quenched When Rhodopsin Is Phosphorylated and Binds the Intrinsic 48-kDa Protein of Rod Outer Segments. Proc Natl Acad Sci USA *83*, 1174-1178.

(86) Benovic, J.L., Kühn, H., I, W., Codina, J., Caron, M.G., and Lefkowitz, R.J. (1987b). Functional Desensitization of the Isolated β-Adrenergic Receptor by the β-Adrenergic Receptor Kinase - Potential Role of an Analog of the Retinal Protein Arrestin (48-kDa Protein). Proc Natl Acad Sci USA *84*, 8879-8882.

(87) Shinohara, T., Dietzschold, B., Craft, C.M., Wistow, G., Early, J.J., Donoso, L.A., Horwitz, J., and Tao, R. (1987). Primary and Secondary Structure of Bovine Retinal S-Antigen (48-kDa Protein). Proc Natl Acad Sci USA *84*, 6975-6979.

(88) Lohse, M.J., Benovic, J.L., Codina, J., Caron, M.G., and Lefkowitz, R.J. (1990). Beta-Arrestin - a Protein that Regulates *β*-Adrenergic Receptor Function. Science *248*, 1547-1550.

(89) Premont, R.T., and Gainetdinov, R.R. (2007). Physiological Roles of G Protein-Coupled Receptor Kinases and Arrestins. Annu Rev Physiol *69*, 511-534.

(90) Bennett, M.R. (1999). One Hundred Years of Adrenaline: the Discovery of Autoreceptors. Clin Auton Res *9*, 145-159.

(91) Rubin, R.P. (2007). A Brief History of Great Discoveries in Pharmacology: In Celebration of the Centennial Anniversary of the Founding of the American Society of Pharmacology and Experimental Therapeutics. Pharmacol Rev *59*, 289-359.

(92) Buck, L., and Axel, R. (1991). A Novel Multigene Family May Encode Odorant Receptors - a Molecular-Basis for Odor Recognition. Cell *65*, 175-187.

(93) Ferretti, L., Karnik, S.S., Khorana, H.G., Nassal, M., and Oprian, D.D. (1986). Total Synthesis of a Gene for Bovine Rhodopsin. Proc Natl Acad Sci USA *83*, 599-603.

(94) Oprian, D.D., Molday, R.S., Kaufman, R.J., and Khorana, H.G. (1987). Expression of a Synthetic Bovine Rhodopsin Gene in Monkey Kidney Cells. Proc Natl Acad Sci USA *84*, 8874-8878.

(95) Sakmar, T.P., Franke, R.R., and Khorana, H.G. (1989). Glutamic Acid-113 Serves as the Retinylidene Schiff-Base Counterion in Bovine Rhodopsin. Proc Natl Acad Sci USA *86*, 8309-8313.

(96) Sakmar, T.P., Franke, R.R., and Khorana, H.G. (1991). The Role of the Retinylidene Schiff-Base Counterion in Rhodopsin in Determining Wavelength Absorbency and Schiff-Base pKa. Proc Natl Acad Sci USA *88*, 3079-3083.

(97) Nakayama, T.A., and Khorana, H.G. (1991). Mapping of the Amino-Acids in Membrane-Embedded Helices that Interact with the Retinal Chromophore in Bovine Rhodopsin. J Biol Chem *266*, 4269-4275.

(98) Liu, X., Garriga, P., and Khorana, H.G. (1996). Structure and Function in Rhodopsin: Correct Folding and Misfolding in Two Point Mutants in the Intradiscal Domain of Rhodopsin Identified in Retinitis Pigmentosa. Proc Natl Acad Sci USA *93*, 4554-4559.

(99) Garriga, P., Liu, X., and Khorana, H.G. (1996). Structure and Function in Rhodopsin: Correct Folding and Misfolding in Point Mutants at and in Proximity to the Site of the Retinitis Pigmentosa Mutation Leu-125->Arg in the Transmembrane Helix C. Proc Natl Acad Sci USA *93*, 4560-4564.

(100) Mollaaghababa, R., Davidson, F.F., Kaiser, C., and Khorana, H.G. (1997). Structure and Function in Rhodopsin: Expression of Functional Mammalian Opsin in Saccharomyces Cerevisiae. Proc Natl Acad Sci USA *94*, 3481-3481.

(101) Kim, J.M., Altenbach, C., Thurmond, R.L., Khorana, H.G., and Hubbell, W.L. (1997). Structure and Function in Rhodopsin: Rhodopsin Mutants with a Neutral Amino Acid at E134 Have a Partially Activated Conformation in the Dark State. Proc Natl Acad Sci USA *94*, 14273-14278.

(102) Han, M., Smith, S.O., and Sakmar, T.P. (1998). Constitutive Activation of Opsin by Mutation of Methionine 257 on Transmembrane Helix 6. Biochemistry *37*, 8253-8261.

(103) Farrens, D.L., Altenbach, C., Yang, K., Hubbell, W.L., and Khorana, H.G. (1996). Requirement of Rigid-Body Motion of Transmembrane Helices for Light Activation of Rhodopsin. Science *274*, 768-770.

(104) Sheikh, S.P., Zvyaga, T.A., Lichtarge, O., Sakmar, T.P., and Bourne, H.R. (1996). Rhodopsin Activation Blocked by Metal-Ion-Binding Sites Linking Transmembrane Helices C and F. Nature *383*, 347-350.

(105) Schertler, G.F.X., Villa, C., and Henderson, R. (1993). Projection Structure of Rhodopsin. Nature *362*, 770-772.

(106) Palczewski, K., Kumasaka, T., Hori, T., Behnke, C.A., Motoshima, H., Fox, B.A., Le Trong, I., Teller, D.C., Okada, T., Stenkamp, R.E., Yamamoto, M., and Miyano, M. (2000). Crystal Structure of Rhodopsin: a G Protein-Coupled Receptor. Science *289*, 739-745.

(107) Teller, D.C., Okada, T., Behnke, C.A., Palczewski, K., and Stenkamp, R.E. (2001). Advances in Determination of a High-Resolution Three-Dimensional Structure of Rhodopsin, a Model of G-Protein-Coupled Receptors (GPCRs). Biochemistry *40*, 7761-7772.

(108) Li, J., Edwards, P.C., Burghammer, M., Villa, C., and Schertler, G.F. (2004). Structure of Bovine Rhodopsin in a Trigonal Crystal Form. J Mol Biol *343*, 1409-1438.

(109) Okada, T., Sugihara, M., Bondar, A.N., Elstner, M., Entel, P., and Buss, V. (2004). The Retinal Conformation and Its Environment in Rhodopsin in Light of a New 2.2 a Crystal Structure. J Mol Biol *342*, 571-583.

(110) Sakmar, T.P., Menon, S.T., Marin, E.P., and Awad, E.S. (2002). Rhodopsin: Insights from Recent Structural Studies. Annu Rev Biophys Biomole Struct *31*, 443-484.

(111) Rosenbaum, D.M., Cherezov, V., Hanson, M.A., Rasmussen, S.G., Thian, F.S., Kobilka, T.S., Choi, H.J., Yao, X.J., Weis, W.I., Stevens, R.C., and Kobilka, B.K. (2007). GPCR Engineering Yields High-Resolution Structural Insights into β_2-Adrenergic ReceptorFunction. Science *318*, 1266-1273.

(112) Rasmussen, S.G., Choi, H.J., Rosenbaum, D.M., Kobilka, T.S., Thian, F.S., Edwards, P.C., Burghammer, M., Ratnala, V.R., Sanishvili, R., Fischetti, R.F., Schertler, G.F., Weis, W.I., and Kobilka, B.K. (2007). Crystal Structure of the Human β_2 Adrenergic G Protein-Coupled Receptor. Nature *450*, 383-387.

(113) Cherezov, V., Rosenbaum, D.M., Hanson, M.A., Rasmussen, S.G., Thian, F.S., Kobilka, T.S., Choi, H.J., Kuhn, P., Weis, W.I., Kobilka, B.K., and Stevens, R.C. (2007). High-Resolution Crystal Structure of an Engineered Human β_2 Adrenergic G Protein-Coupled Receptor. Science *318*, 1258-1265.

(114) Murakami, M., and Kouyama, T. (2011). Crystallographic Analysis of the Primary Photochemical Reaction of Squid Rhodopsin. J Mol Biol *413*, 615-627.

(115) Nakamichi, H., and Okada, T. (2006a). Crystallographic Analysis of Primary Visual Photochemistry. Angew Chem Int Ed *45*, 4270-4273.

(116) Nakamichi, H., and Okada, T. (2006b). Local Peptide Movement in the Photoreaction Intermediate of Rhodopsin. Proc Natl Acad Sci USA *103*, 12729-12734.

(117) Salom, D., Lodowski, D.T., Stenkamp, R.E., Le Trong, I., Golczak, M., Jastrzebska, B., Harris, T., Ballesteros, J.A., and Palczewski, K. (2006). Crystal Structure of a Photoactivated Deprotonated Intermediate of Rhodopsin. Proc Natl Acad Sci USA *103*, 16123-16128.

(118) Ruprecht, J.J., Mielke, T., Vogel, R., Villa, C., and Schertler, G.F. (2004). Electron Crystallography Reveals the Structure of Metarhodopsin I. EMBO J *23*, 3609-3620.

(119) Park, J.H., Scheerer, P., Hofmann, K.P., Choe, H.W., and Ernst, O.P. (2008). Crystal Structure of the Ligand-Free G Protein-Coupled Receptor Opsin. Nature *454*, 183-187.

(120) Scheerer, P., Park, J.H., Hildebrand, P.W., Kim, Y.J., Krauss, N., Choe, H.W., Hofmann, K.P., and Ernst, O.P. (2008). Crystal Structure of Opsin in Its G Protein-Interacting Conformation. Nature *455*, 497-502.

(121) Choe, H.W., Kim, Y.J., Park, J.H., Morizumi, T., Pai, E.F., Krauss, N., Hofmann, K.P., Scheerer, P., and Ernst, O.P. (2011). Crystal Structure of Metarhodopsin II. Nature *471*, 651-655.

(122) Standfuss, J., Edwards, P.C., D'Antona, A., Fransen, M., Xie, G., Oprian, D.D., and Schertler, G.F. (2011). The Structural Basis of Agonist-Induced Activation in Constitutively Active Rhodopsin. Nature *471*, 656-660.

(123) Deupi, X., Edwards, P., Singhal, A., Nickle, B., Oprian, D., Schertler, G., and Standfuss, J. (2012a). Stabilized G Protein Binding Site in the Structure of Constitutively Active Metarhodopsin-II. Proc Natl Acad Sci USA *109*, 119-124.

(124) Singhal, A., Ostermaier, M.K., Vishnivetskiy, S.A., Panneels, V., Homan, K.T., Tesmer, J.J.G., Veprintsev, D., Deupi, X., Gurevich, V.V., Schertler, G.F.X., and Standfuss, J. (2013). Insights into Congenital Stationary Night Blindness Based on the Structure of G90D Rhodopsin. EMBO Rep *14*, 520-526.

(125) Deupi, X., and Kobilka, B.K. (2010). Energy Landscapes as a Tool to Integrate GPCR Structure, Dynamics, and Function. Physiology *25*, 293-303.

(126) Deupi, X., Standfuss, J., and Schertler, G. (2012b). Conserved Activation Pathways in G Protein-Coupled Receptors. Biochem Soc Trans *40*, 383-388.

(127) Deupi, X. (2014). Relevance of Rhodopsin Studies for GPCR Activation. Biochim Biophys Acta *1837*, 674-682.

(128) Altenbach, C., Kusnetzow, A.K., Ernst, O.P., Hofmann, K.P., and Hubbell, W.L. (2008a). High-Resolution Distance Mapping in Rhodopsin Reveals the Pattern of Helix Movement Due to Activation. Proc Natl Acad Sci USA *105*, 7439-7444.

(129) Ye, S., Zaitseva, E., Caltabiano, G., Schertler, G.F., Sakmar, T.P., Deupi, X., and Vogel, R. (2010). Tracking G-Protein-Coupled Receptor Activation Using Genetically Encoded Infrared Probes. Nature *464*, 1386-1389.

(130) Archer, E., Maigret, B., Escrieut, C., Pradayrol, L., and Fourmy, D. (2003). Rhodopsin Crystal: New Template Yielding Realistic Models of G Protein-Coupled Receptors? Trends Pharmacol Sci *24*, 36-40.

(131) Evers, A., and Klabunde, T. (2005). Structure-Based Drug Discovery Using GPCR Homology Modeling: Successful Virtual Screening for Antagonists of the α_{1A} Adrenergic Receptor. J Med Chem *48*, 1088-1097.

(132) Periole, X., Huber, T., Marrink, S.J., and Sakmar, T.P. (2007). G Protein-Coupled Receptors Self-Assemble in Dynamics Simulations of Model Bilayers. J Am Chem Soc *129*, 10126-10132.

(133) Periole, X., Knepp, A.M., Sakmar, T.P., Marrink, S.J., and Huber, T. (2012). Structural Determinants of the Supramolecular Organization of G Protein-Coupled Receptors in Bilayers. J Am Chem Soc *134*, 10959-10965.

(134) Rasmussen, S.G., Choi, H.J., Fung, J.J., Pardon, E., Casarosa, P., Chae, P.S., Devree, B.T., Rosenbaum, D.M., Thian, F.S., Kobilka, T.S., Schnapp, A., Konetzki, I., Sunahara, R.K., Gellman, S.H., Pautsch, A., Steyaert, J., Weis, W.I., and Kobilka, B.K. (2011a). Structure of a Nanobody-Stabilized Active State of the β_2 Adrenoceptor. Nature *469*, 175-180.

(135) Rosenbaum, D.M., Zhang, C., Lyons, J.A., Holl, R., Aragao, D., Arlow, D.H., Rasmussen, S.G., Choi, H.J., Devree, B.T., Sunahara, R.K., Chae, P.S., Gellman, S.H., Dror, R.O., Shaw, D.E., Weis, W.I., Caffrey, M., Gmeiner, P., and Kobilka, B.K. (2011). Structure and Function of an Irreversible Agonist-β_2 Adrenoceptor Complex. Nature *469*, 236-240.

(136) Rasmussen, S.G., DeVree, B.T., Zou, Y., Kruse, A.C., Chung, K.Y., Kobilka, T.S., Thian, F.S., Chae, P.S., Pardon, E., Calinski, D., Mathiesen, J.M., Shah, S.T., Lyons, J.A., Caffrey, M., Gellman, S.H., Steyaert, J., Skiniotis, G., Weis, W.I., Sunahara, R.K., and Kobilka, B.K. (2011b). Crystal Structure of the β_2 Adrenergic Receptor-G_s Protein Complex. Nature *477*, 549-555.

(137) Stevens, R.C., Cherezov, V., Katritch, V., Abagyan, R., Kuhn, P., Rosen, H., and Wuthrich, K. (2013). The GPCR Network: A Large-Scale Collaboration to Determine Human GPCR Structure and Function. Nat Rev Drug Discov *12*, 25-34.

(138) Siu, F.Y., He, M., de Graaf, C., Han, G.W., Yang, D.H., Zhang, Z.Y., Zhou, C.H., Xu, Q.P., Wacker, D., Joseph, J.S., Liu, W., Lau, J., Cherezov, V., Katritch, V., Wang, M.W., and Stevens, R.C. (2013). Structure of the Human Glucagon Class B G Protein-Coupled Receptor. Nature *499*, 444-449.

(139) Wu, H.X., Wang, C., Gregory, K.J., Han, G.W., Cho, H.P., Xia, Y., Niswender, C.M., Katritch, V., Meiler, J., Cherezov, V., Conn, P.J., and Stevens, R.C. (2014). Structure of a Class C GPCR Metabotropic Glutamate Receptor 1 Bound to an Allosteric Modulator. Science *344*, 58-64.

(140) Dore, A.S., Okrasa, K., Patel, J.C., Serrano-Vega, M., Bennett, K., Cooke, R.M., Errey, J.C., Jazayeri, A., Khan, S., Tehan, B., Weir, M., Wiggin, G.R., and Marshall, F.H. (2014). Structure of Class C GPCR Metabotropic Glutamate Receptor 5 Transmembrane Domain. Nature *511*, 557-562.

(141) Grunbeck, A., and Sakmar, T.P. (2013). Probing G Protein-Coupled Receptor-Ligand Interactions with Targeted Photoactivatable Cross-Linkers. Biochemistry *52*, 8625-8632.

(142) Nakayama, T.A., and Khorana, H.G. (1990a). Synthesis of a New Photoactivatable Analog of 11-Cis-Retinal. J Org Chem *55*, 4953-4956.

(143) Nakayama, T.A., and Khorana, H.G. (1990b). Orientation of Retinal in Bovine Rhodopsin Determined by Cross-Linking Using a Photoactivatable Analog of 11-*Cis*-Retinal. J Biol Chem *265*, 15762-15769.

(144) Zhang, H.Z., Lerro, K.A., Yamamoto, T., Lien, T.H., Sastry, L., Gawinowicz, M.A., and Nakanishi, K. (1994). The Location of the Chromophore in Rhodopsin - a Photoaffinity Study. J Am Chem Soc *116*, 10165-10173.

(145) Barger, G., and Dale, H.H. (1910). Chemical Structure and Sympathomimetic Action of Amines. J Physiol *41*, 19-59.

(146) Lefkowitz, R.J., Mukherjee, C., Coverstone, M., and Caron, M.G. (1974). Stereospecific (^{3}H)(-)-Alprenolol Binding Sites, β-Adrenergic Receptors and Adenylate Cyclase. Biochem Bioph Res Co *60*, 703-709.

(147) Williams, L.T., and Lefkowitz, R.J. (1976). Alpha-Adrenergic Receptor Identification by (^{3}H)Dihydroergocryptine Binding. Science *192*, 791-793.

(148) Shaner, N.C., Steinbach, P.A., and Tsien, R.Y. (2005). A Guide to Choosing Fluorescent Proteins. Nat Methods *2*, 905-909.

(149) Goncalves, M.S. (2009). Fluorescent Labeling of Biomolecules with Organic Probes. Chem Rev *109*, 190-212.

(150) Alivisatos, A.P., Gu, W.W., and Larabell, C. (2005). Quantum Dots as Cellular Probes. Annu Rev Biomed Eng *7*, 55-76.

(151) Selvin, P.R. (2002). Principles and Biophysical Applications of Lanthanide-Based Probes. Annu Rev Biophys Biomole Struct *31*, 275-302.

(152) Kobilka, B.K., Kobilka, T.S., Daniel, K., Regan, J.W., Caron, M.G., and Lefkowitz, R.J. (1988). Chimeric α_2-, β_2-Adrenergic Receptors: Delineation of Domains Involved in Effector Coupling and Ligand Binding Specificity. Science *240*, 1310-1316.

(153) Barak, L.S., Ferguson, S.S., Zhang, J., Martenson, C., Meyer, T., and Caron, M.G. (1997). Internal Trafficking and Surface Mobility of a Functionally Intact β_2-Adrenergic Receptor-Green Fluorescent Protein Conjugate. Mol Pharmacol *51*, 177-184.

(154) Tarasova, N.I., Stauber, R.H., Choi, J.K., Hudson, E.A., Czerwinski, G., Miller, J.L., Pavlakis, G.N., Michejda, C.J., and Wank, S.A. (1997). Visualization of G Protein-Coupled Receptor Trafficking with the Aid of the Green Fluorescent Protein. Endocytosis and Recycling of Cholecystokinin Receptor Type A. J Biol Chem *272*, 14817-14824.

(155) Angers, S., Salahpour, A., Joly, E., Hilairet, S., Chelsky, D., Dennis, M., and Bouvier, M. (2000). Detection of β_2-Adrenergic Receptor Dimerization in Living Cells Using Bioluminescence Resonance Energy Transfer (BRET). Proc Natl Acad Sci USA *97*, 3684-3689.

(156) Gales, C., Rebois, R.V., Hogue, M., Trieu, P., Breit, A., Hebert, T.E., and Bouvier, M. (2005). Real-Time Monitoring of Receptor and G Protein Interactions in Living Cells. Nat Methods *2*, 177-184.

(157) Bohme, I., and Beck-Sickinger, A.G. (2009). Illuminating the Life of GPCRs. Cell Commun Signal *7*.

(158) Lohse, M.J., Nuber, S., and Hoffmann, C. (2012). Fluorescence/Bioluminescence Resonance Energy Transfer Techniques to Study G Protein-Coupled Receptor Activation and Signaling. Pharmacol Rev *64*, 299-336.

(159) Hoffmann, C., Gaietta, G., Bunemann, M., Adams, S.R., Oberdorff-Maass, S., Behr, B., Vilardaga, J.P., Tsien, R.Y., Ellisman, M.H., and Lohse, M.J. (2005). A FlAsH-Based FRET Approach to Determine G Protein-Coupled Receptor Activation in Living Cells. Nat Methods *2*, 171-176.

(160) Hoffmann, C., Gaietta, G., Zurn, A., Adams, S.R., Terrillon, S., Ellisman, M.H., Tsien, R.Y., and Lohse, M.J. (2010). Fluorescent Labeling of Tetracysteine-Tagged Proteins in Intact Cells. Nat Protoc *5*, 1666-1677.

(161) Rashidian, M., Dozier, J.K., and Distefano, M.D. (2013). Enzymatic Labeling of Proteins: Techniques and Approaches. Bioconjugate Chem *24*, 1277-1294.

(162) Rush, J.S., and Bertozzi, C.R. (2008). New Aldehyde Tag Sequences Identified by Screening Formylglycine Generating Enzymes *in Vitro* and *in Vivo*. J Am Chem Soc *130*, 12240-12241.

(163) Popp, M.W., Antos, J.M., Grotenbreg, G.M., Spooner, E., and Ploegh, H.L. (2007). Sortagging: a Versatile Method for Protein Labeling. Nat Chem Biol *3*, 707-708.

(164) Chen, I., Howarth, M., Lin, W.Y., and Ting, A.Y. (2005). Site-Specific Labeling of Cell Surface Proteins with Biophysical Probes Using Biotin Ligase. Nat Methods *2*, 99-104.

(165) Slavoff, S.A., Chen, I., Choi, Y.A., and Ting, A.A.Y. (2008). Expanding the Substrate Tolerance of Biotin Ligase through Exploration of Enzymes from Diverse Species. J Am Chem Soc *130*, 1160-1162.

(166) Pober, J.S., Iwanij, V., Reich, E., and Stryer, L. (1978). Transglutaminase-Catalyzed Insertion of a Fluorescent Probe into the Protease-Sensitive Region of Rhodopsin. Biochemistry *17*, 2163-2168.

(167) Keppler, A., Gendreizig, S., Gronemeyer, T., Pick, H., Vogel, H., and Johnsson, K. (2003). A General Method for the Covalent Labeling of Fusion Proteins with Small Molecules *in Vivo*. Nat Biotechnol *21*, 86-89.

(168) Keppler, A., Pick, H., Arrivoli, C., Vogel, H., and Johnsson, K. (2004). Labeling of Fusion Proteins with Synthetic Fluorophores in Live Cells. Proc Natl Acad Sci USA *101*, 9955-9959.

(169) Maurel, D., Comps-Agrar, L., Brock, C., Rives, M.-L., Bourrier, E., Ayoub, M.A., Bazin, H., Tinel, N., Durroux, T., Prezeau, L., Trinquet, E., and Pin, J.-P. (2008). Cell-

Surface Protein-Protein Interaction Analysis with Time-Resolved FRET and Snap-Tag Technologies: Application to GPCR Oligomerization. Nat Methods *5*, 561-567.

(170) Emami-Nemini, A., Roux, T., Leblay, M., Bourrier, E., Lamarque, L., Trinquet, E., and Lohse, M.J. (2013). Time-Resolved Fluorescence Ligand Binding for G Protein-Coupled Receptors. Nat Protoc *8*, 1307-1320.

(171) Los, G.V., Encell, L.P., McDougall, M.G., Hartzell, D.D., Karassina, N., Zimprich, C., Wood, M.G., Learish, R., Ohana, R.F., Urh, M., Simpson, D., Mendez, J., Zimmerman, K., Otto, P., Vidugiris, G., Zhu, J., Darzins, A., Klaubert, D.H., Bulleit, R.F., and Wood, K.V. (2008). Halo Tag: a Novel Protein Labeling Technology for Cell Imaging and Protein Analysis. ACS Chem Biol *3*, 373-382.

(172) Snaar-Jagalska, B.E., Cambi, A., Schmidt, T., and de Keijzer, S. (2013). Single-Molecule Imaging Technique to Study the Dynamic Regulation of GPCR Function at the Plasma Membrane. G Protein-Coupled Receptors: Trafficking and Oligomerization *521*, 47-67.

(173) Gronemeyer, T., Godin, G., and Johnsson, K. (2005). Adding Value to Fusion Proteins through Covalent Labeling. Curr Opin Biotech *16*, 453-458.

(174) Glazer, A.N. (1970). Specific Chemical Modification of Proteins. Annu Rev Biochem *39*, 101-130.

(175) Sletten, E.M., and Bertozzi, C.R. (2009). Bioorthogonal Chemistry: Fishing for Selectivity in a Sea of Functionality. Angew Chem Int Ed *48*, 6974-6998.

(176) Rousselet, A., and Devaux, P.F. (1978). Interaction between Spin-Labeled Rhodopsin and Spin-Labeled Phospholipids in Retinal Outer Segment Disk Membranes. FEBS Lett *93*, 161-164.

(177) Chen, Y.S., and Hubbell, W.L. (1978). Reactions of Sulfhydryl-Groups of Membrane-Bound Bovine Rhodopsin. Membrane Biochem *1*, 107-130.

(178) Resek, J.F., Farahbakhsh, Z.T., Hubbell, W.L., and Khorana, H.G. (1993). Formation of the Meta II Photointermediate Is Accompanied by Conformational Changes in the Cytoplasmic Surface of Rhodopsin. Biochemistry *32*, 12025-12032.

(179) Yang, K., Farrens, D.L., Hubbell, W.L., and Khorana, H.G. (1996). Structure and Function in Rhodopsin. Single Cysteine Substitution Mutants in the Cytoplasmic Interhelical E-F Loop Region Show Position-Specific Effects in Transducin Activation. Biochemistry *35*, 12464-12469.

(180) Gether, U., Lin, S., Ghanouni, P., Ballesteros, J.A., Weinstein, H., and Kobilka, B.K. (1997). Agonists Induce Conformational Changes in Transmembrane Domains III and VI of the β_2 Adrenoceptor. EMBO J *16*, 6737-6747.

(181) Wu, C.W., and Stryer, L. (1972). Proximity Relationships in Rhodopsin. Proc Natl Acad Sci USA *69*, 1104-1108.

(182) Stryer, L. (1978). Fluorescence Energy-Transfer as a Spectroscopic Ruler. Annu Rev Biochem *47*, 819-846.

(183) Altenbach, C., Yang, K., Farrens, D.L., Farahbakhsh, Z.T., Khorana, H.G., and Hubbell, W.L. (1996). Structural Features and Light-Dependent Changes in the Cytoplasmic Interhelical E-F Loop Region of Rhodopsin: a Site-Directed Spin-Labeling Study. Biochemistry *35*, 12470-12478.

(184) Hubbell, W.L., Altenbach, C., Hubbell, C.M., and Khorana, H.G. (2003). Rhodopsin Structure, Dynamics, and Activation: a Perspective from Crystallography,

Site-Directed Spin Labeling, Sulfhydryl Reactivity, and Disulfide Cross-Linking. Adv Protein Chem *63*, 243-290.

(185) Altenbach, C., Kusnetzow, A.K., Ernst, O.P., Hofmann, K.P., and Hubbell, W.L. (2008b). High-Resolution Distance Mapping in Rhodopsin Reveals the Pattern of Helix Movement Due to Activation. Proc Natl Acad Sci USA *105*, 7439-7444.

(186) Farrens, D.L., and Khorana, H.G. (1995). Structure and Function in Rhodopsin. Measurement of the Rate of Metarhodopsin II Decay by Fluorescence Spectroscopy. J Biol Chem *270*, 5073-5076.

(187) Dunham, T.D., and Farrens, D.L. (1999). Conformational Changes in Rhodopsin. Movement of Helix F Detected by Site-Specific Chemical Labeling and Fluorescence Spectroscopy. J Biol Chem *274*, 1683-1690.

(188) Ghanouni, P., Gryczynski, Z., Steenhuis, J.J., Lee, T.W., Farrens, D.L., Lakowicz, J.R., and Kobilka, B.K. (2001). Functionally Different Agonists Induce Distinct Conformations in the G Protein-Coupling Domain of the β_2 Adrenergic Receptor. J Biol Chem *276*, 24433-24436.

(189) Yao, X., Parnot, C., Deupi, X., Ratnala, V.R., Swaminath, G., Farrens, D., and Kobilka, B. (2006). Coupling Ligand Structure to Specific Conformational Switches in the β_2-Adrenoceptor. Nat Chem Biol *2*, 417-422.

(190) Mathiasen, S., Christensen, S.M., Fung, J.J., Rasmussen, S.G., Fay, J.F., Jorgensen, S.K., Veshaguri, S., Farrens, D.L., Kiskowski, M., Kobilka, B., and Stamou, D. (2014). Nanoscale High-Content Analysis Using Compositional Heterogeneities of Single Proteoliposomes. Nat Methods *11*, 931-934.

(191) Davis, L., and Chin, J.W. (2012). Designer Proteins: Applications of Genetic Code Expansion in Cell Biology. Nat Rev Mol Cell Bio *13*, 168-182.

(192) Huber, T., and Sakmar, T.P. (2014). Chemical Biology Methods for Investigating G Protein-Coupled Receptor Signaling. Chem Biol *21*, 1224-1237.

(193) Noren, C.J., Anthonycahill, S.J., Griffith, M.C., and Schultz, P.G. (1989). A General-Method for Site-Specific Incorporation of Unnatural Amino-Acids into Proteins. Science *244*, 182-188.

(194) Mendel, D., Ellman, J.A., and Schultz, P.G. (1991). Construction of a Light-Activated Protein by Unnatural Amino-Acid Mutagenesis. J Am Chem Soc *113*, 2758-2760.

(195) Judice, J.K., Gamble, T.R., Murphy, E.C., Devos, A.M., and Schultz, P.G. (1993). Probing the Mechanism of Staphylococcal Nuclease with Unnatural Amino-Acids - Kinetic and Structural Studies. Science *261*, 1578-1581.

(196) Kimata, Y., Shimada, H., Hirose, T., and Ishimura, Y. (1995). Role of Thr-252 in Cytochrome P450 - a Study with Unnatural Amino-Acid Mutagenesis. Biochem Bioph Res Co *208*, 96-102.

(197) Nowak, M.W., Kearney, P.C., Sampson, J.R., Saks, M.E., Labarca, C.G., Silverman, S.K., Zhong, W., Thorson, J.S., Abelson, J.N., Davidson, N., Schultz, P.G., Dougherty, D.A., and Lester, H.A. (1995). Nicotinic Receptor-Binding Site Probed with Unnatural Amino Acid Incorporation in Intact Cells. Science *268*, 439-442.

(198) Wang, L., Brock, A., Herberich, B., and Schultz, P.G. (2001). Expanding the Genetic Code of Escherichia Coli. Science *292*, 498-500.

(199) Sakamoto, K., Hayashi, A., Sakamoto, A., Kiga, D., Nakayama, H., Soma, A., Kobayashi, T., Kitabatake, M., Takio, K., Saito, K., Shirouzu, M., Hirao, I., and Yokoyama, S. (2002). Site-Specific Incorporation of an Unnatural Amino Acid into Proteins in Mammalian Cells. Nucleic Acids Res *30*, 4692-4699.

(200) Deiters, A., Cropp, T.A., Mukherji, M., Chin, J.W., Anderson, J.C., and Schultz, P.G. (2003). Adding Amino Acids with Novel Reactivity to the Genetic Code of Saccharomyces Cerevisiae. J Am Chem Soc *125*, 11782-11783.

(201) Chin, J.W., Cropp, T.A., Anderson, J.C., Mukherji, M., Zhang, Z.W., and Schultz, P.G. (2003a). An Expanded Eukaryotic Genetic Code. Science *301*, 964-967.

(202) Chin, J.W., Cropp, T.A., Chu, S., Meggers, E., and Schultz, P.G. (2003b). Progress toward an Expanded Eukaryotic Genetic Code. Chem Biol *10*, 511-519.

(203) Huang, L.Y., Umanah, G., Hauser, M., Son, C., Arshava, B., Naider, F., and Becker, J.M. (2008). Unnatural Amino Acid Replacement in a Yeast G Protein-Coupled Receptor in Its Native Environment. Biochemistry *47*, 5638-5648.

(204) Ye, S., Köhrer, C., Huber, T., Kazmi, M., Sachdev, P., Yan, E.C.Y., Bhagat, A., RajBhandary, U.L., and Sakmar, T.P. (2008). Site-Specific Incorporation of Keto Amino Acids into Functional G Protein-Coupled Receptors Using Unnatural Amino Acid Mutagenesis. J Biol Chem *283*, 1525-1533.

(205) Ye, S., Huber, T., Vogel, R., and Sakmar, T.P. (2009). FTIR Analysis of GPCR Activation Using Azido Probes. Nat Chem Biol *5*, 397-399.

(206) Grunbeck, A., Huber, T., Sachdev, P., and Sakmar, T.P. (2011). Mapping the Ligand-Binding Site on a G Protein-Coupled Receptor (GPCR) Using Genetically Encoded Photocrosslinkers. Biochemistry *50*, 3411-3413.

(207) Grunbeck, A., Huber, T., Abrol, R., Trzaskowski, B., Goddard, W.A., and Sakmar, T.P. (2012). Genetically Encoded Photo-Cross-Linkers Map the Binding Site of an Allosteric Drug on a G Protein-Coupled Receptor. ACS Chem Biol *7*, 967-972.

(208) Valentin-Hansen, L., Park, M., Huber, T., Grunbeck, A., Naganathan, S., Schwartz, T.W., and Sakmar, T.P. (2014). Mapping Substance P Binding Sites on the Neurokinin-1 Receptor Using Genetic Incorporation of a Photoreactive Amino Acid. J Biol Chem *289*, 18045-18054.

(209) Ray-Saha, S., Huber, T., and Sakmar, T.P. (2014). Antibody Epitopes on G Protein-Coupled Receptors Mapped with Genetically Encoded Photoactivatable Cross-Linkers. Biochemistry *53*, 1302-1310.

(210) Zhong, W.G., Gallivan, J.P., Zhang, Y.O., Li, L.T., Lester, H.A., and Dougherty, D.A. (1998). From *Ab Initio* Quantum Mechanics to Molecular Neurobiology: A Cation-π Binding Site in the Nicotinic Receptor. Proc Natl Acad Sci USA *95*, 12088-12093.

(211) Dougherty, D.A. (2000). Unnatural Amino Acids as Probes of Protein Structure and Function. Curr Opin Chem Biol *4*, 645-652.

(212) Pless, S.A., Galpin, J.D., Frankel, A., and Ahern, C.A. (2011). Molecular Basis for Class Ib Anti-Arrhythmic Inhibition of Cardiac Sodium Channels. Nat Commun *2*, 351.

(213) Klippenstein, V., Ghisi, V., Wietstruk, M., and Plested, A.J.R. (2014). Photoinactivation of Glutamate Receptors by Genetically Encoded Unnatural Amino Acids. J Neurosci *34*, 980-991.

(214) Pless, S.A., and Ahern, C.A. (2013). Unnatural Amino Acids as Probes of Ligand-Receptor Interactions and Their Conformational Consequences. Annu Rev Pharmacol *53*, 211-229.

(215) Deiters, A., Cropp, T.A., Summerer, D., Mukherji, M., and Schultz, P.G. (2004). Site-Specific Pegylation of Proteins Containing Unnatural Amino Acids. Bioorg Med Chem Lett *14*, 5743-5745.

(216) Brustad, E.M., Lemke, E.A., Schultz, P.G., and Deniz, A.A. (2008). A General and Efficient Method for the Site-Specific Dual-Labeling of Proteins for Single Molecule Fluorescence Resonance Energy Transfer. J Am Chem Soc *130*, 17664-17665.

(217) Nguyen, D.P., Elliott, T., Holt, M., Muir, T.W., and Chin, J.W. (2011). Genetically Encoded 1,2-Aminothiols Facilitate Rapid and Site-Specific Protein Labeling via a Bio-Orthogonal Cyanobenzothiazole Condensation. J Am Chem Soc *133*, 11418-11421.

(218) Seo, M.H., Lee, T.S., Kim, E., Cho, Y.L., Park, H.S., Yoon, T.Y., and Kim, H.S. (2011). Efficient Single-Molecule Fluorescence Resonance Energy Transfer Analysis by Site-Specific Dual-Labeling of Protein Using an Unnatural Amino Acid. Anal Chem *83*, 8849-8854.

(219) Seo, M.H., Park, J., Kim, E., Hohng, S., and Kim, H.S. (2014). Protein Conformational Dynamics Dictate the Binding Affinity for a Ligand. Nat Commun *5*, 3724.

(220) Plass, T., Milles, S., Koehler, C., Schultz, C., and Lemke, E.A. (2011). Genetically Encoded Copper-Free Click Chemistry. Angew Chem Int Ed *50*, 3878-3881.

(221) Reddington, S.C., Tippmann, E.M., and Jones, D.D. (2012). Residue Choice Defines Efficiency and Influence of Bioorthogonal Protein Modification via Genetically Encoded Strain Promoted Click Chemistry. Chem Commun *48*, 8419-8421.

(222) Borrmann, A., Milles, S., Plass, T., Dommerholt, J., Verkade, J.M., Wiessler, M., Schultz, C., van Hest, J.C., van Delft, F.L., and Lemke, E.A. (2012). Genetic Encoding of

a Bicyclo[6.1.0]Nonyne-Charged Amino Acid Enables Fast Cellular Protein Imaging by Metal-Free Ligation. ChemBioChem *13*, 2094-2099.

(223) Wang, K., Sachdeva, A., Cox, D.J., Wilf, N.W., Lang, K., Wallace, S., Mehl, R.A., and Chin, J.W. (2014). Optimized Orthogonal Translation of Unnatural Amino Acids Enables Spontaneous Protein Double-Labelling and FRET. Nat Chem *6*, 393-403.

(224) Molday, R.S., and Mackenzie, D. (1983). Monoclonal-Antibodies to Rhodopsin - Characterization, Cross-Reactivity, and Application as Structural Probes. Biochemistry *22*, 653-660.

(225) Venkatakrishnan, A.J., Deupi, X., Lebon, G., Tate, C.G., Schertler, G.F., and Babu, M.M. (2013). Molecular Signatures of G Protein-Coupled Receptors. Nature *494*, 185-194.

(226) Jaakola, V.P., Griffith, M.T., Hanson, M.A., Cherezov, V., Chien, E.Y., Lane, J.R., Ijzerman, A.P., and Stevens, R.C. (2008). The 2.6 Angstrom Crystal Structure of a Human A_{2A} Adenosine Receptor Bound to an Antagonist. Science *322*, 1211-1217.

(227) Tan, Q., Zhu, Y., Li, J., Chen, Z., Han, G.W., Kufareva, I., Li, T., Ma, L., Fenalti, G., Zhang, W., Xie, X., Yang, H., Jiang, H., Cherezov, V., Liu, H., Stevens, R.C., Zhao, Q., and Wu, B. (2013). Structure of the CCR5 Chemokine Receptor-HIV Entry Inhibitor Maraviroc Complex. Science *341*, 1387-1390.

(228) Wu, B., Chien, E.Y., Mol, C.D., Fenalti, G., Liu, W., Katritch, V., Abagyan, R., Brooun, A., Wells, P., Bi, F.C., Hamel, D.J., Kuhn, P., Handel, T.M., Cherezov, V., and Stevens, R.C. (2010). Structures of the CXCR4 Chemokine GPCR with Small-Molecule and Cyclic Peptide Antagonists. Science *330*, 1066-1071.

(229) Chien, E.Y., Liu, W., Zhao, Q., Katritch, V., Han, G.W., Hanson, M.A., Shi, L., Newman, A.H., Javitch, J.A., Cherezov, V., and Stevens, R.C. (2010). Structure of the Human Dopamine D3 Receptor in Complex with a D2/D3 Selective Antagonist. Science *330*, 1091-1095.

(230) Ballesteros, J.A., and Weinstein, H. (1995). [19] Integrated Methods for the Construction of Three-Dimensional Models and Computational Probing of Structure-Function Relations in G Protein-Coupled Receptors. Methods Neurosci *25*, 366-428.

(231) Huber, T., Botelho, A.V., Beyer, K., and Brown, M.F. (2004). Membrane Model for the G Protein-Coupled Receptor Rhodopsin: Hydrophobic Interface and Dynamical Structure. Biophys J *86*, 2078-2100.

(232) Ridge, K.D., Lu, Z.J., Liu, X., and Khorana, H.G. (1995). Structure and Function in Rhodopsin - Separation and Characterization of the Correctly Folded and Misfolded Opsins Produced on Expression of an Opsin Mutant-Gene Containing Only the Native Intradiscal Cysteine Codons. Biochemistry *34*, 3261-3267.

(233) Reeves, P.J., Hwa, J., and Khorana, H.G. (1999). Structure and Function in Rhodopsin: Kinetic Studies of Retinal Binding to Purified Opsin Mutants in Defined Phospholipid-Detergent Mixtures Serve as Probes of the Retinal Binding Pocket. Proc Natl Acad Sci USA *96*, 1927-1931.

(234) Ning, X., Guo, J., Wolfert, M.A., and Boons, G.J. (2008). Visualizing Metabolically Labeled Glycoconjugates of Living Cells by Copper-Free and Fast Huisgen Cycloadditions. Angew Chem Int Ed *47*, 2253-2255.

(235) Debets, M.F., van Berkel, S.S., Dommerholt, J., Dirks, A.T., Rutjes, F.P., and van Delft, F.L. (2011). Bioconjugation with Strained Alkenes and Alkynes. Acc Chem Res *44*, 805-815.

(236) Strop, P., and Brunger, A.T. (2005). Refractive Index-Based Determination of Detergent Concentration and Its Application to the Study of Membrane Proteins. Protein Sci *14*, 2207-2211.

(237) Cheng, X., Jo, S., Lee, H.S., Klauda, J.B., and Im, W. (2013). Charmm-Gui Micelle Builder for Pure/Mixed Micelle and Protein/Micelle Complex Systems. J Chem Inf Model *53*, 2171-2180.

(238) Phillips, J.C., Braun, R., Wang, W., Gumbart, J., Tajkhorshid, E., Villa, E., Chipot, C., Skeel, R.D., Kale, L., and Schulten, K. (2005). Scalable Molecular Dynamics with Namd. J Comput Chem *26*, 1781-1802.

(239) Menon, S.T., Han, M., and Sakmar, T.P. (2001). Rhodopsin: Structural Basis of Molecular Physiology. Physiol Rev *81*, 1659-1688.

(240) Henselman, R.A., and Cusanovich, M.A. (1976). Characterization of the Recombination Reaction of Rhodopsin. Biochemistry *15*, 5321-5325.

(241) Cornish, V.W., Hahn, K.M., and Schultz, P.G. (1996). Site-Specific Protein Modification Using a Ketone Handle. J Am Chem Soc *118*, 8150-8151.

(242) Hang, H.C., and Bertozzi, C.R. (2001). Chemoselective Approaches to Glycoprotein Assembly. Acc Chem Res *34*, 727-736.

(243) Bayer, E.A., Ben-Hur, H., and Wilchek, M. (1988). Biocytin Hydrazide--a Selective Label for Sialic Acids, Galactose, and Other Sugars in Glycoconjugates Using Avidin-Biotin Technology. Anal Biochem *170*, 271-281.

(244) Wang, L., Zhang, Z., Brock, A., and Schultz, P.G. (2003). Addition of the Keto Functional Group to the Genetic Code of Escherichia Coli. Proc Natl Acad Sci USA *100*, 56-61.

(245) Shi, X., Jung, Y., Lin, L.-J., Liu, C., Wu, C., Cann, I.K.O., and Ha, T. (2012). Quantitative Fluorescence Labeling of Aldehyde-Tagged Proteins for Single-Molecule Imaging. Nat Methods *9*, 499-503.

(246) Fleissner, M.R., Brustad, E.M., Kalai, T., Altenbach, C., Cascio, D., Peters, F.B., Hideg, K., Peuker, S., Schultz, P.G., and Hubbell, W.L. (2009). Site-Directed Spin Labeling of a Genetically Encoded Unnatural Amino Acid. Proc Natl Acad Sci USA *106*, 21637-21642.

(247) Huber, T., Naganathan, S., Tian, H., Ye, S.X., and Sakmar, T.P. (2013). Unnatural Amino Acid Mutagenesis of GPCRs Using Amber Codon Suppression and Bioorthogonal Labeling. Method Enzymol *520*, 281-305.

(248) Ahn, B., Rhee, S.G., and Stadtman, E.R. (1987). Use of Fluorescein Hydrazide and Fluorescein Thiosemicarbazide Reagents for the Fluorometric Determination of Protein Carbonyl Groups and for the Detection of Oxidized Protein on Polyacrylamide Gels. Anal Biochem *161*, 245-257.

(249) Stadtman, E.R., and Levine, R.L. (2003). Free Radical-Mediated Oxidation of Free Amino Acids and Amino Acid Residues in Proteins. Amino Acids *25*, 207-218.

(250) Stadtman, E.R. (1993). Oxidation of Free Amino Acids and Amino Acid Residues in Proteins by Radiolysis and by Metal-Catalyzed Reactions. Annu Rev Biochem *62*, 797-821.

(251) Grimsrud, P.A., Xie, H., Griffin, T.J., and Bernlohr, D.A. (2008). Oxidative Stress and Covalent Modification of Protein with Bioactive Aldehydes. J Biol Chem *283*, 21837-21841.

(252) Zhang, Z., Smith, B.A.C., Wang, L., Brock, A., Cho, C., and Schultz, P.G. (2003). A New Strategy for the Site-Specific Modification of Proteins *in Vivo*. Biochemistry *42*, 6735-6746.

(253) Zeng, Y., Ramya, T.N.C., Dirksen, A., Dawson, P.E., and Paulson, J.C. (2009). High-Efficiency Labeling of Sialylated Glycoproteins on Living Cells. Nat Methods *6*, 207-209.

(254) Kiick, K.L., Saxon, E., Tirrell, D.A., and Bertozzi, C.R. (2002). Incorporation of Azides into Recombinant Proteins for Chemoselective Modification by the Staudinger Ligation. Proc Natl Acad Sci USA *99*, 19-24.

(255) Saxon, E., and Bertozzi, C.R. (2000). Cell Surface Engineering by a Modified Staudinger Reaction. Science *287*, 2007-2010.

(256) van Berkel, S.S., Dirks, A.T.J., Debets, M.F., van Delft, F.L., Cornelissen, J.J.L.M., Nolte, R.J.M., and Rutjes, F.P.J.T. (2007). Metal-Free Triazole Formation as a Tool for Bioconjugation. ChemBioChem *8*, 1504-1508.

(257) Agard, N.J., Prescher, J.A., and Bertozzi, C.R. (2004). A Strain-Promoted [3 + 2] Azide-Alkyne Cycloaddition for Covalent Modification of Biomolecules in Living Systems. J Am Chem Soc *126*, 15046-15047.

(258) Sletten, E.M., and Bertozzi, C.R. (2011). From Mechanism to Mouse: a Tale of Two Bioorthogonal Reactions. Acc Chem Res *44*, 666-676.

(259) Tsao, M.-L., Tian, F., and Schultz, P.G. (2005). Selective Staudinger Modification of Proteins Containing P-Azidophenylalanine. ChemBioChem *6*, 2147-2149.

(260) Debets, M.F., van der Doelen, C.W., Rutjes, F.P., and van Delft, F.L. (2010). Azide: a Unique Dipole for Metal-Free Bioorthogonal Ligations. ChemBioChem *11*, 1168-1184.

(261) Schilling, C.I., Jung, N., Biskup, M., Schepers, U., and Brase, S. (2011). Bioconjugation via Azide-Staudinger Ligation: An Overview. Chem Soc Rev *40*, 4840-4871.

(262) Yanagisawa, T., Ishii, R., Fukunaga, R., Kobayashi, T., Sakamoto, K., and Yokoyama, S. (2008). Multistep Engineering of Pyrrolysyl-tRNA Synthetase to Genetically Encode N_{ε}-(O-Azidobenzyloxycarbonyl) Lysine for Site-Specific Protein Modification. Chem Biol *15*, 1187-1197.

(263) Blomquist, A.T., and Liu, L.H. (1953). Many-Membered Carbon Rings .7. Cyclooctyne. J Am Chem Soc *75*, 2153-2154.

(264) Wittig, G., and Krebs, A. (1961). Zur Existenz Niedergliedriger Cycloalkine .1. Chem Ber-Recl *94*, 3260-3275.

(265) Seitz, G., Pohl, L., and Pohlke, R. (1969). 5,6-Didehydro-11,12-Dihydrodibenzo[a,E]Cyclooctene. Angew Chem Int Ed *8*, 447-448.

(266) Jewett, J.C., Sletten, E.M., and Bertozzi, C.R. (2010). Rapid Cu-Free Click Chemistry with Readily Synthesized Biarylazacyclooctynones. J Am Chem Soc *132*, 3688-3690.

(267) van Geel, R., Pruijn, G.J.M., van Delft, F.L., and Boelens, W.C. (2012). Preventing Thiol-Yne Addition Improves the Specificity of Strain-Promoted Azide-Alkyne Cycloaddition. Bioconjugate Chem *23*, 392-398.

(268) Staros, J.V., Bayley, H., Standring, D.N., and Knowles, J.R. (1978). Reduction of Aryl Azides by Thiols: Implications for the Use of Photoaffinity Reagents. Biochem Bioph Res Co *80*, 568-572.

(269) Nehring, S., Budisa, N., and Wiltschi, B. (2012). Performance Analysis of Orthogonal Pairs Designed for an Expanded Eukaryotic Genetic Code. PLoS One *7*, e31992.

(270) Liu, W., Brock, A., Chen, S., and Schultz, P.G. (2007). Genetic Incorporation of Unnatural Amino Acids into Proteins in Mammalian Cells. Nat Methods *4*, 239-244.

(271) Fairbanks, B.D., Sims, E.A., Anseth, K.S., and Bowman, C.N. (2010). Reaction Rates and Mechanisms for Radical, Photoinitated Addition of Thiols to Alkynes, and Implications for Thiol-Yne Photopolymerizations and Click Reactions. Macromolecules *43*, 4113-4119.

(272) Hoogenboom, R. (2010). Thiol-Yne Chemistry: a Powerful Tool for Creating Highly Functional Materials. Angew Chem Int Ed *49*, 3415-3417.

(273) Mielke, T., Alexiev, U., Glasel, M., Otto, H., and Heyn, M.P. (2002). Light-Induced Changes in the Structure and Accessibility of the Cytoplasmic Loops of Rhodopsin in the Activated Meta-II State. Biochemistry *41*, 7875-7884.

(274) Blaskovic, S., Blanc, M., and van der Goot, F.G. (2013). What Does S-Palmitoylation Do to Membrane Proteins? FEBS J *280*, 2766-2774.

(275) Sarramegna, V., Talmont, F., Demange, P., and Milon, A. (2003). Heterologous Expression of G Protein-Coupled Receptors: Comparison of Expression Systems from the Standpoint of Large-Scale Production and Purification. Cell Mol Life Sci *60*, 1529-1546.

(276) Almen, M.S., Nordström, K.J., Fredriksson, R., and Schioth, H.B. (2009). Mapping the Human Membrane Proteome: a Majority of the Human Membrane Proteins Can Be Classified According to Function and Evolutionary Origin. BMC Biol *7*, 50.

(277) Bosmann, H.B., Hagopian, A., and Eylar, E.H. (1968). Cellular Membranes: the Isolation and Characterization of the Plasma and Smooth Membranes of Hela Cells. Arch Biochem Biophys *128*, 51-69.

(278) Milo, R. (2013). What Is the Total Number of Protein Molecules per Cell Volume? A Call to Rethink Some Published Values. Bioessays *35*, 1050-1055.

(279) Okayasu, T., Ikeda, M., Akimoto, K., and Sorimachi, K. (1997). The Amino Acid Composition of Mammalian and Bacterial Cells. Amino Acids *13*, 379-391.

(280) Hern, J.A., Baig, A.H., Mashanov, G.I., Birdsall, B., Corrie, J.E., Lazareno, S., Molloy, J.E., and Birdsall, N.J. (2010). Formation and Dissociation of M_1 Muscarinic Receptor Dimers Seen by Total Internal Reflection Fluorescence Imaging of Single Molecules. Proc Natl Acad Sci USA *107*, 2693-2698.

(281) Calebiro, D., Rieken, F., Wagner, J., Sungkaworn, T., Zabel, U., Borzi, A., Cocucci, E., Zurn, A., and Lohse, M.J. (2013). Single-Molecule Analysis of Fluorescently Labeled G Protein-Coupled Receptors Reveals Complexes with Distinct Dynamics and Organization. Proc Natl Acad Sci USA *110*, 743-748.

(282) Sommerhage, F., Helpenstein, R., Rauf, A., Wrobel, G., Offenhäusser, A., and Ingebrandt, S. (2008). Membrane Allocation Profiling: a Method to Characterize Three-Dimensional Cell Shape and Attachment Based on Surface Reconstruction. Biomaterials *29*, 3927-3935.

(283) Beatty, K.E., Szychowski, J., Fisk, J.D., and Tirrell, D.A. (2011). A Bodipy-Cyclooctyne for Protein Imaging in Live Cells. ChemBioChem *12*, 2137-2139.

(284) Beatty, K.E., Fisk, J.D., Smart, B.P., Lu, Y.Y., Szychowski, J., Hangauer, M.J., Baskin, J.M., Bertozzi, C.R., and Tirrell, D.A. (2010). Live-Cell Imaging of Cellular Proteins by a Strain-Promoted Azide-Alkyne Cycloaddition. ChemBioChem *11*, 2092-2095.

(285) Hughes, L.D., Rawle, R.J., and Boxer, S.G. (2014). Choose Your Label Wisely: Water-Soluble Fluorophores Often Interact with Lipid Bilayers. PLoS One *9*, e87649.

(286) Naganathan, S., Ray-Saha, S., Park, M., Tian, H., Sakmar, T.P., and Huber, T. (2015). Multiplex Detection of Functional G Protein-Coupled Receptors Harboring Site-Specifically Modified Unnatural Amino Acids. Biochemistry *54*, 776-786.

(287) Srinivasan, G., James, C.M., and Krzycki, J.A. (2002). Pyrrolysine Encoded by Uag in Archaea: Charging of a Uag-Decoding Specialized Trna. Science *296*, 1459-1462.

(288) Polycarpo, C., Ambrogelly, A., Berube, A., Winbush, S.A.M., McCloskey, J.A., Crain, P.F., Wood, J.L., and Soll, D. (2004). An Aminoacyl-Trna Synthetase That Specifically Activates Pyrrolysine. Proc Natl Acad Sci USA *101*, 12450-12454.

(289) Blight, S.K., Larue, R.C., Mahapatra, A., Longstaff, D.G., Chang, E., Zhao, G., Kang, P.T., Green-Church, K.B., Chan, M.K., and Krzycki, J.A. (2004). Direct Charging of tRNA(CUA) with Pyrrolysine *in Vitro* and *in Vivo*. Nature *431*, 333-335.

(290) Neumann, H., Peak-Chew, S.Y., and Chin, J.W. (2008). Genetically Encoding N_{ε}-Acetyllysine in Recombinant Proteins. Nat Chem Biol *4*, 232-234.

(291) Hancock, S.M., Uprety, R., Deiters, A., and Chin, J.W. (2010). Expanding the Genetic Code of Yeast for Incorporation of Diverse Unnatural Amino Acids via a Pyrrolysyl-tRNA Synthetase/tRNA Pair. J Am Chem Soc *132*, 14819-14824.

(292) Wan, W., Tharp, J.M., and Liu, W.R. (2014). Pyrrolysyl-tRNA Synthetase: an Ordinary Enzyme but an Outstanding Genetic Code Expansion Tool. Biochim Biophys Acta *1844*, 1059-1070.

(293) Nguyen, D.P., Lusic, H., Neumann, H., Kapadnis, P.B., Deiters, A., and Chin, J.W. (2009). Genetic Encoding and Labeling of Aliphatic Azides and Alkynes in Recombinant Proteins via a Pyrrolysyl-tRNA Synthetase/tRNA(CUA) Pair and Click Chemistry. J Am Chem Soc *131*, 8720-8721.

(294) Lang, K., Davis, L., Torres-Kolbus, J., Chou, C., Deiters, A., and Chin, J.W. (2012). Genetically Encoded Norbornene Directs Site-Specific Cellular Protein Labelling via a Rapid Bioorthogonal Reaction. Nat Chem *4*, 298-304.

(295) Plass, T., Milles, S., Koehler, C., Szymanski, J., Mueller, R., Wiessler, M., Schultz, C., and Lemke, E.A. (2012). Amino Acids for Diels-Alder Reactions in Living Cells. Angew Chem Int Ed *51*, 4166-4170.

(296) Kaya, E., Vrabel, M., Deiml, C., Prill, S., Fluxa, V.S., and Carell, T. (2012). A Genetically Encoded Norbornene Amino Acid for the Mild and Selective Modification of Proteins in a Copper-Free Click Reaction. Angew Chem Int Ed *51*, 4466-4469.

(297) Seitchik, J.L., Peeler, J.C., Taylor, M.T., Blackman, M.L., Rhoads, T.W., Cooley, R.B., Refakis, C., Fox, J.M., and Mehl, R.A. (2012). Genetically Encoded Tetrazine

Amino Acid Directs Rapid Site-Specific *in Vivo* Bioorthogonal Ligation with *Trans*-Cyclooctenes. J Am Chem Soc *134*, 2898-2901.

(298) Lee, Y.J., Wu, B., Raymond, J.E., Zeng, Y., Fang, X., Wooley, K.L., and Liu, W.R. (2013). A Genetically Encoded Acrylamide Functionality. ACS Chem Biol *8*, 1664-1670.

(299) Lang, K., and Chin, J.W. (2014a). Bioorthogonal Reactions for Labeling Proteins. ACS Chem Biol *9*, 16-20.

(300) Lang, K., and Chin, J.W. (2014b). Cellular Incorporation of Unnatural Amino Acids and Bioorthogonal Labeling of Proteins. Chem Rev *114*, 4764-4806.

(301) Hoyle, C.E., and Bowman, C.N. (2010). Thiol-Ene Click Chemistry. Angew Chem Int Ed *49*, 1540-1573.

(302) Jewett, J.C., and Bertozzi, C.R. (2010). Cu-Free Click Cycloaddition Reactions in Chemical Biology. Chem Soc Rev *39*, 1272-1279.

(303) Schadel, S.A., Heck, M., Maretzki, D., Filipek, S., Teller, D.C., Palczewski, K., and Hofmann, K.P. (2003). Ligand Channeling within a G Protein-Coupled Receptor: the Entry and Exit of Retinals in Native Opsin. J Biol Chem *278*, 24896-24903.

(304) Sanchez-Martin, M.J., Ramon, E., Torrent-Burgues, J., and Garriga, P. (2013). Improved Conformational Stability of the Visual G Protein-Coupled Receptor Rhodopsin by Specific Interaction with Docosahexaenoic Acid Phospholipid. ChemBioChem *14*, 639-644.

(305) Rattner, A., Sun, H., and Nathans, J. (1999). Molecular Genetics of Human Retinal Disease. Annu Rev Genet *33*, 89-131.

(306) Middleton, R.J., and Kellam, B. (2005). Fluorophore-Tagged GPCR Ligands. Curr Opin Chem Biol *9*, 517-525.

(307) Cohen, B.E., McAnaney, T.B., Park, E.S., Jan, Y.N., Boxer, S.G., and Jan, L.Y. (2002). Probing Protein Electrostatics with a Synthetic Fluorescent Amino Acid. Science *296*, 1700-1703.

(308) Pantoja, R., Rodriguez, E.A., Dibas, M.I., Dougherty, D.A., and Lester, H.A. (2009). Single-Molecule Imaging of a Fluorescent Unnatural Amino Acid Incorporated into Nicotinic Receptors. Biophys J *96*, 226-237.

(309) Li, J., Xu, Q., Cortes, D.M., Perozo, E., Laskey, A., and Karlin, A. (2002). Reactions of Cysteines Substituted in the Amphipathic N-Terminal Tail of a Bacterial Potassium Channel with Hydrophilic and Hydrophobic Maleimides. Proc Natl Acad Sci USA *99*, 11605-11610.

(310) Roy, R., Hohng, S., and Ha, T. (2008). A Practical Guide to Single-Molecule Fret. Nat Methods *5*, 507-516.

(311) Costanzi, S. (2011). Homology Modeling of Class a G Protein-Coupled Receptors. Methods Mol Biol *857*, 259-279.

(312) Bockenhauer, S., Furstenberg, A., Yao, X.J., Kobilka, B.K., and Moerner, W.E. (2011). Conformational Dynamics of Single G Protein-Coupled Receptors in Solution. J Phys Chem B *115*, 13328-13338.

(313) Huber, T., and Sakmar, T.P. (2011). Escaping the Flatlands: New Approaches for Studying the Dynamic Assembly and Activation of GPCR Signaling Complexes. Trends Pharmacol Sci *32*, 410-419.

(314) Starace, D.M., and Knox, B.E. (1998). Cloning and Expression of a Xenopus Short Wavelength Cone Pigment. Exp Eye Res *67*, 209-220.

(315) Knepp, A.M., Grunbeck, A., Banerjee, S., Sakmar, T.P., and Huber, T. (2011). Direct Measurement of Thermal Stability of Expressed CCR5 and Stabilization by Small Molecule Ligands. Biochemistry *50*, 502-511.

(316) Shichi, H. (1970). Spectrum and Purity of Bovine Rhodopsin. Biochemistry *9*, 1973-1977.

(317) Rushton, W.A. (1961). Dark-Adaptation and the Regeneration of Rhodopsin. J Physiol *156*, 166-178.

(318) Lamb, T.D., and Pugh, E.N. (2006). Phototransduction, Dark Adaptation, and Rhodopsin Regeneration - the Proctor Lecture. Invest Ophth Vis Sci *47*, 5138-5152.

(319) Dowling, J.E., and Wald, G. (1960). The Biological Function of Vitamin-a Acid. Proc Natl Acad Sci USA *46*, 587-608.

(320) Cooper, A. (1981). Rhodopsin Photoenergetics: Lumirhodopsin and the Complete Energy Profile. FEBS Lett *123*, 324-326.

(321) Schick, G.A., Cooper, T.M., Holloway, R.A., Murray, L.P., and Birge, R.R. (1987). Energy Storage in the Primary Photochemical Events of Rhodopsin and Isorhodopsin. Biochemistry *26*, 2556-2562.

(322) Kühne, W. (1978). Über Den Sehpurpur. Heidelberg: Unters Physiol Inst Univ Heidelberg, 113 pp.

(323) Hecht, S., Chase, A.M., Shlaer, S., and Haig, C. (1936). The Regeneration of Visual Purple in Solution. Science *84*, 331-333.

(324) Chase, A.M., and Smith, E.L. (1940). Regeneration of Visual Purple in Solution. J Gen Physiol *23*, 21-39.

(325) Zorn, M., and Futterman, S. (1973). Extraction, Regeneration after Bleaching, and Ion-Exchange Chromatography of Rhodopsin in Tween 80. Arch Biochem Biophys *157*, 91-99.

(326) Matsumoto, H., and Yoshizawa, T. (1975). Existence of a *β*-Ionone Ring-Binding Site in the Rhodopsin Molecule. Nature *258*, 523-526.

(327) Matsumoto, H., Horiuchi, K., and Yoshizawa, T. (1978). Effect of Digitonin Concentration on Regeneration of Cattle Rhodopsin. Biochim Biophys Acta *501*, 257-268.

(328) Mccaslin, D.R., and Tanford, C. (1981). Effects of Detergent Micelles on the Recombination Reaction of Opsin and 11-*Cis*-Retinal. Biochemistry *20*, 5207-5212.

(329) Sakamoto, T., and Khorana, H.G. (1995). Structure and Function in Rhodopsin: The Fate of Opsin Formed upon the Decay of Light-Activated Metarhodopsin II *in Vitro*. Proc Natl Acad Sci USA *92*, 249-253.

(330) Gross, A.K., Rao, V.R., and Oprian, D.D. (2003a). Characterization of Rhodopsin Congenital Night Blindness Mutant T94I. Biochemistry *42*, 2009-2015.

(331) Gross, A.K., Xie, G., and Oprian, D.D. (2003b). Slow Binding of Retinal to Rhodopsin Mutants G90D and T94D. Biochemistry *42*, 2002-2008.

(332) Piechnick, R., Ritter, E., Hildebrand, P.W., Ernst, O.P., Scheerer, P., Hofmann, K.P., and Heck, M. (2012). Effect of Channel Mutations on the Uptake and Release of the Retinal Ligand in Opsin. Proc Natl Acad Sci USA *109*, 5247-5252.

(333) Degrip, W.J. (1982a). Thermal-Stability of Rhodopsin and Opsin in Some Novel Detergents. Methods Enzymol *81*, 256-265.

(334) Hjelmeland, L.M., and Chrambach, A. (1984). Solubilization of Functional Membrane-Proteins. Methods Enzymol *104*, 305-318.

(335) Xie, G., Gross, A.K., and Oprian, D.D. (2003). An Opsin Mutant with Increased Thermal Stability. Biochemistry *42*, 1995-2001.

(336) Sanders, C.R., and Prosser, R.S. (1998). Bicelles: a Model Membrane System for All Seasons? Structure *6*, 1227-1234.

(337) Whiles, J.A., Deems, R., Vold, R.R., and Dennis, E.A. (2002). Bicelles in Structure-Function Studies of Membrane-Associated Proteins. Bioorg Chem *30*, 431-442.

(338) Durr, U.H., Gildenberg, M., and Ramamoorthy, A. (2012). The Magic of Bicelles Lights up Membrane Protein Structure. Chem Rev *112*, 6054-6074.

(339) McKibbin, C., Farmer, N.A., Jeans, C., Reeves, P.J., Khorana, H.G., Wallace, B.A., Edwards, P.C., Villa, C., and Booth, P.J. (2007). Opsin Stability and Folding: Modulation by Phospholipid Bicelles. J Mol Biol *374*, 1319-1332.

(340) Tian, H., Naganathan, S., Kazmi, M.A., Schwartz, T.W., Sakmar, T.P., and Huber, T. (2014). Bioorthogonal Fluorescent Labeling of Functional G Protein-Coupled Receptors. ChemBioChem *15*, 1820-1829.

(341) Pierce, M.M., Raman, C.S., and Nall, B.T. (1999). Isothermal Titration Calorimetry of Protein-Protein Interactions. Methods *19*, 213-221.

(342) Litman, B.J. (1982). Purification of Rhodopsin by Concanavalin A Affinity Chromatography. Methods Enzymol *81*, 150-153.

(343) Degrip, W.J. (1982b). Purification of Bovine Rhodopsin over Concanavalin A-Sepharose. Methods Enzymol *81*, 197-207.

(344) Srinivasan, S., Ramon, E., Cordomi, A., and Garriga, P. (2014). Binding Specificity of Retinal Analogs to Photoactivated Visual Pigments Suggest Mechanism for Fine-Tuning GPCR-Ligand Interactions. Chem Biol *21*, 369-378.

(345) Navratilova, I., Sodroski, J., and Myszka, D.G. (2005). Solubilization, Stabilization, and Purification of Chemokine Receptors Using Biosensor Technology. Anal Biochem *339*, 271-281.

(346) Oates, J., and Watts, A. (2011). Uncovering the Intimate Relationship between Lipids, Cholesterol and GPCR Activation. Curr Opin Struct Biol *21*, 802-807.

(347) Kawaguchi, T., Hamanaka, T., and Kito, Y. (1986). Kinetic Study of Transfer of 11-*Cis*-Retinal between Rod Outer Segment Membranes Using Regeneration of Rhodopsin. Biophys Chem *24*, 5-12.

(348) Kefalov, V.J., Crouch, R.K., and Cornwall, M.C. (2001). Role of Noncovalent Binding of 11-*Cis*-Retinal to Opsin in Dark Adaptation of Rod and Cone Photoreceptors. Neuron *29*, 749-755.

(349) Cornwall, M.C., and Fain, G.L. (1994). Bleached Pigment Activates Transduction in Isolated Rods of the Salamander Retina. J Physiol *480 (Pt 2)*, 261-279.

(350) Cornwall, M.C., Matthews, H.R., Crouch, R.K., and Fain, G.L. (1995). Bleached Pigment Activates Transduction in Salamander Cones. J Gen Physiol *106*, 543-557.

(351) Surya, A., Foster, K.W., and Knox, B.E. (1995). Transducin Activation by the Bovine Opsin Apoprotein. J Biol Chem *270*, 5024-5031.

(352) Matsumoto, H., Tokunaga, F., and Yoshizawa, T. (1975). Accessibility of the Iodopsin Chromophore. Biochim Biophys Acta *404*, 300-308.

(353) Crescitelli, F. (1984). The Gecko Visual Pigment: the Dark Exchange of Chromophore. Vision Res *24*, 1551-1553.

(354) Kefalov, V.J., Estevez, M.E., Kono, M., Goletz, P.W., Crouch, R.K., Cornwall, M.C., and Yau, K.W. (2005). Breaking the Covalent Bond - a Pigment Property that Contributes to Desensitization in Cones. Neuron *46*, 879-890.

(355) Defoe, D.M., and Bok, D. (1983). Rhodopsin Chromophore Exchanges among Opsin Molecules in the Dark. Invest Ophth Vis Sci *24*, 1211-1226.

(356) Baylor, D.A., Matthews, G., and Yau, K.W. (1980). Two Components of Electrical Dark Noise in Toad Retinal Rod Outer Segments. J Physiol *309*, 591-621.

(357) Liu, J., Liu, M.Y., Nguyen, J.B., Bhagat, A., Mooney, V., and Yan, E.C. (2009). Thermal Decay of Rhodopsin: Role of Hydrogen Bonds in Thermal Isomerization of 11-*Cis*-Retinal in the Binding Site and Hydrolysis of Protonated Schiff Base. J Am Chem Soc *131*, 8750-8751.

(358) Liu, J., Liu, M.Y., Fu, L., Zhu, G.A., and Yan, E.C.Y. (2011). Chemical Kinetic Analysis of Thermal Decay of Rhodopsin Reveals Unusual Energetics of Thermal Isomerization and Hydrolysis of Schiff Base. J Biol Chem *286*, 38408-38416.

(359) Hubbard, R. (1966). The Stereoisomerization of 11-*Cis*-Retinal. J Biol Chem *241*, 1814-1818.

(360) Fernando, H., Nagle, G.T., and Rajarathnam, K. (2007). Thermodynamic Characterization of Interleukin-8 Monomer Binding to CXCR1 Receptor N-Terminal Domain. FEBS J *274*, 241-251.

(361) Nisius, L., Rogowski, M., Vangelista, L., and Grzesiek, S. (2008). Large-Scale Expression and Purification of the Major HIV-1 Coreceptor CCR5 and Characterization of Its Interaction with Rantes. Protein Expres Purif *61*, 155-162.

(362) Rajarathnam, K., and Rosgen, J. (2014). Isothermal Titration Calorimetry of Membrane Proteins - Progress and Challenges. Biochim Biophys Acta *1838*, 69-77.

(363) Cooper, A., and Converse, C.A. (1976). Energetics of Primary Processes in Visula Escitation: Photocalorimetry of Rhodopsin in Rod Outer Segment Membranes. Biochemistry *15*, 2970-2978.

(364) Cooper, A. (1979). Energetics of Rhodopsin and Isorhodopsin. FEBS Lett *100*, 382-384.

(365) Hubbard, R. (1958). The Thermal Stability of Rhodopsin and Opsin. J Gen Physiol *42*, 259-280.

(366) Manalan, A.S., Besch, H.R., Jr., and Watanabe, A.M. (1981). Characterization of [^{3}H](+/-)Carazolol Binding to *β*-Adrenergic Receptors. Application to Study of *β*-Adrenergic Receptor Subtypes in Canine Ventricular Myocardium and Lung. Circ Res *49*, 326-336.

(367) Contreras, M.L., Wolfe, B.B., and Molinoff, P.B. (1986). Thermodynamic Properties of Agonist Interactions with the *β* Adrenergic Receptor-Coupled Adenylate Cyclase System. II: Agonist Binding to Soluble Beta Adrenergic Receptors. J Pharmacol Exp Ther *237*, 165-172.

(368) Alberty, R.A., and Hammes, G.G. (1958). Application of the Theory of Diffusion-Controlled Reactions to Enzyme Kinetics. J Phys Chem *62*, 154-159.

(369) Kusnetzow, A.K., Altenbach, C., and Hubbell, W.L. (2006). Conformational States and Dynamics of Rhodopsin in Micelles and Bilayers. Biochemistry *45*, 5538-5550.

(370) Lee, A.G. (2004). How Lipids Affect the Activities of Integral Membrane Proteins. Biochim Biophys Acta *1666*, 62-87.

(371) Wang, T., and Duan, Y. (2007). Chromophore Channeling in the G Protein-Coupled Receptor Rhodopsin. J Am Chem Soc *129*, 6970-6971.

(372) Wang, T., and Duan, Y. (2009). Ligand Entry and Exit Pathways in the β_2-Adrenergic Receptor. J Mol Biol *392*, 1102-1115.

(373) Papermaster, D.S., and Dreyer, W.J. (1974). Rhodopsin Content in the Outer Segment Membranes of Bovine and Frog Retinal Rods. Biochemistry *13*, 2438-2444.

(374) Botelho, A.V., Gibson, N.J., Thurmond, R.L., Wang, Y., and Brown, M.F. (2002). Conformational Energetics of Rhodopsin Modulated by Nonlamellar-Forming Lipids. Biochemistry *41*, 6354-6368.

(375) Dieterle, J.M., and Robeson, C.D. (1954). Crystalline Neoretinene B. Science *120*, 219-220.

(376) Brown, P.K., and Wald, G. (1956). Neo-B Isomer of Vitamin-A and Retinene. J Biol Chem *222*, 865-877.

(377) Kühn, H., and Wilden, U. (1987). Deactivation of Photoactivated Rhodopsin by Rhodopsin-Kinase and Arrestin. J Recept Res *7*, 283-298.

(378) Richard, E.A., and Lisman, J.E. (1992). Rhodopsin Inactivation Is a Modulated Process in Limulus Photoreceptors. Nature *356*, 336-338.

(379) Ranganathan, R., and Stevens, C.F. (1995). Arrestin Binding Determines the Rate of Inactivation of the G Protein-Coupled Receptor Rhodopsin *in Vivo*. Cell *81*, 841-848.

(380) Katritch, V., Cherezov, V., and Stevens, R.C. (2012). Diversity and Modularity of G Protein-Coupled Receptor Structures. Trends Pharmacol Sci *33*, 17-27.

(381) Hildebrand, P.W., Scheerer, P., Park, J.H., Choe, H.W., Piechnick, R., Ernst, O.P., Hofmann, K.P., and Heck, M. (2009). A Ligand Channel through the G Protein-Coupled Receptor Opsin. PLoS One *4*, e4382.

(382) Frederiksen, R., Boyer, N.P., Nickle, B., Chakrabarti, K.S., Koutalos, Y., Crouch, R.K., Oprian, D., and Cornwall, M.C. (2012). Low Aqueous Solubility of 11-*Cis*-Retinal Limits the Rate of Pigment Formation and Dark Adaptation in Salamander Rods. J Gen Physiol *139*, 493-505.

(383) Tsukamoto, H., and Farrens, D.L. (2013). A Constitutively Activating Mutation Alters the Dynamics and Energetics of a Key Conformational Change in a Ligand-Free G Protein-Coupled Receptor. J Biol Chem *288*, 28207-28216.

(384) Schafer, C.T., and Farrens, D.L. (2015). Conformational Selection and Equilibrium Governs the Ability of Retinals to Bind Opsin. J Biol Chem *290*, 4304-4318.

(385) Vogel, R., and Siebert, F. (2001). Conformations of the Active and Inactive States of Opsin. J Biol Chem *276*, 38487-38493.

(386) Sachs, K., Maretzki, D., Meyer, C.K., and Hofmann, K.P. (2000). Diffusible Ligand All-*Trans*-Retinal Activates Opsin via a Palmitoylation-Dependent Mechanism. J Biol Chem *275*, 6189-6194.

(387) Okada, T. (2004). X-Ray Crystallographic Studies for Ligand-Protein Interaction Changes in Rhodopsin. Biochem Soc Trans *32*, 738-741.

(388) McGaughey, G.B., Gagne, M., and Rappe, A.K. (1998). Pi-Stacking Interactions. Alive and Well in Proteins. J Biol Chem *273*, 15458-15463.

(389) Tsukamoto, H., Terakita, A., and Shichida, Y. (2010). A Pivot between Helices V and VI near the Retinal-Binding Site Is Necessary for Activation in Rhodopsins. J Biol Chem *285*, 7351-7357.

(390) Wang, T., and Duan, Y. (2011). Retinal Release from Opsin in Molecular Dynamics Simulations. J Mol Recognit *24*, 350-358.

(391) Ludeke, S., Beck, R., Yan, E.C.Y., Sakmar, T.P., Siebert, F., and Vogel, R. (2005). The Role of Glu181 in the Photoactivation of Rhodopsin. J Mol Biol *353*, 345-356.

(392) Sekharan, S., and Buss, V. (2008). Glutamic Acid 181 Is Uncharged in Dark-Adapted Visual Rhodopsin. J Am Chem Soc *130*, 17220-17221.

(393) Lewis, J.W., Szundi, I., Kazmi, M.A., Sakmar, T.P., and Kliger, D.S. (2004). Time-Resolved Photointermediate Changes in Rhodopsin Glutamic Acid 181 Mutants. Biochemistry *43*, 12614-12621.

(394) Janz, J.M., and Farrens, D.L. (2004). Role of the Retinal Hydrogen Bond Network in Rhodopsin Schiff Base Stability and Hydrolysis. J Biol Chem *279*, 55886-55894.

(395) Adamian, L., and Liang, J. (2002). Interhelical Hydrogen Bonds and Spatial Motifs in Membrane Proteins: Polar Clamps and Serine Zippers. Proteins-Structure Function and Genetics *47*, 209-218.

(396) Tikhonova, I.G., Best, R.B., Engel, S., Gershengorn, M.C., Hummer, G., and Costanzi, S. (2008). Atomistic Insights into Rhodopsin Activation from a Dynamic Model. J Am Chem Soc *130*, 10141-10149.

(397) Moitra, S., Tirupula, K.C., Klein-Seetharaman, J., and Langmead, C.J. (2012). A Minimal Ligand Binding Pocket within a Network of Correlated Mutations Identified by

Multiple Sequence and Structural Analysis of G Protein-Coupled Receptors. Bmc Biophys *5*.

(398) Tian, H., Sakmar, T.P., and Huber, T. (2013a). Site-Specific Labeling of Genetically Encoded Azido Groups for Multicolor, Single-Molecule Fluorescence Imaging of GPCRs. Receptor-Receptor Interactions *117*, 267-303.

(399) Sage, D., Neumann, F.R., Hediger, F., Gasser, S.M., and Unser, M. (2005). Automatic Tracking of Individual Fluorescence Particles: Application to the Study of Chromosome Dynamics. IEEE T Image Process *14*, 1372-1383.

(400) Tian, H., Sakmar, T.P., and Huber, T. (2013b). Site-Specific Labeling of Genetically Encoded Azido Groups for Multicolor, Single-Molecule Fluorescence Imaging of GPCRs. Methods Cell Biol *117*, 267-303.

(401) Holden, S.J., Uphoff, S., Hohlbein, J., Yadin, D., Le Reste, L., Britton, O.J., and Kapanidis, A.N. (2014). Defining the Limits of Single-Molecule FRET Resolution in TIRF Microscopy. Biophys J *106*, 2082-2082.